THE DEVELOPMENT OF CILIA ON THE *CIONA INTESTINALIS* EMBRYO AND THE EVOLUTION OF CHORDATE LEFT-RIGHT ASYMMETRY



The Development of Cilia on the *Ciona intestinalis* Embryo and the Evolution of Chordate Left-right Asymmetry

HELEN THOMPSON

Department of Zoology,

University of Oxford

October 2011

A DISSERTATION SUBMITTED
FOR THE DEGREE OF
DOCTOR OF PHILOSOPHY
AT THE UNIVERSITY OF OXFORD

ACKNOWLEDGEMENTS

I should firstly like to thank my supervisors, Sebastian Shimeld and Helen Dawe, for all their scientific help and guidance during my DPhil. I am also particularly grateful to the BBSRC who provided the funding for this project.

For their help and advice in lab meetings, I should also like to thank Peter Holland and Keith Gull and their respective labs. A special thank you to the Holland lab for accommodating me for the entirety of my DPhil.

I cannot thank Michael Shaw enough for his time and patience in helping me with my Electron Microscope work, as well as for his general scientific advice. Without his expertise and willingness to help I would not have been able to complete this project.

I owe all my knowledge of *Ciona intestinalis* and molecular biology to the expertise of Wei-Chung Chen who was a brilliant Post-doc while she was in Oxford and was greatly missed when she left.

Maths will never be my favourite subject but with the excellent help of Michael Bonsall I was able to complete the Statistics section of my project with relative calm!

It has been great to have the help and support of Michiel Plugge and Matthew Hodges from day one of my DPhil and later of Kyle Martin. They have provided me with scientific advice and guidance as well as friendship and much needed fun over the last 4 years. In particular, I need to thank them for carrying many, many tanks of sea water and collecting *Ciona* in the rain on Hayling Island when they had no obligation to help.

I should like to thank Mum, Dad and my sister, Claire for all their support with all my

education and, particularly my DPhil, over the last 4 years. I would not have been able to achieve any of this without their unrelenting support and encouragement throughout my life. Claire, you know far more about *Ciona* then any non-biologist ever should!

Lastly, I should like to thank Tom who has been on the other end of all the frustration of failed experiments or mass *Ciona* deaths over my time in Oxford. I really appreciate his support and, in particular, the last 6 months when he has encouraged me through finishing my experiments and writing up.

ABSTRACT

Most multicellular organisms have body plans that exhibit an element of symmetry; either radial or bilateral symmetry. Bilateral symmetry refers to organisms which have a single plane of symmetry with each side a mirror image of the other. Although externally these species appear symmetrical, internally, the organs are positioned in an asymmetric manner. This left-right axis is the last axis established after the Anterior-Posterior (AP) axis and Dorsal-ventral (DV) axis and recent research has analysed how this asymmetry is established. In the mouse it has been shown that monocilia on the organiser region, the mouse ventral node, rotate and generate a leftward fluid flow across the node. This flow, termed nodal flow, is essential for the left-sided localised expression of *nodal*, *lefty* and *pitx2* and subsequent asymmetric patterning of organs. Nodal flow is highly conserved in the vertebrates but, although the conservation of asymmetric gene expression extends into the invertebrates, whether this is established through directional flow is unknown. This research has investigated the extent of nodal flow conservation in a basal chordate, the urochordate, *Ciona intestinalis*.

Here I have shown, through Electron Microscopy (EM) and immunofluorescence, that cilia are present, at the posterior of each cell of the *Ciona intestinalis* embryo, at the time point indicative to a role in the establishment of left-right asymmetry. They do not appear to be homologous to the cilia of the mouse ventral node because they are not motile and have a disorganised microtubule structure. However, the cilia may still have an important role in the development of left-right asymmetry in a sensory capacity or provide the site for H^+/K^+-ATPase channels already known to be involved in *Ciona intestinalis* left-right asymmetry.

CONTENTS

List of Figures *xiv*

List of Tables *xix*

1 Introduction **1**

1.1 ASYMMETRY 1

1.1.1 Asymmetry in nature 3

1.1.2 Vertebrate asymmetry 3

1.1.3 The general model of asymmetry 4

1.2 ASYMMETRY IN VERTEBRATES 5

1.2.1 Asymmetric gene expression of genes 5

1.2.2 Human laterality diseases 5

1.3 LEFT-RIGHT ASYMMETRY IN MOUSE 6

1.3.1 Mouse ventral node 6

1.3.2 Ventral node cells 7

1.3.3 Cilia 8

1.3.3.1 Motile cilia 8

1.3.3.2 Primary cilia 11

1.3.4 Mouse mutants with laterality defects 11

1.3.5 The generation of a leftward flow by node cilia 13

1.3.6 The posterior positioning of nodal cilia on cells of the mouse node 14

1.3.7 Nodal cilia movement 15

1.3.8 Nodal cilia structure 16

1.4 HOW IS THE LEFTWARD NODAL FLOW TRANSLATED TO MOLECULAR ASYMMETRIES? 16

1.4.1 The Chemical Hypothesis 17

1.4.2 The Physical Hypothesis 19

1.4.3 Cilia as mechanosensors 20

1.5 LEFT-RIGHT ASYMMETRY DETERMINATION IN OTHER VERTEBRATE SPECIES 22

1.5.1 Rabbit 23

1.5.2 Zebrafish (*Danio rerio*) 24

1.5.3 *Xenopus* 27

1.5.4 Chick (*Gallus gallus*) 29

1.6 THE DEVELOPMENT OF LEFT-RIGHT ASYMMETRY IN THE INVERTEBRATES 32

1.6.1 *Ciona intestinalis* *33*

1.6.2 Amphioxus (*Branchiostoma floridae)* 36

1.6.3 Sea urchin 37

1.7 ECDYSOZOANS – *DROSOPHILA MELANOGASTER* 39

1.8 LOPHOTROCHOZOANS – SNAILS 40

1.9 SUMMARY 41

1.10 AIMS 43

2 Materials and Methods **45**

2.1 MOUSE EMBRYOS 45

2.1.1 Collection and dissection of mouse embryos 45

2.2 ELECTRON MICROSCOPY 45

2.2.1 Scanning Electron Microscopy 45

2.2.2 Transmission Electron Microscopy 46

2.3 BIOINFORMATICS 47

2.3.1 Proteins linked with left-right asymmetry 47

2.3.2 Identification of homologues 47

2.4 *CIONA INTESTINALIS* ANIMALS 48

2.4.1 Fertilisation 49

2.4.2 De-chorionation 49

2.5 *CIONA INTESTINALIS* PROBES 49

2.5.1 Cloning 49

2.5.2 Double digest 50

2.5.3 Sequencing 50

2.5.4 DNA linearization 52

2.5.5 Phenol/Chloroform extraction 52

2.5.6 Riboprobe synthesis and cleaning 53

2.5.7 *In situ* hybridisations 53

2.6 ANTIBODY STAINING 54

2.6.1 Acetylated α- and γ-tubulin 54

2.6.2 Phalloidin 55

2.7 DE-CILIATION OF *CIONA INTESTINALIS* EMBRYOS 56

2.7.1 Microinjection 56

2.7.1.1 Morpholinos 56

2.7.1.2 Microinjection of *Ciona intestinalis* embryos 57

2.8 Cilia positional measurements 58

2.8.1 Position along the AP axis 58

2.8.2 Angle from the centre of the cell 58

3 An electron microscope study of the early stages of *Ciona intestinalis* development 59

3.1 INTRODUCTION 59

3.2 RESULTS 61

3.2.1 Morphology of the node 61

3.2.2 Structure of mouse gastrula ectoderm cilia 63

3.2.3 Early *Ciona intestinalis* development 65

3.2.3.1 Early *Ciona intestinalis* embryos 65

3.2.3.2 Late *Ciona intestinalis* embryos 68

3.2.3.3 Anti-acetylated α-tubulin staining of embryos 73

3.2.4 Transmission Electron Microscopy of *Ciona intestinalis* neurula stage embryos 74

3.2.4.1 Transmission Electron Microscopy of early tailbud *Ciona intestinalis* embryos 74

3.2.4.2 The ultrastructure of *Ciona intestinalis* neurula stage cilia 77

3.2.4.3 The ultrastructure of a *Ciona intestinalis* chorion and follicle cells 85

3.2.4.4 The ultrastructure of a *Ciona intestinalis* sperm head and tail 88

3.3 DISCUSSION 89

3.3.1 Microtubule fixation experimentation 90

3.3.2 The structure of cilia on mouse gastrula embryo epithelia 91

3.3.3 *Ciona intestinalis* cleavage stage embryos 93

3.3.4 Cilia on *Ciona intestinalis* embryos 94

3.3.5 Timing of cilia presence on *Ciona intestinalis* embryos 95

3.3.6 *Ciona intestinalis* cilia and left-right asymmetry 96

3.3.7 *Ciona intestinalis* cilia structure and motility 97

3.3.8 Role of cilia as mechanosensors or sites of signalling 100

3.3.9 The role of the chorion in the development of left-right asymmetry in *Ciona intestinalis* 103

3.3.10 Conclusion 106

4 The role of cilia on the neurula stage *Ciona intestinalis* embryo 107

4.1 INTRODUCTION 107

4.2 RESULTS 109

4.2.1 The distance along the AP axis of a cell a cilium is positioned on a *Ciona intestinalis* embryo 109

4.2.2 The angle from the centrepoint of a cell a cilium is positioned on a *Ciona intestinalis* embryo 111

4.2.3 The effect cell location on the embryo has on cilia position 113

4.2.4 The effect of de-chorionation on cilia formation 115

4.2.5 Experimental manipulation of cilia on a *Ciona intestinalis* embryo 117

4.2.6 The effect of exposure to 4.45M NaCl on *Ci-Pitx* expression in *Ciona intestinalis* embryos 123

4.3 DISCUSSION 127

4.3.1 Polarisation of *Ciona intestinalis* cilia 128

4.3.2 Planar Cell Polarity in organisms 129

4.3.3 Planar Cell Polarity pathway in vertebrates 129

4.3.4 The control of cilia organisation in the vertebrate inner ear 131

4.3.5 PCP in left-right asymmetry 131

4.3.6 PCP genes in *Ciona intestinalis* 132

4.3.7 The position of cilia at different locations on the late neurula/early tailbud *Ciona intestinalis* embryo 134

4.3.8 The effect of de-chorionation on cilia presence 135

4.3.9 The effect of experimental manipulation on cilia 137

4.3.10 Conclusion 138

5 The distribution of proteins linked with the establishment of left-right asymmetry across the eukaryotes 141

5.1 INTRODUCTION 141

5.2 RESULTS 143

5.2.1 Identification of proteins involved in the initial break in symmetry

in humans and mice 143

5.2.2 Phylogenetic distribution of left-right linked proteins 144

5.2.2.1 Phylogenetic distribution of the structural proteins essential for ciliogenesis 152

5.2.2.2 Phylogenetic distribution of known Transcription Factors (TFs) involved in left-right asymmetry 157

5.2.2.3 Phylogenetic distribution of proteins involved in the movement of cilia and other factors in the development of laterality 159

5.2.3 The presence of left-right asymmetry proteins in *Ciona intestinalis* 163

5.2.3.1 *Ciona intestinalis* proteins 163

5.2.3.2 The presence of proteins involved in left-right asymmetry in *Ciona intestinalis* 165

5.2.3.3 The expression patterns of *DNAH11* in the developing *Ciona intestinalis* embryo 166

5.3 DISCUSSION 168

5.3.1 The presence and absence of proteins involved in left-right asymmetry and nodal flow in the human and mouse models 170

5.3.1.1 Structural proteins 170

5.3.1.2 Transcription Factors 172

5.3.1.3 Other proteins 174

5.3.2 Protein presence and left-right asymmetry mechanisms 176

5.3.3 Proteins involved in the establishment of left-right asymmetry in *Ciona intestinalis* 177

5.3.4 Conclusion 178

6 Conclusions **180**

References *187*

Appendices *207*

LIST OF FIGURES

Chapter 1

1.1 Types of symmetry in the Metazoa 2

1.2 A typical 9+2 motile cilium from the basal body to the ciliary tip 9

1.3 The ciliary beat pattern in motile cilia of the trachea and the monocilia of the mouse ventral node 10

1.4 The current two models for the establishment of left-right asymmetry in the mouse model 18

1.5 Holozoan Phylogeny 32

Chapter 3

3.1 Morphology of the mouse ventral node and surrounding endoderm at the Theiler stage 10 (7.0 d.p.c) 62

3.2 The disorganised ultrastructure axoneme arrangement of cilia on the surface of the Theiler stage 10 (7.0 d.p.c) 3 somite mouse embryo 64

3.3 Early *Ciona intestinalis* development 66

3.4 The surface texture and microvilli structures of an early 8-16 cell *Ciona intestinalis* embryo 67

3.5 The surface texture and microvilli structures of a late 8-16 cell *Ciona intestinalis* embryo 68

3.6 The surface texture and structures of 32 cell stage to gastrula stage *Ciona intestinalis* embryos 69

3.7 The surface texture and morphology of a neurula *Ciona intestinalis* embryo 70

3.8 The presence of cilia on the tailbud stage *Ciona intestinalis* embryos 71

3.9 The surface texture and morphology of late tailbud stage *Ciona intestinalis* embryos 72

3.10 The presence of cilia on the tailbud stage *Ciona intestinalis* embryo through immunofluorescence and DAPI staining 73

3.11 A summary of the results from SEM and immunolocalisation in early *Ciona intestinalis* embryogenesis 75

3.12 Experimentation with different TEM fixes on neurula stage *Ciona intestinalis* embryos showed that Fix 2 as the optimum fixative to preserve membranes and organelles 76

3.13 The ultrastructure of a *Ciona intestinalis* neurula embryo cilium showing the collapsed doublet microtubule organisation 79

3.14 The ultrastructure of cilia on a neurula stage *Ciona intestinalis* embryo shows the disintegration of doublet microtubule organisation 80

3.15 The longitudinal ultrastructure of cilia on a neurula stage *Ciona intestinalis* embryo shows the disintegration of doublet microtubule organisation 81

3.16 The ultrastructure of cilia on a neurula stage *Ciona intestinalis* embryo shows the presence of a single microtubule in the centre of the axoneme 82

3.17 The ultrastructure of a cilium on a neurula stage *Ciona intestinalis* embryo shows the cilium within a pocket 83

3.18 The mean measurements of *Ciona intestinalis* tailbud stage cilia 85

3.19 The morphology and ultrastructure of the *Ciona intestinalis* embryo chorion with large vacuous follicle cells on the outside and test cells on the inside 87

3.20 The ultrastructure of a *Ciona intestinalis* sperm flagellum 88

Chapter 4

4.1 Polarisation of cilia on the developing *Ciona intestinalis* embryo to the posterior of each cell 110

4.2 The angle of cilia from the centre of each cell on a late neurula stage *Ciona intestinalis* embryo 112

4.3 The location of a cell on a neurula stage *Ciona intestinalis* embryo affects cilia position along the AP axis but not the angle from the centrepoint 114

4.4 De-chorionation at fertilisation does not remove cilia on tailbud stage *Ciona intestinalis* embryos 116

4.5 The position of cilia along the AP axis on *Ciona intestinalis* 10 and 30 mins after exposure to NaCl 119

4.6 The effect of NaCl exposure on the cilia position along the AP axis on a developing *Ciona intestinalis* embryo 0 mins after exposure 120

4.7 The effect of NaCl exposure on the cilia position along the AP axis on a developing *Ciona intestinalis* embryo 10 mins after exposure 121

4.8 The effect of NaCl exposure on the cilia position along the AP axis on a developing *Ciona intestinalis* embryo 30 mins after exposure 122

4.9 The effect of NaCl exposure on *Ciona intestinalis* neurula stage cilia angle from the centre of each cell 124

4.10 The localisation of *Ci-Pitx* expression in the left ectoderm and mesenchyme of 4.45M NaCl exposed *Ciona intestinalis* embryos 125

4.11 *Ci-Pitx* expression in *Ciona intestinalis* early and late tailbud embryos after exposure to 4.45M NaCl 127

Chapter 5

5.1 Phylogenetic relationships of the eukaryotes 148

5.2 Distribution of proteins involved in left-right asymmetry in vertebrates among the eukaryotes 150

5.3 Distribution of proteins involved in left-right asymmetry in vertebrates among the eukaryotes and the known mechanisms involved in the establishment of left-right asymmetry in Metazoa 151

5.4 DNAH11 Phylogeny 153

5.5 INV Phylogeny 160

5.6 EST expression of 13 genes in the adult and embryo *Ciona intestinalis* gene collection 165

5.7 *DNAH11* is not expressed in the early stages of *Ciona intestinalis* embryogenesis 167

Appendices

A1.1 DNAH5 Phylogeny 209

A1.2 DNAI1 Phylogeny 211

A1.3 DNAI2 Phylogeny 212

A1.4 KIF3A Phylogeny 213

A1.5 FOXJ1 Phylogeny 214

A1.6 RFX3 Phylogeny 215

A1.7 ZIC3 Phylogeny 216

A1.8 GDF1 Phylogeny 218

A1.9 PKD2 Phylogeny 220

A1.10 BICC1 Phylogeny 221

A1.11 DAND5 Phylogeny 222

LIST OF TABLES

Chapter 5

5.1 Human diseases with the phenotype, *situs inversus* 145

5.2 Mouse mutants with the phenotype, *situs inversus* 146

5.3 Genes of interest 147

Appendices

A1.1 Source and version of the genome used in the analysis 207

A1.2 Accession numbers of the proteins included in the phylogenetic inferences 223

CHAPTER 1

Introduction

1.1 ASYMMETRY

Symmetry in biology is the balanced distribution of duplicate body parts or shapes on either side of a plane of symmetry. Most multicellular organisms have body plans that exhibit an element of symmetry; either radial or bilateral symmetry. Radial symmetry is when an organism has multi planes of symmetry that produce almost identical repeated sections (Fig. 1.1A). This type of symmetry is most common in sessile animals such as sea anemones, floating jellyfish and slow moving organisms like star fish. Radial symmetry is also present in plants which often display this type of symmetry in the distribution of flower petals. Bilateral symmetry refers to organisms which have a single plane of symmetry with each side a mirror image of the other (Fig. 1.1A). Animals which display this type of symmetry at some point in their development belong to the group Bilateria. Particular organisms, such as the sponges, do not display any form of body symmetry and are termed, asymmetric.

Asymmetry is the absence or violation of symmetry and occurs throughout development even if the resulting or overall organism is classified as bilaterally or radially symmetrical. During development molecular assemblies, subcellular structures, cell types and tissue architecture are all distributed asymmetrically in order to develop highly complex organisms. For example, asymmetry at a subcellular level is required for cell division, cell fusion and axon

specification through the establishment of persistent polarity of growth to generate the distinct cell shapes (Li and Bowerman 2010). In early amphibian and avian development the egg divides asymmetrically to form a blastodisc at the animal pole and the yolk resides at the larger vegetal pole. Many organisms have asymmetric positioning of organs which differentiates the left side of the organism from the right which is known as the left-right axis.

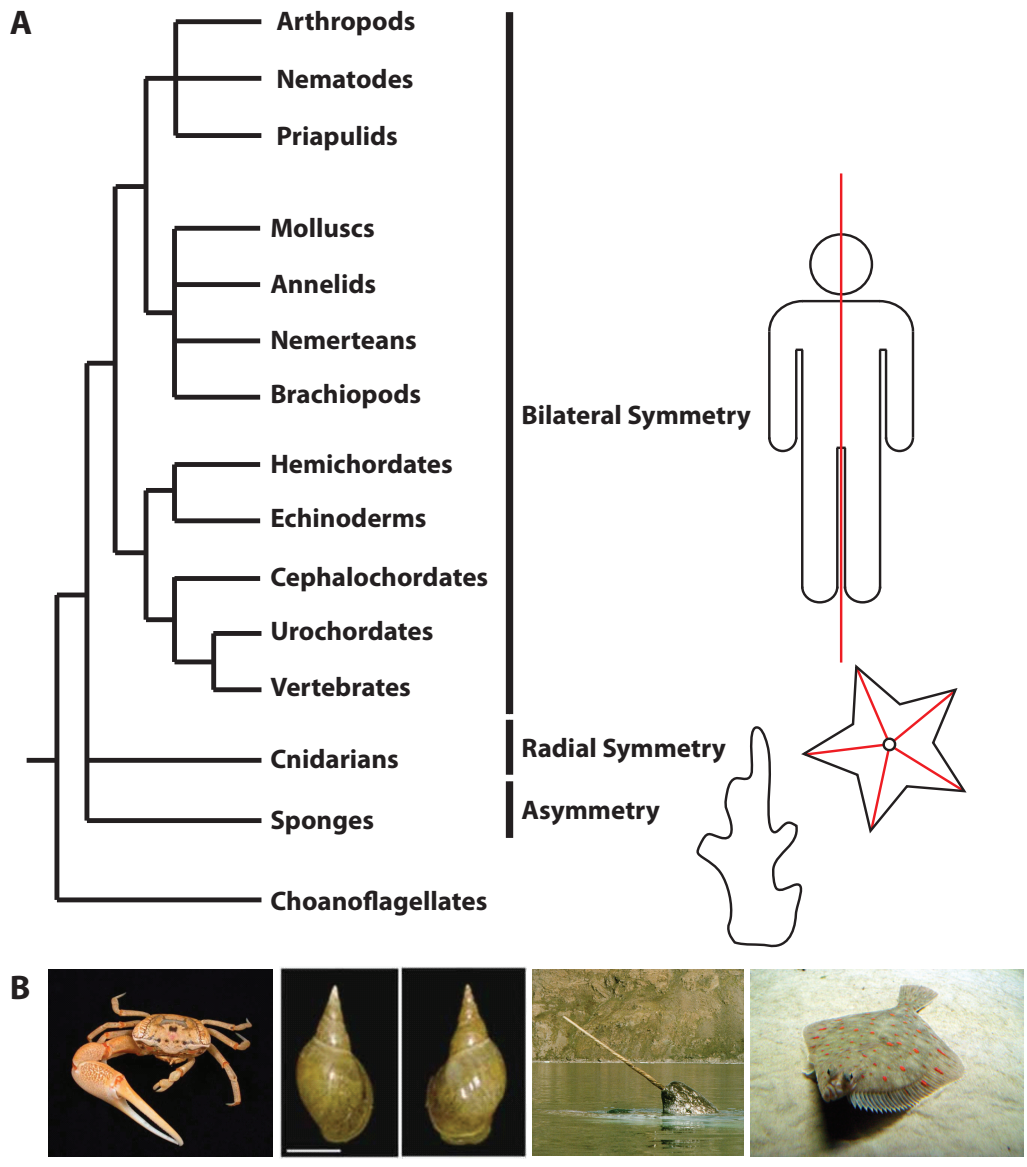


Figure 1.1: Types of symmetry in the Metazoa

A: Bilateral and Radial symmetry in the Bilaterians and Cnidarians and asymmetry in the sponges. Red lines indicate the plane(s) of symmetry. **B**: Examples of asymmetry in the bilaterians; male fiddler crab, sinstral and dextral shell coiling in snails, incisors in narwhals and the flatfish body plan.

1.1.1 Asymmetry in nature

The dramatic asymmetry of the claws of the male fiddler crab and the anteriorly directed incisors of narwhals are examples of asymmetry on otherwise predominantly symmetrical organisms. However, there are also other more subtle cases of asymmetry such as the twisted abdomen of many male insects and asymmetry of the whole body plan in flatfishes and coiled shells of snails (Fig. 1.1B). The varieties of asymmetry can be segregated into three main groups; fluctuating asymmetries, antisymmetry and directional asymmetry. Fluctuating asymmetries are not inherited and are the deviation from perfect bilateral symmetry due to environmental stressors, developmental instability and genetic problems during development. The other two groups are both heritable asymmetries with antisymmetry encompassing species in which individuals have a 50% chance of displaying one sided asymmetry and of 50% displaying the mirror image. Directional asymmetry is a fixed asymmetry observed in all the members of the population and is consistent with regulation of developmental processes on either side of the midline (Boorman & Shimeld 2002b). In all the examples of asymmetry, at some point symmetry is broken which requires a particular switch to begin the break in symmetry. Although there are many types and forms of asymmetry in the development of organisms, throughout this thesis the term asymmetry will only refer to the asymmetric left-right axis.

1.1.2 Vertebrate asymmetry

Asymmetry is found throughout nature in many different species and relies on a switch which causes the mediolateral on one side to differ from the axis on the other. Externally, humans

look symmetrical but internally, the organ arrangement is asymmetric with the heart and spleen on the left-hand side and the gall bladder on the right-hand side. The left-right axis is the third axis established after the anterior-posterior (AP) and dorsal-ventral (DV) axes. The first morphological asymmetry in the vertebrate body plan is when the somites emerge and the embryo begins to turn along the AP axis. Molecular asymmetries occur early in development and subsequent organ morphologies display left-right asymmetry such as heart tube looping (Kaufman 1992). Although molecular and morphological asymmetries are well understood, the mechanisms which create these asymmetries are less well known. Over the years it has become clear that cilia have a crucial role in the development of vertebrate left-right asymmetry.

1.1.3 The general model of asymmetry

The first model proposed to explain asymmetry was a model for handedness which contains three components; conversion, random generation of asymmetry and tissue specific interpretation processes (Brown & Wolpert 1990). The first component, conversion, proposed that molecular handedness is converted into handedness at the cellular level in some form. This then generates a reaction diffusion process caused by a higher concentration of a particular molecule on one side then the other. Finally, the tissue of the organism responds to the difference between the two sides which results in the development of particular structures on the left and the right. This model has provided the foundation for many experiments to try and elucidate the molecules and interactions involved.

1.2 ASYMMETRY IN VERTEBRATES

1.2.1 Asymmetric expression of genes

Approximately 16 years ago biologists found certain genes were expressed asymmetrically prior to morphological asymmetries, such as the heart looping. The first identified asymmetric genes involved in left-right asymmetry are *sonic hedgehog* (*shh*), *activin receptor IIa* (*cAct-RIIa*) and chick *nodal related 1* (*cNR-1*) which are all expressed at the left-side of the Henson's node and lateral plate (Levin et al. 1995). This was later followed by the discovery of left-sided *nodal* (Collignon et al. 1996; Lowe et al. 1996), *lefty* (Meno et al. 1996) and *pitx2* (Ryan et al. 1998) expression on the mouse ventral node and lateral plate mesoderm (LPM). Nodal, a secretory protein that belongs to the Transforming Growth Factor-beta (TGF-β) family, acts as a left-sided determinant and is regulated by the nodal antagonists, *lefty-1* and *lefty-2*, both also TGF-β family members. *Lefty-1* prevents bleeding of *nodal* signal to the right side of the node at the midline and *lefty-2* inhibits overexpression of *nodal* on the left-side of the node. Additionally, expression of *pitx2*, a paired homeobox transcription factor, is activated by *nodal* on the left-side of the node (Levin & Palmer 2007). The left-sided *nodal* expression is later transferred from the node to the LPM which is essential for downstream morphological asymmetries (Brennan et al. 2002; Kawasumi et al. 2011).

1.2.2 Human laterality diseases

Like many vertebrates, humans display internal asymmetries with organs positioned on different sides of the body. The failure to establish correct organ positioning results in

heterotaxy, which can assume several forms, including the complete reversal of organs or individual organ misplacement (see reviews Kosaki & Casey 1998; Belmont et al. 2004). The human disease, Primary Ciliary Dyskinesia (PCD), also known as immotile cilia syndrome, is characterised by defects in respiratory cilia, sperm motility and, in 50% of cases, *situs inversus* (Afzelius et al. 1976; Noone et al. 1999). *Situs inversus*, present in ~1 in 20,000 births, is the complete mirror-image reversal of internal organs and is the most common laterality defect in humans (Narayan et al. 1994). Other forms of left-right asymmetry defects such as isomerism, single organ inversions, or heterotaxia occur in fewer births because they have a higher chance of embryonic lethality (Kosaki & Casey 1998). This *situs inversus* subset of PCD is known as Kartagener's syndrome, an inherited autosomal recessive syndrome (Kartagener & Stucki 1962). Transmission Electron Microscopy of the cilia in numerous organs of sufferers, including the trachea, showed that they lack the dynein arms required for ciliary beating (Afzelius 1976). Ciliary defects as well as disruption to *situs* in this human ciliary disease first implied that embryonic cilia could function in correct positioning of organs within the body.

1.3 LEFT-RIGHT ASYMMETRY IN MOUSE

1.3.1 Mouse ventral node

Early mouse embryos have a cylindrical structure whose inside is the dorsal side and is lined with epiblast, and outside is the ventral side, which is covered in hypoblast. Scanning Electron Microscopy (SEM) of gestational 7-9 days post coitum (d.p.c) mice showed the presence of cilia on the mouse ventral node with one cilium projection per cell (Sulik et al. 1994). The ventral node in mouse embryos is homologous to the Spemann's organiser in *Xenopus* (Spemann &

Mangold 1924; Blum et al. 1992; Beddington 1994) which determines tissue specification in very early development (Spemann & Mangold 1924). A homologous structure is present in both the avian (Waddington 1932) and zebrafish (Kupffer 1896; Shih & Fraser 1996) embryo called the Henson's node and the Kupffer's Vesicle (KV), respectively. The ventral node is positioned at the most posterior part of the notochordal plate which is a primordium of the notochord (Kinder et al. 2001). The node is a concave triangular region transiently formed during gastrulation at the ventral midline and is 50-100 μm in width and 10-20 μm in depth (Sulik et al. 1994).

1.3.2 Ventral node cells

SEM analysis of the mouse ventral node demonstrated that cells of the notochordal plate differ from other cells of the embryo because of the presence of a single cilium on each cell. Initially these cells are covered by a squamous endoderm layer (Lee & Anderson 2008), which is hypothesised to be removed through either cell death or movement. Additionally, these ventral node cells differ from the surrounding mesodermal cells by their small ventral surface area at the apex of the developing embryo. The cilia are ~5 μm in length and 0.3 μm in diameter (Hirokawa et al. 2009) but further experimentation was required to determine if these cilia were linked with human immotile cilia disease and the establishment of left-right asymmetry which will be discussed in 1.3.5.

1.3.3 Cilia

Cilia and flagella are membrane-bound microtubule containing projections which emanate from the cell surface. They are derived from the centriole of each cell and motile cilia are reabsorbed at the initiation of the cell cycle and assembled once the cell has exited the cell cycle into a stationary or differentiated state (Quarmby & Parker 2005). Cilia and flagella are structurally and functionally identical but are termed differently due to their independent discovery in different species and unless stated in this thesis the research in cilia is also applicable to flagella and vice versa. The inner core of a cilium consists of a microtubule-based cytoskeleton known as an axoneme which provides strength and, in some cases, motility for cilia. Microtubules are polymers of α- and β-tubulin dimers with a diameter of 25 nm and have important roles in cell structure, mitosis, cytokinesis and vesicular transport. Cilia are assembled through the movement of Intraflagellar Transport Proteins (IFTs) along the axoneme from the cell body to the assembling tip (Kozminski et al. 1993) (a review of IFT: Rosenbaum & Witman 2002). IFT particles are transported towards the tip by the molecular motor, cytoplasmic kinesin-2, and back towards the base by another molecular motor, dynein-2 (Rosenbaum & Witman 2002). Proteomics have shown that this method of ciliary transport is an ancient trait and is found in most types of organisms and cilia (Fliegauf & Omran 2006).

1.3.3.1 Motile cilia

Generally, cilia are separated into two groups; motile and immotile, which have different structures. Motile cilia have a 9+2 structure in which the nine doublet microtubules surround a central pair whereas immotile cilia do not possess a central pair (Fig. 1.2) (Porter 1957; Satir

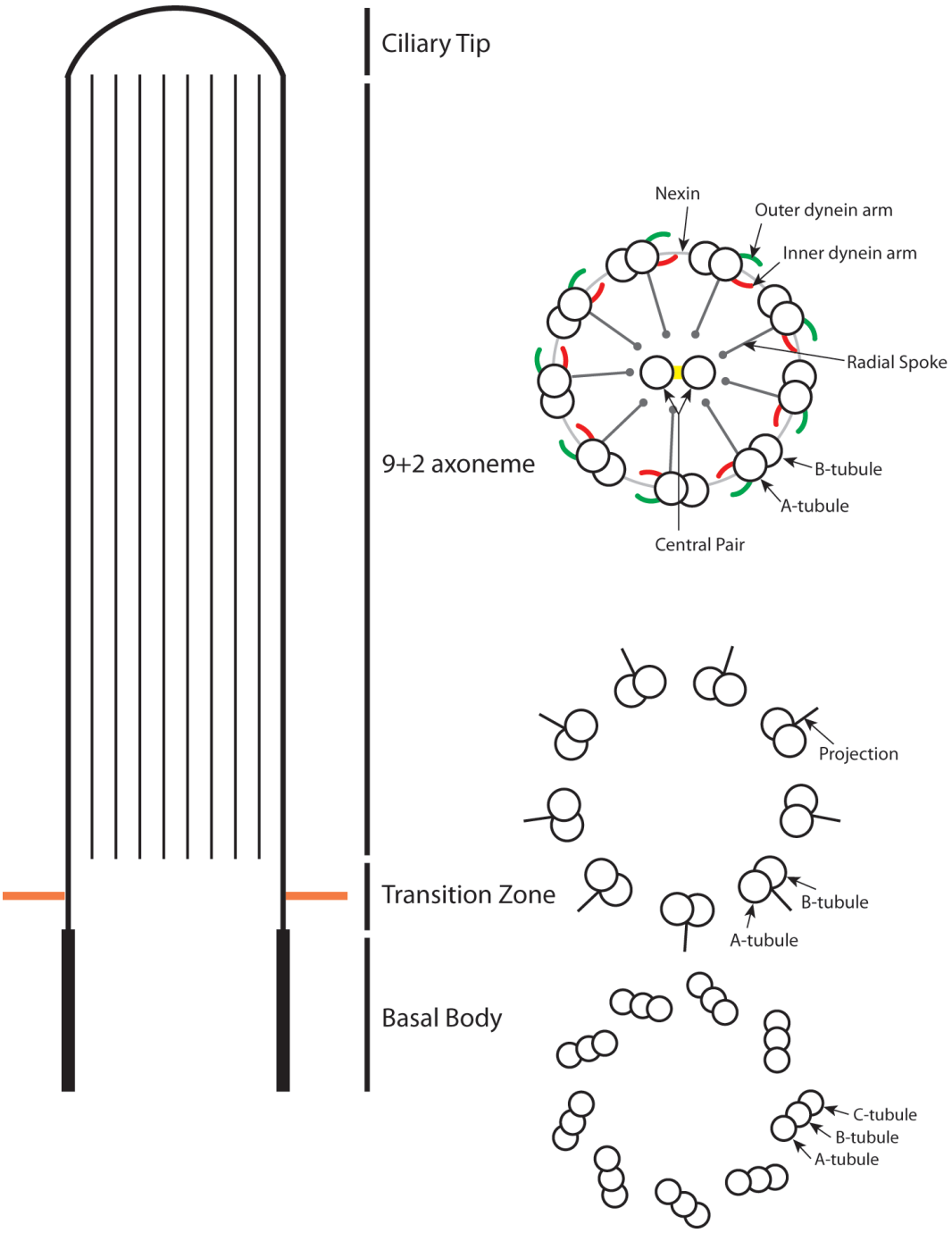


Figure 1.2: A typical 9+2 motile cilium from the basal body to the ciliary tip.

2005). Additionally, motile cilia have other structures to generate motility, such as dynein arms and radial spokes. Motile cilia are usually found in large numbers to co-ordinate wave-like motions that move particles and fluids across cell surfaces, for example removing mucus and dirt from the trachea. Motile cilia can beat at a maximum of 100Hz, although mammalian cilia

beat at a much lower frequency of 10-20 Hz (Satir & Christensen 2007). There are two types of strokes to generate movement; the effective stroke and the recovery stroke. The effective stroke is vertical and extends into the mucus whereas the recovery stroke is a horizontal action through the relatively stationary fluid layer beneath the mucus (Fig. 1.3A) (Boucher 2004). Cilia are decorated with other structures and molecules such as dynein motor proteins which hydrolysis of ATP causes to walk towards the base of the neighbouring doublet which

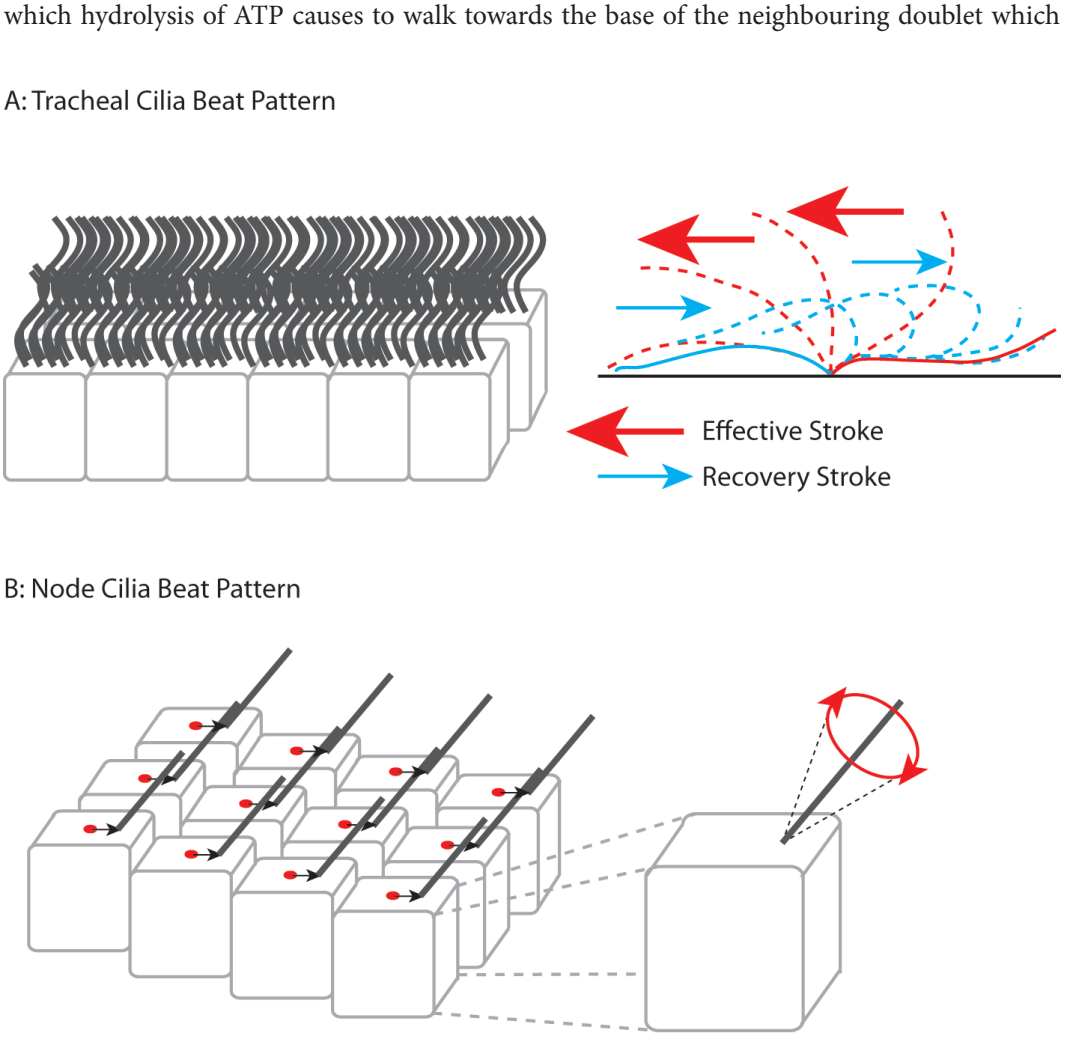


Figure 1.3: The ciliary beat pattern in motile cilia of the trachea and the monocilia of the mouse ventral node

A: The ciliary beat of the trachea cilia can be separated into two types of stroke; the powerful effective stroke, which generates the force and the recovery stroke, which is a horizontal stroke beneath the mucus layer.
B: The monocilia of the mouse ventral node project from the posterior of each cell at a 40°±10° angle which enables the cilia to generate a leftward flow across the node through vortical rotation. Cilia project from the centre of each cell (red dot) when they first emerge and then move to the posterior.

generates a sliding motion (Numata et al. 2008). Experiments in *Chlamydomonas reinhardtii* have shown that the outer dynein arm plays a major role in generating cilia beat frequency and inner dynein arms influence the beat waveform (van's Gravesande & Omran 2005). Inner dynein arms (IDAs) and outer dynein arms (ODAs) are often mutated in diseases where cilia are unable to beat such as in 60% of patients with PCD (Noone et al. 2007).

1.3.3.2 Primary cilia

Immotile cilia, also known as primary cilia, are found on the surface of virtually all the cells of the mammalian body and have a nine doublet microtubule structure axoneme. However, they lack the central pair and accessories, such as dynein arms and radial spokes, which promote motility. The lack of motility associated structures suggests that they are unnecessary for their role which has led to the assumption that they function as chemosensors and mechanosensors (Wheatley 2005). A role for primary cilia as mechanosensors was demonstrated by mechanically bending the cilia in the mammalian kidney cells. This bending of the cilium caused an increase in intracellular Ca^{2+} which demonstrated that they act as mechanosensors which dose the cell with periodic increases in Ca^{2+} (Praetorius & Spring 2001).

1.3.4 Mouse mutants with laterality defects

Two famous mouse mutants are characterised by perturbation to normal left-right asymmetry: (1) *Situs inversus viscerum* (*iv*) where individuals either develop normally or are mirror-image reversed (Layton 1976; Singh et al. 1991; Lowe et al. 1996) and (2) *inversion of embryonic turning* (*inv*) where all individuals exhibit *situs inversus* (Yokoyama et al. 1993). Normal left-

sided expression of *nodal* at the mouse node was not observed in either mouse mutant. *iv* mice may have left-sided, right-sided or bilateral *nodal* expression which suggests the 50% incidence of *situs inversus* is due to this randomised *nodal* expression (Lowe et al. 1996). In contrast, *inv* mice which display a 100% incidence of *situs inversus* all have right-sided *nodal* expression (Lowe et al. 1996).

Another mouse mutant, *legless* (*lgl*), also displayed left-right asymmetry defects in addition to limb, brain, and craniofacial malformations (Singh et al. 1991). 50% of *lgl* mice display *situs inversus*, an identical phenotype to *iv* mutants, which suggests that a similar mechanism and gene are involved (Schreiner et al. 1993). The *iv* and *lgl* mouse mutants are a result of a point mutation in the left-right dynein (*lrd*) gene which alters the encoding of an outer arm axonemal dynein expressed in cells of the mouse node (Supp et al. 1997). The *lrd* gene, also known as *DNAH11*, is a dynein axonemal heavy chain protein that acts as a molecular motor at the cilia axoneme and is required for motility. *Lrd* is expressed throughout the node at embryonic day 7.5 but by embryonic day 8.0 becomes restricted to the left of the node (Supp et al. 1997). The *inv* mouse was generated through a recessive insertional mutation within the *inversin* gene which removes a coding sequence of 1000 amino acids (Yokoyama et al. 1993; Morgan et al. 1998; Mochizuki et al. 1998). The *inversin* gene encodes an intracellular protein with ankyrin repeats in the C-terminal domain (Morgan et al. 1998). The mouse mutations further enhanced the debate that cilia observed on the mouse ventral node are important in the establishment of left-right asymmetry. The mutation in the *DNAH11* gene in both the *iv* and *lgl* mice also implied that the motility of these cilia was also important.

1.3.5 The generation of a leftward flow by node cilia

Cilia were observed on the mouse ventral node at 7.0 d.p.c but there was debate as to whether they were motile. The presence of *lrd* mRNA in cells that do not possess motile cilia (Supp et al. 1997) led many to believe that the cilia were immotile, although videomicroscopy of the node region showed fluid disturbance suggesting the cilia are in fact motile (Bellomo et al. 1996). A kinesin motor protein, KIF3B, was disrupted by gene targeting in mice to assess the presence of cilia at the node and the *situs* of the organism (Nonaka et al. 1998). KIFs move various types of cargo over long distances along microtubules in many kinds of cells. The kinesin-2 anterograde motor protein family member, KIF3B, forms a heterodimer with KIF3A and an associated protein KAP3 and is essential for ciliogenesis as a motor protein to transport complexes to the minus end of microtubules (Goldstein 1993; Yamazaki et al. 1995; Yamazaki et al. 1996). The KIF3B deficient mice exhibited randomised left-right asymmetry and bilateral or absent *lefty-2* expression (Nonaka et al. 1998). For the first time a direct link between the node cilia and left-right asymmetry was shown as KIF3B deficient mutants had absent node cilia and left-right defects (Nonaka et al. 1998).

The experiments in the KIF3B$^{-/-}$ mutants showed that cilia at the mouse ventral node are essential for the development of left-right asymmetry and also demonstrated that they are motile. Videomicroscopy of the mouse node showed that cilia were motile and beating in a vortical fashion. The addition of fluorescent latex beads enabled the leftward flow across the node generated by these cilia to be observed for the first time (Nonaka et al. 1998). This leftward flow is required from somite stage 1 to 6, which is 7 days into development (Shiratori & Hamada 2006) and is named nodal flow. The reversal of this flow, assessed through analysis

of asymmetrically expressed genes, caused the reversal of left-right asymmetry in mice (Nonaka et al. 2002). Videomicroscopy of the other mouse mutants has shown the effect that the different gene mutations have on nodal flow and how disruption to the nodal flow has led to randomised or reversal of left-right asymmetry. In the *iv* and *lgl* mice, the ventral node cilia are paralysed due to the mutation in the outer dynein arm protein, DNAH11 so that only Brownian movement is observed. In the *inv* mouse the cilia are still motile but the flow is disorganised and turbulent (Okada et al. 1999). It is hypothesised that the disruption to nodal flow fails to generate a signal which can be read by a particular population of cells on the left of the ventral node. Therefore, downstream left-right asymmetry effectors, such as *nodal* are not restricted to the left-side of the node but instead signals are read all over the node which creates symmetrical *nodal* expression.

1.3.6 The posterior positioning of nodal cilia on cells of the mouse node

Cilia in the node protrude from a cell at a posterior tilt to enable the vortical rotation to generate a leftward flow (Fig. 1.3B) (Nonaka et al. 2005; Okada et al. 2005). Videomicroscopy showed that nodal cilia trajectories are elliptical and therefore appear to be posteriorly tilted (Nonaka et al. 2005). Measurements from SEMs of the nodal cilia found that cilia are positioned at a tilt of between 15° and 35° towards the posterior of the node. Immunofluorescence confirmed that cilia emanate from the posterior of ventral node cells (Nonaka et al. 2005; Okada et al. 2005). Basal bodies of nodal cilia are positioned centrally on each cell and then gradually migrate to the posterior (Hashimoto et al. 2010). The removal of a gene, *Bicaudal C* (*BicC*), affects the

positioning of cilia in the mouse ventral node and as a result disrupts nodal flow and left-right asymmetry (Maisonneuve et al. 2009). *BicC* can uncouple *dishevelled-2* (*dsh-2*) signalling from the canonical Wingless (Wnt) pathway, which has been previously implicated in planar cell polarity (PCP) and the positioning of cilia (Hashimoto et al. 2010). In *dsh* mouse mutants the posterior positioning is disrupted and nodal flow impaired while inhibition of *Rac1*, a member of the Rho family of GTPases and a component of the non-canonical Wnt signalling pathway which regulates actin assembly and organisation, affected cilia posterior positioning. *Dvl2* and *3* are localised to the apical surface of the nodal cells and are polarised to the posterior of cells. It has been hypothesised that the posterior positioning of basal bodies creates the posterior tilt of cilia which is determined by planar polarisation mediated by non-canonical Wnt signalling (Hashimoto et al. 2010).

1.3.7 Nodal cilia movement

Node cilia beat at a rapid speed of ~600rpm which generates both a fast (20-50 μm/s) and a smooth leftward flow of the extraembryonic fluid in the ~5 μm above the node surface (Okada et al. 1999; Hirokawa et al. 2006). The flow moves upwards along the left side-wall and a slower rightward counterflow returns ~20 μm above the surface of the node (Okada et al. 2005). Unlike tracheal cilia, which normally beat in a back and forth motion perpendicular to the cell the nodal cilia rotate at a tilt of 40°±10° to the posterior from a vertical angle (Hirokawa et al. 2006). The tilt causes cilia to make a leftward swing away from the surface and a rightward sweep near the surface. The laws of hydrodynamics determine that a stationary surface, in this case the cell, prevents the movement of fluids by shear resistance which itself has been shown

to be essential for the generation of leftward flow (Buceta et al. 2005). As a result the leftward sweep is far more effective than the rightward sweep at generating fluid movement. Due to this distinction between the two strokes, the leftward sweep is called the effective stroke and the rightward sweep, the recovery stroke (Fig. 1.3) (Okada et al. 2005).

1.3.8 Nodal cilia structure

Motile cilia have a conserved 9+2 structure (discussed earlier in the Chapter) which is required to generate the forces necessary for cilia to beat. Inner and outer dynein arms have been observed through TEM on the nine doublet microtubules of node cilia and an outer dynein arm antibody, AD2 (Yoshida et al. 1989) localised to the monocilia of the mouse node (Takeda et al. 1999). However, the mouse node cilia do not have a central pair previously believed to be necessary for cilia motility. The central pair is required for cilia to beat in a back and forth motion but could restrict the rotational movement observed in the mouse node and has therefore, been lost. The 9+0 with dynein arms structure of node cilia has only been documented before in *Thalassiosira pseudonana* (Merchant et al. 2007; Wickstead & Gull 2007) but this structure in nodal cilia could be a result of, or result in, the unique rotational movement of cilia at the mouse node.

1.4 HOW IS THE LEFTWARD NODAL FLOW TRANSLATED TO MOLECULAR ASYMMETRIES?

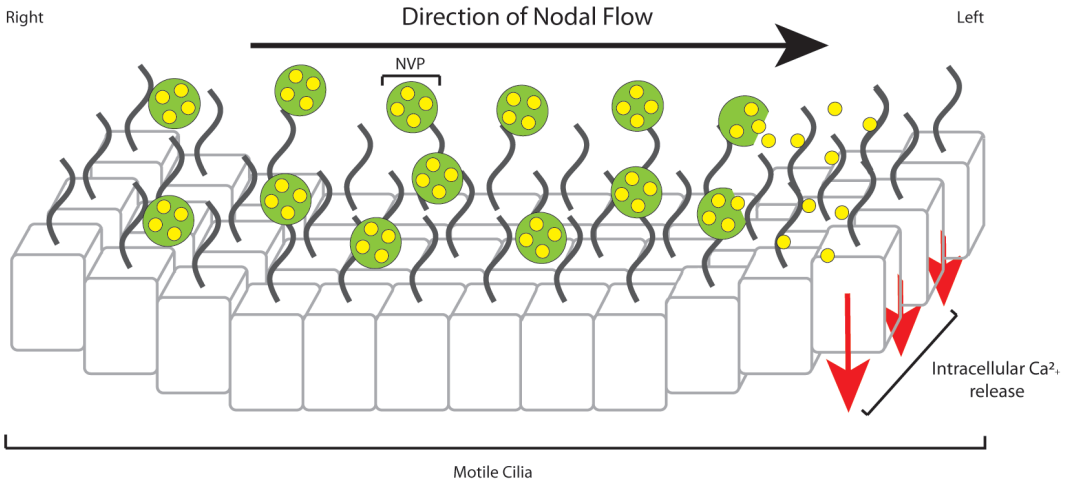
While a role for cilia in the development of left-right asymmetry is now generally accepted, the

precise mechanism whereby ciliary beating sets up the left-right axis remains controversial. The two main hypotheses used to explain this expression are the chemical hypothesis and the physical hypothesis (Fig. 1.4). The chemical hypothesis is based on the idea that a morphogen is transported to the left of the node by the nodal cilia which will produce a concentration gradient in the cavity of the ventral node (Nonaka et al. 1998; Okada et al. 2005). On the other hand, the physical hypothesis assumes that the leftward flow is mechanically detected by immotile cilia on the periphery of the ventral node (McGrath et al. 2003). Both methods have tried to resolve the issues proposed by mouse mutant models that have right sided, left-sided and bilateral molecular asymmetries when nodal flow is removed or disrupted.

1.4.1 The Chemical Hypothesis

The chemical hypothesis was first proposed by Nonaka et al. (1998), and later by Okada et al. (2005), who both suggest that leftward flow could lead to the accumulation of a morphogen on the left-hand side of the node, which in turn generates a concentration gradient across the node. This model suggests that cilia on the left are informed that they are left-sided cilia by sensing a currently unknown morphogen. FGF8 and Nodal are both candidates for the unknown morphogen because proteins the right size for both candidates, 20-40kDa, generated a stationary concentration gradient across the node (Okada et al. 2005). Further analysis has suggested that a morphogen could be transported across the node in particles. Small (0.3-5 μm) particles were detected by fluorescent lipophilic dye being transported to, and accumulating on, the left by nodal flow (Tanaka et al. 2005). These particles have been termed nodal vesicular parcels (NVPs) but very little is known about them and how they work. One

A: Chemical Hypothesis



B: Physical Hypothesis

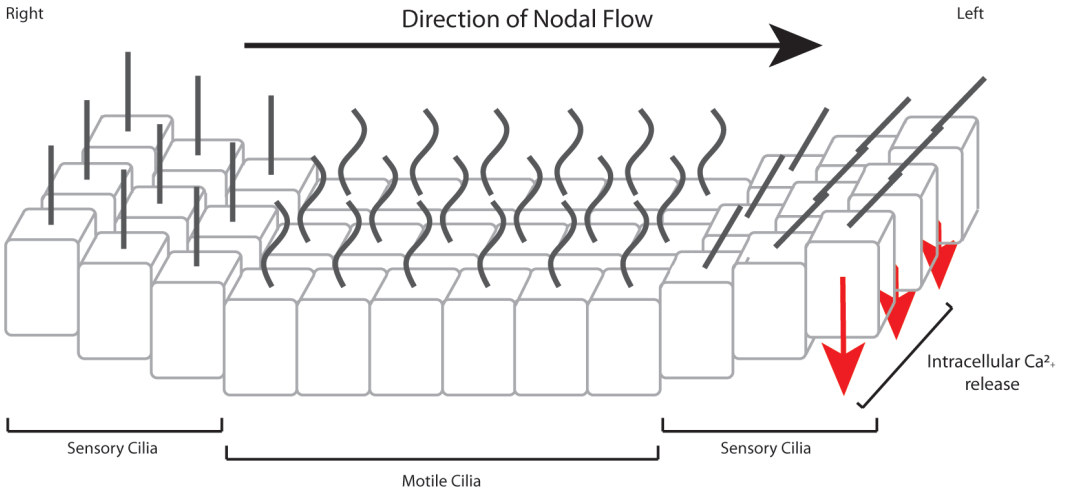


Figure 1.4: The current two models for the establishment of left-right asymmetry in the mouse model

A: The Chemical Hypothesis suggests that nodal vesicular parcels (NVPs) are released from the right-hand side of the node and are transported across the node by the nodal flow generated by motile cilia. At the left-hand side of the node, cilia burst the NVPs and they release their contents which are detected by trans-membrane receptors on the cilia. The receptos trigger an intracellular calcium release which results in left-sided nodal expression. **B**: The Physical Hypothesis contrasts with the previous hypothesis because it suggests that there are two populations of cilia on the mouse ventral node. It predicts that motile cilia in the centre of the node generate a leftward flow which bends the sensory cilia at the periphery of the node which in turn triggers an intracellular calcium release.

model suggests that NVPs leave the cell from a rod like structure, are transported to the left of the node above the rotating cilia and burst when they hit a cilium. The burst NVPs are absorbed by the surface of nodal crown cells but the contents of the Nodal vesicular parcels remain unidentified. Pharmacological experiments, with an inhibitor of FGFR, suppress NVP release and Ca^{2+} elevation observed at the left of the node (Fig. 1.4A). Retinoic acid (RA) or sonic hedgehog (shh) rescue both NVP release and Ca^{2+} elevation to maintain the left-sided dominance (Hirokawa et al. 2006) which suggests that they control the release of NVPs.

1.4.2 The Physical Hypothesis

Brueckner (2001) proposed an alternative hypothesis called the 'two-cilia hypothesis' which states that two populations of cilia exist in the node. The hypothesis was constructed due to problems with the simplistic chemical hypothesis in relation to the mouse mutants discussed earlier. *iv* mouse mutants, that are due to a mutation in the *lrd* gene normally required for cilia motility, show numerous different asymmetric gene expressions including left-sided/ right-sided/bilateral and no *nodal* expression. *Kif3A* and *Kif3B* mutants are devoid of all cilia at the mouse ventral node and result in bilateral or no asymmetric gene expression. The simple morphogen hypothesis would suggest the two mouse mutants should have the same downstream effect on *nodal* expression but do not. The lack of cilia and the inability of cilia to generate a leftward flow would both prevent the accumulation of a morphogen at the left-side of the node and therefore the signal would be expected to be lost or randomised in both conditions.

To overcome this difference the physical hypothesis was proposed which relies on the

presence of two populations of cilia in the mouse ventral node. One of these populations generates a leftward flow, as described above, and the other senses the flow (Fig. 1.4B). SEM and GFP-tagged left-right dynein (lrd) fusion protein studies show there is a distinct arrangement of cilia within the node. The experiments concluded *lrd*-containing motile monocilia were centrally located and non-*lrd* containing node monocilia located peripherally (McGrath et al. 2003). This suggests that cilia in the centre are motile and those on the periphery are mechanosensors. The mechanosensors may transmit the signal generated by motile cilia through intracellular signalling. The presence of cilia in the *iv* mouse mutant would mean that although they were not capable of generating a leftward flow they could still function as mechanosensors. *Kif3A* and *Kif3B* lacked all cilia so had neither motile cilia nor the mechanosensory cilia. The difference in the asymmetric *nodal* expression in the two mouse mutant models could be explained.

1.4.3 Cilia as mechanosensors

The physical hypothesis has proposed that immotile cilia at the mouse node detect the fluid flow generated by centrally located motile cilia. The hypothesis suggests that immotile cilia at the periphery of the node are forcibly bent by the leftward flow which results in elevated Ca^{2+} signal through PKD2 (McGrath et al. 2003). Primary cilia are known to function as photoreceptors, chemosensors and mechanosensors (Pazour & Whitman 2003) with a significant role as sensory organelles. It has been observed that there is an elevation in Ca^{2+} levels at the left periphery of the node which is reliant on node monocilia that contain polycystin-cation channels (McGrath et al. 2003). The lack of elevated levels of Ca^{2+} results in

a lack of *nodal* and *lefty-2* expression in the LPM and randomisation of left-right asymmetry (McGrath et al. 2003; Pennekamp et al. 2002).

PKD1 and *PKD2* are two of the genes that, when mutated, cause Polycystic Kidney Disease (Torres & Harris 2006) and encode the proteins, polycystin-1, a large membrane protein that could act as a receptor (Woolf et al. 1995), and polycystin-2, a calcium selective cation channel. Polcystin-1 and -2 interact to produce new calcium permeable non-selective cation currents which they are unable to generate on their own (Hanaoka et al. 2000). Mutations in *PKD1* (16p13.3) account for ~90% of adult PKD cases whereas mutations in *PKD2* (4q21-23) account for ~10% of affected families. PKD1 contains a large structurally robust extracellular domain which potentially acts as a flow sensor and PKD2 has been characterised as a six transmembrane spanning protein of the voltage activated calcium family with an intracellular amino- and carboxyl-terminal (Mochizuki et al. 1996; Koulen et al. 2002). A *Pkd1*-related locus (*Pkd1|1*) mouse mutant displays left-right asymmetry defects as well as a failure to express asymmetric genes suggesting that the nodal signalling cascade is not initiated. Additionally, results have shown that Pkd1|1 is the binding partner of Pkd2 in left-right asymmetry determination and they co-localise to cilia (Field et al. 2011).

Physical manipulation of primary cilia, using a micropipette to force cilia to bend, was followed by an increase in intracellular calcium. Calcium levels were detected using Fluo-4 as an indicator (Praetorius & Spring 2001). After the sudden rise in calcium levels, IP_3 is released from sensitive stores, which sends a signal across neighbouring cells. Ca^{2+} elevation is a characteristic of left-right asymmetry at the node and the PKD2 proteins EF-hand domains are a specialised helix-loop-helix motif that has calcium binding activity (Mochizuki et al. 1996). In ~70% of proteins in which the domains occur there is evidence of a role in calcium

activity which suggests that *PKD2* has a role in intracellular signalling via calcium channels. All the evidence suggests that PKD2 could have a role on the mechanosensory cilia at the periphery of the mouse ventral node and is required to control the level of Ca^{2+} elevation.

These findings could go some way to explain how reversed nodal flow generates reversed left-right asymmetry (Nonaka et al. 2002). Reversed asymmetry through the generation of a reversed flow would not manifest unless a signal could be interpreted on the right as well as the left of the node. The prediction proposes a signalling cascade is initiated on the side of the embryo with the higher concentration of molecule X. Unless the right is a default pathway that is overcome by leftward flow, in normal circumstances some sort of receptor is required to initiate a cascade of asymmetric gene expression on the right. Could this be the role of primary cilia?

1.5 LEFT-RIGHT ASYMMETRY DETERMINATION IN OTHER VERTEBRATE SPECIES

Although the experiments discussed previously have been conducted in the mouse model where nodal cilia were first observed, not all the research in the development of left-right asymmetry was first conducted in this model. Simultaneously to mouse left-right asymmetry studies, research has been conducted in other vertebrate organisms to maximise the overall knowledge of the mechanisms which establish left-right asymmetry. Analysis of other vertebrate model systems has validated and in some cases added new light to the mechanisms involved. Research has focused on four frequently used models in developmental biology; the frog (*Xenopus*), fish (zebrafish – *Danio rerio*), rabbit (*Oryctolagus cuniculus*) and chick (*Gallus*

gallus). The similarities and differences between these species and the mouse model will be discussed in more detail in the next section. Frog and *Xenopus* are valuable in the analysis of the first stages of development because their eggs can be manipulated to enable insight into the very early mechanisms in the establishment of left-right asymmetry. Numerous characteristics of the mouse nodal flow are highly conserved in other model systems but there are also a few differences which could be a consequence of contrasting mechanisms in viviparous and oviparous organisms. The next section reviews the research in these mammalian and non-mammalian organisms, firstly focussing on the closely related organisms, the rabbit.

1.5.1 Rabbit

The rabbit is a prototype mammalian embryo, which is known to develop via a flat blastodisc rather than the cup-shaped egg cylinder embryo in mouse. Analysis of the rabbit embryogenesis provides a much closer model to human development in which to compare mechanisms such as left-right asymmetry. Experimentation has established the existence of a leftward fluid flow and cilia in rabbit development and has also provided some evidence of the position and structure of cilia in the node (Feistel & Blum 2006). SEM, TEM and immunofluorescence show cilia projected from cells on the notochordal plate and positioned to the posterior; a common and conserved finding in cilia involved in left-right asymmetry (Feistel & Blum 2006; Okada et al. 2005).

The cilia of the notochordal plate are motile and produce a rotational movement which generates a leftward flow, although the flow is slower than observed in the mouse ventral node. Cilia were not observed on the organiser region, termed the Hensen's node in rabbits, but

left-sided *nodal* expression demonstrated that the notochordal plate was in fact a homologous structure to the mouse ventral node (Okada et al. 2005). The addition of fluorescent beads demonstrated that the leftward flow accumulates 10kDa sized proteins at the left side of the notochordal plate for over 2 mins (Okada et al. 2005).

Several genes involved in ciliogenesis and left-right asymmetry were analysed in the rabbit embryo around the time of nodal cilia activity. As well as clarifying known mechanisms in a novel model system their research also discovered a previously unknown cilia structure in the node. Initial experiments showed that rabbit notochordal cilia do not have a central pair but are 9+0 in structure (Okada et al. 2005) but later experiments have shown that 9+2 and even 9+4 axoneme structures are interwoven with the 9+0 cilia (Feistel & Blum 2006). These results led to the conclusion that despite a highly conserved ciliogenic program, the axonemal structures may vary widely within vertebrates. A replication of this work in other model systems will determine if this is a characteristic restricted to rabbit or a more general phenomenon. The rabbit and mouse models provide an interesting insight into the conservation of nodal flow and the mammalian mechanisms involved in the development of left-right asymmetry. However, to establish the extent of conservation across the vertebrates other non-mammalian models have also been analysed including the fish, *Danio rerio*.

1.5.2 Zebrafish (*Danio rerio*)

A non-mammalian organism zebrafish, a tropical freshwater fish, is frequently used in developmental biology due to its ability to develop rapidly, develop outside the mother in transparent eggs and be mutants screened and propagated easily. It was also one of the first

model systems analysed to discover the extent of nodal flow conservation (Essner et al. 2002). *Nodal* (Rebagliati et al. 1998), *lefty* (Meno et al. 1999) and *pitx2* (Campione et al. 1999) asymmetric expression in the Kupffer's vesicle (KV) is conserved in zebrafish embryogenesis and is required for the normal development of left-right asymmetry. The Kupffer's vesicle, a homologous structure to the mouse ventral node, is a transient spherical organ conserved in all teleost fishes which is composed from a group of two-dozen cells called dorsal forerunner cells (DFCs) that migrate to the leading edge of the embryonic shield. A homologue of the gene *lrd*, a dynein axonemal heavy chain protein expressed in the mouse ventral node, was identified in zebrafish and localised at the end of gastrulation in the dorsal forerunner cells that migrate ahead of the organiser region. These forerunner cells give rise to the Kupffer's vesicle which also contains monocilia (Essner et al. 2002) which suggests that the presence of nodal cilia is a conserved mechanism. Later on in development after gastrulation, the KV is found ventral to the notochord in the tailbud next to the yolk cell.

The monocilia on the cells of the KV generate a directional leftward flow across the KV prior to the onset of molecular asymmetries (Essner et al. 2002; Okada et al. 2005). Disruption of these cells through ablated DFCs and morpholinos against *lrd*, led to defects in left-right asymmetry in the brain, heart and gut and randomised left-right asymmetry of asymmetric gene expression (Essner et al. 2005). *lrdr1* is controlled by upstream regulators such as *no tail*, a T-box transcription factor, and *nodal* signalling (Essner et al. 2005). Small fluorescent beads were injected into the lumen of KV of 8-10 somite embryos which when videoed showed counter-clockwise movement (Kramer-Zucker et al. 2005). Analysis of mutant zebrafish embryos demonstrated small alterations to cilia and IFT in the KV and results in an obliteration of fluid movement. The lack of *lrd* expression led to paralysed monocilia and a

lack of directional flow identical to results in the mouse ventral node (Essner et al. 2005). An absence of *pitx2* and the near-complete absence of *southpaw* expression in *hippi*SP-injected embryos showed the loss of asymmetry in mutant zebrafish (Kramer-Zucker et al. 2005). It could be concluded that the results demonstrated that fluid flow is a conserved feature of gastrulation-stage midline structures which regulate left-right asymmetry (Kramer-Zucker et al. 2005). These results were profound because they showed for the first time that ciliated cells functioned in the development of left-right asymmetry in a non-murine embryo.

Mouse ventral node cilia are positioned posteriorly in the cell at a 40° ± 10° tilt which is also apparent through electron microscopy in zebrafish (Kramer-Zucker et al. 2005). The cilia are tilted to the posterior at approximately 45° relative to the surface of the roof in the KV. Vangl2, a core and specific component of the PCP pathway, controls the posterior positioning of cilia in the KV (Borovina et al. 2010). The cilia of the medaka KV do not have a central pair, consistent with mouse ventral node cilia (Okada et al. 2005), but are still capable of movement whereas the zebrafish KV cilia do have a central pair (Kramer-Zucker et al. 2005). They also observed that the cell membrane and cytoplasm adjacent to the cilium insertion appeared to be a site of active vesicle fusion. Overall, experiments suggest there is a similar mechanism involved in laterality determination in zebrafish as in mouse. However, a second system is also known to function in laterality determination in the zebrafish embryo.

H^+/K^+-ATPase channels work through the intracellular accumulation of K^+ ions in exchange for H^+ ions which is mediated by ATPases that convert energy from the ATP into an electrochemical K^+ gradient (Levin et al. 2002). The movement of ions generates a net negative membrane potential (Meneton et al. 1999). Treatment of zebrafish early stage embryos with Omeprazole, an inhibitor of H^+/K^+-ATPase, resulted in reversed heart looping and randomised

expression of *pitx2* and *southpaw*, a nodal related TGF-β family member (Kawakami et al. 2005). In particular, H^+/K^+-ATPase inhibitor treatment before the midblastula transition resulted in high numbers of left-right defects which indicate that H^+/K^+-ATPase relevant for left-right patterning is maternally transcribed. Additionally, it has been shown that H^+/K^+-ATPase acts upstream of Notch signalling which is required for normal nodal cilia length, left-sided *nodal* expression and normal left-right asymmetry (Kawakami et al. 2005; Raya et al. 2004; Lopes et al. 2010). H^+/K^+-ATPase is the first known step in the development of left-right asymmetry in zebrafish embryos and is prior to monocilia and the leftward flow. Zebrafish provide an interesting model in which to analyse these two mechanisms that each have an apparently independent role in setting up left-right asymmetry in vertebrates.

1.5.3 *Xenopus*

Xenopus laevis, an African Clawed Frog, is an amphibian model system commonly used in research due in part to its large oocytes which can be easily manipulated. Studies in this species have shown that the amphibian Gastrocoel Roof Plate (GRP), homologous to the mouse ventral node and zebrafish KV (Shook et al. 2004), has cilia which generate a leftward flow essential for left-sided *nodal* expression and downstream left-right asymmetry (Schweickert et al. 2007). Cilia are first observed at stage 14 where they are initially positioned at the centre of each GRP cell but by stage 18 they are positioned more to the posterior pole of each cell. Vangl2, a PCP protein, is also essential for posterior positioning of GRP *Xenopus* cilia (Antic et al. 2010). *Nodal* (Lustig et al. 1996), *lefty* (Cheng et al. 2000) and *pitx2* (Ryan et al. 1998) are all expressed asymmetrically in this structure during early X*enopus* development. Other

known genes expressed in cilia of the node in mice and zebrafish, *lrd*, *inversin* and *polycystin-2* are also localised to cilia in the GRP which suggests homology with the structures in these species (Schweickert et al. 2007).

Transverse sections through the GRP demonstrated the existence of a leftward fluid flow in *Xenopus* which itself is a characteristic of the mouse nodal flow. Cilia beat in a clockwise fashion at a speed of 20-25 Hz which is comparable to the zebrafish cilia but a much faster rate than known in mice and rabbit (Schweickert et al. 2007). Additionally, fluorescent beads moved across the GRP in a leftward direction as seen in both the mouse ventral node and zebrafish KV (Schweickert et al. 2007). It appears from all the experimentation in these different model systems that there is a conserved role for cilia in the development of the left-right axis.

However, molecular asymmetries in *Xenopus* also appear much earlier during development than mouse and other vertebrate asymmetries. This has raised the issue of a potential mechanism other than cilia which has the ability to determine laterality. During the very early stages of *Xenopus* embryogenesis maternal H^+/K^+-ATPase mRNA is symmetrically expressed but becomes asymmetrically distributed during the first two cell divisions (Levin et al. 2002). Embryos treated with the H^+/K^+-ATPase inhibitor Omeprazole displayed heart left-right asymmetry defects and bilateral or right sided *Nodal*, *Pitx2* and *lefty* expression (Levin et al. 2002). This asymmetric H^+/K^+-ATPase localisation is the first known step in left-right asymmetry determination in vertebrates and is prior to the presence of node cilia and nodal flow. Evidence has not shown that a similar method is present in mouse embryos and H^+/K^+-ATPase appears to be a feature of non-viviparous species. It is still not know what mechanism generates the asymmetric expression of H^+/K^+-ATPase mRNA which is likely to be one of the first initiation steps in left-right determination. It could be that left-right laterality

is established early by H^+/K^+-ATPase but that cilia and nodal flow enhance the signal later in development.

Serotonin, also known as 5-hydroxytryptamine (5-HT), is a monoamine neurotransmitter with crucial roles in physiology and cognition. In *Xenopus*, pharmacological screens were conducted to determine if serotonin signalling was involved in the establishment of left-right asymmetry (Fukumoto et al. 2005). The results implicated endogenous serotonin signalling through the receptors R3 and R4 and monoamine oxidase. *Xnr-1* normal left-sided expression was altered in embryos exposed to inhibitors of R3, R4 and monoamine oxidase. Maternal serotonin is observed in the *Xenopus* egg and early cleavage stages where it begins to degrade. Serotonin localisation in the plane perpendicular to the animal-vegetal axis during later cleavage stages is dependent on H^+/K^+-ATPase and gap junctions (Fukumoto et al. 2005). The data together demonstrate that serotonin is important for the establishment of left-right asymmetry in conjunction with H^+/K^+-ATPase and gap junctions.

1.5.4 Chick (*Gallus gallus*)

Most assumptions concerning left-right asymmetry involve the analysis of mouse mutants but studies in an avian model, the chick show different results. Research in the chick, *Gallus gallus*, has shown that the mechanisms involved in the establishment of left-right asymmetry differ in the avian model from the mammalian, amphibian and fish models. The first morphological sign of asymmetry appears in chick with the appearance of Kohler's sickle and then the primitive streak, after which there is clear right-sided looping of the heart tube. Evidence of left-right asymmetry in the chick embryo in the establishment of an early midline

barrier prevents cell mixing from the left and right (Kelly et al. 2002) and is required for *Nodal* and *shh* expression. *Nodal*, *pitx2* and *lefty* are all expressed asymmetrically in the chick mouse ventral node homologue, the Hensens's node (Levin et al. 1995). *Lefty* generates a later midline barrier as it suppresses *nodal* signalling on the right (Levin et al. 1995). Many of the genes expressed asymmetrically in the chick embryo are expressed symmetrically in mouse development and in chick embryos the sidedness of *nodal* is determined by *shh* (Levin et al. 1995). In addition to *shh*, asymmetric *nodal* expression is controlled by Wnt, Notch and PKA signalling (Raya et al. 2004; Kawakami & Nakanishi 2001; Rodriguez-Esteban et al. 2001) (A full list of asymmetrically expressed genes on the left and right side of Hensen's node in the chick embryo can be found in Schlueter & Brand (2007)).

Although cilia are present on the developing chick embryo and there are monociliated cells on the node (Essner et al. 2002), they are short, immotile and emanate from various regions of the embryo. The cilia are also present on the endodermal cells of the node and not the mesodermal cells seen in other vertebrates. Additionally, in the chick mutant, *Talpid*, the mutated *talpid3* gene which normally encodes a centrosomal protein essential for primary cilia formation, is devoid of cilia on the node but has no left-right asymmetry disruption (Yin et al. 2009). It is, therefore, unlikely that nodal flow is occurring in the development of left-right asymmetry in chick embryos. Later research has shown that cellular rearrangement of the node creates leftward movement of cells around the node which is required for normal left-right asymmetry (Gros et al. 2009; Cui et al. 2009). The chick was the first vertebrate model tested that does not in some way use nodal cilia for the establishment of left-right asymmetry.

In early cultured chick embryos the removal of the left or right blastoderm adjacent to the emerging primitive streak results in ectopic, or a lack of, *nodal* expression (Levin &

Mercola 1999). Treatment with lindane, which diminishes gap junctional communication disrupts normal left-sided *nodal* expression and expression is bilateral. Gap junction channels are formed by assembly and docking of hexamers of proteins from the connexin family (Jiang & Goodenough 1996). This research led to the proposal that the left-sided *shh* expression at the Hensen's node is due to left-right information transferred uni-directionally throughout the epiblast by gap junction channels (Levin & Mercola 1999). However, the molecule transported through the gap junction is not known; although serotonin has been implicated as a candidate (Fukumoto et al. 2005) although not definitive. Serotonin has been shown to act upstream of *shh* in the chick embryo and alter normal left-sided expression (Fukumoto et al. 2005). Another early step in establishing left-right asymmetry are H^+/K^+-ATPase channels which have a role in developing chick left-right asymmetry as well as *Xenopus* and zebrafish (discussed previously). H^+/K^+-ATPase channels generate a membrane potential at Hamburger Hamilton stage 3 and 4 and are essential for normal left-right asymmetry (Levin et al. 2002). It remains unknown as to how the H^+/K^+-ATPase, gap junctions and serotonin are all related.

All the above research provided an invaluable insight into left-right asymmetry and the conservation of the mechanisms within the vertebrate clade. Further elucidation of how the uni-directional fluid flow is converted into left-sided *nodal*, *lefty* and *pitx2* expression has not yet been achieved through the analysis of other vertebrate models. The ability to analyse asymmetry in very early embryogenesis, something that cannot be achieved easily in the mouse model, has indicated that asymmetries may be defined earlier in development than previously thought. Nodal cilia are important in the development of left-right asymmetry but they could also have an unknown link to earlier methods of laterality development and

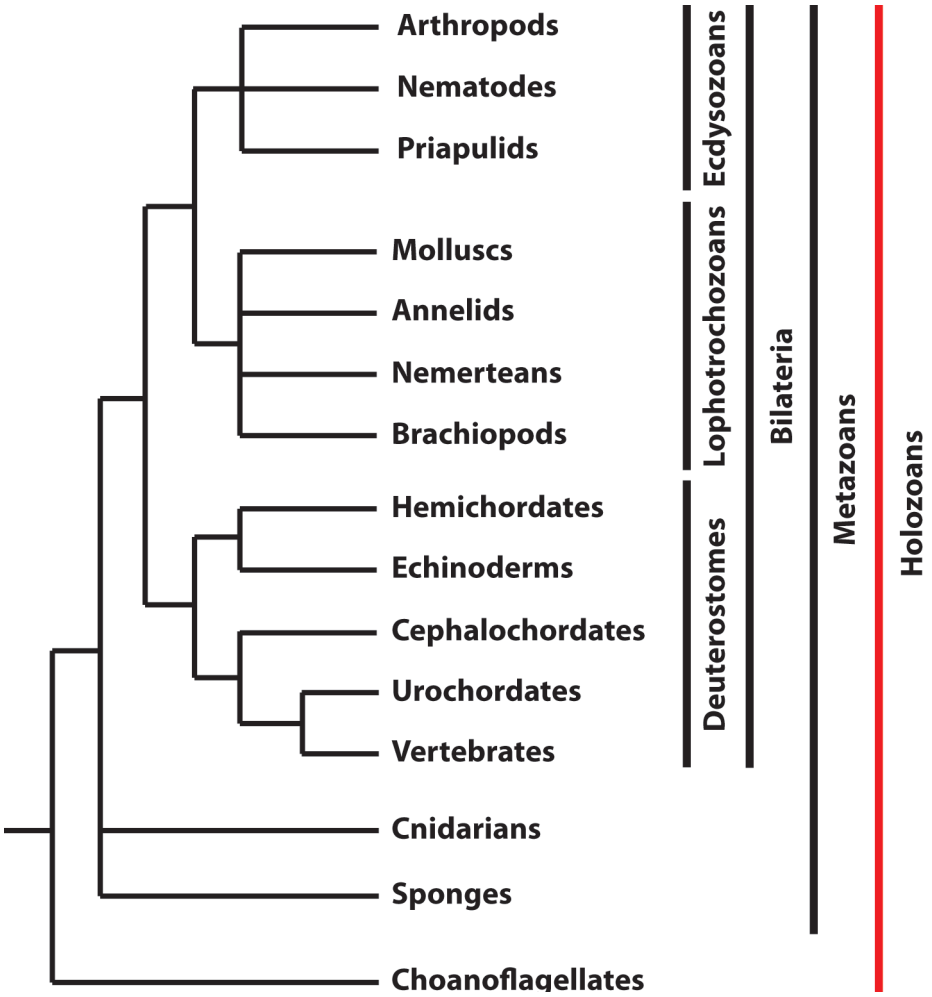


Figure 1.5: Holozoan Phylogeny

should be studied together. One way to help establish the evolutionary progress of left-right asymmetry is to extend our knowledge beyond the vertebrates.

1.6 THE DEVELOPMENT OF LEFT-RIGHT ASYMMETRY IN THE INVERTEBRATES

Structural asymmetry is present throughout evolution and across the Bilateria. In polychaete annelids, which usually appear externally symmetrical, the pharayngeal apparatus is

often asymmetrical, as is the operculum in Serpulidae. Most people are aware of claw size asymmetry in lobsters, members of the arthropod phylum, and shell coiling in molluscs, but many asymmetries are internal or only occur during particular stages of development. Most research on left-right asymmetry has focused on the vertebrates but gradually, the mechanisms involved in invertebrate asymmetry are beginning to be understood.

The bilaterians consist of three main groups: Ecdysozoans, Lophotrochozoans and Deuterostomes (Fig. 1.5). The deuterostomes consist of five major clades including vertebrates which have been the main group of organisms analysed in regard to left-right asymmetry. The other four clades are echinoderms, hemichordates, cephalochorates and urochordates, with the latter most closely related to the vertebrates. *Amphioxus*, sea urchins and *Ciona intestinalis* are the most commonly used non-vertebrate deuterostome models in biological research and have provided a potential area of research for analysis of left-right asymmetry. This section will review these organisms as model systems for laterality determination and summarise the experiments which have already been conducted.

1.6.1 *Ciona intestinalis*

Ascidians are urochordates which, together with cephalochordates and vertebrates, constitute the phylum Chordata. At some point in their lifecycle all chordates share the same distinctive characteristics including a notochord, dorsal neural tube, endostyle and postanal tail. Molecular phylogenetic data demonstrate that urochordates are the closest living relatives to vertebrates (Delsuc et al. 2006) with cephalochordates now placed as the most basal extant chordate lineage. Taxonomically ascidians are often divided into three distinct taxonomic

groups, Aplousobranchiata, Phlebobranchiata and Stolidobranchiata with the model species *Ciona intestinalis* representing Phlebobranchiata and *Halocynthia roretzi*, Stolidobranchiata (Tsagkogeorga et al. 2009). These species are distantly related and probably diverged several hundred million years ago (Lemaire 2009), yet still exhibit very similar early development (Nishida 1987; Nishida 1983; Nishida & Satoh 1985).

Adult *Ciona intestinalis* and *Halocynthia roretzi* are sessile filter feeders commonly found in large clumps on submerged marine substrate. They are hermaphroditic broadcast spawners but are typically not capable of self-fertilisation (Harada et al. 2008). The adult ascidian differs dramatically from the typical chordate body plan, however, during ascidian embryogenesis they develop a motile tadpole larva with clear similarities to vertebrates. The small number of cells in the ascidian larva, at around 2600, with fewer than 20 major tissues, plus rapid and stereotyped development makes the ascidian an efficient and important model system in developmental biology. *Ciona intestinalis* and *Ciona savignyi* are now most commonly used in molecular laboratories, primarily due to the availability of genome sequences (Dehal et al. 2002; Small et al. 2007), the existence of EST (Expressed Sequence Tag) collections (Satou et al. 2003) and their widespread availability.

The *Ciona intestinalis* larva has asymmetric positioning of two sensory pigment spots, the ocellus and otolith, the adjoining regions of the brain and in the adult an asymmetrically folded gut (Boorman & Shimeld 2002). *Nodal* has been described in *Halocynthia roretzi* (Morokuma et al. 2002), *Ciona intestinalis* (Mita & Fujiwara 2007) and *Molgula oculata* (Schumpert et al. 2000). *Nodal* is first observed in a pair of lateral blastomeres in *Ciona intestinalis* embryos and later in six vegetal blastomeres at the 32 cell stage (Morokuma et al. 2002; Imai et al. 2004). It is also vital in patterning the neural tube along the medial-lateral axis in *Ciona intestinalis*

(Hudson & Yasuo 2005). *Nodal* is initially expressed symmetrically in the zygote at the 32-cell stage but becomes asymmetric by the tail-bud stage of development (Morokuma et al. 2002) through regulation by *Ci-Lefty* (Mita & Fujiwara 2007). The pro-orthologue of *Pitx2*, *Ci-Pitx*, is expressed asymmetrically in the left head mesoderm and throughout the left sided ectoderm but not in the dorsal and ventral midline cells at the tailbud stage (Boorman & Shimeld 2002). *Ci-Nodal* signalling is required to drive *Ci-Pitx* expression in the left epidermis of the embryo, a characteristic of vertebrate *pitx2* expression (Yoshida & Saiga 2008). Similar results have been observed in the other ascidian species although this section has focused on results in *Ciona intestinalis*. This expression precedes the first morphological signs of left-right asymmetry, as seen in the development of vertebrate left-right asymmetry.

So far laterality research in *Ciona intestinalis* has focused upstream of *nodal*/*pitx* expression, on the role of ion flux, a mechanism discovered in *Xenopus* (Levin et al. 2002). In *Xenopus*, H^+/K^+-ATPase mRNA reverts from a symmetrical distribution of expression at the 1 cell stage to an asymmetrical distribution during the first two cell divisions. Disruption of H^+/K^+-ATPase results in ectopic expression of asymmetric genes and heterotaxia. *Ciona intestinalis* embryos exposed to Omerpazole, which blocks H^+/K^+-ATPase, relatively late in development display disrupted *Ci-Pitx* expression (Shimeld & Levin 2006). The most sensitive time-point for exposure to Omerpazole corresponds with the time frame prior to asymmetric gene expression. However, left-right asymmetry is also disrupted in embryos when the protective shell, the chorion is removed at fertilisation (Shimeld & Levin 2006), which implies that it has an important role in left-right asymmetry in *Ciona intestinalis*.

1.6.2 Amphioxus (*Branchiostoma floridae*)

Amphioxus are members of the phylum Chordata along with vertebrates and urochodates. They share the same distinctive anatomical characteristics such as the notochord, dorsal neural tube, endostyle and postanal tail. Amphioxus development begins with cell-divison to create a 32-cell blastula which undergoes three types of cleavage; radial, bilateral and spiral, to develop a 256-cell spherical blastula surrounding a spacious cavity called the blastocoel. Next, the embryo undergoes gastrulation which generates the DV axis with the blastopore situated on the dorsal side. At this stage the ectodermal cells begin to project motile cilia, which are important once the embryo has ruptured from the follicle to become free-swimming. The ciliated ectoderm links Amphioxus (Fig. 1.4) with invertebrates where it is common but in vertebrates is entirely unknown. The role of cilia at this time is expected to be more of a behavioural trait rather than a prerequisite for left-right asymmetry (Stokes & Holland 1995).

It is once the embryo becomes pelagic that the first signs of asymmetry emerge (Medawar 1951). The head-cavities of the Amphioxus arise as a pair of sacs in front of the notochord and myocoelomic pouches. The right sac becomes enlarged and the cells lose their cubical shape to become a flattened pavement epithelium. At the same time the left sac remains the same shape and size but moves to lie transversely below the notochord. The right sac becomes the praeoral body-cavity or coelom of the 'head' while the left sac becomes the praeoral pit. Other asymmetric events which occur in the development of Amphioxus include the formation of the gill slits which begin on the right side and then later in development migrate to the left as well as somites out of register.

Nodal is expressed asymmetrically in Amphioxus by the 13 hr neurula stage and *Nodal*, is

first detected in the early gastrula just within the dorsal lip of the blastopore in a region of the hypoblast. All the gene expression data from this region has marked it as a potentially homologous region to the Spemann's organiser (Yu et al. 2002; Yu et al. 2007). *Nodal* expression remains bilaterally symmetrical until the 13hr neurula when expression is lost on the right-hand side. Asymmetry begins in the paraxial mesoderm of the neurula and spreads along the left-side of the endoderm in areas where left-right asymmetrical morphological structures will develop (Yu et al. 2002). Additionally, the pro-orthologue to *pitx2* has been discovered and the left-sided expression patterns shown in two amphioxus species *Branchiostoma belcheri* (Yasui et al. 2000) and *Branchiostoma floridae* (Boorman & Shimeld 2002a). Although *nodal* and *pitx* left-sided expression is conserved in cephalochordates, there has been no research conducted in this model to analyse the mechanisms which establish this asymmetric expression.

1.6.3 Sea urchin

Research has shown that conservation of mechanisms regulating left-right asymmetry reached as far as the sea urchin, a basal deuterostome, with evidence of *nodal* signalling (Duboc et al. 2005). Interestingly, however, *nodal* expression was found on the right side of the embryo unlike the left-sided expression seen in chordates. Likewise, *pitx* and *lefty* are expressed unilaterally in the Mediterranean sea urchin, *Paracentrotus lividus*, and are also expressed on the right. Both the embryo and larvae of the sea urchin are bilaterally symmetrical but during the process of transition to radial symmetry in the adult they undergo an asymmetric period where a rudiment forms on the left side of the larvae. The main components of the rudiment, the hydropore canal, hydrocoel and primary vestibule, are found only on the left side. Early

nodal expression is required for the establishment of the oral-aboral axis but inhibition of *nodal* later disrupted left-right asymmetry. *Nodal* was the first gene to be expressed on the right side of the larvae at 22hr then *lefty*, *pitx2* and *sox9* were expressed by 26hr (Duboc et al. 2005). It was determined that *nodal*, *pitx2* and *lefty* are continuously expressed between 18hr and 24hr which is a period essential for left-right signalling. *Nodal* expression on the right of the larva prevents the formation of the rudiment on the right so, therefore, it develops on the left (Duboc et al. 2005).

To analyse if H^+/K^+-ATPase channels, known to have a role in left-right asymmetry across the vertebrates as well as the urochordate *Ciona intestinalis*, also affect rudiment position in sea urchins, embryos were treated with Omerpazole (Hibino et al. 2006). Larvae displayed disrupted asymmetry of the adult rudiment which normally resides on the left of the larvae. This evidence suggested that endogenous spatially-regulated early H^+/K^+-ATPase transport functions in the establishment of left-right asymmetry in sea urchins (Hibino et al. 2006). This study also showed that there appeared to be no role for calcium channels in left-right asymmetry in sea urchins, which is in contrast to vertebrates.

Cilia are observed on the developing sea urchin embryo but it is still not known if they have the potential to affect laterality. A population of 9+2 structure cilia exist in the primary pore canal (PPC) and they beat from the time the cilia emerge to 55 hr post fertilisation, when they stop. The cilia on the right disappeared by 55 hr creating asymmetry by 60 hr and the cilia beat is a much slower beat than required for the movement of water. The observations have led to debates concerning the function of the cilia themselves. Removal of both or just the left hand side cilia, in *Temnopleurus hardwicki*, embryos restricted the width of the sea urchin later in development. The role of cilia in creating a flow necessary for the establishment of

left-right asymmetry in sea urchin is a possibility since asymmetrical activity arose soon after the formation of the ciliary bundle, by 28 hr and before morphological asymmetry (Hara et al. 2003). Further research is required to determine if the function of the cilia in the PPC is to restrict formation of the rudiment on the right. If there is a role for the nodal flow in a similar fashion to vertebrates it would be expected to be reversed as a result of *nodal* expression on the right not the left.

1.7 ECDYSOZOANS - *DROSOPHILA MELANOGASTER*

For many years the only invertebrate investigated for left-right asymmetry was *Drosophila melanogaster*, a genetic model system which can be easily manipulated with genetics. Although, the AP and DV axes were both well established in *Drosophila melanogaster* there was no evidence of left-right asymmetry. Klingenberg et al. (1998) were the first to show subtle left-right asymmetry in the size and shape of *Drosophila melanogaster* wings. Another form of asymmetry in *Drosophila melanogaster* is observed at embryonic stage 13 in *Drosophila melanogaster*, when the ventrally bending hindgut tube twists 90º to the left before further coiling occurs at stage 15 (Coutelis et al. 2008).

In 2001, the first two stable mutants which displayed left-right asymmetry defects in the coiling of the proventriculus in the gut were generated (Ligoxygakis et al. 2001). The mutants, *dicephalic* and *wunen*, meant for the first time that left-right asymmetry could be reversed through genetic and developmental manipulation. The mutant phenotype showed a reversal in the coiling of the gut but failed to show left-right asymmetry in other aspects of the organism. It has been shown that left-right asymmetry in the gut is controlled by information from the

surrounding maternal tissues but it was unable to prove that this was the only mechanism involved in left-right asymmetry (Ligoxygakis et al. 2001). However, the conclusion that the asymmetric coiling of the *Drosophila melanogaster* gut was due to predetermined maternal signals was debated due to results which suggests that left-right asymmetry is actually specified in relation to the AP and DV polarities in the embryo (Hayashi et al. 2005).

Another mechanism shown to be involved in the handedness of *Drosophila melanogaster* is a myosin I motor, Myo31DF, which results in the reversal of handedness when absent. Overexpression of Myo61DF in *Drosophila melanogaster* mimics the loss of Myo31DF which suggests that it is part of a complex system initiating the break in left-right asymmetry (Hozumi et al. 2006; Speder et al. 2006). Much more research in this area is required to understand fully the mechanisms at work in *Drosophila melanogaster* in establishing left-right asymmetry.

1.8 LOPHOTROCHOZOANS – SNAILS

It has been thought for the some years that due to a lack of the *nodal* gene in the ecdysozoans, *nodal* emerged concomitantly with the development of the mouth in deuterostomes. However, recently research in *nodal* conservation has migrated out of the deuterostomes into other protostomes, including the molluscs.

The other clade which comprises the Bilateria, the lophotrochozoans, contains snails, molluscs and annelids which all display some asymmetric characteristics. The chirality in snails, which incorporates the body handedness and direction of shell coiling, has particularly interested scientists for many years. The two main forms of shell coiling are termed dextral (right-turning) and sinistral (left-turning) with most extant species of snail displaying dextral

shell coiling. Body chirality occurs early in gastropod development when the direction of spiral cleavage at the third cleavage determines body direction. Mechanical manipulation of the third cleavage chirality in one gastropod, *Lymnaea stagnalis* leads to the reversal of embryonic handedness (Kuroda et al. 2009).

Experimentation to analyse *nodal* and *pitx2* conservation in the lophotrochozoans focused on dextral, *Lottia gigantea* and sinistral, *Biomphalaria glabrata*, forms of snail. *Nodal* expression was detected in two ectodermal domains on the right side of the *Lottia gigantea* trochophore stage embryo and in the ectodermal region on the left side of the *Biomphalaria glabrata* trochophore stage embryo (Grande & Patel 2009). *Pitx2* expression was shown in the cells adjacent to the cells expressing *nodal*. The first evidence of either *nodal* or *pitx2* expression was at the 32-64 cell stage of development with *nodal* expression upstream of *pitx2* expression. An inhibitor of *nodal* signalling, SB-431542, added to the embryos prior to blastula formation led to non-coiled shells in *Biomphalaria glabrata* (Grande & Patel 2009). These experiments clearly show that *nodal* and *pitx2* expression has a conserved role in left-right asymmetry outside of the deuterostomes and the asymmetric expression of these two genes is an ancestral feature of the bilaterians. Additionally, mechanical manipulation of the third cleavage chirality leads to the reversal of *nodal* expression and embryonic handedness in *Lymnaea stagnalis* (Kuroda et al. 2009) which suggest that there are early mechanisms involved in left-right asymmetry as observed in *Xenopus*, Zebrafish and chick.

1.9 SUMMARY

Major progress has been made in the quest to uncover the mechanisms that establish left-right

asymmetry in organisms. Most research has focussed on the elucidation of the mechanisms which generate the asymmetric positioning of organs in vertebrates, and in particular the mouse, rabbit, frog, fish and chick. In the mammalian, fish and amphibian models, cilia on the organiser generate a leftward flow through vortical rotation. Disruption to the directional flow results in bilateral, right sided or no expression of normally left-sided asymmetric genes and culminates in disordered organ positioning. Two conflicting models have been proposed to explain how the leftward flow generates a left-right axis; the chemical and the physical hypothesis. Research has shown support for both theories, but to date there has not been a consensus on which hypothesis is correct.

The mechanisms involved in the establishment of left-right asymmetry have been further complicated by findings in other vertebrate models. Although the node mechanism is highly conserved in mammals, fish and amphibians, other mechanisms are known in the fish, amphibian and avian models which subsequently affect the generation of left-right asymmetry. H^+/K^+-ATPase channels, gap junctions and serotonin are all essential in very early development for the correct positioning of organs in later development. Due to the inability to study very early mammalian embryos it is not known if these other mechanisms are also involved in the mammals. It is still not understood if all these mechanisms work in conjunction to generate the normal vertebrate body plan or work independently. Serotonin requires both H^+/K^+-ATPase and gap junctions for normal development of left-right asymmetry which suggests that the several of these mechanisms are working together. One proposal has been that nodal cilia are required in some organisms to transmit left-right asymmetry that has previously been set up through H^+/K^+-ATPase, gap junctions and serotonin during the cleavage stages of development.

Most research about the establishment of left-right asymmetry has been conducted in vertebrates but asymmetric gene expression is conserved in several phyla in the invertebrates. The extent to which the conservation of cilia and H^+/K^+-ATPase extend back into more basal organisms will be achieved by the analysis of basal chordates within the deuterostomes and then by extending research to the protostomes.

1.10 Aims

The presence of monocilia which rotate, generate a leftward flow and disruption to which results in left-right defects in most vertebrate species analysed suggests it is a highly conserved mechanism in the establishment of left-right asymmetry. Although research has shown high levels of conservation in the presence and asymmetric localisation of particular genes, including *nodal*, *pitx2* and *lefty* in non-vertebrates, the upstream mechanisms have not been widely analysed. Evidence has suggested that H^+/K^+-ATPase channels are critical in the establishment of left-right asymmetry in *Ciona intestinalis* but as yet the possible role of cilia had not been explored in a member of the closest living relatives to the vertebrates, the urochordates. This project aims to analyse and evaluate whether cilia are present on the developing *Ciona intestinalis* embryo prior to asymmetric gene expression, if they are motile, can generate a leftward flow and are required for normal left-right asymmetry development.

Detailed SEM analysis of the surface structures of *Ciona intestinalis* embryos from fertilisation to the late tailbud stage showed that cilia are present, one per cell, on every cell of late neurula and early tailbud embryos (Chapter 3). TEM of the late neurula stage embryo cilia show that they do not have the standard structure related to motile cilia, 9+2 but immediately after they

exit the cell the nine doublet microtubules become disorganised and degenerate into singlets. Accessories related to motility; a central pair, dynein arms and radial spokes, are not observed on any *Ciona intestinalis* embryo cilia. The late neurula and early tailbud stage cilia are positioned universally at the posterior of each cell on the embryo. Subdivision of the embryo into nine regions showed that statistically, although cilia are positioned in the posterior of each cell they are positioned in a significantly different position along the AP axis on cells on the left of the embryo in the region between the head and tail (Chapter 4).

The timing of cilia presence immediately prior to asymmetric gene expression on the embryo suggested there could be a link with the establishment of left-right asymmetry, so embryos were manipulated to remove cilia. Experimentation was not able to fully remove the cilia from the embryo but disruption to their positioning through exposure to high concentrations of NaCl did not affect the asymmetric gene expression of *Ci-Pitx*. Further experimentation is required to establish whether the cilia observed on the late neurula and early tailbud stages of *Ciona intestinalis* development have a role in the development of left-right asymmetry.

Additionally, genes, that when mutated in humans and mice prevent the normal distribution of organs, were analysed for their presence across the eukaryotes (Chapter 5). 13 genes were collated from a screen of both human disorders and mouse mutants. Orthologues were searched for in species that represent a wide spread of eukaryote evolution, produce cilia at some point in their life cycle and, within the Metazoa, have different known mechanisms in the development of left-right asymmetry. Ancient structural proteins were found in the majority of ciliated species whereas, proteins that encode transcription factors were only observed within the Holozoa. Other proteins that are involved in the establishment of left-right asymmetry are predominantly restricted to the Metazoa, except for PKD2, a protein involved in calcium signalling.

CHAPTER 2

Materials and Methods

2.1 MOUSE EMBRYOS

2.1.1 Collection and dissection of mouse embryos

Mouse embryos were provided by Elizabeth Robertson's lab (Sir William Dunn School of Pathology) and Dominic Norris' lab (Medical Research Council, Harwell). All the embryos were aged by somite number and photographed on a dissection microscope before they were processed for Electron Microscopy as described below.

2.2 ELECTRON MICROSCOPY

2.2.1 Scanning Electron Microscopy

The samples were fixed at Room Temperature (RT) (2.5% glutaraldehyde, 2% paraformaldehyde in 100 mM cacodylate buffer (pH 7.0) with 1 mM ethylene glycol tetraacetic acid (EGTA) and 2 mM $MgCl_2$, 0.01% picric acid and 100mM sucrose) and left in the fixative for 1-2 days at 4°C. After the primary fixation the samples were washed in cacodylate buffer (0.2 M, pH 7.4) and post-fixed with 1% osmium tetroxide in 100 mM cacodylate buffer (pH 7.0) followed by several rinses in cacodylate buffer. The samples were washed with distilled water to remove fixative/buffer. The samples were dehydrated with ethanol to 100% EtOH, critically point-dried

for 10 mins, and then mounted on aluminium SEM stubs using double-sided carbon tabs. After sputter-coating with gold the samples were examined using a scanning electron microscope (JEOL JSM 6390).

2.2.2 Transmission Electron Microscopy

The samples were fixed at RT (2.5% glutaraldehyde, 2% paraformaldehyde in 100 mM cacodylate buffer (pH 7.0) with 1 mM ethylene glycol tetraacetic acid (EGTA) and 2 mM $MgCl_2$ and picric acid) for 10 mins. The fixative was replaced with fresh fixative and left for 16-24h at 4°C. After the primary fixation the samples were washed with cacodylate buffer (0.2 M, pH 7.4) and post-fixed with 1% osmium tetroxide in 100 mM cacodylate buffer (pH 7.0) for 1h at 4°C followed by several rinses in distilled water. En bloc stain with 0.5% aqueous uranyl acetate for 16 h at 4°C in dark. The sample was then moved through a dehydration gradient (30%, 50%, 70% and 90% EtOH) for 15 mins each step and then 100% EtOH for 3x 30 mins. After dehydration the embryo is passed through 2x15 mins changes of Propylene oxide and then embedded in resin (Agar 100 resin) through a series of steps. Infiltration of the resin begins with a 2:1 mix of propylene oxide:resin, then a 1:1 mix of propylene oxide:resin then a 1:2 mix of propylene oxide:resin which all stand for 1 hr. The sample was left overnight in 100% resin and then changed into fresh resin for 1 hr. The fresh resin was transferred to an embedding mould for 12-24 hrs at 60-70°C.

Resin containing embryos was sectioned using a diamond knife on an ultra-microtome. 50-70nm sections were cut, placed on a grid, dried and then covered in 0.2% lead citrate for 30 secs before they were viewed using a transmission electron microscope (FEI Technai). Each section was examined for the presence of cilia and those found were photographed. Photos were taken

on negatives, developed and refined on a photo software programme (Adobe photoshop).

2.3 BIOINFORMATICS

2.3.1 Proteins linked with Left-right asymmetry

A set of proteins with a known role in left-right asymmetry were selected on the basis that they were either involved in human disorders and diseases or were mouse mutants that display *situs inversus*. Proteins involved in human disorders and diseases with the phenotype, *situs inversus*, were collated through the Online Mendelian Inheritance in Man website. Additionally, mouse mutants from the Mouse Genome Informatics database that have the *situs inversus* phenotype were selected and the proteins involved were added to the OMIM protein list. 13 proteins that cause *situs inversus* in greater than 48% of cases were carried forward to the next stage of analysis. The 13 human protein sequences downloaded from NCBI (http://www.ncbi.nlm.nih.gov/) and were used to query the predicted proteomes of 45 eukaryotic organisms for which complete or near-complete genome sequence is publically available. The 45 eukaryotic organisms were selected for their wide evolutionary spread and different left-right mechanisms.

2.3.2 Identification of homologues

Homologues to the 13 human protein sequences were identified using an approach developed by Wickstead and Gull (2007) which relies on clustering of proteins by BLASTp scores. Initially, potential orthologues of the human protein sequence for each gene, were identified by a reciprocal best BLASTp search with an e-value threshold of 10^{-5}. Orthologues found by this

method in the other 45 proteomes (e-value threshold of $<10^{-2}$) were also used to perform RBB to find additional instances missed originally. Results from this search were then formed into clusters using a distance matrix derived from BLASTp scores (Wickstead & Gull 2007). The orthologous cluster was further defined by eye, aligned, trimmed and then used in Maximum Likelihood phylogenetic inference (Guindon & Gascuel 2003; Ronquist 2003).

Highly truncated sequences and sequences with a >95% identity were removed to reduce redundancy and aid both alignment and phylogenetic reconstruction (Wickstead & Gull 2007). The sequences were aligned using MAFFT (Katoh et al. 2002) and analysed manually to refine the alignment. A Maximum Likelihood phylogeny (PHYML) (Guindon & Gascuel 2003) and then a Bayesian phylogeny were inferred using the Markov chain Monte Carlo method as implemented by MrBayes v3.1.2 (Ronquist 2003). The WAG substitution matrix was used (Whelan & Goldman 2001) and 4 chains were run for 250,000 generations from a random starting tree sampling every 200 generations and with a "temperature" of 0.2. 2 runs enabled a consensus phylogeny to be inferred and bootstrap values.

2.4 *CIONA INTESTINALIS* ANIMALS

2.4.1 Fertilisation

Adult *Ciona intestinalis* were collected from Northney and Sparkes Marinas, Portsmouth and maintained in a closed sea water system at ~16°C. Oocytes and sperm were removed through dissection into separate dishes of RT filtered sea water. The sperm and oocytes were mixed and left for 15 mins before the sperm was removed and the fertilised oocytes washed. The fertilised oocytes were left to develop at 12°C. Developing embryos were collected every hour for *in situ*

hybridisations and SEM.

2.4.2 De-chorionation

Before embryos were fixed for experimentation the chorion was removed chemically in a de-chorionation solution (2% Sodium glycoylate and 0.1% protease in Filtered Sea Water (FSW)) (Mita-Miyazawa et al. 1985) for approximately 5 mins. The time altered depending on the embryos stage of development, with early stages 4 mins was sufficient but by the tailbud stage 8 mins was required. The de-chorionation solution was removed once the embryos settled and was replaced with 2 washes of FSW.

2.5 *CIONA INTESTINALIS* PROBES

2.5.1 Cloning

Ciona genes were extracted from the *Ciona intestinalis* gene collection in pBluescript SK (+/-), spread on Amp^+ agarose/LB plates and left in a 37°C incubator overnight. 10 white colonies were picked and left to grow in 3 ml Amp^+ LB in a 37°C shaker overnight. 1ml of Amp^+ LB was transferred to a Quiagen Miniprep Kit and the plasmid DNA collected according to the manufacturer's protocol. A double digest using EcoR1 and Xho1 was conducted for 2 hrs in a 37°C water bath to determine EST size.

2.5.2 Double Digest

Reagent	Quantity (µl)
Plasmid DNA	2
Buffer	1
Restriction Enzyme 1	0.5
Restriction Enzyme 2	0.5
H_2O	6

2.5.3 Sequencing

Cut pDNA with an insert of the correct size was sequenced to check if the insert/EST was the correct sequence or gene. The pDNA was sequenced in each direction using T7, T3, M13F or M13R with Bigdye.

Reagent	Quantity (µl)
Bigdye	1
5x Sequening Buffer	1.5
Primer (T3, T7 or Sp6)	1
DNA template	3
H_20	3.5

The pDNA, primer and Bigdye mixture were then placed in a thermocycler on the programme described below.

95.0°C	3 minutes	
95.0°C	30 seconds	Repeat 35 times
50.0°C	20 second	
60.0°C	4 minutes	
Repeat		
4.0°C	Hold	

Reagent	Quantity (µl)
3M NaOAc	1.5
100% EtOH	31.25
H_2O	7.25

The sample was centrifuged at 1400-2000g for 45 mins then washed with 75 µl 70% EtOH and spun at 50g for 1 min. The resulting pellet was dried and sent to the Zoology Department Sequencing facility. Each gene sequence was checked against NCBI (http://www.ncbi.nlm.nih.gov/) and JGI (http://genome.jgi-psf.org/) databases using BLAST (Altschul et al. 1990). Plasmid DNA containing the correct EST was processed for *in situ* hybridisation probes.

2.5.4 DNA linearization

Reagent	Quantity (µl)
Plasmid DNA	15
Restriction Enzyme	2
10x Buffer	5
H_2O	28

The mix was placed in a 37°C water bath for 2 hrs, then 2 µl more restriction enzyme was added before being returned to the water bath for another 1 hr. 200 µl of DEPC H_2O was added prior to the Phenol/Chloroform extraction. Probes were made for the sense and antisense direction.

2.5.5 Phenol/Chloroform Extraction

125 µl chloroform and 125 µl phenol was added to the linearised DNA, shaken and centrifuged at 13,000 rpm for 10 mins. The aqueous solution was transferred to a new tube and 250 µl chloroform added. The mix was centrifuged at 13,000 rpm for 5 mins and the aqueous solution transferred to a clean tube. 25 µl 3M NaOAc and 750 µl 100% EtOH were added and left at -20°C for 15 mins before being centrifuged at 13,000 rpm for 10 mins. The 100% EtOH was removed and replaced with 70% EtOH and centrifuged at 13,000 rpm for 3 mins. The EtOH was removed and the pellet left to dry for ~10 mins. 30 µl DEPC H_2O was added to re-suspend the pellet.

2.5.6 Riboprobe Synthesis and Cleaning

Synthetic RNA was made from the DNA in the sense and antisense direction and labelled with digoxygenin-rUTP.

Reagent	Quantity (µl)
linearised DNA	10
5x RNA polymerase buffer	4
0.1M DTT	2
Dig-rUTP label mix	2
RNAsin	1
RNA polymerase (T3, T7 or Sp6)	1

The mix was placed in the 37°C water bath for 2 hrs. The riboprobes were cleaned with Roche Sephadex Columns according to the manufacturer's protocol.

2.5.7 *In situ* hybridisations

The embryos collected for *in situ* hybridisation were fixed in 4% paraformaldehyde (PFA) and stored at 4°C. They were then taken through a dehydration gradient of 70% and 100% EtOH and once in the third wash of 100% were stored at -20°C. All embryos were then run through a pre-hybridisation treatment to permeabilise the embryo and block non-specific binding of RNA. They were washed in 50:50 xylene:EtOH, 75:25 xylene:EtOH for 1 hour and back to 50:50

xylene:EtOH, 100% EtOH 3 times, MeOH once and PBT (1% PBS and 0.1% Tween 20) 3 times. Embryos were then incubated in PBT and 4 μg/ml proteinase K for 5 mins, fixed in 4% PFA for 25 mins, washed in PBT 3 times and then hybridisation solution (50% formamide, 5x SSC pH 4.5, 100μg/ml yeast RNA, 50ug/ml heparin, 0.1% Tween 20 in 0.1% DEPC H_2O) twice. The hybridisation solution was replaced and the embryos were incubated at 55-65°C overnight.

The following day an empirical amount of probe, calculated from RNA concentration, from a 50 μl digoxygenin riboprobe synthesis was added to the hybridisation solution and incubated overnight at 55-65°C. The embryos were then washed in *Ciona* wash (50% formamide, 5xSSC pH 4.5, 0.1% Tween 20 in 0.1% DEPC H_20) 6 times at the hybridisation temperature for 20 mins each and PBT 3 times at RT. Block (20% heat treated sheep serum in PBT) was then added for at least 2 hours at RT before replacement with the antibody (anti-fab fragment) in a 1:3000 dilution of block. Whilst the antibody was on the embryos were stored at 4°C overnight. The embryos were washed with PBT 3 times, APT (100mM NaCl, 100mM Tris HCL pH 9.5, 50mM $MgCl_2$, 0.1% Tween 20 in 0.1% DEPC H_2O) 3 times for 15 mins each before 700 μl staining solution (6 μl BCIP/NBT in APT) was added. The embryos in 4 well plates were kept in the dark.

After staining, the embryos were fixed in 4% PFA for 25 mins, washed in PBT 3 times and mounted in 80% glycerol on slides. The slides were viewed with an Axioscope fitted with axiocam.

2.6 ANTIBODY STAINING

2.6.1 Acetylated α- and γ-tubulin

The primary antibodies used were anti-acetylated alpha tubulin clone C3B9 (Woods et al. 1989) and rabbit anti-γ-tubulin (Sigma-Aldrich). Embryos were fertilised as previously stated (4.2.1)

and allowed to develop at 18°C for 7 hours until they reached the neurula stage. Embryos were fixed in -20°C MeOH for a minimum of 2 hours before they were rehydrated in 3 x 10 mins PBS (1%), 1x Triton-X-PBS (Tx-PBS) (0.05%) and 1x PBS washes. Primary antibodies were used at 1:2 (C3B9 (Woods et al. 1989)) and 1:250 (anti-γ-tubulin (Sigma-Aldrich Co. Ltd, Poole, UK)) in Tx-PBS (0.1%) and incubated for 1 hour at RT. Embryos were washed for at least 10 mins 3x in Tx-PBS (0.1%) at RT, and then the secondary antibodies (Alexa-fluor 488- and Alexa-fluor 594-conjugated goat anti-mouse and goat anti-rabbit (MolecularProbes)) was used at 1:500 in Tx-PBS (0.1%) before at least 10 mins 3x Tx-PBS (0.1%). Finally, DAPI was added at 1:1000 in Tx-PBS (0.1%), washed for at least 10 mins 3x in Tx-PBS (0.1%) and mounted in Anti-fade Vectashield (Vectashield, Vector Laboratories Ltd., Peterborough, UK). The embryos were then viewed on an Axioscope and the images processed in Metamorph (Universal Imaging) and figures assembled in Adobe photoshop CS4.

2.6.2 Phalloidin

Alex-Fluor-633-phalloidin conjugate (Molecular Probes) were used to visualise F-actin. Embryos were collected as described previously and fixed in 4% formaldehyde-1.6% NaCl in Cytoskeleton Buffer (CB) (10mM Mes pH 6.1, 138mM KCl, 3mM $MgCl_2$, 10mM EGTA pH 7.0 and 200mM sucrose) overnight at 4°C. The embryos were then washed 3x in PBS (1%), rinsed in Tx-PBS (0.5%) and further washed 3x in Tx-PBS (0.1%). A block of 2% Bovine Serum Albumin (BSA) in Tx-PBS (0.1%) was added for 30 mins whilst the embryos were rocked. Phallodin was used at 1:100 for 30 mins at RT and then washed for at least 10 mins each 3x Tx-PBS (0.1%) and mounted in anti-fade Vectashield (Vectashield, Vector Laboratories Ltd., Peterborough,

UK). The embryos were then viewed on an Axioscope and the images processed in Metamorph (Universal Imaging) and figures assembled in Adobe photoshop CS4.

2.7 DE-CILIATION OF *CIONA INTESTINALIS* EMBRYOS

Control and Experimental *Ciona intestinalis* embryos were grown in FSW until the late neurula stage when cilia first emerge. 720 µl 4.45M NaCl was added to 6 ml of FSW and embryos for 2 mins and then 7.2 ml of FSW was added to dilute the 4.45M NaCl, as previously described by Casano et al. 1998. Control embryos had 720 µl FSW added and then diluted with 7.2 ml of FSW. All the embryos were transferred to FSW in 90mm petri dishes until embryos were fixed for SEM (2.5% glutaraldehyde, 2% paraformaldehyde in 100 mM cacodylate buffer (pH 7.0) with 1 mM ethylene glycol tetraacetic acid (EGTA) and 2 mM $MgCl_2$, 0.01% picric acid and 100mM sucrose) at 0, 10 and 30 mins after exposure to 4.45M NaCl or *in situ* hybridisation (4% PFA and 5X MOPS) at 60, 90 and 120 mins after exposure.

2.7.1 Microinjection

2.7.1.1 Morpholinos

Morpholinos were made to order (Gene Tools, LLC). For IFT88, a complementary morpholino was designed to target a sequence containing the putative initiation codon (5'-ACCGAACATTGGCAAGCCCGGACAT-3' (the nucleotide sequence that correspond to the initiation codon of the gene is underlined)). 15 fmoles of morpholino in 30 pl of solution

(morpholino and dH_2O) was injected using a Eppendorf Femtojet Microinjector.

2.7.1.2 Micoinjection of *Ciona intestinalis* embryos

The morpholino, at 0.5 μM stock solution, was centrifuged at 1300g for 10 mins to pellet any impurities which could clog the needle. The Femtotip II (Eppendorf) needles were back filled with 5 μl of morpholino and attached to the Femtojet. Injection pressure (Pi) was set to 250 hPa, injection time (ti) set to 5 secs and the compensation pressure (Pc) to 750 hPa.

Fertilisation and de-chorionation was performed in the same way as *in situ* hybridisations except the sea water was more thoroughly millipore-filtered (0.22 μm). 1% seawater agarose plates were produced in 30 and 90mm Petri dishes and the larger plates were left to dry on a slope with a cover slip placed on the top of the agarose at the shallow end of the plate. Once these plates had dried the coverslip was removed. All pipettes were coated in sigmacote to prevent the embryos from sticking.

After fertilisation and de-chorionation, the de-chorionation solution was removed and replaced with 0.22 μm FSW twice and then placed in a flat dried 1% seawater agarose petri dish. The embryos were then collected with a 3 ml pipette and placed along the edge of the indentation made by the coverslip. The filled Femtotip II was lowered and each embryo injected. Injected embryos were removed and placed in a 1% seawater agarose petri dish containing Millipore-filtered seawater in a 12°C incubator for 16 hrs.

2.8 CILIA POSITIONAL MEASUREMENTS

2.8.1. Position along the AP axis

Embryos were fixed and imaged on a JEOL JSM 6390 SEM as described in 2.2.1. Photographs were taken of each embryo and refined in Adobe Photoshop. Each embryo was aligned along its AP axis, all the cells which are parallel to the surface of the specimen were traced in Adobe Illustrator and the position of the base of the cilium recorded with a blue circle. The centre of each cell was calculated and the length of the AP axis of the cell through the centre recorded. The length through the centre of the cell the cilium was situated along the AP axis was measured and converted into a percentage of the total cell AP axis.

2.8.2 Angle from the centre of the cell

A SEM image of each embryo was aligned along its AP axis, all the cells which are parallel to the the surface of the specimen were traced in Adobe Illustrator and the location of each cilium anchor (red) and direction of each cilium projection (blue). The centre of the each cell was located and the distance from the anterior to the centre of the cell marked as 0°. The angle from this point to the cilium was measured and recorded. Statistics used ANOVA and analyses were conducted in R 2.12.2 (R Foundation for Statistical Computing, Vienna, Austria).

CHAPTER 3

An Electron Microscope Study of the Early Stages of *Ciona intestinalis* Development

3.1 INTRODUCTION

A lot of research in the field of left-right asymmetry development has been focused in the mouse model system, in part due to the famous mouse mutants which provided valuable clues into the mechanisms that are disrupted during the development of left-right asymmetry. Node monocilia and their ability to generate a directional flow across the ventral node which is necessary for normal laterality development was also first observed in this model. As a result, the level of conservation was assessed in other vertebrate species. Monocilia and their directional flow were observed on the mouse ventral node and also the homologous organiser structures in rabbit, *Xenopus* and zebrafish which indicates a high level of conservation throughout the vertebrates. The high level of asymmetric gene expression conservation outside the vertebrates has led to experimentation in some invertebrate species, including the ascidian *Ciona intestinalis* to determine if the same mechanisms are also present outside the vertebrates.

Ascidians are urochordates which, together with cephalochordates and vertebrates, constitute the phylum Chordata, with the urochordates being the closet living relatives to the vertebrates (Delsuc et al. 2006). Their phylogenetic position next to the vertebrates as well as their asymmetric gene expression and organ distribution, during the larva stage, makes *Ciona intestinalis* an

interesting model to research the conservation of left-right asymmetry mechanisms outside the vertebrates. This chapter will investigate whether the mechanisms known to establish left-right asymmetry in the mouse model are present in the more primitive invertebrate *Ciona intestinalis* model.

In mouse the first morphological sign of asymmetry is heart tube looping (Kaufman 1992) whereas during *Ciona intestinalis* development it is in the swimming larva stage when the two sensory pigment spots, the ocellus and otolith are positioned asymmetrically along with the adjoining regions of the brain (Boorman & Shimeld 2002). However, the first molecular sign of asymmetry is much earlier in development at the mid to late tailbud stage, when *Ci-Nodal* and *Ci-Pitx* are expressed asymmetrically in the left head mesoderm and throughout the left sided ectoderm but not in the dorsal and ventral midline cells (Boorman & Shimeld 2002). This expression precedes the first morphological signs of left-right asymmetry, which is seen in the development of vertebrate left-right asymmetry.

Research in *Ciona intestinalis* left-right asymmetry establishment has focused on the role of ion flux, a mechanism discovered in *Xenopus* (Levin et al. 2002) (described in Chapter 1). Drug inhibitor work has demonstrated that *Ciona intestinalis* embryos exposed to Omeprazole, which blocks H^+/K^+-ATPase, relatively late during development display disrupted *Ci-Pitx* expression (Shimeld & Levin 2006). Although H^+/K^+-ATPase channels are important in *Ciona intestinalis* asymmetrical development it has been demonstrated in other vertebrate species, *Xenopus* and zebrafish, that nodal flow and H^+/K^+-ATPase are both important for normal laterality development.

Although, H^+/K^+-ATPase channels are known to affect left-right asymmetry in the *Ciona intestinalis* embryo it is still unknown if they also have motile cilia on the ectoderm of the embryo

which could generate a flow within the chorion. This research will focus on whether there is a structure akin to the node present on the developing *Ciona intestinalis* embryo and whether there are cilia present on the embryo at a time consistent with a role in the development of left-right asymmetry. The presence of cilia on the embryo prior to asymmetric gene expression would indicate that there is a potential role for cilia in the establishment of left-right asymmetry external to the vertebrates, in their closest living relative.

Here I show that there are cilia present on the ectoderm of the *Ciona intestinalis* embryo although they are not confined to a node like structure but emanate from every cell of the surface ectoderm. They emerge for a brief period of time at the end of neurulation and the beginning of the tailbud stage but are lost by the mid-tailbud stage when asymmetric gene expression is first observed. The presence of cilia led to experiments to assess the structure of these cilia to see if they have the same structure as nodal cilia on the mouse embryo. It is shown that the *Ciona intestinalis* cilia are a 9+0 structure without dynein arms or radial spokes but there is progressive collapse of the ring structure along the length of the axoneme, a finding common with the non-node cilia of the mouse gastrula embryo. These results indicate that if these cilia have a role in the establishment of left-right asymmetry, it is not an identical role to those of the mouse ventral node.

3.2 RESULTS

3.2.1 Morphology of the mouse node

Characterisation of the mouse ventral node morphology and the monocilia that populate the node have been intensively studied through the use of Scanning Electron Microscopy (SEM)

(Lee & Anderson, 2008; Sulik et al., 1994). In order to analyse mechanisms involved in the establishment of left-right asymmetry in the invertebrate species, *Ciona intestinalis*, SEM of the whole ectoderm surface of mouse embryo at gastrulation prior to molecular asymmetries was reviewed. Initial mouse SEM experiments focused on the ventral node pit region before the rest of the surface was surveyed for microtubule structures. 7.0 d.p.c mice embryos were dissected, the Reichart's membrane removed, fixed to preserve microtubule structures and viewed in a JEOL JSM 6390 SEM.

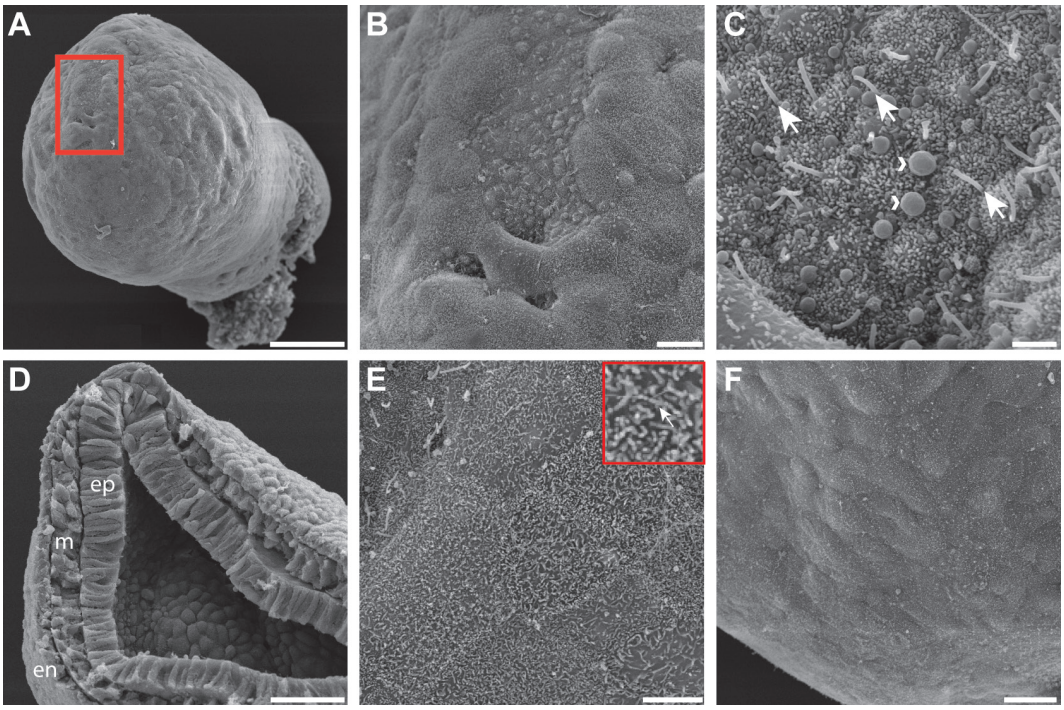


Figure 3.1: Morphology of the mouse ventral node and surrounding endoderm at the Theiler stage 10 (7.0 d.p.c).

A: SEM image of the apex of the egg cylinder with the visceral yolk sac and Reichart's membrane have been removed. The node is outlined by a red box. **B**: Higher magnification of the node. The cells in the node have a smaller ventral surface area. The outer epithelium still covers parts of the node. **C**: Higher magnification of the exposed node area with cilia projections (arrows) and vesicles (arrowheads). **D**: Cross-section of the mouse epithelia cells on a gastrula embryo showing the three cell layers. E: High magnification of microvilli on the epithelia of the embryo (arrows in inset). **F**: Image of the large, flat cells of the epithelium. ep = epiblast, m = mesoderm and en = endoderm.
Bar = 100µm (A); bar = 50µm (D); bar = 25 µm (F); bar = 10µm (B); bar = 5µm (E); bar = 2µm (C).

In all the wild-type embryos analysed, a concave, oblong shaped area with cilial projections was located at the rostral end of the primitive streak (Fig. 3.1A, B, C), known as the mouse ventral node. The pit was approximately 40 μm in width and 70 μm, in length which is fractionally smaller than the size of the mature node, 50-60 μm wide and 70-90 μm long, observed by (Sulik et al. 1994; Yamanaka et al. 2007). The ciliated region had one cilium projection per cell of approximately 2-3 μm in length (Fig. 3.1C, arrows point to cilia) which is consistent with previous analyses of the node (Jurand 1974; Sulik et al. 1994). The ciliated region was covered by endodermal 'bridges' which appear to move to expose the underlying cells, and 1-1.5 μm vesicles populated the pit (Fig. 3.1C, arrowheads). At this stage cilia are unlikely to generate a leftward flow as it is too early in development and the node is not fully mature with areas still covered by the endodermal sheet. The mesodermal cells outside the mouse ventral node region have an increased apical surface which makes them larger and flatter than the node cells. All the cells on the surface of the embryo were covered in thousands of microvilli (Fig. 3.1E, F). No cilia were observed on the non-node cells by SEM, but they could be present but not detected due to their small size and the number of microvilli.

3.2.2 Structure of mouse gastrula stage ectoderm cilia

Cilia were not observed on the surface of the mouse embryos analysed using SEM, except in the mouse ventral node, but their small size and the number and size of microvilli could camouflage the cilia. To search for cilia within the microvilli, thin sections of the mouse embryo were cut and viewed on a FEI Technai Transmission Electron Microscope (TEM). Each section was examined for the presence of cilia and those found were photographed. All images are independent and are

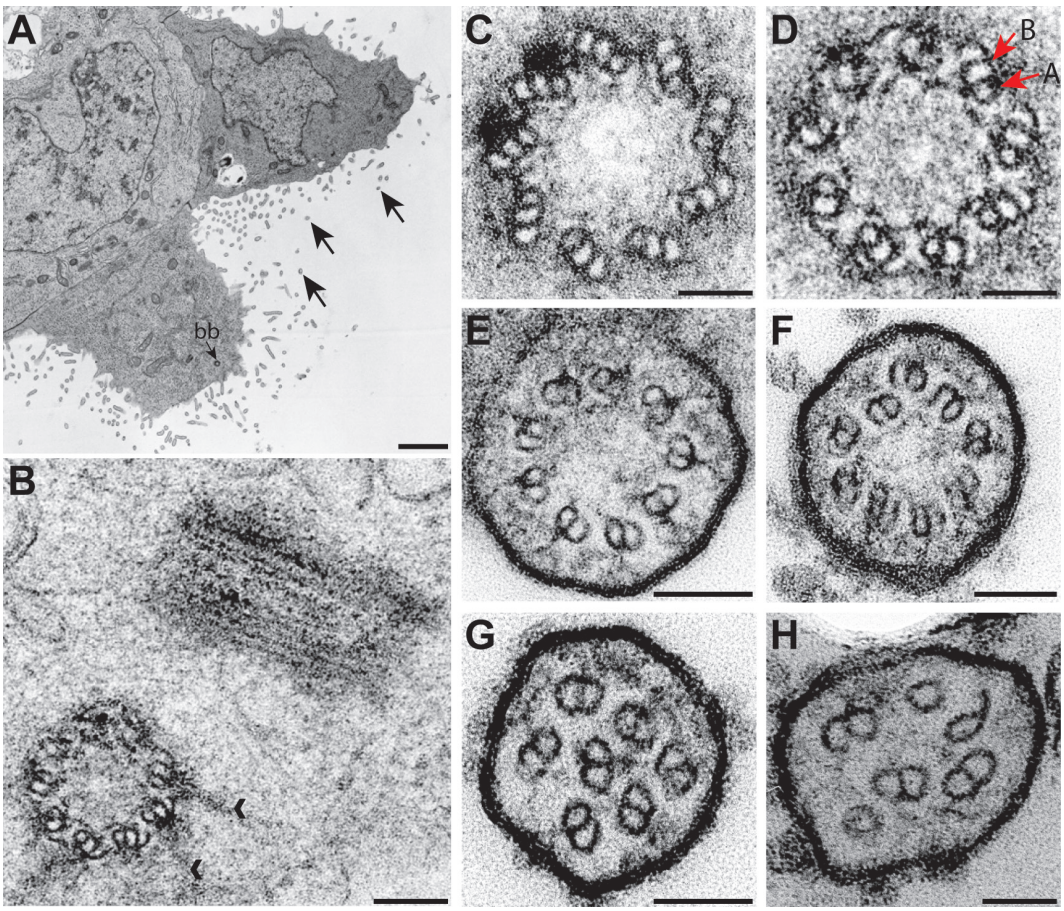


Figure 3.2: The disroganised ultrastucture axoneme arrangement of cilia on the surface of the Theiler stage 10 (7.5 d.p.c.) 3 somite mouse embryo.

A: TEM of the suspected mouse node with lots of microvilli (arrows) and a basal body (bb) within a cell of the endoderm. **B**: Basal body and daughter centriole with projections (arrowheads). **C**: Triplet basal body. **D**: Triplet to doublet basal body with links between microtubule A and microtuble C (red arrows). **E**: Transition zone as the cilium exits the cell with doublet microtubules. **F**: Doublet microtubules of a cilium outisde the cell with a collapsed axoneme. **G**: Collapse of the 9 doublet ring structure. **H**: A cilium with both doublet and singlet microtubules.
Bar = 2µm (A); bar = 0.1µm (B, C, D, E, F, G, H)

not serial sections of a cilium.

The mouse embryo was covered in large microvilli (Fig. 3.2A, large arrows). The basal body of cilia in the epithelium of a mouse embryo at 3 somite stage had a canonical nine triplet microtubule arrangement (Fig. 3.2C). As the triplets became doublets they appeared to be linked on both the inner (microtubule A to microtubule C) and outer doublet (*n*=8) (Fig 3.2D, red arrows). Projections radiated from the cilium to the surrounding tissue and on some occasions a longitudinal section of a daughter centriole was present nearby (*n*=6) (Fig. 3.2B, arrowheads).

In the transition zone, the doublets were arranged in a nine ring with small projections from the centre of the two microtubules to the outer membrane of the cilium (Fig. 3.2E). The transition zone of the cilium was observed as the cilium was exiting the cell and once the cilium was had exited the cell cytoplasm the nine doublet ring structure collapsed. The number of doublets within the cilium decreased from nine to seven or eight and even as few as three with some partial microtubule structures (*n*=43/45), towards the distal end of the cilium, suggesting progressive collapse. Singlet microtubules were observed in sections close to the ciliary tip (*n*=11/45) (Fig 3.2H). A central pair, a characteristic of almost all motile cilia, was not observed in any cilium viewed (*n*=0/54). No additional structures, such as radial spokes or dynein arms, were observed on any surface cilia (Fig. 3.2G, F, H).

3.2.3 Early *Ciona intestinalis* development

3.2.3.1 Early *Ciona intestinalis* embryos

SEM has been a valuable tool to study the surface of a developing mouse embryo in search of microtubule structures that have a role in the determination of laterality (Sulik et al. 1994). This experiment utilised the same method to examine the external surface of *Ciona intestinalis* embryos at different stages of development for microtubule structures. The stages of development were categorised for consistency (Fig. 3.3). Embryos were harvested hourly, fixed and viewed in a JEOL JSM 6390 SEM. Embryos were fixed in a glutaraldehyde and paraformaldehyde (PFA) fixative to preserve microtubule structures on the cell surfaces of the embryos. Sucrose was added to preserve osmotic balance when embryos were transferred from their sea water environment to the fixative. This method has shown that early 8-16 cell embryos (Fig. 3.4) are

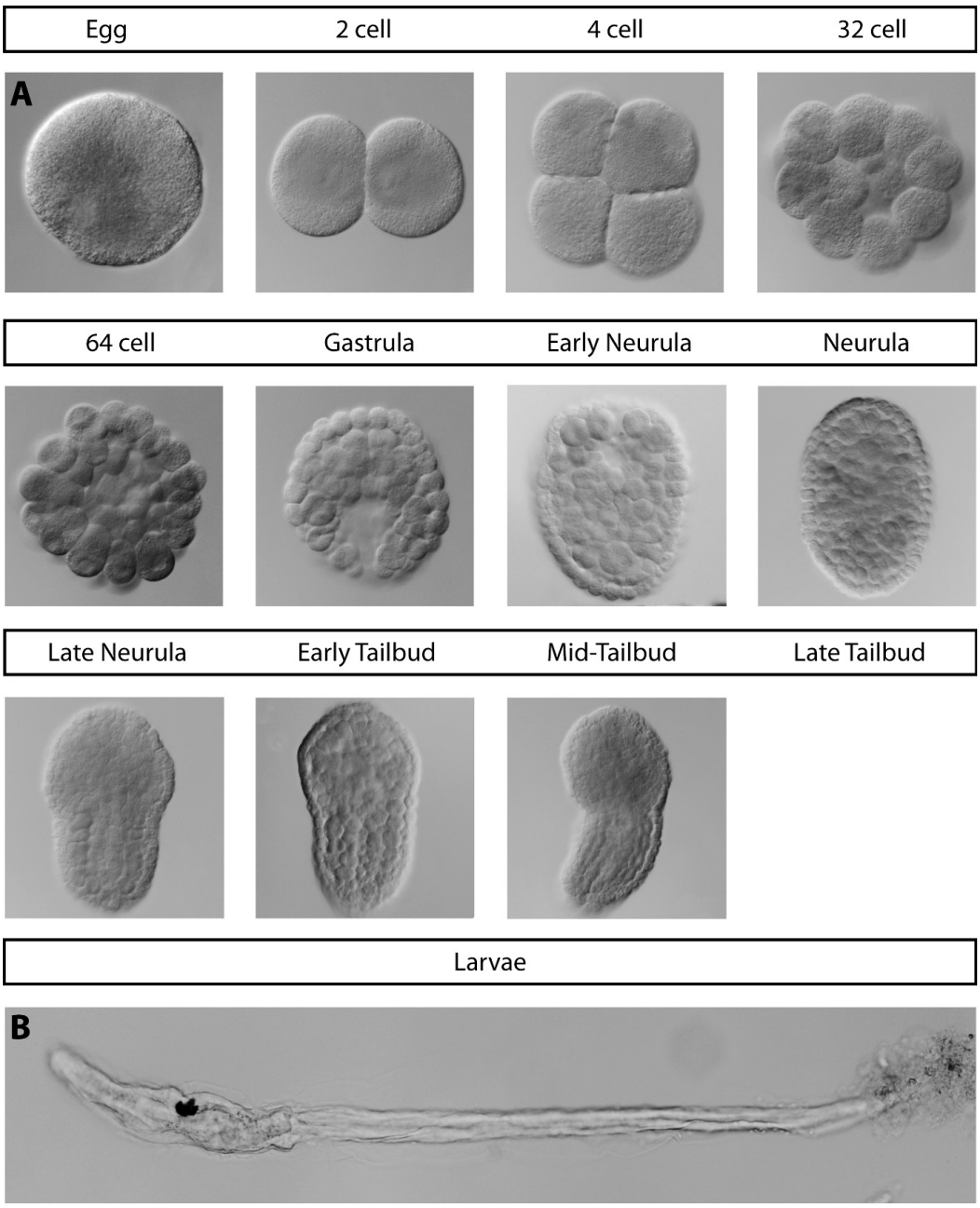


Figure 3.3: Early *Ciona intestinalis* development.

A: The Early development of a *Ciona intestinalis* embryo from oocyte to mid tailbud. **B**: A hatched larvae.

covered in microvilli projections (arrows) (Fig. 3.4B, arrows) which emanated from a rough, crinkled cell surface. The projections varied in length from less than 1.0 μm to 1.5 μm. Thin, long projections, up to 8.5 μm in length, were present between some cells of the developing embryo. This embryo was undergoing cleavage from an early 8-16 cell embryo with a defined cleavage furrow (asterisk) (Fig. 3.4A). In later 8-16 cell embryos (Fig. 3.5A) the surface still

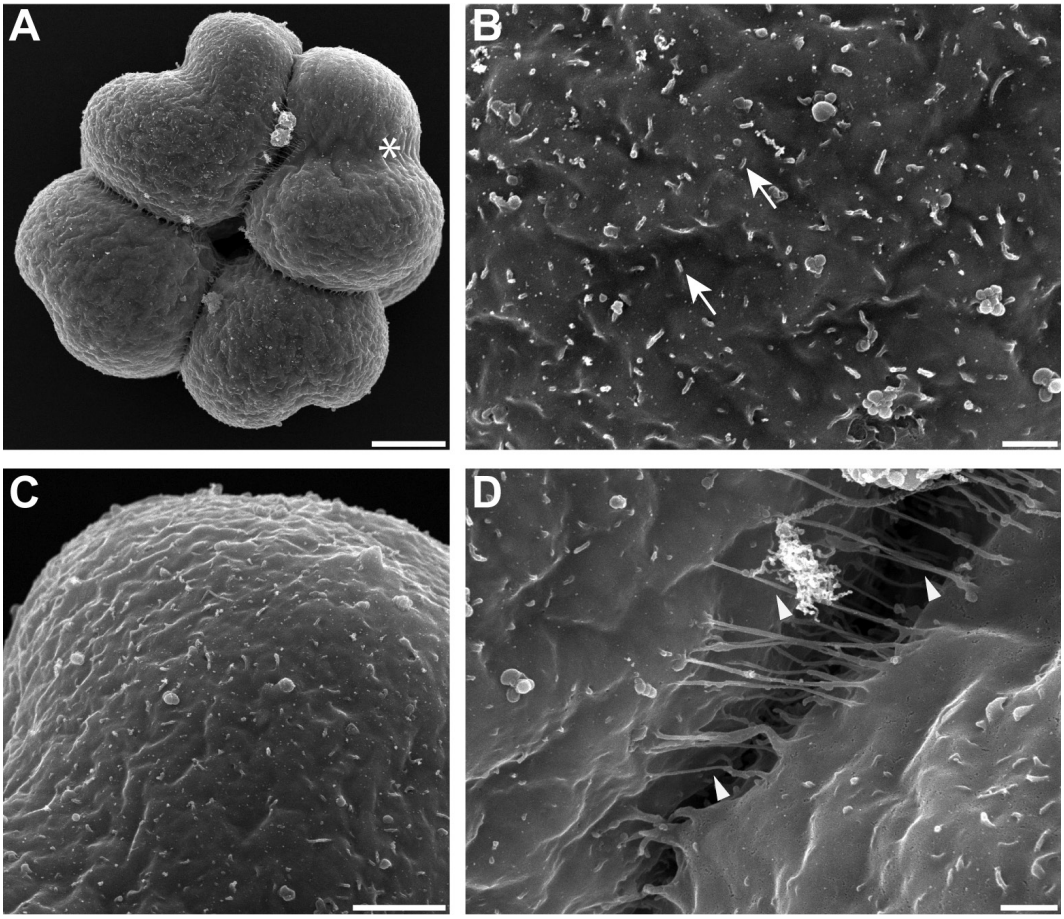


Figure 3.4: The surface texture and microvilli structures of an early 8-16 cell *Ciona intestinalis* embryo.

A: SEM image of an embryo at the early 8-16cell stage with the chorion removed. The embryo is undergoing cleavage from a 8 to 16 cell embryo. The cleavage furrow is depicted by an asterisk. **B**, **C**: Higher magnification of the cell surface of the developing embryo. The surface appears crinkled and microvilli are present (arrows). **D**: Higher magnification of the area between individual cells. Thin projections are present between some cells (block arrows).
Bar = 20μm (A); bar = 5μm (C); bar = 2μm (B, D)

appeared crinkled and covered in microvilli (arrows) (Fig. 3.5B). Projections were seen between cells with some as long as 12 μm (Fig. 3.5D). Dividing cells were covered in microvilli and had deep furrows which interlocked (Fig. 3.5C).

32 cell, 44 cell and 110 cell embryos (Fig. 3.6) had a much smoother cell surface and there was an absence of microvilli seen in earlier embryos (Fig. 3.6A-F). These embryos had no evidence of cells undergoing division and the gastrula embryo (Fig. 3.6G, H) had crinkled surface texture. As seen in earlier embryos, projections were observed between cells of the 32 cell embryo (arrowhead) (Fig 3.6B) but not in any of the other embryos. The remains of the chorion could

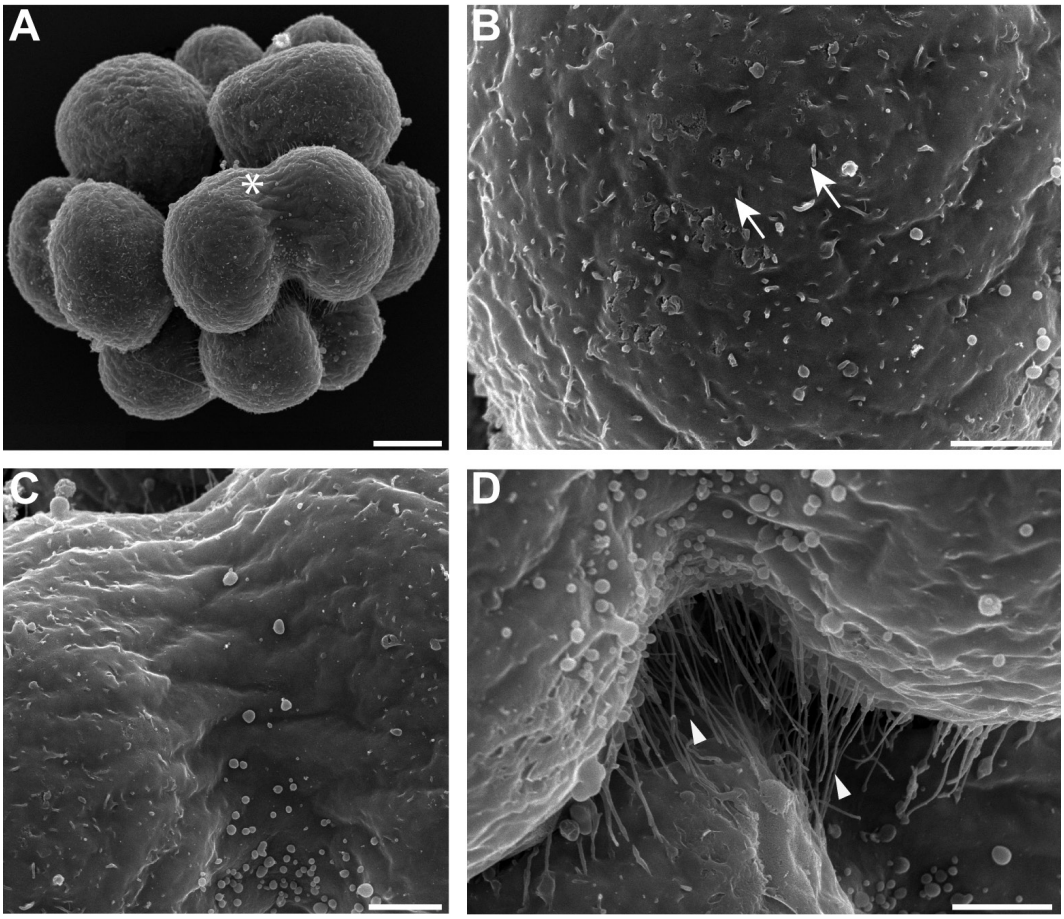


Figure 3.5: The surface texture and microvilli structures of a late 8-16 cell *Ciona intestinalis* embryo.

A: SEM image of an embryo at the late 8-16 stage with the chorion removed. The cleavage furrow is depicted by an asterisk. **B**: Higher magnification of the cell surface of the developing embryo. The surface appears crinkled and microvilli are present (arrows). **C**: A closer image of a dividing cell with furrows on the embryo. **D**: Higher magnification of the area between individual cells. Thin projections are present between some cells (block arrows).
Bar = 20μm (A); bar = 5μm (B, C, D)

still be seen to the top left of the image as well as some residual chorion and test cells on the surface of the gastrula embryo (Fig. 3.6G).

3.2.3.2 Late *Ciona intestinalis* embryos

The early neurula stage embryo (Fig. 3.7A) was still in the process of neurulation with six cells not joined leaving a large cranial neuropore. The cells of the embryo were smooth around the neuropore and showed no sign of cilia or projections. Anterior to the neuropore the cells were crinkled, similar to the early cleavage stage embryos (Fig. 3.7D) but this phenomenon appeared

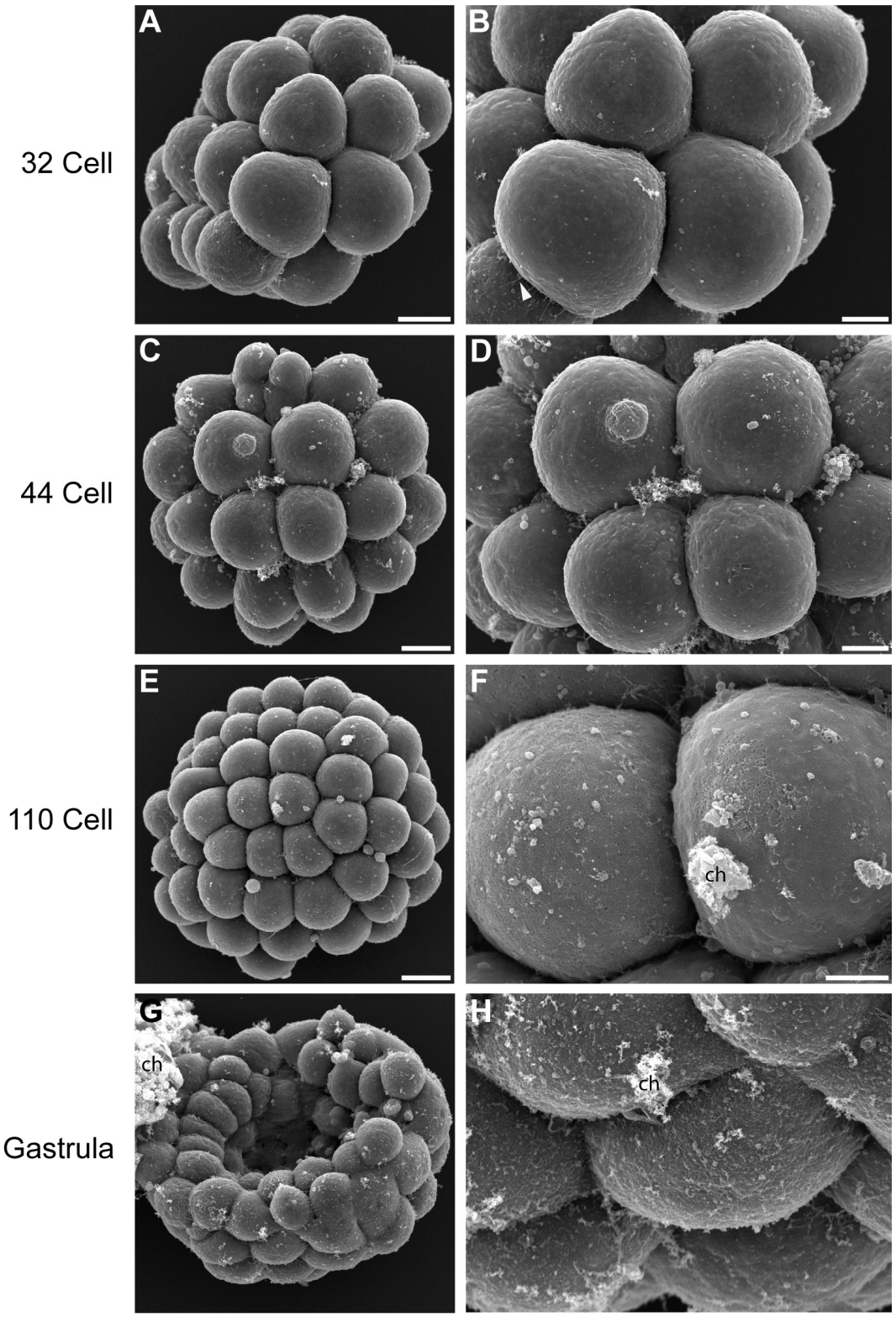


Figure 3.6: The surface texture and structures of 32 cell stage to gastrula stage *Ciona intestinalis* embryos.

A, **C**, **E**, **G**: SEM images of 32 cell, 44 cell, 110 cell and gastrula embryos with the chorion removed. **B**, **D**, **F**, **H**: Higher magnification of cells of the embryo with a smooth surfaces. **B**: Small, thin projections can be seen between some cells of the embryo (block arrows). Some chorion (ch) debris remains on the cells of the 110 cell and gastrula embryo.
Bar = 20µm (A, C, E, G); bar = 10µm (B, D); bar = 5µm (F, H)

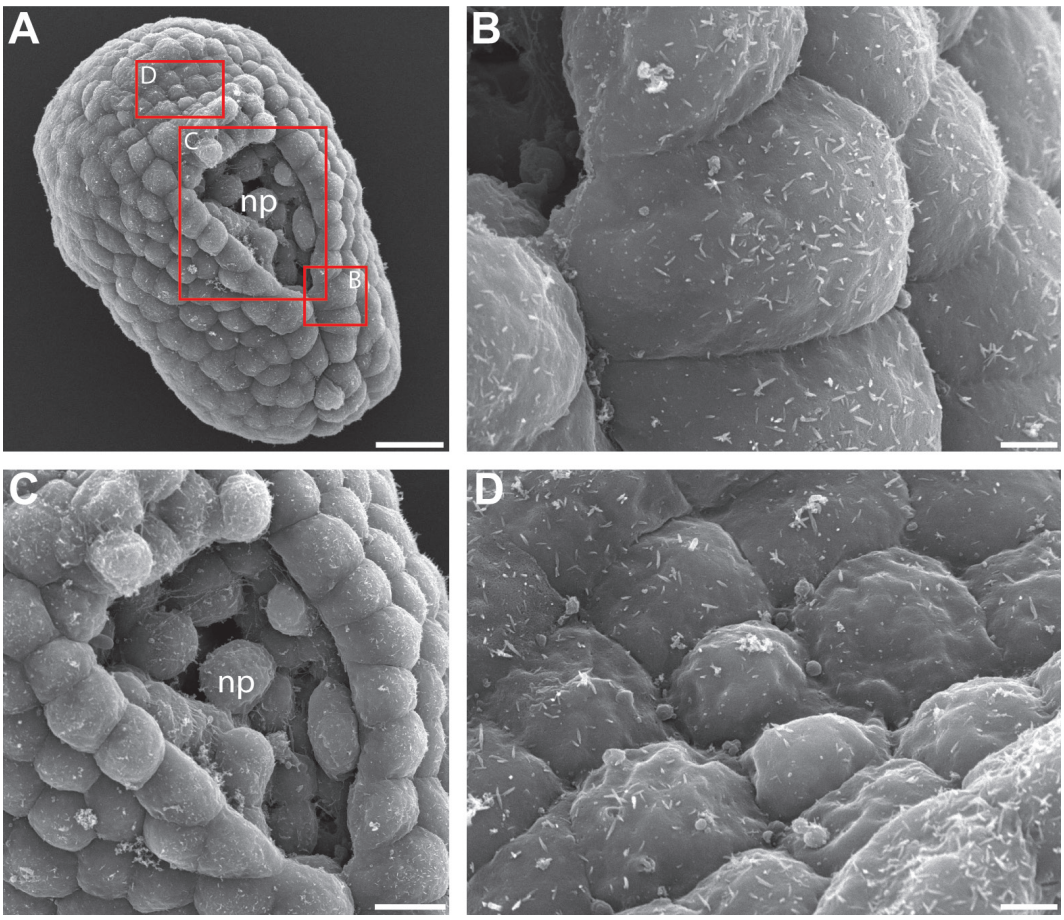


Figure 3.7: The surface texture and morphology of a neurula *Ciona intestinalis* embryo.

A: An SEM image of an embryo at the neurula stage with the chorion removed. **B**, **D**: Higher magnification of the crinkled surface of the developing embryo. **C**: The embryo is undergoing neuropore (np) closure and cells inside the embryo can be seen. **D**: A high magnification image of the cells anterior to the neuropore. Bar = 20µm (A); bar = 10µm (C); bar = 2µm (B, D)

to be restricted to this one region. Due to the de-chorionation process some residual pieces of chorion and test cells remain on the cells but should not be confused with microvilli (Fig. 3.7B).

At the tailbud stage of *Ciona intestinalis* development, the cell surface was smooth and the chorion sufficiently removed to have a clear view of the embryo (Fig. 3.8). By the late neurula stage the neuropore had further closed and a difference between the anterior and posterior region was more pronounced. At the early tailbud stage the posterior region of the embryo had begun to lengthen and bend to generate an early tailbud and the anterior region of the embryo had expanded ventrally to create a head region. On both the late neurula and early tailbud stage

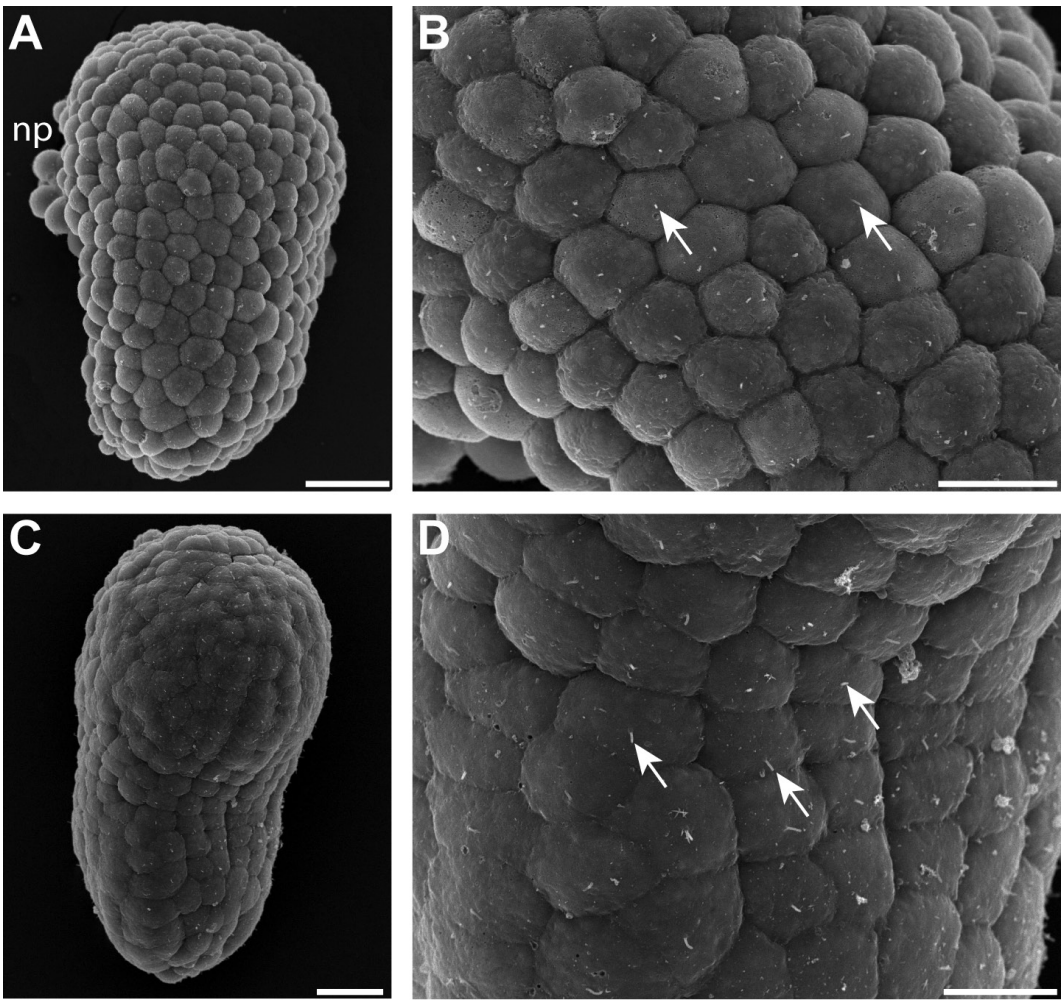


Figure 3.8: The presence of cilia on the tailbud stage *Ciona intestinalis* embryos.

A: SEM image of the right lateral side of an early tailbud embryo with the chorion removed. **B**: Higher magnification shows cilia projecting from the cells of the embryo. There is one cilium per cell (arrows). **C**: SEM image of a left lateral side of a tailbud embryo with chorion removed. **D**: One cilium projects from each cell (arrows). np = neuropore.
Bar = 20μm (A, C); bar = 10μm (B, D)

embryos the cells of the ectoderm all possessed a single cilium projection from their apical surface (arrows) (*n*=54). The cilia were 1.5 μm to 2 μm in length and appeared to emanate from the posterior of each cell (Fig. 3.8D). The apical surface of each cell was domed so the cilia project posteriorly (Further explained in Chapter 4).

At the mid tailbud stage the posterior tail bud had bent ventrally (Fig. 3.9A) and begun to curl around to the head region by the late tailbud stage (Fig. 3.9G). The cells were small (5 μm) and did not possess any cilia projections (*n*=21) (Fig. 3.9B, D, F, H). Cilia were not observed on

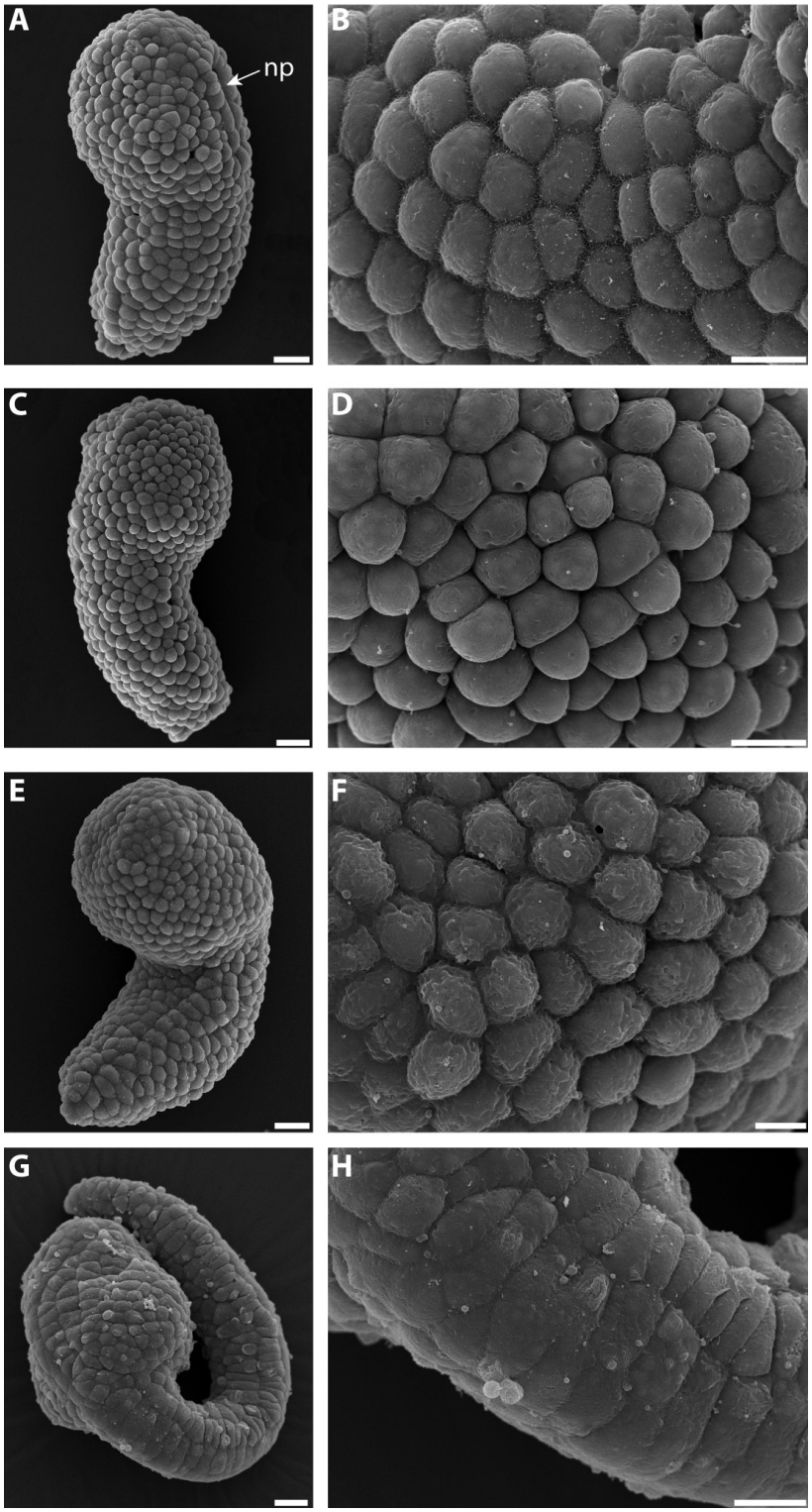


Figure 3.9: The surface texture and morphology of late tailbud stage *Ciona intestinalis* embryos.

A,**C**,**E**,**G**: SEM image of tailbud embryos with the chorion removed. **B**,**D**,**F**,**H**: Higher magnification shows an absence of cilia projecting from the cells of the embryo. **H**: A high magnification image of a late tailbud stage embryo with rectangular cells on the dorsal side. np = neuropore.
Bar = 20 µm (A, C, E, G): bar = 10 µm (B, D, H); bar = 5 µm (F)

any of the cells of the embryos in any embryo region. There was also no evidence of projections between the cells of the embryo. By the late tailbud stage the neuropore had completely closed and the cell shape changed from round to rectangular (Fig. 3.9H).

3.2.3.3 Anti-acetylated α-tubulin staining of embryos

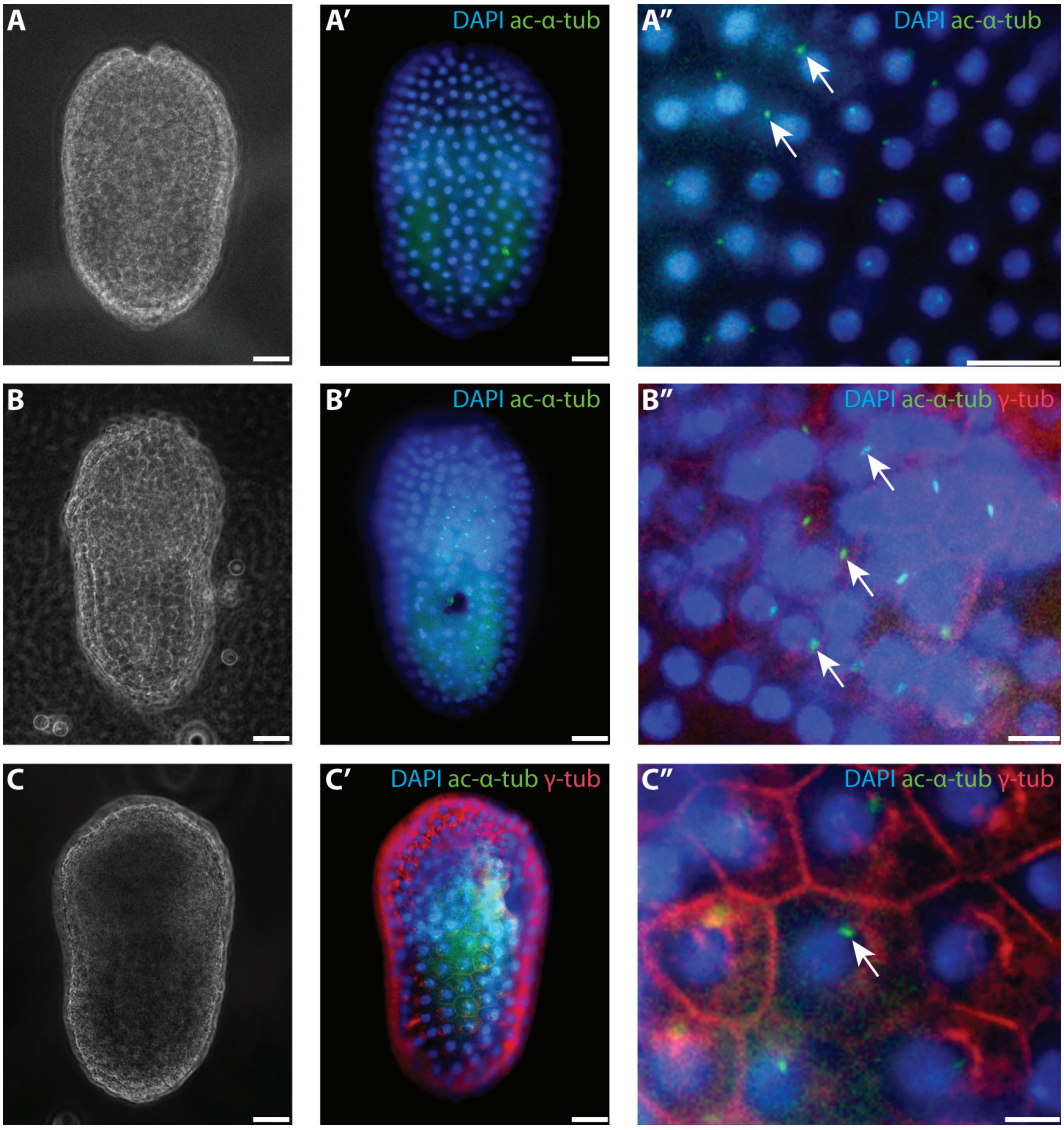


Figure 3.10: The presence of cilia on the tailbud stage *Ciona intestinalis* embryo through immunofluorescence and DAPI staining

A, **B**, **C**: A dark-field image of tailbud *Ciona intestinalis* embryos. **A'**, **B'**, **C'**: Staining of Tailbud *Ciona intestinalis* embryos showing primary cilia (white arrows), visualised using anti-acetylated α-tubulin (green) (centre and right columns). γ-tubulin staining (red) is focused at the cell boundaries. Full colour merged images including the cell nuclei (visualised with DAPI, a fluorescent stain which binds to DNA) are shown in B'', C', C''. Bar = 20 μm (A, A', B, B', C, C'); bar = 10 μm (A''); bar = 5 μm (B''); bar = 2 μm (C'').

SEM had shown cilia-like projections at the late neurula/early tailbud stage of embryogenesis but immunological staining was required to confirm that the projections were cilia. Late neurula and tailbud stage *Ciona intestinalis* embryos were stained with anti-acetylated α-tubulin, a marker for cilia, γ-tubulin, a basal body marker and DAPI which stains cell nuclei (Fig. 3.10). Anti-acetylated α-tubulin, a cilia marker (green) indicated one cilium per nuclei (demonstrated with DAPI (blue)) on neurula and tailbud embryos (*n*=9) (Fig. 3.10A-C") which measured 1.5 μm in length. γ-tubulin, a basal body marker (red) was expressed at the cell boundaries on the ectoderm and revealed that only one cilium was present within each boundary indicating there is only one cilium per cell (Fig. 3.10C") Focusing through the embryo showed that anti-acetylated α-tubulin staining was only found around the periphery of the embryo. Cilia were only found universally on the ectoderm of the embryo with no evidence of internal cilia. The cilia were located at the posterior of each cell as previously shown by SEM.

The timing of ciliogenesis and the presence of cilia on the *Ciona intestinalis* embryo is consistent with a role for cilia in the establishment of left-right asymmetry because it immediately precedes and overlaps with the establishment of asymmetric gene expression (Fig. 3.11).

3.2.4 Transmission Electron Microscopy of *Ciona intestinalis* neurula stage embryos

3.2.4.1 Transmission Electron Microscopy of neurula *Ciona intestinalis* embryos

Immunofluorescence experiments have demonstrated that the projections observed on the ectoderm of late neurula and early tailbud *Ciona intestinalis* embryos were microtubule cilia structures. Cilia are generally grouped into two types; motile and immotile, through analysis of

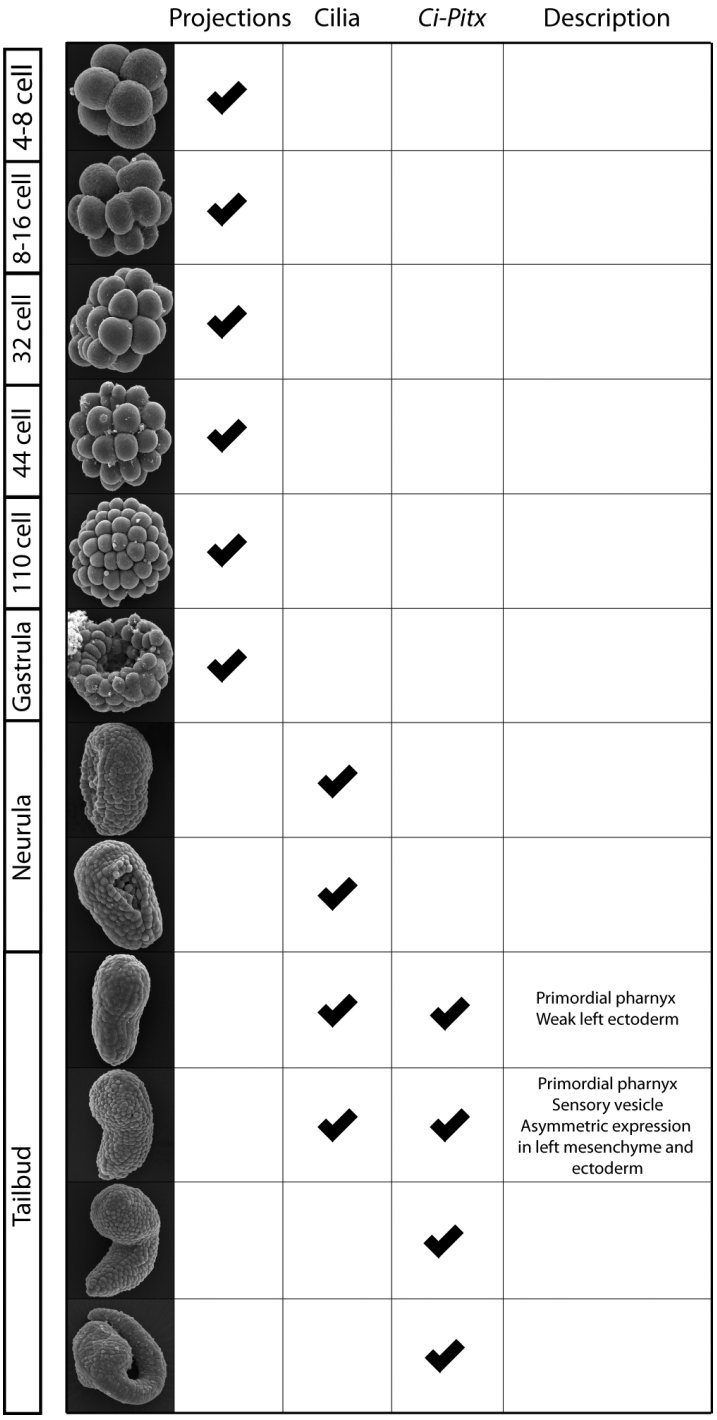


Figure 3.11: A summary of the results from SEM and immunolocalisation in early *Ciona intestinalis* embryogenesis.

A tick chart to summarise the results observed in SEM analyses, at specific stages of *Ciona intestinalis* embryo development, combined with previous *in situ* hybridisation experiments (Boorman and Shimeld 2002).

their ultrastructure by Transmission Electron Microscopy (TEM). TEM was used here to assess the ultrastructure of *Ciona intestinalis* embryo cilia to try and place the cilia into one of these

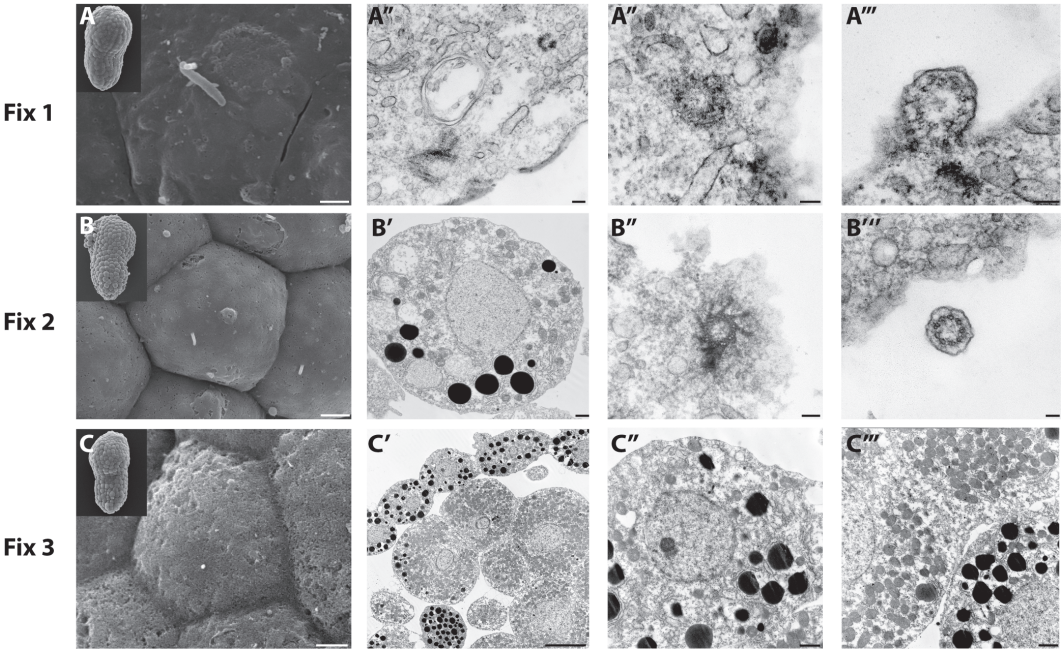


Figure 3.12: Experimentation with different TEM fixes on neurula stage *Ciona intestinalis* embryo showed Fix 2 as the optimum fixation for preservation of membranes and organelles.

Ciona intestinalis neurula embryos imaged through SEM (left column) and TEM (right-hand columns) to optimise the fixation. **A**: Fix 1 (2.5% glutaraldehyde, 2% paraformaldehyde in 100 mM cacodylate buffer (pH 7.0) with 1 mM EGTA and 2 mM $MgCl_2$, 200mM sucrose and picric acid). **B**: Fix 2 (2.5% glutaraldehyde, 200mM cacodylate buffer and 1.6% NaCl). **C**: Fix 3 (2.5% glutaraldehyde, 2% paraformaldehyde in 100 mM cacodylate buffer (pH 7.0) with 1 mM EGTA and 2 mM $MgCl_2$, picric acid,100mM Sucrose and 0.8% NaCl) Bar = 10 µm (C'); bar = 2 m (C, B); bar = 1 µm (A, B′, C″, C‴); bar = 100 nm (A′, A″, A‴, B″, B‴)

two groups and therefore, understand more about their role in development. Embryos in the initial TEM experiments on the structure of *Ciona intestinalis* tailbud cilia were fixed in the same fixative used in the SEM experiments (2.5% glutaraldehyde, 2% paraformaldehyde in 100 mM cacodylate buffer (pH 7.0) with 1mM ethylene glycol tetraacetic acid (EGTA) and 2mM $MgCl_2$, 0.01% picric acid and 200mM sucrose) (Fig 3.12A). Embryos were embedded in resin, sectioned and then observed on a FEI Technai TEM. Cell composition, internal structures and cilia were assessed and analysed to determine the quality of the embryo fixation. Basal body (Fig. 3.12A") and cilia (Fig. 3.12A‴) structures were clear and the cytoplasm dense but the clarity of organelle and cell membranes was unclear (Fig. 3.12A').

To enhance the membrane clarity a fixative used previously on another ascidian, *Botryllus*

schlosseri (Degasperi et al. 2009) was used (2.5% glutaraldehyde, 200mM cacodylate buffer (pH 7.2) and 1.6% NaCl). To check that microtubule structures were not damaged by the new fixative, the presence of cilia was tested using SEM which showed identical results to SEM experiments using the previously described fixative (Fig. 3.12B). On the late neurula/early tailbud embryos one cilium was observed at the posterior of each cell, at a length of 1.5-2 μm (Fig. 3.12B), which showed that microtubule structures were preserved in the different fixative. TEM was conducted on the embryos fixed with the 1.6% NaCl fixative and the clarity of the membranes assessed. The basal body (Fig. 3.12B") and cilia (Fig. 3.12B"') structures were clear and not disrupted but the density of the cytoplasm was low in comparison to the first fixative (Fig. 3.12B').

To maintain membrane clarity and cilia structure but increase cytoplasm density, so information was not lost, a mixture of the previous fixatives was used. Embryos were fixed in a third fixative (2.5% glutaraldehyde, 200mM sodium cacodylate, 0.8% NaCl and 100mM sucrose) and presence of microtubules tested through SEM (Fig. 3.12C). Cilia were observed on all the ectoderm cells of neurula and tailbud embryos and were the length observed previously (Fig. 3.12C). TEM analysis showed disorganised cytoplasm and broken membranes (Fig. 3.12C", C"'). Cilia were not analysed as problems with the cytoplasm and membrane fixation renders this untenable. It was therefore concluded that the best fixative for *Ciona intestinalis* neurula/tailbud TEM was fixative two (2.5% glutaraldehyde, 200mM cacodylate buffer (pH 7.2) and 1.6% NaCl) and would be used for further TEM experiments.

3.2.4.2 The ultrastructure of *Ciona intestinalis* neurula stage cilia

Ciona intestinalis embryos were grown in FSW, de-chorionated, fixed in fixative 2 (as described above) and 70 nm thick serial sections cut to analyse the ultrastructure of late neurula/early

tailbud cilia along the whole length of each cilium (*n*=76). As observed through SEM, one cilium emanates from each cell with no instances of multiple cilia emerging from one cell. The basal body of the cilium was found within the cytoplasm of the cell and has nine triplet microtubules with transitional fibres extending into the cell cytoplasm. A nine doublet microtubule ring with connections between the microtubule doublets and the ciliary membrane, indicative of the transition zone were observed as the cilium exited the cell. These connections were only observed in 140 nm length of the cilium at the point along the axoneme when it leaves the cell and extends into the external environment. Immediately after the cilium has exited the cell the axoneme had a nine doublet ring structure with no evidence of a central pair, dynein arms or radial spokes but within 70 nm of this the nine doublet microtubules were no longer in a ring. Towards the distal tip of the cilium the doublet microtubules became more disorganised and the doublets became singlet microtubules (Fig. 3.13). The outer nine doublet microtubules first showed evidence of a loss of doublet structure ~210 nm after the cilium has exited the cell (*n*=9) (Fig 3.14 and 3.16). At the most distal tip of the cilium the microtubules were no longer present but were replaced by a dense region (*n*=4).

Without an anchor or reference point there is no way of confirming if a particular MT doublet leads the disorganisation as discussed in *Leishmania mexicana* (Gluenz et al. 2010). The disorganised doublet microtubule structure was also observed in longitudinal cilia (Fig 3.15A) with microtubules not parallel to the cilia membrane. On all the cilia recorded (cilia *n*=76) axoneme accessories required for motility were not observed including no evidence of a central pair, radial spokes or connections between doublets. In two cilia analysed there was a singlet microtubule in the centre of nine doublet microtubules which persisted for ~210 nm. One

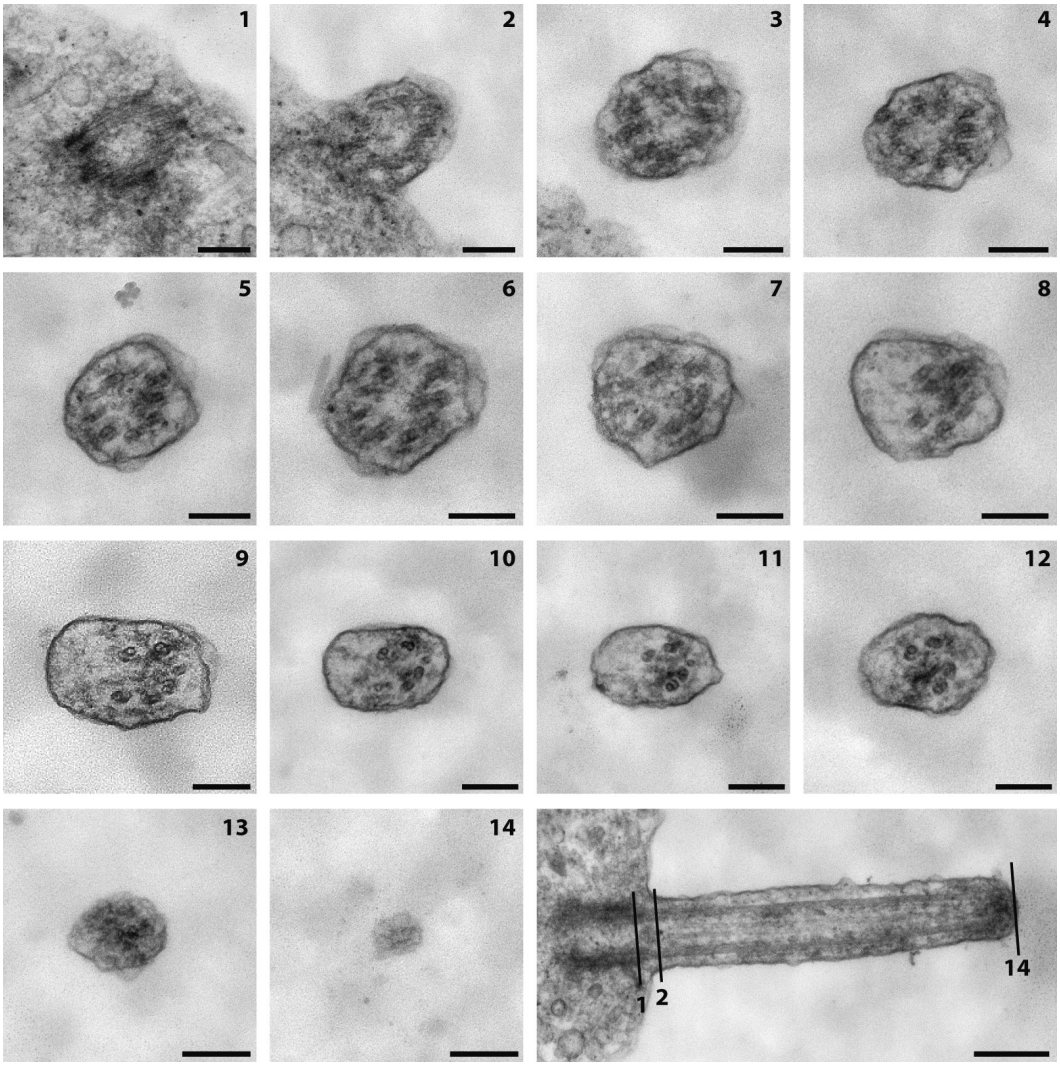


Figure 3.13: The ultrastructure of a *Ciona intestinalis* neurula embryo cilium showing the collapsed doublet microtubule organisation.

The ultrastructure of a cilium from a neurula stage embryo from the basal body (1) through the transition zone (2) to the distal tip (14). Microtubule doublets are not positioned in a ring structure but become disorganised as the sections move towards the distal tip of the cilium. The cilium near the tip does not have the full complement of nine doublet microtubules. Numbers indicate adjacent serial sections along a *Ciona intestinalis* neurula stage embryo cilium. The longitudinal cilium shows the equivalent location of each section along the cilium.
Bar = 200 nm (1-12); bar = 100 nm (13-14 and longitudinal)

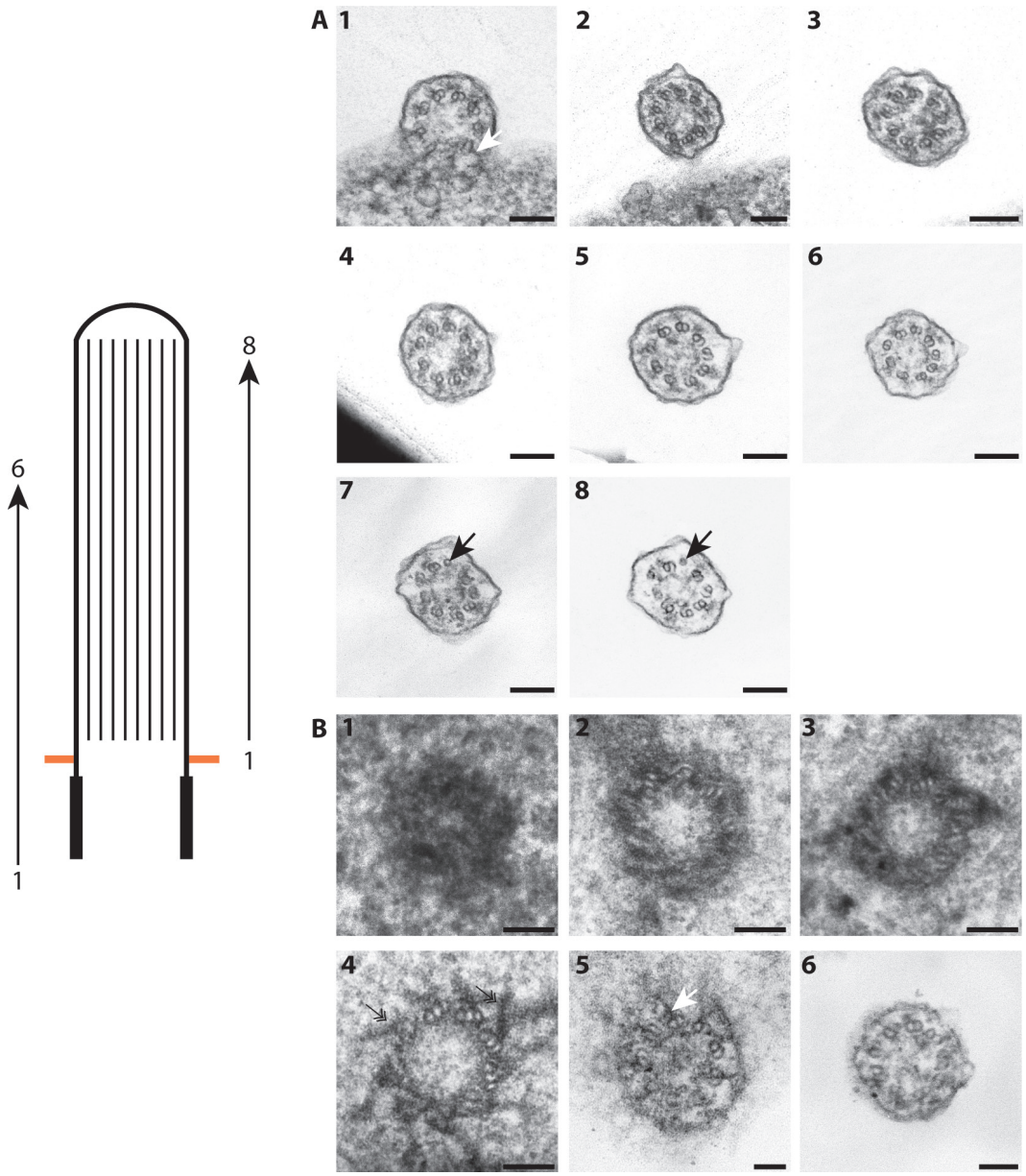


Figure 3.14: The ultrastructure of cilia on a neurula stage *Ciona intestinalis* embryo shows the disintegration of doublet microtubule organisation.

A: Serial sections of a neurula stage embryo from the transition zone (1) towards the distal tip of the axoneme (8). Doublet microtubules taper towards the centre of the axoneme and some doublets turn to singlets near the distal tip (arrow). **B**: The ultrastructure of a cilium from basal body (1) to the cilium axoneme (6). The basal body has the standard triplet microtubule organisation with transition fibres (double arrows) emanating from the triplets. The transition zone has nine doublet microtubules which are attached to the membrane through projections (white arrow). The cilium once it has exited from the cell has nine doublet microtubules in a ring structure.
Bar = 100 nm (All)

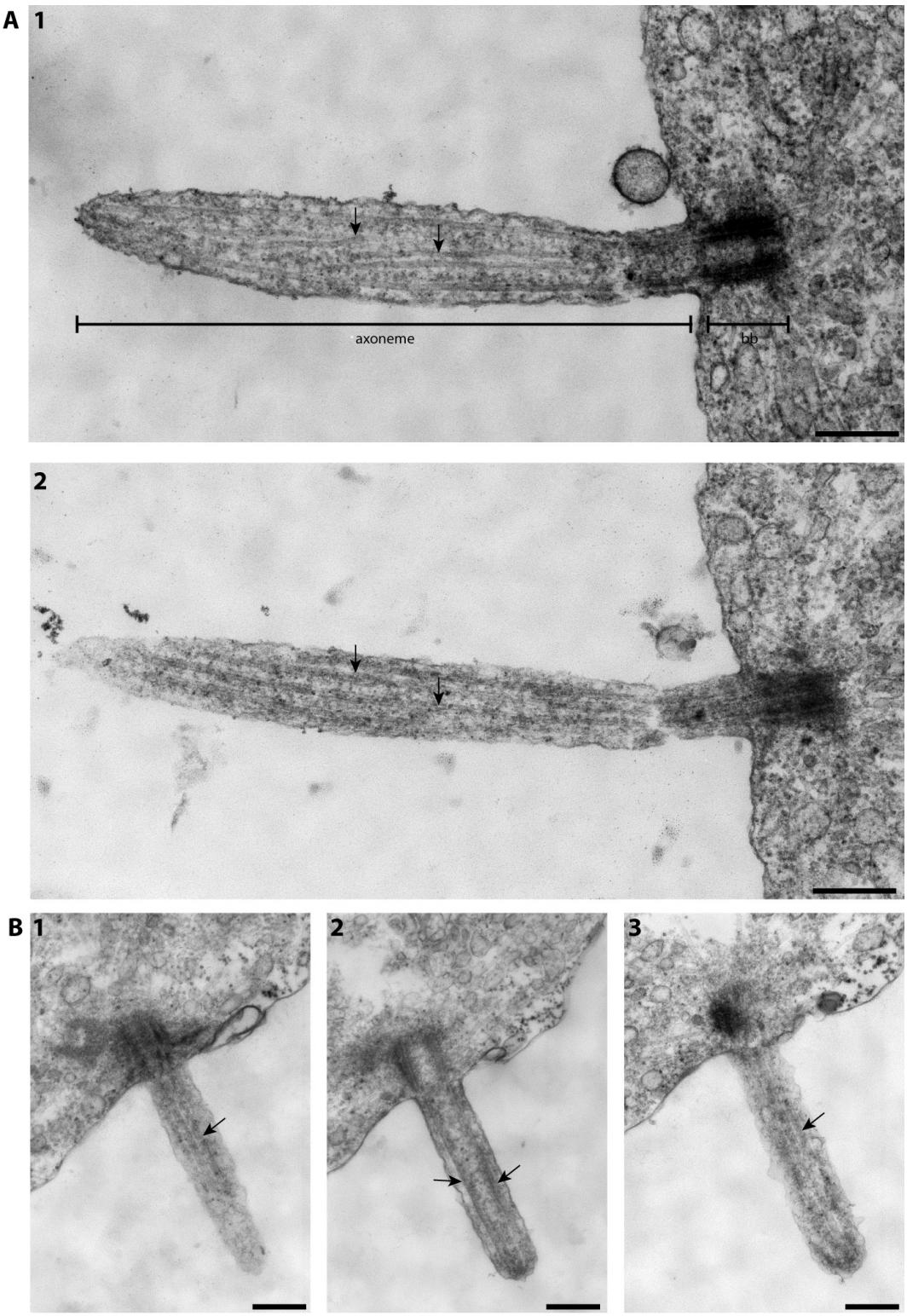


Figure 3.15: The longitudinal ultrastructure of cilia on a neurula stage *Ciona intestinalis* embryo shows the disintegration of doublet microtubule organisation.

A: Longitudinal serial sections of a neurula stage cilium axoneme and basal body (bb) with disorganised microtubule structure (arrows). **B**: Longitudinal sections (1-3) of another cilium which has the appearance of organised microtubule structures but it is unknown if all the doublet microtubules are intact and parallel. Bar = 200 nm (A, B)

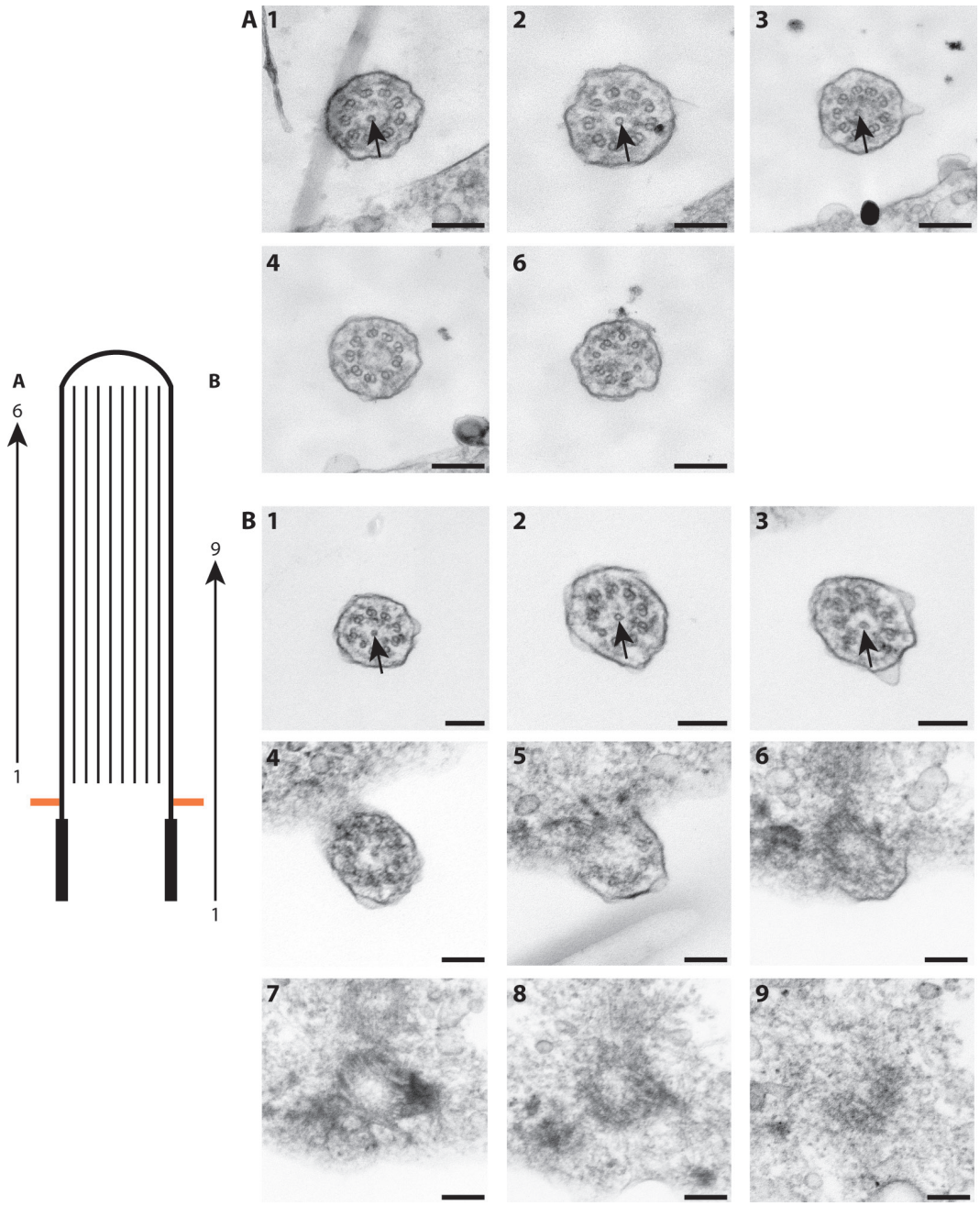


Figure 3.16: The ultrastructure of cilia on a neurula stage *Ciona intestinalis* embryo shows the presence of a single microtubule in the centre of the axoneme.

A, **B**: Serial sections of a neurula stage embryo from the axoneme (A) and from the basal body to the the axoneme (B) with a singlet microtubule in the centre of the axoneme (arrow). The singlet did not persist for the full length of the axoneme and was only observed on two cilia. The outer doublet microtubules tapered towards the centre of the axoneme and some doublets turned to singlets near the distal tip (arrow).
Bar = 100 nm (All)

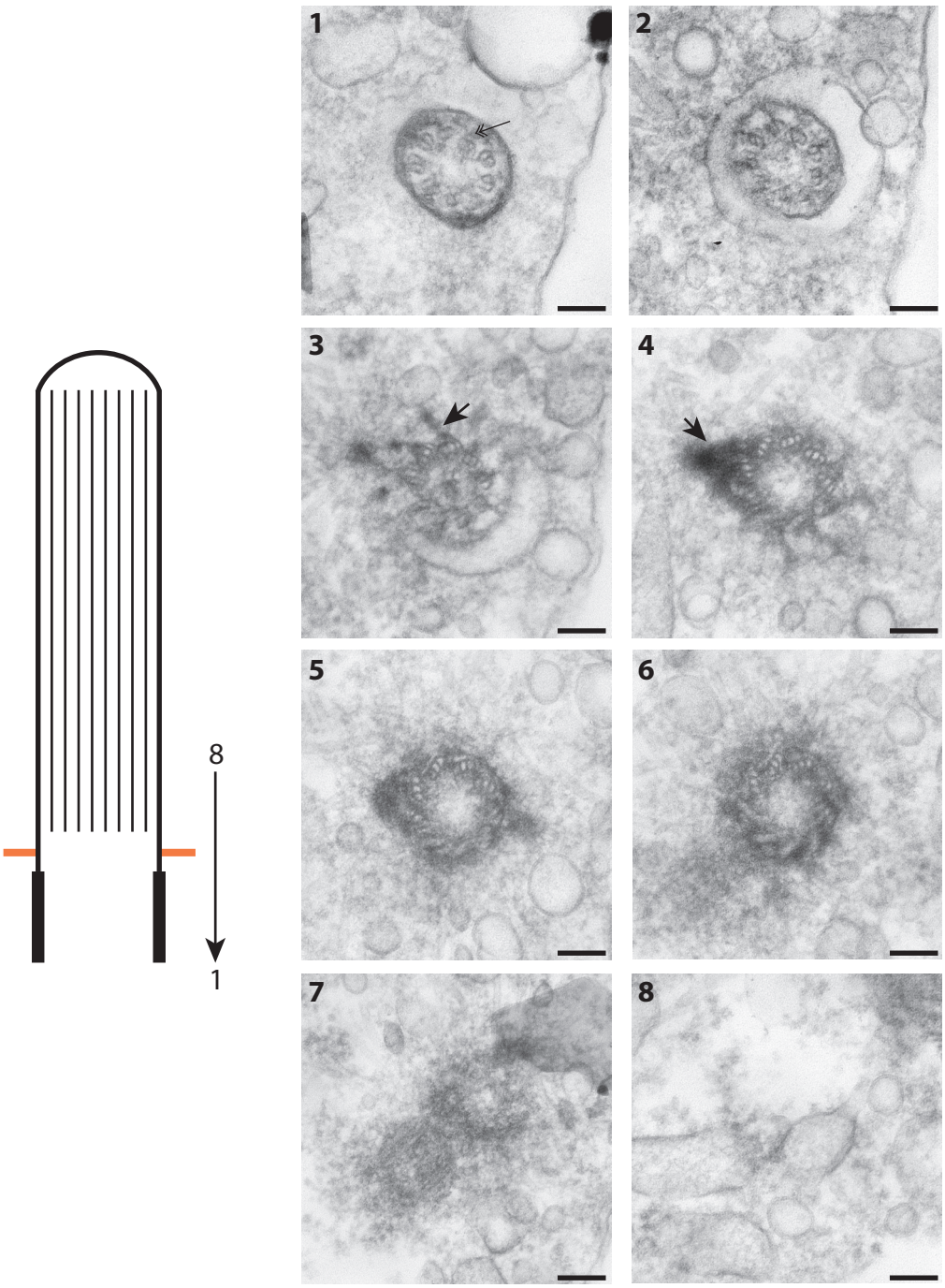


Figure 3.17: The ultrastructure of a cilium on a neurula stage *Ciona intestinalis* embryo shows the cilium within a pocket.

Figure 3.17: The ultrastructure of a cilium on a neurula stage *Ciona intestinalis* embryo shows the cilium within a pocket.

Serial sections of the ultrastructure of a cilium within cytoplasm moving proximally from the axoneme of the cilium (1) to the basal body (8). Intraflagella transport proteins were observerd in the axoneme of the cilium (double arrow). The cilium has a nine doublet microtubule ring structure axoneme and a triplet microtubule basal body structure with transition fibres and a basal foot (arrows). The transition zone (3) and cilium axoneme (2) are both enclosed within a pocket which is surrounded by the cytoplasm.
Bar = 100 nm

cilium did not exit the cell but remained surrounded by the cell cytoplasm (Fig. 3.17). The cilium had the conventional triplet microtubule basal body structure and at the transition zone of the cilium nine doublet microtubules were tethered to the cilia membrane through projections. Transition fibres and a basal foot were observed on the basal body of this cilium which indicates a successfully docked basal body. In all the other cilia analysed (*n*=76) the transition zone was only an average of 140 nm but after this point of the cilium in this case it did not exit the cell but remained within the cell cytoplasm but was separated by a membrane (Fig. 3.17). In the distal region to the transition zone the doublet microtubules were no longer organised in a nine complete doublet microtubule structure (Fig. 3.17). At this point the membrane separating the cilium with the cyptoplasm had disappeared and the cilium was in direct contact with the cell cytoplasm. IFT particles were observed which show that neurula stage *Ciona intestinalis* cilium are built in the same way as previously described cilia (Fig. 3.17).

The arrangement of cilia microtubules was depicted in cartoon form to represent the position of each individual microtubule at each position along the length of the cilium (Fig. 3.18). The microtubule arrangement immediately after the cilium has exited the cell is a nine doublet microtubule ring structure but the organised ring structure becomes disorganised along the length of the cilium towards the tip. Numerous measurements were taken from several cilia serial sections (*n*=8) and averaged to generate a summary of the average length and width of a neurula stage embryo cilium. The mean total length of a cilium from basal body to tip was 1.59 μm ±0.18, with the basal body length 0.27 μm and from transition zone to tip 1.32 μm (Fig. 3.18). The mean length of a cilium is similar to those shown through SEM in previous experiments. The mean diameter of each cilium was 0.27±0.01 μm whereas the diameter of the transition zone and basal body was smaller at 0.24±0.008 μm.

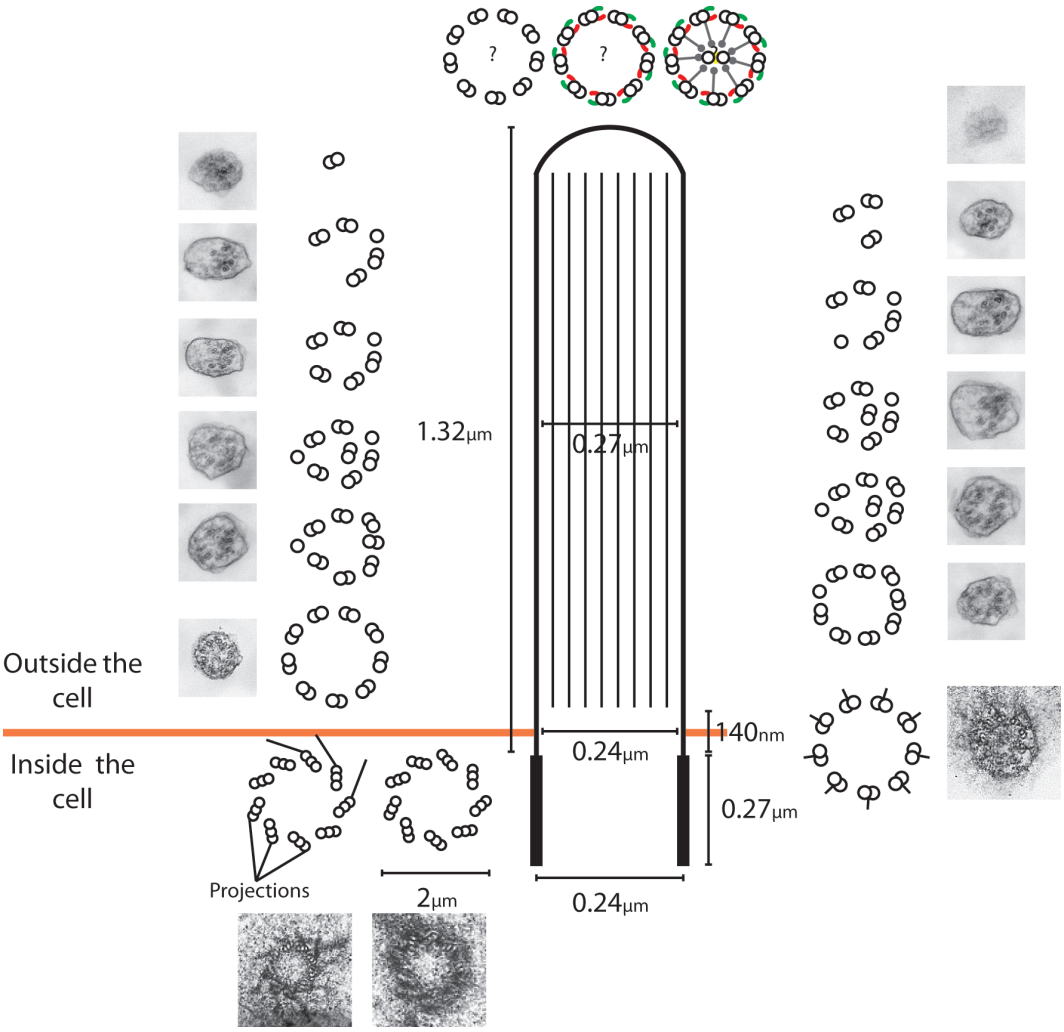


Figure 3.18: The mean measurements of *Ciona intestinalis* tailbud stage cilia

Mean measurements from the 75 cilia analsyed from the neurula stage *Ciona intestinalis* embryo are shown in a schematic which demonstrates the disorganisation of the nine doublet microtubules towards the distal stip of the cilium. Measurements were taken at different regions of the cilium and the mean recorded as shown. The transition zone and basal body sections are from a different cilium from the same embryo but illustrate the ultrstructure of the proximal region of the cilium.

3.2.4.3 The ultrastructure of a *Ciona intestinalis* chorion and follicle cells

The removal of the *Ciona intestinalis* chorion has a very dramatic effect on molecular asymmetry (Shimeld & Levin 2006) so if the cilia on the embryo have a role in left-right asymmetry it is likely there is a link with the chorion. The *Ciona intestinalis* chorion is a thick cuticle layer which protects the embryo during the early stages of embryogenesis and has numerous protruding follicle cells (Fig. 3.19A). The composition of the chorion is not fully known but

embryos allowed to develop without the protection of the chorion have a higher susceptibility to arresting at the egg and gastrula stage of development. Additionally, recent experiments have shown that the removal of the chorion at fertilisation disrupts asymmetric *Ci-Pitx* expression (Shimeld & Levin 2006). It has been previously suggested that the follicle cells have a role in buoyancy as the embryos within the chorion sink to the bottom of a petri dish if the follicle cells are removed. As a result of Shimeld and Levin's (2006) experiments it has been shown that the chorion has an important role in establishing correct molecular asymmetries at the tailbud stage of development. To understand the role the chorion plays in the development of laterality in the *Ciona intestinalis* embryo, SEM images and TEM sections of embryos contained within the chorion and with the chorion partially removed were analysed. SEM of a broken follicle cell and a TEM cross-section show that follicle cells are composed of large empty hexagonal spaces in between thin membranes. At the distal tip of the follicle cell there is a dark, circular, dense area (Fig. 3.19D) which corresponds with the TEM section of a follicle cell tip (Fig. 3.19C). Adjacent to the dark, dense region is an area of small dark dots which are only found in this position and not in other regions of the follicle cell (Fig. 3.19E, F). Below the base of the follicle cells the membrane of the chorion is present (Fig. 3.19G) which is 7 nm in thickness (Fig. 3.19H). Immediately inside the chorion, next to the embryo, there are high numbers of circular, 5 μm wide cells, known as test cells. SEM has demonstrated that these test cells are attached to the chorion around the entire embryo (Fig. 3.19 JK) and comprise a nucleus, clear, empty cytoplasm and aggregates of pigment (Fig. 3.19J).

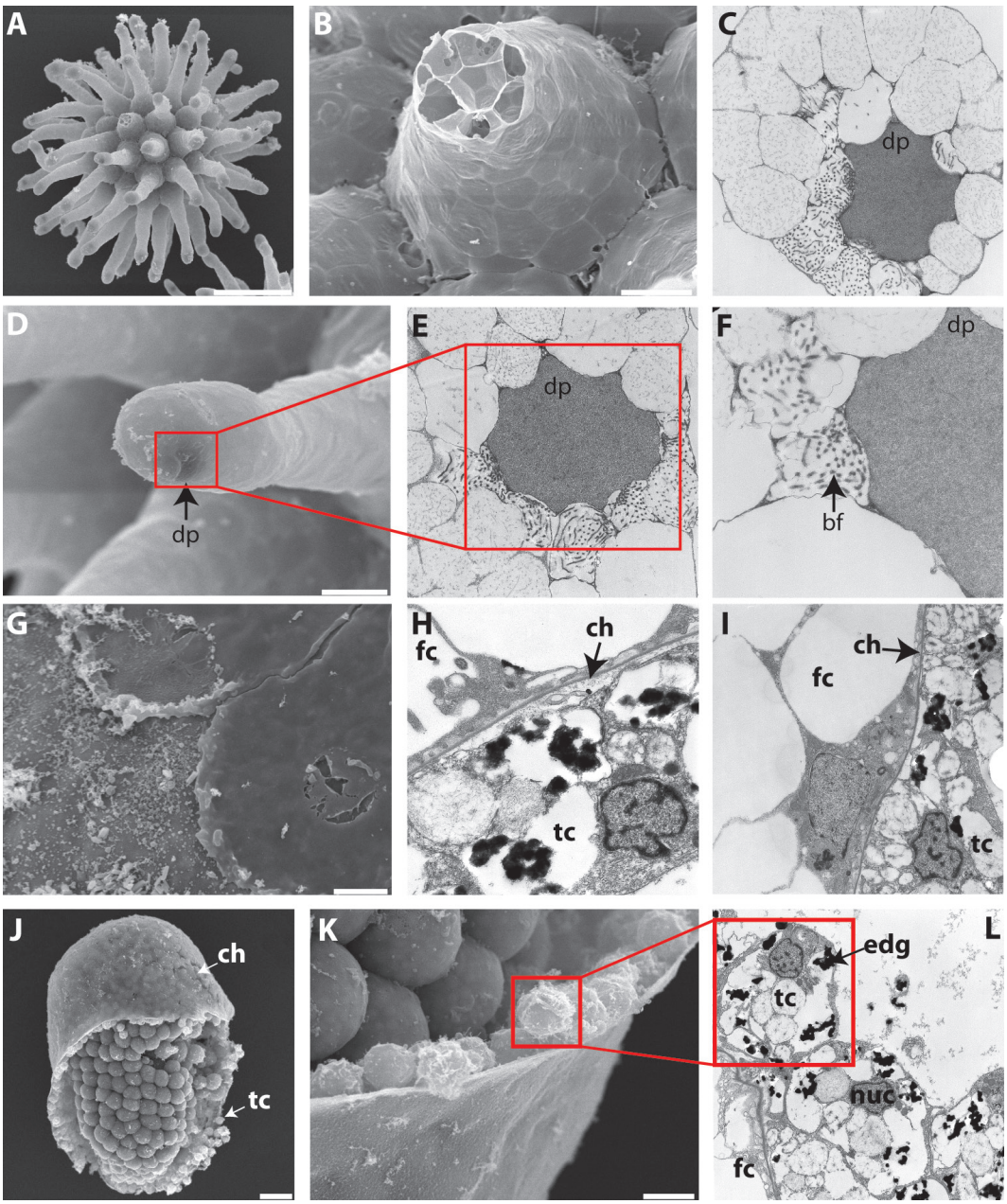


Figure 3.19: The morphology and ultrastructure of the *Ciona intestinalis* embryo chorion with large vacuous follicle cells on the outside and test cells on the inside.

A: SEM of a *Ciona intestinalis* embryo within the chorion and follicle cells. **B**: SEM of a broken follicle cell with clear, hexagonal cell membranes within the structure. **C**: A TEM cross-section of a follicle cell with empty cells consistent with the SEM. **D**: High magnification of the distal tip of a follicle cell. A circular region of dark pigmentation (dp) is present at the tip of each follicle cell. **E**: A TEM cross-section of the dark pigmentation region of the follicle cell with a dense cytoplasm and adjacent small pigment cells. **F**: A high magnification TEM image of the dense cytoplasm and small beaded filaments (bf). **G**: A SEM image of the base of the follicle cells and the chorion beneath. **H**: A TEM cross-section of the chorion membrane (ch). **I**: A TEM cross-section of a chorion membrane with the large empty follicle cells (fc) attached. **J**: A SEM image of a *Ciona intestinalis* tailbud stage embryo with the follicle cells removed and the chorion partially removed. **K**: A high magnification SEM image of a test cell (tc) beneath the chorion membrane and adjacent to the cells of the embryo. **L**: A TEM cross-section of a test cell beneath the chorion and follicle cells. The test cell has a nucleus (nuc), empty cytoplasm and electron dense granules (edg).
Bar = 100 µm (A, D): bar = 50 µm (G): bar = 20 µm (H, J): bar = 10 µm (B, C, F, I); bar = 5 µm (E, K, L)

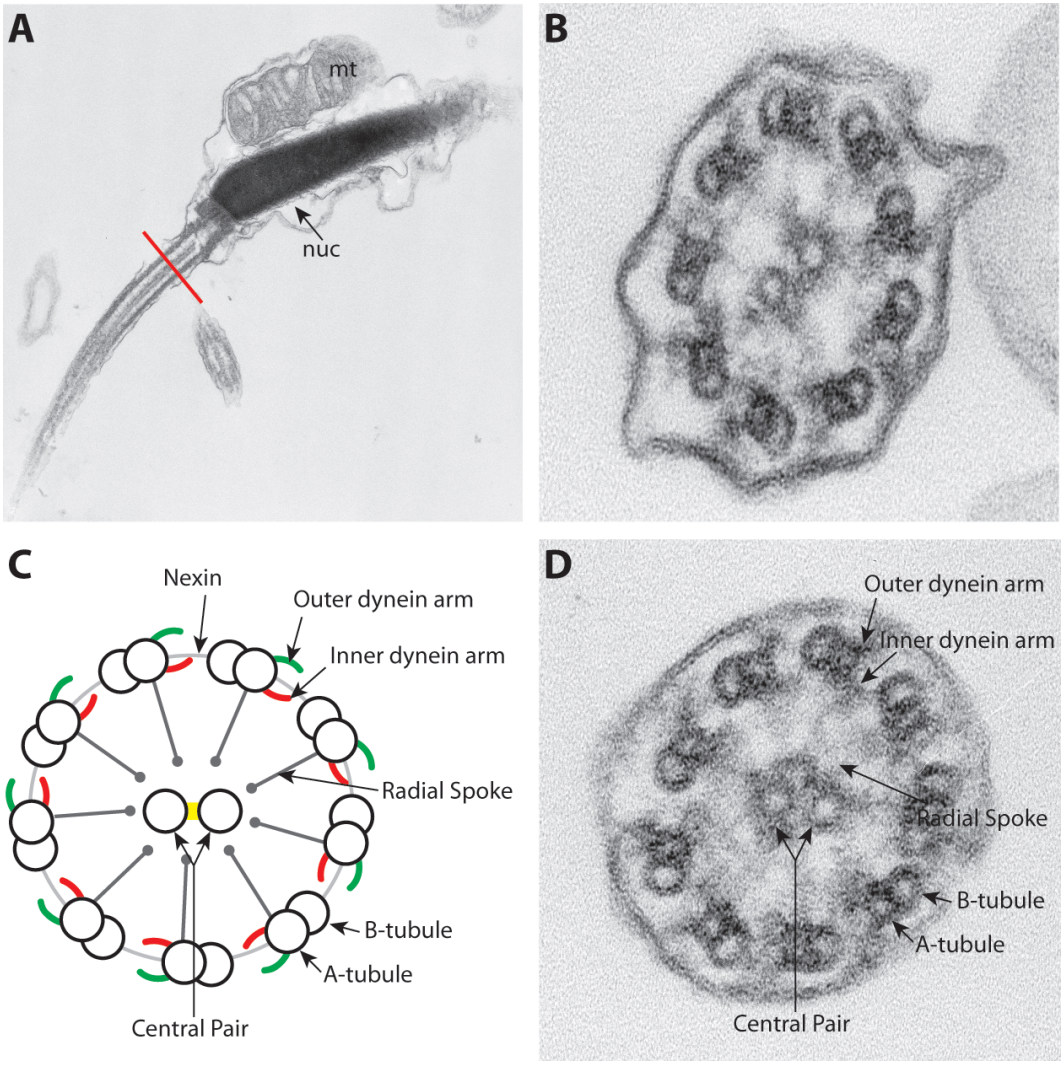


Figure 3.20: The ultrastructure of a *Ciona intestinalis* sperm flagellum

A: A longitudinal section of the head and tail of a *Ciona intestinalis* sperm flagellum with a large nucleus and mitochondria in the head region. **B**: A cross section of a sperm flagellum, from the region of the red line in A, showing a 9+2 structure. **C**: A cartoon of a motile cilium/flagellum. **D**: A cross section of a sperm flagellum with the characteristic structures of a motile cilium/flagellum marked.
Bar = 2µm (A); bar = 0.1µm (B, C, D, E, F, G, H)

3.2.4.4 The ultrastructure of a *Ciona intestinalis* sperm head and tail

Sperm with a 9+2 ultrastructure with dynein arms and radial spokes were found exclusively on *Ciona intestinalis* embryos fixed and sectioned within their chorion. All of the sperm were observed emanating from the cell and were found near the chorion. The chorion is important for sperm association and fertilisation which led to the hypothesis that when these stuctures were first examined they were believed to be 9+2 cilia but were in fact sperm tails that were

still attached to the chorion at fixation. In order to establish if there were sperm attached to the chorion, sperm were fixed independently of embryos, centrifuged to form a pellet, processed using the same method for whole *Ciona intestinalis* embryos and sectioned. The ultrastructure of the sperm flagella was analysed to eliminate any cilia which possess the same structure and were not shown to originate within the cell.

Ciona intestinalis sperm flagella had a nine doublet microtubule ring structure with a central pair of microtubules in the centre. Additional structures which are essential for flagella motility and, therefore, the sperm's role were also detected. Outer and inner dynein arms were located on the B microtubule of the nine doublet microtubules and radial spokes emanated from near the doublet microtubules towards the central pair (Fig. 3.20B, D). A longitudinal section through the sperm head shows a large nucleus, one mitochondrion contained within a membrane with a flagella tail protruding from the posterior (Fig. 3.20A).

3.3 DISCUSSION

Over the last 15 years there has been a rapid advancement in our knowledge of the mechanisms which generate left-right asymmetry in the model vertebrate species. *Nodal* and *pitx2* molecular asymmetries are highly conserved in vertebrate species and have more recently been shown to also have a role in left-right asymmetry in distant phyla such as molluscs (Grande & Patel 2009). Similar mechanisms have been shown to be involved in establishing these molecular asymmetries in the vertebrates with nodal cilia and H^+/K^+-ATPase acting independently or concurrently in different species. Ascidians, as the closest living relatives to the vertebrates, provide an excellent model to examine the primitive vertebrate condition. Recent experimentation has focused on the

role of H^+/K^+-ATPase in ascidian left-right asymmetry (Shimeld & Levin 2006) but my analysis aimed to investigate if nodal cilia and flow were present in a more primitive chordate. Initial analysis concentrated on the mouse epithelia and the presence and structure of microtubule structures outside the ventral node. This analysis was extended to the ascidian, *Ciona intestinalis* to assess for the presence of cilia on the developing embryo and the potential role of nodal flow on an organism which lies outside the vertebrates.

3.3.1 Microtubule fixation experimentation

Scanning Electron Microscopy (SEM) is a powerful method used for analysing the surface structures and textures on quickly developing embryos. In these experiments the technique enabled detailed analysis of the surface structures of *Mus musculus* and *Ciona intestinalis* embryos early in development. The early stages of the related ascidian species *Halocynthia roretzi* had previously been analysed using SEM but this is the first time SEM had been used to study the surface structures on the early developing *Ciona intestinalis* embryo. The SEM fixative composition was picked due to its ability to maintain microtubule structures which are often very delicate and lost or reabsorbed with other less sensitive fixatives.

Another Electron Microscopy (EM) technique, Transmission Electron Microscopy (TEM), allows very high magnification without the loss of detail in ultra thin sections of a specimen. TEM has been a very important tool in the discovery and elucidation of cilia/flagella ultrastructure. Again, like the SEM experiments, very careful consideration of the fixation method used, in these experiments, was undertaken so that the cilia structure of *Ciona intestinalis* embryos could be analysed. Experimentation with different TEM fixatives has enabled the elucidation

of the ultrastructure of the *Ciona intestinalis* late neurula/early tailbud cilia. The fixative used successfully for the SEM analysis did not maintain the membranes when sections were analysed by TEM so different fixatives were trialled for optimisation. The fixative with the optimum results had been successfully used on another ascidian, *Botryllus schlosseri* (Degasperi et al. 2009) and maintained the cytoplasm, membrane and cilia microtubule structures. The main difference between the three fixatives was an alternative method for maintaining the osmotic balance as the embryos were moved from Filtered Sea Water (FSW) to fixative. The fixative used for further *Ciona intestinalis* cilia analysis used 1.6% NaCl instead of sucrose to maintain osmotic balance. The careful consideration of the fixative used on both mouse and *Ciona intestinalis* has resulted in detailed images of previously unseen surface structures and their ultrastructure which has led to interesting new findings in the early development of *Ciona intestinalis*.

3.3.2 The structure of cilia on mouse gastrula embryo epithelia

SEM analysis of the early mouse embryo has shown previously that up to 6 μm in length cilia monopolise the mouse ventral node and their presence and current functioning are essential in the establishment of left-right asymmetry (Sulik et al. 1994; Nonaka et al. 1998). The exact ultrastructure of the cilia of the mouse node has been debated over recent years but most data suggest that they have a 9+0 ring structure with dynein arms providing the required motility (Hirokawa et al. 2006). In order to compare any cilia presence on the ectoderm of the *Ciona intestinalis* embryo, I first analysed the structure of non-node mouse cilia. In contrast this analysis of epithelia, outside the node, are 9+0 with the nine doublet microtubules in a ring shape immediately after the cilium has exited the cell but the ring arrangement disintegrates

and the doublet microtubules arrangement becomes disorganised. A central pair, dynein arms and radial spokes which are all involved with cilia motility were absent from the epithelia cilia. At the distal tip of the cilia some microtubule doublets are absent and other doublets are now a single microtubule. The lack of a doublet ring which extends the full length of the cilium would suggest that the cilia are not motile and must have another role on the embryo. The results here have shown that the cilia structure of the mouse epithelia are not the same structure as those found in the mouse ventral node.

The structure of these cilia is a phenomenon that has been described over the last 50 years but is still not well understood. Dahl (1963) observed numerous cilia in the rat cerebral cortex which have a distinct eight peripheral and one central doublet ultrastructure (8+1) with a peripheral doublet of a 9+0 cilium displaced to the centre. Additionally, Allen (1965) found a similar structure in isolated cilia in inner retinal neurons and in retinal pigment epithelium. This ultrastructure arrangement is never found as a basal body but begins approximately 0.5 μm distal to the cell surface. The apparent collapse of the axoneme could occur because there is an absence of connections between doublets which maintain the 9+0 ring structure (Dahl 1963). More recently, the incursion of one or more microtubule doublets into the axoneme core was described in mammalian epithelial cell lines and the amastigote *Leishmania mexicana*, the parasite responsible for Leishmaniasis (Gluenz et al. 2010). These studies have analysed the progressive collapse of the 9+0 ring structure along the length of the axoneme which this thesis has demonstrated is also a feature of the mouse epithelia cilia. The role of a cilium/flagellum with this conserved axoneme architecture has been suggested to be sensory which is likely to be their role on the mouse surface epithelia.

3.3.3 *Ciona intestinalis* cleavage stage embryos

To analyse the surface ectoderm of *Ciona intestinalis* embryos, SEM was conducted on all the early stages of development in order to search for microtubule structures that could be cilia. The SEM images of *Ciona intestinalis* early cleavage embryos show two contrasting surface textures, smooth and crinkled. This phenomenon has been attributed to the position of these cells within the cell cycle. This has previously been described in *Halocynthia roretzi*, with microvilli present just before cell division and cytokinesis but absent after the cell divides (Satoh & Deno 1984). It was noted that the number of microvilli were not restricted to the cleavage furrow region, as demonstrated in my experiments (Fig. 3.4B), but cover the whole of the developing embryo (Satoh & Deno, 1984). This transition between two types of surface texture progressed until the 32 cell stage in *Halocynthia roretzi* whereas it was also present at the gastrula stage here (Fig. 3.6H).

The presence of microvilli and a rough texture is shown on the early neurula embryo (Fig. 3.7D) which is later then seen in the *Halocynthia roretzi* embryo experiments conducted by Satoh & Deno (1984) although they did state 'up to at least the 32 cell'. This experiment has shown that their assumption that this phenomenon could occur later in development is correct. The reason for the crinkling and presence of microvilli is not fully understood but is assumed to be a result of the hardening of the microfilaments in the cell cortex to aid the rounding up of cells prior to division (Satoh & Deno 1984). Once the cells flatten after division the microvilli disappear. The SEM analysis in *Ciona intestinalis* has reinforced the proposal that the rough texture is linked to cell division because it is only observed on embryos which are undergoing division. Until the 64

cell stage, the cells of the embryo divide in a synchronous fashion so it is expected that the whole embryo would either have a rough or smooth texture. Problems of fixation and shrinkage due to dehydration can be discarded as having a role here because both smooth and crinkled textures were observed on one SEM stub which has undergone the same process.

Another common feature in cleavage embryos is long, thin projections that extend between cells. They are observed in unison with the rough, microvilli texture discussed above which has been linked to the cells stage in the cell cycle. The length of the projections differs from, 2 μm in length to as long as 12 μm in length. These projections have been previously witnessed in *Halocynthia roretzi* and were termed 'cytoplasmic processes' by Satoh & Deno (1984) but this is the first time they have been shown to exist in *Ciona intestinalis*. Satoh & Deno (1984) suggested that these projections are potentially microvilli that are originally short projections near the cleavage plane that elongate across the plane during cell division (Satoh & Deno 1984). Apart from this there has been no further work conducted on these projections and their structure and function are still undefined. Depending on their structure and composition there is the possibility that these projections could have a very important role in communication between cells in the very early stages of development. Multicellular organisms require cell to cell communication between closely positioned cells and at the early embryo stages these projections could adopt this role.

3.3.4 Cilia on *Ciona intestinalis* embryos

One of the most interesting findings from this SEM study of the early stages of *Ciona intestinalis* development is that one cilium projection emanates from every cell of the late neurula/early

tailbud stage embryo. Although, microvilli were observed periodically during the first cleavage stages there were no other projections observed from the surface of the cells. Cilia were first detected, on some of the cells, at the mid-neurula stage but were seen all over the embryo by the early tailbud stage. The cilia are small, 1.5-2 μm in length, and appear to emanate at the posterior of each cell for the whole period they are present (further analysis of positioning in Chapter 4). Cilia have never been described on the developing embryo of the distantly related ascidian, *Halocynthia roretzi* or any other ascidian embryo before, although detailed SEM images have been examined (Satoh 1978; Satoh & Deno 1984). The careful consideration of fixation for the preservation of microtubule structures has enabled these cilia to be shown for the first time even though previous ascidian SEM studies have been carried out.

3.3.5 Timing of cilia presence on *Ciona intestinalis* embryos

The timing of the emergence of cilia on the *Ciona intestinalis* embryo has suggested a possible link between these cilia and a role in left-right asymmetry previously described in vertebrates. Cilia are first present at the late neurula/early tailbud stage of development and persist for approximately one hour until the mid-tailbud stage. This is a very small window so their role is likely to be specific to that precise time point in development. Interestingly, this time point is immediately prior to asymmetric *Ci-Nodal* and *Ci-Pitx* expression which is first observed at the mid to late tailbud stage (Boorman & Shimeld 2002a; Morokuma et al. 2002; Mita & Fujiwara 2007). This could mean that the cilia are involved in the mechanism which sets up the left-sided *Ci-Pitx* expression in the ectoderm and mesenchyme as in several vertebrate species.

3.3.6 *Ciona intestinalis* cilia and left-right asymmetry

There are differences between the situations in mouse laterality development and the observations made through SEM in *Ciona intestinalis*. The mouse node is a defined pit with one 5-10 μm length cilia emanating from each cell. In contrast the cilia on a *Ciona intestinalis* embryo are much shorter at 1.5-2 μm and emanate from every ectoderm cell of the embryo. Videomicroscopy of the mouse node cilia has demonstrated that the cilia rotate to create a leftward flow across the node pit but these cilia are at least 5x longer then the *Ciona intestinalis* cilia. The flow moves leftwards across the pit just above the surface of the node, continues along the left side wall and returns to the right side in a counter-flow above the surface (Okada et al. 2005). The ventral node is a pit which enables a leftward flow to be generated and a recovery rightward flow to occur above the pit, however, the cilia on the *Ciona intestinalis* embryo are not positioned within a pit but are positioned on every cell of the ascidian embryo. This could be a result of the absence of an organiser on the *Ciona intestinalis* embryo (Dehal et al. 2002) which would normally be the location of nodal cilia. The lack of a pit structure would mean that if a leftward flow is generated it would involve the whole embryo rather than the small area of the organiser region and the chorion would be essential to encase the flow. *Ciona intestinalis* cilia were examined live under an Axioscope microscope but no cilia movement was observed which initially suggests that these cilia are immotile but to confirm this result the ultrastructure of the cilia was analysed.

3.3.7 *Ciona intestinalis* cilia structure and motility

In order for these cilia to have a conserved role as the generators of a leftward flow in the urochordate species, *Ciona intestinalis*, they must be motile. To analyse the role of the cilia, their structure was analysed and compared to that of the cilia of the mouse ventral node and epithelia. The majority of cilia analysed through TEM had nine doublet microtubules axoneme structure immediately after the cilia have exited the cell and then the nine doublet ring organisation disintegrates and some doublets become singlets. On only two cilia was a single microtubule present in the centre of the nine doublet ring and never a central pair, a characteristic of motile cilia. Although at present, research suggests that mouse node cilia do not have a central pair, they do have dynein arms. There is also no evidence that additional structures, such as dynein arms or radial spokes essential for motility are present on the cilia of the neurula/tailbud *Ciona intestinalis* embryos. The cilia had a collapsed axoneme, reduction in doublets and at the most distal tip of the cilium, singlet microtubules.

Although cilia have not been observed on early stages of *Ciona intestinalis* development prior to these experiments, cilia are present on the larvae stage in numerous tissues (Manni et al. 2005; Katz 1983; Dilly 1969; Crowther & Whittaker 1994; Torrence & Cloney 1982) and a comprehensive TEM analysis of the structure of these cilia was recently conducted (Konno et al. 2010). The cilia structures observed were grouped into six different categories; (1) 9+2 with dynein arms and radial spokes, (2) 9+2 without dynein arms, (3) 9+2 with electron dense bridges to the cilia membrane, (4) 9+0 with an electron dense area in the centre of the axoneme, (5) 9+0 without dynein arms and radial spokes and (6) short axoneme cilia-like protrusions. Early stage embryos were not analysed in this research but the only type of cilia observed on the

late neurula/early tailbud stage embryos in my experiments were the same structure as group 5 on the larvae. The disorganised doublet microtubule structure close to the distal tip observed on late neurula/early tailbud was also observed on these later larvae stage embryos so is a conserved structure throughout *Ciona intestinalis* development. The role of the cilia on the larval stage embryos has not been elucidated so cannot provide potential roles for the cilia observed here by SEM and TEM.

In comparison with the cilia of the mouse ventral node which are 9+0 with dynein arms, and with the collapsed axoneme structure of the mouse epithelia cells, it is likely from TEM analysis that cilia of the *Ciona intestinalis* embryo have a role similar to the latter. The absence of the central pair, radial spokes and nexin from the *Ciona intestinalis* and mouse non-node cilia suggest that they are not motile because these two structures are important for the generation of movement in motile cilia. Radial spokes and the central pair are required for cilia motility through their interaction with the motor proteins, the dynein arms. Radial spokes are a structurally conserved T-shaped macromolecular complex which repeats in pairs or triplets along the doublet microtubules (Warner 1970; Warner & Satir 1974; Goodenough 1985). One end of the T-shaped complex is anchored to the doublet microtubule near the dynein arms and projects to the centre of the axoneme. The other end of the spoke is called the head region and it potentially interacts with projections from the central pair to relay signals from the central pair to the dynein arms (Warner & Satir 1974; Witman 1978; Goodenough 1985; Smith & Yang 2004). These experiments have shown that the absence of radial spokes paralyses cilia.

It is not fully understood how the central pair facilitates cilia motility: some experiments have shown that the central pair rotation seen in *Chlamydomonas reinhardtii* and *Paramecium tetramelia* is important in some organisms (Mitchell & Nakatsugawa 2004; Omoto & Kung 1979;

Wargo & Smith 2003) although not all (Tamm & Tamm 1981; Gadelha et al. 2006). The slide motion in cilia motility is constrained by nexin links between adjacent outer-doublets which facilitate bending (Downing & Sui 2007). The absence of these structures limits the chances that these cilia are motile.

However, cilia of the mouse ventral node do not have these central structures and are known to be motile. This is in part due to presence of dynein arms which are essential for motility and can work independently of radial spokes and the central pair. Research has shown that the central pair and radial spokes are not required for high frequency oscillatory beating and as long as dynein arms are present certain cilia are able to beat, as in the case in nodal cilia (Yagi & Kamiya 2000). The dynein arms undergo hydrolysis of ATP so they can walk towards the base of the neighbouring doublet. Dynein arms on individual doublets hydrolyse ATP at different times to generate a synchronised movement to bend the cilium (Numata et al. 2008). The lack of dynein arms, a central pair and radial spokes which all generate cilia bending and therefore, movement of the cilia are all absent from the non-node epithelia and *Ciona intestinalis* cilia. This strongly suggests that neither population of cilia are motile, which would dismiss a conserved nodal flow mechanism in the ascidian model. The cilia are therefore more likely to have an additional role on the surface of the embryo which is able to function without these motile accessories and disorganised microtubule structure.

Recent analysis has suggested that this microtubule disorganisation could be advantageous for cilia that are not required to be motile but instead have a sensory role (Gluenz et al. 2010). All the evidence from the TEM of *Ciona intestinalis* indicates that the late neurula/early tailbud stage cilia are not motile, on the ascidian model, so are not homologous to the nodal cilia observed in the vertebrates. However, it does not mean that these cilia do not have a role in the establishment

of left-right asymmetry in *Ciona intestinalis*. The cilia could have an important sensory role in laterality development or be the site of H^+/K^+-ATPase ion flux.

The role of these cilia is unknown but cilia have multiple roles in development as both mechanosensors and chemosensors. Cilia cover many organisms as they develop, such as Amphioxus (Stokes & Holland 1995) and Sea urchins (Emlet 1995), and are often involved in the embryos movement and rotation. *Ciona intestinalis* cilia contrast to the large cilia observed in swimming embryos (Stokes & Holland 1995) which would suggest a more specific and localised role on the developing embryo. Future experiments are required to elucidate the function of *Ciona intestinalis* cilia by establishing the downstream effects that result from the loss of cilia on a developing *Ciona intestinalis* embryo.

3.3.8 Role of cilia as mechanosensors or sites of signalling

However, over recent years more and more research is indicating that motile and primary cilia have a very important role in cell signalling, which due to a lack of motility could be the likely role of cilia on the surface ectoderm of the *Ciona intestinalis* embryo. Motile cilia are known to have an important sensory role in *Chlamydomonas reinhardtii* mating. During the mating of *Chlamydomonas reinhardtii* the motile flagella are required to touch the flagella of an opposing mating type to initiate a Ca^{2+} signalling pathway and enable the fusion of the gametes (Huang et al. 2007). Cleaved PKD2 protein is localised in the *Chlamydomonas reinhardtii* flagellar membrane where it is essential for the Ca^{2+} signalling pathway in gamete mating (Huang et al. 2007). Additionally, polycystins, a feature of Primary cilia signalling have also been found localised to the motile cilia of the oviduct (Teilmann et al. 2005; Teilmann et al. 2006) and Vangl2,

a protein in the non-canonical Wnt pathway is not confined to the Primary cilia but is found on motile respiratory epithelial cells (Ross et al. 2005; Torban et al. 2004). Although, motile cilia are implicated in cellular signalling, the ultrastructure of *Ciona intestinalis* cilia indicates that they are not motile and would probably have a sensory role more attributed to that of the Primary cilia.

Hedgehog (Hh) and Wingless (Wnt) signalling are two pathways with multiple and essential roles in development and along with the polycystins (discussed in Chapter 1), are involved in signalling in Primary cilia. Components of the Hh signalling pathway localise to the cilia (Corbit et al. 2005; Haycraft et al. 2005) and cells lacking cilia are unable to induce the pathway in response to exogenous Sonic Hh ligand (Shh) (Ocbina & Anderson 2008; Han et al. 2008; Rohatgi et al. 2007). IFT is required for Hh signalling in the cilium by transporting Gli proteins and Suppressor of Fused (SuFu) to the ciliary tip (May et al. 2005; Haycraft et al. 2005; Liu et al. 2005). In mammalian cilia, the absence of the hedgehog ligand binding to the patched receptor represses the activation of the seven transmembrane spanning protein, smoothened (Smo) (Corbit et al. 2005; Rohatgi et al. 2007). The main transcriptional response to Hh is mainly driven by Gli proteins, which due to the repression of Smoothened (Smo) results in Gli3 being constantly proteolytically cleaved into the repressor, GliR (Haycraft et al. 2005; Kiprilov et al. 2008; Nielsen et al. 2008). The repressor is subsequently transported back towards the cell body. In the presence of Hh the patched receptor releases the seven transmembrane spanning protein, Smo which is transported to the ciliary tip where it interacts with SuFu and stops the proteolytic cleavage of Gli and the activated Gli3A is shuttled to the nucleus where it induces the expression of genes. Research has only implicated primary cilia in Hh signalling in mammalian species and is unlikely to operate in *Drosophila melanogaster* which is believed to have cilium independent

Hh signalling (Huangfu & Anderson 2006). (See reviews (Berbari et al. 2009; Veland et al. 2009)

Like Hh signalling, the primary cilia have been implicated in Wnt signalling which also requires IFT for normal regulation. The Wnt pathway can be divided into two main pathways which all utilise the Wnt ligand and the Frizzled receptor but have different downstream pathways. The canonical pathway involves the regulation of β-catenin levels, through the β-catenin destruction complex which in the absence of wnt signalling maintains low β-catenin levels. The binding of the Wnt ligand to the Frizzled receptor activates Dishevelled (Dsh) which stabilises β-catenin, which like Gli, serves as a transcriptional activator. The other pathway, the non-canonical pathway, acts through aPCK, CamK and JNK to control cellular polarity, migration and the Planar Cell Polarity (PCP) (The pathway is reviewed in more detail in Logan & Nusse 2004). The exact link between both Wnt pathways and cilia is not known but research has shown that in cells that possess a cilium, the canonical Wnt signalling pathway activity is restricted in mouse embryos (Corbit et al. 2008). Inversin, a protein localised to the base of cilia, regulates Dsh and is the switch between the canonical and the non-canonical pathways, although this is widely believed to be over-simplified.

In *Ciona intestinalis* embryos, two hedgehog genes have been described, *Ci-hh1*, which is maternally expressed gene and *Ci-hh2*, which is zygotically expressed (Takatori et al. 2002). *Ci-hh2* is expressed at the correct time point for a role in signalling in the ectoderm cilia, but is only expressed in a row of internal cells in the tail region running along the anterio-posterior axis and not in the ectoderm (Takatori et al. 2002). The lack of *Ci-hh2* gene expression in the embryo region where the cilia are located suggests that the cilia are not involved in Hh signalling. Similarly, Wnt signalling is also unlikely to be present in the cilia as Wnt genes involved in the pathway are not expressed at the right time and place for their involvement (Ikuta et al. 2010).

Polycystins were also absent from the tailbud embryo. Additionally, gene expression of other components of the Hh and Wnt signalling pathways were absent entirely or not in the ectoderm of the embryo. It is, therefore, unlikely that Hh, Wnt signalling or the Ca^{2+} channel generated by polycystins are operating in the *Ciona intestinalis* cilia at this stage of development.

3.3.9 The role of the chorion in the development of left-right asymmetry in *Ciona intestinalis*

One known link between the establishment of left-right asymmetry in *Ciona intestinalis* and disruption to the asymmetric expression of *Ci-Pitx* is the removal of the chorion at fertilisation (Shimeld & Levin 2006). To examine the chorion more closely, SEM and TEM was conducted on embryos within the chorion to establish if there was any evidence of an interaction between the chorion and cilia. The *Ciona intestinalis* embryo remains within a chorion, sometimes known as the vitelline membrane, during early development and whilst left-right asymmetry is established. The chorion is a thin membrane between the cone shaped follicle cells on the outside and circular test cells on the inside. The chorion protects the embryo in the early stages of development and is covered in follicle cells believed to be important for buoyancy (Lambert & Lambert 1978). The chorion is the site of sperm binding and is involved in species-specific recognition of gametes (De Santis et al. 1980; Rosati & De Santis 1978). It is a 60 nm thick membrane which is composed of fine filaments arranged in a thick interwoven meshwork (Cotelli et al. 1981). The chorion and associated structures are generated during oogenesis in the adult *Ciona intestinalis* and surround the embryo until the larvae is ready to hatch (Burighel & Cloney 1997; Kessel & Kemp 1962; Mancuso 1965; Cotelli et al. 1981). No interaction between the chorion and the cilia of the

embryo were observed which indicates that if the chorion is involved it is not through direct communication from the cilia.

The follicle cells are cone shaped and highly vacuolated with an expanded basal surface where the nucleus lies and a narrow apical surface. They are involved in embryo buoyancy and are thought to limit the number of sperm that can interact with the chorion during fertilisation (De Santis et al. 1980). TEM of the apical surface of the follicle cells has shown for the first time an area of dark pigmentation which appears to correspond to the molecule observed at the tip of follicle cells under the light microscope (Fig. 3.19). Immediately adjacent to this area were cells which contained thin beaded filaments exclusively. Cells of a similar composition have been described in *Styela plicata* test cells but it is not known what is their function (Burighel & Cloney 1997).

As well as the chorion, there are also two closely positioned groups of cells, the test cells and the follicle cells. Test cells are found between the embryo and the chorion whereas the follicle cells are located on the outside of the chorion in direct contact with the surrounding environment. Test cells are able to move about in the space between the chorion and the *Halocynthia roretzi* embryo (Satoh et al. 1982; Mancuso 1973). There is no vertebrate counterpart to the test cells which likely to be linked to their role as tunic (or test cell) producers (Burighel & Cloney 1997). The chorion is directly associated with the test cells when analysed through TEM and each test cell contains a nucleus, electron dense granules and empty vacuoles (Fig. 3.19). In *Halocynthia roretzi*, the test cells form aggregates and by the mid to late tailbud stage the test cells become closely associated with the tail region. At the larval stage of development, test cells are observed along the tail and are essential for successful metamorphosis and tunic formation (Sato & Morisawa 1999; Satoh et al. 1982). The space between the *Halocynthia roretzi* embryo and the

chorion is much larger than in the case of *Ciona intestinalis* so it is likely that the test cells do not move about as much as in *Halocynthia roretzi*. All through early *Ciona intestinalis* development the test cells are very closely associated with the embryo (Fig. 3.19) and, therefore, do not require the test cells to move to the tailbud as they are already in close proximity to the tailbud.

The removal of the chorion disrupts asymmetric gene expression which suggests a role of the chorion in the establishment of *Ciona intestinalis* left-asymmetry. The exact role is unknown and the abnormal later embryo development suggests that although the chorion could have a direct role in asymmetry development it could also be a result of general development disruption. The presence of cilia at the precise time point prior to asymmetric gene expression led me to postulate that if the cilia generate a flow, as in the mouse ventral node, the chorion could be providing a physical boundary to fluid flow generated by the cilia and has the same role as the mouse node pit. However, since the discovery that the cilia are not motile the chorion cannot be working in this way. One possibility is that the chorion is interacting with the cilia in some way which is disrupted when the chorion is removed. TEM analysis of the chorion and cilia show that the chorion and cilia do not interact through a physical proximity which is broken when the chorion is removed as the longitudinal cilia observed are not adjoined with the chorion. Additionally, the test cells are present between the chorion and the embryo universally so any interaction would be between the test cells and the cilia. These test cells are vital in tunic formation later in development (Takamura et al. 1996) but whether they also have a role in *Ciona intestinalis* left-right asymmetry is not known.

3.3.10 Conclusion

The ascidian *Ciona intestinalis* is one of the closest living relatives to the vertebrates which makes it an interesting model for analysis of conserved vertebrate mechanisms. Left-right asymmetry has been researched in mouse, *Xenopus* and Zebrafish, and nodal cilia are important for laterality development across the vertebrates. Extensive SEM experiments have shown here that cilia are also present on *Ciona intestinalis* embryos immediately prior to molecular asymmetries but are shorter and are found universally on the late neurula/early tailbud embryo. *Ciona intestinalis* cilia structure is similar to immotile cilia from mammalian cells to the amastigote *Leishmania mexicana* which suggests that the nodal motile cilia role is not conserved in the ascidian species but does not mean that the cilia are not involved in left-right asymmetry. Additionally, consideration of preservation of microtubule structures in these experiments has demonstrated how information can be unintentionally omitted and leads to the suggestion that similar structures may be present on other ascidian species but have not been identified due to use of the wrong fixation.

CHAPTER 4

The Role of Cilia on the Neurula Stage *Ciona intestinalis* Embryo

4.1 INTRODUCTION

This study has shown for the first time that cilia are present on the early stages of *Ciona intestinalis* embryos. Cilia are observed in several sensory and neuronal organs of the larvae stage embryo but prior to this much later stage it was previously thought that cilia were not present. The careful consideration of fixation for EM to preserve microtubule structures has led to the observation of cilia at the late neurula/early tailbud stage of development for the first time. The cilia are present on every cell of the embryo ectoderm and appear localised to the posterior of each cell. They are 1.5 – 2 μm in length and persist on the ectoderm for ~1 hr of development until the mid-tailbud stage of development.

TEM analyses of the structure of these cilia demonstrate that it is highly unlikely that they are motile and are more likely to have a sensory role on the embryo. The cilia are 9+0 without dynein arms and radial spokes immediately after the cilium has exited the cell but the organisation becomes disorganised towards the distal tip. The nine doublet microtubules were no longer organised in a ring structure but taper towards the centre of the axoneme and some doublets become singlets. The lack of a central pair, organised ring structure along the length of the cilium and accessories such as dynein arms and radial spokes suggest that the cilia are immotile. Research has previously reported that the loss of the organised standardised cilia structure may

be a result of the cilia acting as sensory antennae on the cell surface which does not require the rigid axoneme structure of motile cilia. The suggestion that cilia on the *Ciona intestinalis* embryo are not motile has dismissed any idea that their role could be in the generation of a leftward flow on the embryo.

Although, the cilia on the developing *Ciona intestinalis* embryo do not appear motile they do appear to be positioned in a conserved manner to the cilia of the mouse ventral node. Initial observations suggest that the cilia are positioned at the posterior of each cell, a characteristic of cilia in the mouse ventral node. Cilia are initially positioned centrally on the cells of the mouse ventral node and before they then migrate posteriorly (Hashimoto et al. 2010). This characteristic is required for the tilt and therefore, the ability of cilia to rotate and generate an overall leftward flow across the node (Nonaka et al. 2005; Okada et al. 2005). A non-canonical Wnt signalling pathway, PCP, has been implicated as important in this precise patterning and positioning of cilia. Whether the posterior positioning of cilia is a feature of *Ciona intestinalis* embryos is interesting to determine whether characteristics from the vertebrate model of nodal flow is conserved in the ascidian model.

The cilia on the *Ciona intestinalis* embryo are immotile so the motile cilia of the vertebrate organiser regions are not conserved on the ascidian embryo. However, they may still be involved in the establishment of left-right asymmetry but in a different capacity. The cilia are present immediately prior to the asymmetric expression of *nodal* and *pitx2* orthologues and disappear at the time point when the asymmetry is established which suggests a role in the development of left-right asymmetry. The timing of cilia on the embryo led me to analyse whether the absence of cilia on the embryo affects the left-sided expression of *Ci-Pitx* expression and downstream organ asymmetry.

Here I show statistically that cilia are indeed positioned at the posterior of the cell on the *Ciona intestinalis* late neurula/early tailbud embryo. However, the cilia of the embryo are not universally situated in the same position along the Anterior-Posterior (AP) axis of the cell with the cilia of a sub-population of cells on the ventral face of the embryo halfway along the embryo AP positioned at a significantly different position. Although, they are still positioned in the posterior half of the cell they were not positioned as far to the posterior as the other regions. Experiments were also conducted to assess if the cilia on the surface of the embryo have a role in left-right asymmetry. The techniques used failed to perturb ciliogenesis on the embryo but the sudden exposure to high levels of NaCl did result in cilia positioned at the very posterior of the cells AP axis. This change in cilia patterning did not affect the asymmetric *Ci-Pitx* expression so if these cilia are involved in the establishment of left-right asymmetry a tight control on positioning is not required.

4.2 RESULTS

4.2.1 The distance along the AP axis of a cell a cilium is positioned on a *Ciona intestinalis* embryo

SEM of *Ciona intestinalis* late neurula and early tailbud stage embryos has shown that 1.5-2 μm cilia are present on every cell of the ectoderm. Initial analysis suggested that the cilia of each cell on the ectoderm on the *Ciona intestinalis* embryo was positioned in the posterior half of the cell based on the AP axis of the embryo. Measurements were collected from SEM images, to determine if that initial observation was correct and whether it differed on different regions of the embryo. Each embryo was aligned along its AP axis (Fig. 4.1A), all the cells which are

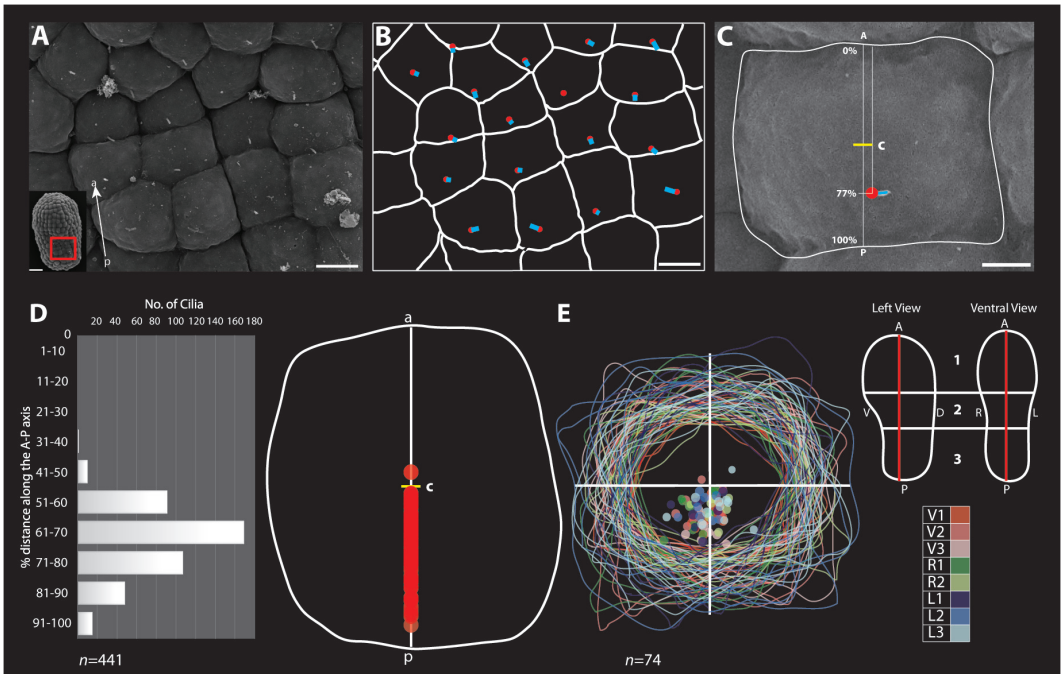


Figure 4.1: Polarisation of cilia on the developing *Ciona intestinalis* embryo to the posterior of each cell.

A: A High magnification SEM image of a late neurula embryo showing the presence of one cilium per cell on the outer ectoderm. Low magnification image of the embryo in the inset shows the anterior (a) and posterior (p). The red boxed area is shown at a higher magnification in A. **B**: A corresponding cartoon of A with an outline of each cell with the location of each cilium anchor (red) and direction of each cilium projection (blue) (Maisonneurve et al. 2009). **C**: A diagram to show the method used to determine the percentage along the embryo and cell AP a cilium was positioned. **D**: A graph to demonstrate the location of each cilium projection as a percentage along the AP axis of each individual cell (*n*=441) on 54 neurula stage embryos. In 432 of cells (98%) the cilium projects posterior to the centrepoint (c, yellow line) of the cell. No cilia project from the anterior 40% of any cell. All the cilia (represented by a red circle) aligned along the centre AP axis of the cell are positioned posterior to the centre point (yellow c). **E**: A comparison of cell location to the position of the cilia. Cells from the future head region (1), middle region (2) tail region (3) on three sides (ventral (red), right (green), left (blue)) of a *Ciona intestinalis* neurula embryo were analysed with the cell outline and position of cilia overlaid to demonstrate the posterior position of cilia. The inset shows the location of each group of cells on a cartoon neurula stage embryo.
Bar = 20 µm (inset A): bar = 5 µm (A, B); bar = 2 µm (C).

parallel to the specimen were traced in Adobe Illustrator and the position of the base of the cilium recorded with a red circle (Fig. 4.1B). The centre of each cell was calculated (c in Fig. 4.1C) and the length of the AP axis of the cell through the centre recorded (Fig. 4.1C). The length through the centre of the cell the cilium was situated along the AP axis was measured and converted into a percentage of the total cell AP axis (Fig. 4.1C). The results of each individual cell (*n*=441) on 54 neurula embryos were collated and a graph to map the distribution calculated (Fig. 4.1D). In 432 of the cells (98%) measured the cilium projects posterior to the centre-point

of the cell, with no cilium projections from the anterior 40% of the cell (Fig. 4.1D).

All the individual cilia (*n*=441) were aligned along the AP axis to demonstrate their position posterior to the centre-point. The embryo was divided into nine regions; three faces (ventral, right and left) and three positions (anterior, 1; middle, 2; posterior, 3) (Fig. 4.1E). Each cell calculated in Fig. 4.1D was traced and assigned a colour depending on the location of the cell on the embryo (red, ventral; green, right; blue, left) with dark colours for cells at the anterior of each face and light colours for the posterior (Fig. 4.1E). The traced cells with their individual cilium were overlain by the centrepoint. All regions of the embryo have cilia posterior to the centrepoint (Fig. 4.1E).

4.2.2 The angle from the centre-point of a cell a cilium is positioned on a *Ciona intestinalis* embryo

Measurements were recorded to analyse whether positioning constraints localise cilia to a particular region of each cell of the *Ciona intestinalis* late neurula/early tailbud stage embryo ectoderm. In addition to information gathered about the location of each cilium along the AP axis, the angle from the centrepoint was also recorded. Each embryo was aligned along its AP axis (Fig. 4.2A), all the cells which are parallel to the specimen were traced in Adobe Illustrator and the location of each cilium anchor (red) and direction of each cilium projection (blue) (Maisonneuve et al. 2009) shown. The centre of the each cell was located and the distance from the anterior to the centre of the cell marked as 0°. The angle from this point to the cilium was measured and recorded (Fig. 4.2A). The embryo was separated into eight segments at 45° angles (Fig. 4.2B) and the number of cilia found in these segments documented (Fig. 4.2C). 83% of cilia were positioned

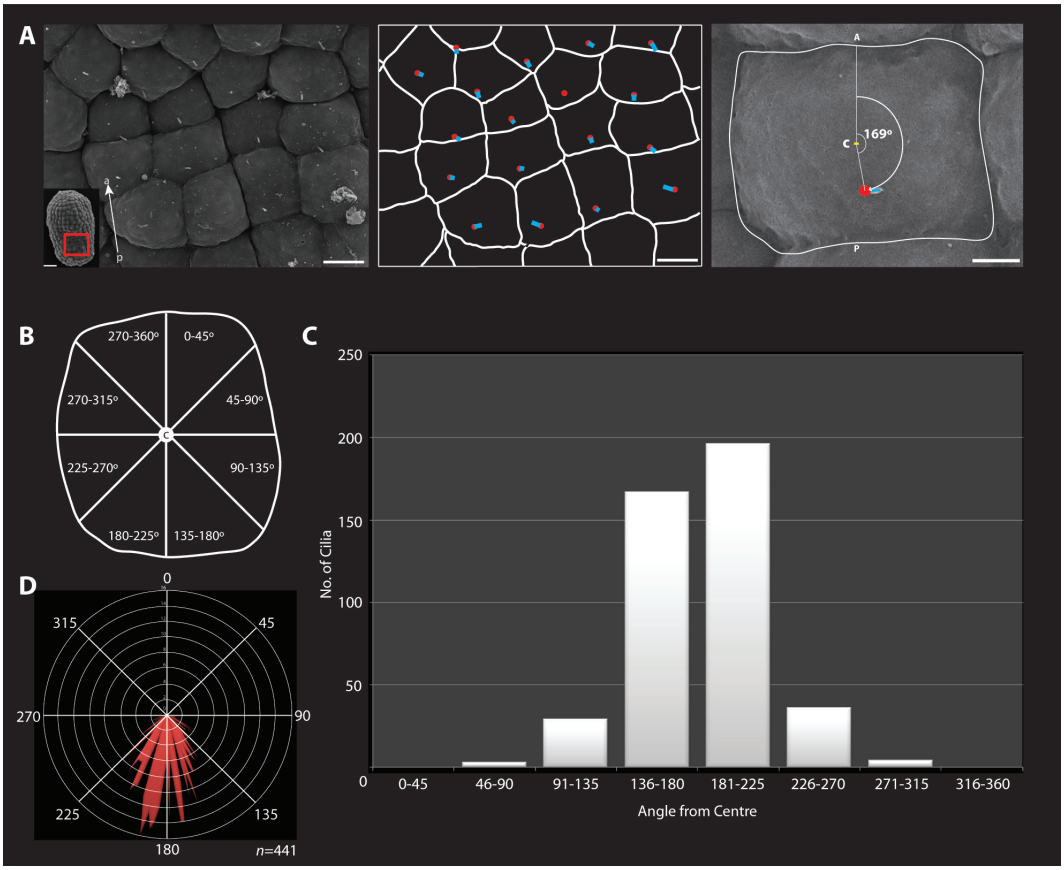


Figure 4.2: The angle of cilia from the centre of each cell on a late neurula stage *Ciona intestinalis* embryo.

A: A High magnification SEM image of a neurula embryo showing the presence of one cilium per cell on the outer ectoderm. Low magnification image of the embryo in the inset shows the anterior (a) and posterior (p). The red boxed area is shown at a higher magnification in A. A corresponding cartoon of A with an outline of each cell with the location of each cilium anchor (red) and direction of each cilium projection (blue) (Maisonneurve et al. 2009) (same images from Fig. 4.1). A diagram to show the method used to determine the angle from the centre of a cell each cilium was positioned. **B**: Each embryo was separated into 45° segments. **C**: A bar chart to demonstrate the distribution of cilia in these 45° segments. 83% of cilia are positioned between 136-225° from the centre of the cell and no cilia are positioned between 0-45° and 316-360°. The highest number of cilia are positioned between 181-225° (*n*=196). **D**: A radar chart to show the frequency of cilia (*n*=441) at each degree from the centre of the cell. 98.9% of cilia were positioned between 90-270° (*n*=436) from the centre.
Bar = 20 µm (inset A): bar = 5 µm (ectoderm); bar = 2 µm (individual cell).

in the 136-225° (*n*=196) segments and no cilia were positioned between 0-45° and 316-360°. The highest number of cilia were positioned between 181-225° (*n*=436). The exact position of each cilium was depicted on a radar graph with the frequency of cilia (*n*=441) at each degree from the centre of the cell shown (Fig. 4.2D). The majority of cilia were positioned between 135 and 225° from the centre of the cell. There were fewer cilia recorded between 90-135° and 225-270°.

4.2.3 The effect cell location on the embryo has on cilia position

The embryo was split into nine different locations; the Face of the embryo (right, ventral and left) and Position along the AP axis (1, 2 and 3) and the cilia position and angle on each cell recorded. The position of each cilium was collected in an identical way to the original positioning experiments. The dorsal face was not incorporated because the closing of the neuropore limited the number of cells that could be accurately measured. Both position and face were taken individually to analyse the mean distance along the AP axis and the angle from the centre each cilium was located. The mean angle position of each cilium did not differ between the different Positions and Faces of the embryo (Fig. 4.3C, E). However, the mean distance along the AP axis at which each cilium was located did differ between the three Positions and also the three Faces (Fig. 4.3B, D). The cilia found on the tailbud region (Position 3) of the embryo had a mean position further along the AP axis than the other two Positions (Fig. 4.3B). Additionally, the cilia on the Ventral face were positioned further along the AP axis (Fig. 4.3D). The different Position and Face percentages and angles were merged and statistically tested by using an ANOVA test incorporating the subtle differences in embryos as a random affect. The location of the cell on the embryo had no affect on the angle of the cilium from the centre of the cell ($F_{4,426}$, $p>0.05$). However, there was a significant difference in cilia position along the AP axis of a cell when the cell is located on the left side of the embryo in the centre of the embryo ectoderm ($F_{4,426,}$ $p<0.01$).

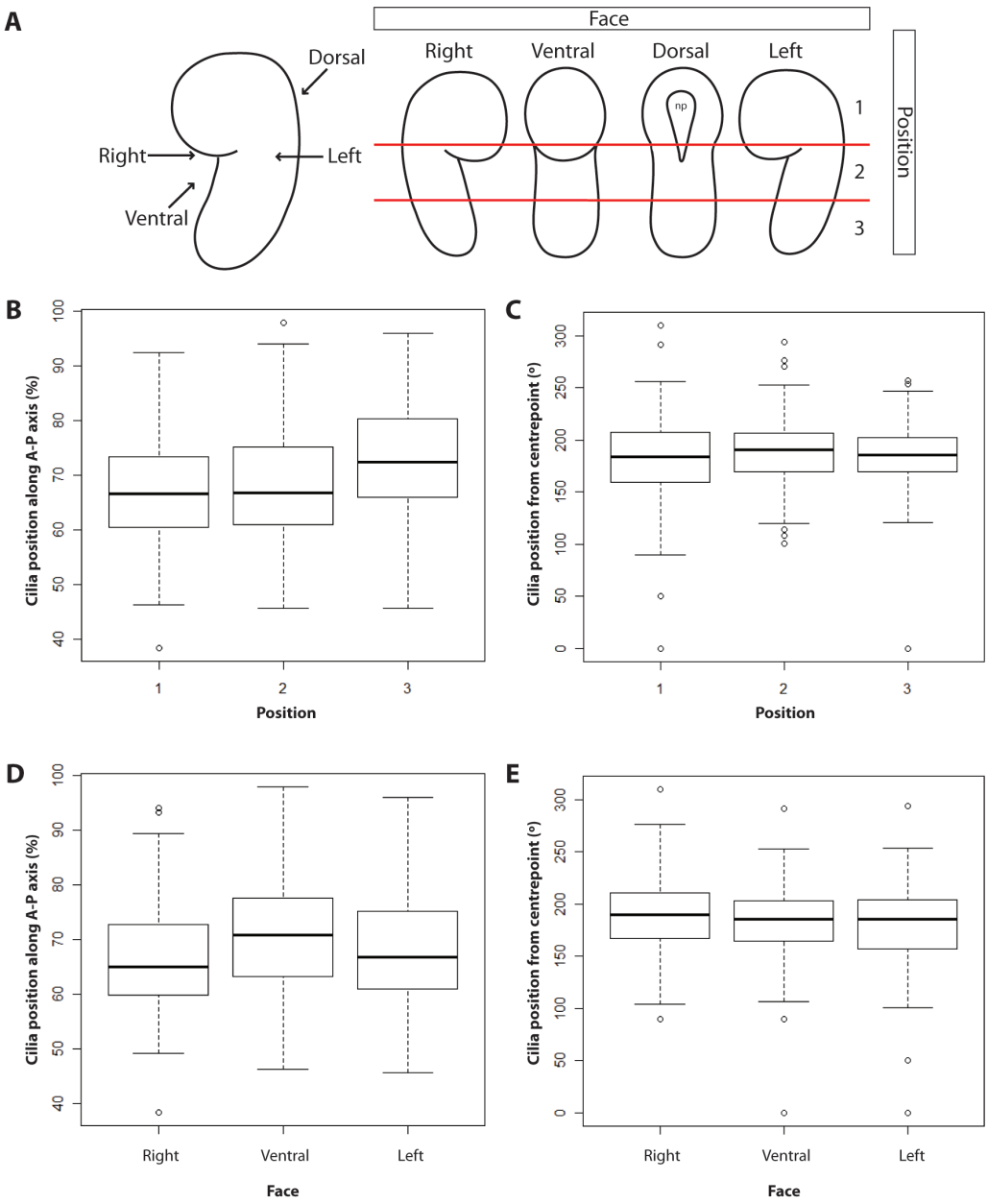


Figure 4.3: The location of a cell on a neurula stage *Ciona intestinalis* embyro affects cilia position along the AP axis but not the angle from the centrepoint.

A: A cartoon representation to demonstrate the segregration of areas on a neurula embryo by face and position. **B**: A boxplot to show the effect cell position on the embryo along the AP axis has on cilia position along the cell AP axis. **C**: A boxplot to show the effect cell position on the embryo along the AP axis has on cilia position from the centrepoint. **D**: A boxplot to show the effect cell position on different faces of the embryo has on cilia position along the cell AP axis. **E**: A boxplot to show the effect cell position on different faces of the embryo has on cilia position from the centrepoint.

4.2.4 The effect of de-chorionation on cilia formation

Cilia are positioned in the posterior half of each cell on the *Ciona intestinalis* embryo at the late neurula and early tailbud stage prior to asymmetric expression of *Ci-Pitx*. The precise timing of the emergence of cilia at the point before molecular asymmetries led to the hypothesis that they have a role in establishing laterality in *Ciona intestinalis*. Previous experiments have shown that the removal of the chorion at fertilisation disrupted molecular asymmetries (Shimeld & Levin 2006). As a result of the timing of cilia emergence prior to molecular asymmetries it was hypothesised that the removal of the chorion at fertilisation could disrupt ciliogenesis and, therefore, left-right asymmetry. To determine if there was a link between cilia and left-right asymmetry, SEM was used to determine if cilia are still present on late neurula and early tailbud embryos de-chorionated at fertilisation. A lack of cilia could explain why de-chorionated embryos displayed bi-lateral *Ci-Pitx* expression. *Ciona intestinalis* embryos were de-chorionated at fertilisation and grown on 1% FSW-agarose in FSW and 30mg/ml gentamycin. At the late neurula and early tailbud stages of development the embryos were fixed for SEM. Control embryos (n=120) were allowed to develop within the chorion and were de-chorionated at neurula and tailbud stages and immediately placed in the fixative.

Control embryos were identical to previously described SEM experiments with a clear cilium at the posterior of each cell on the embryo ectoderm at both neurula (Fig. 4.4A-C) and tailbud (Fig, 4.4D-F) stages. Cilia are indicated by a white arrow and the cell boundaries by a white chevron. The control embryo ectoderm cells were spherical and the apical surface domed with distinct cell boundaries. In contrast, the embryos de-chorionated at fertilisation and grown outside the chorion had cells with a flatter apical surface and less distinct cell boundaries at

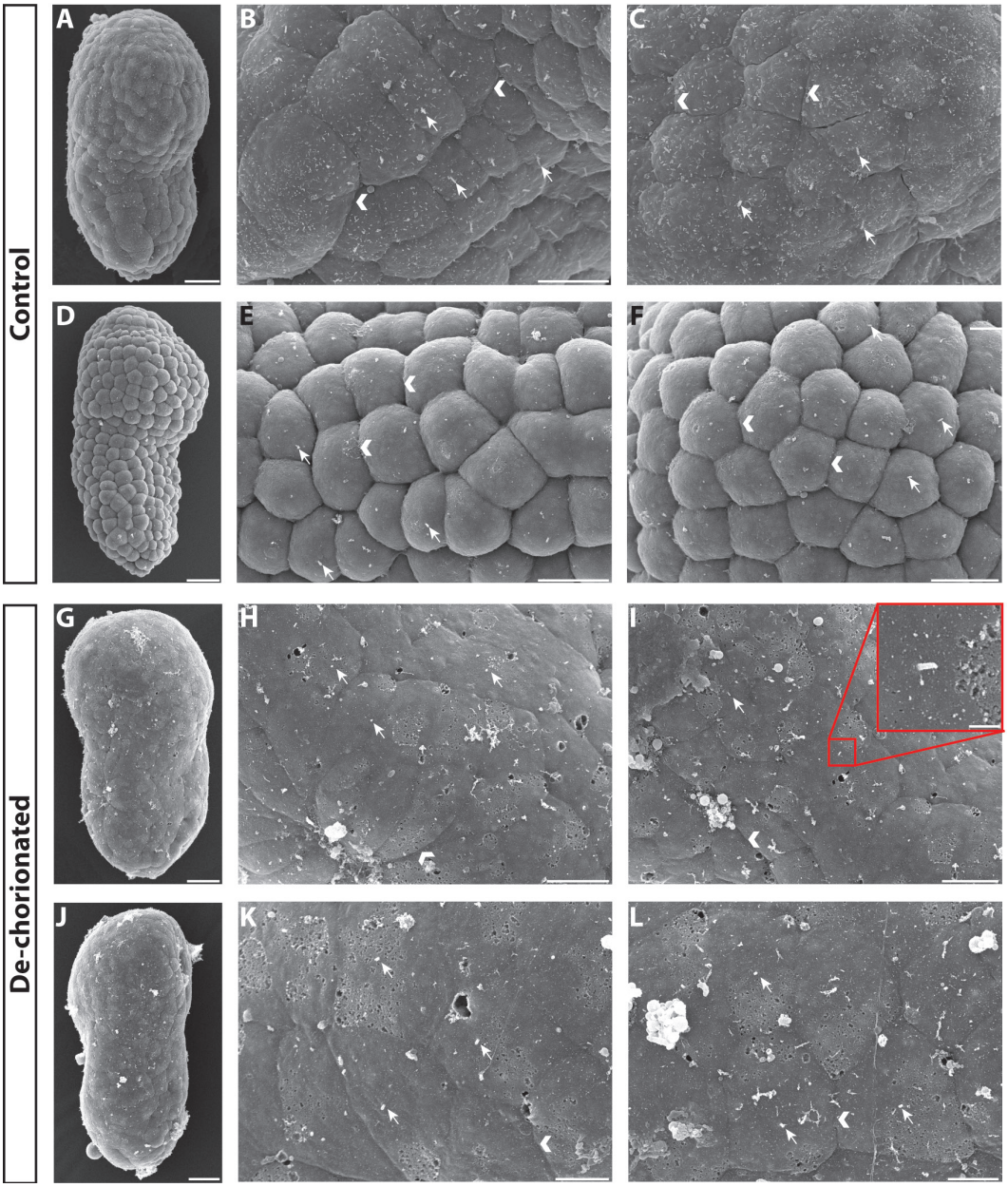


Figure 4.4: De-chorionation at fertilisation does not remove cilia on tailbud stage *Ciona intestinalis* embryos.

A,**D**: Tailbud embryo allowed to develop within the chorion which is removed using protease and sodium glycolate just prior to fixation. **B**: An image from the tail region and **C**: the head region of the control neurula embryo showing the presence of cilia (white arrows) and clear cell boundaries (white chevron). **E**: An image from the tail region and **F**: the head region of the control tailbud embryo showing the presence of cilia (white arrows) and clear cell boundaries (white chevron). **G**, **J**: Tailbud embryo de-chorionated using protease and sodium glycolate immediately after fertilisation and grown independently from the chorion on 2% FSW agarose in 30 mg/ml gentamycin. At the correct stage embryos were removed from the agarose and fixed for SEM. **H**, **K**: An image from the tail region and **I**,**L**: the head region of their respective stage embryos showing the presence of some cilia (white arrows) and indistinct cell boundaries (white chevron). Bar = 20 µm (A, D, G, J); bar = 10 µm (B, E, F, H, I); bar = 5 µm (C, K, L); 1 µm (inset I)

both the neurula (Fig. 4.4G-H) and tailbud (Fig. 4.4J-L) stages. Importantly, both stages of embryo also showed distinct cilia (Fig. 4.4 Insert in I) at ~1.0 μm in length. The lack of clear cell boundaries inhibited the definition that each cilium was positioned to the posterior of each cell. Both condition embryos showed signs of damage on the ectoderm cells with holes and areas of disintegrated membrane which was a result of mechanical damage post-fix (Fig. 4.4 Insert in I). The shape of the experimental de-chorionated embryo contrasted with the control embryos at both stages. In the control embryos the tailbud bends around towards the ventral, head of the embryo but in the experimental embryos the tailbud remained straight with no bend towards the head region. In some experimental embryos analysed the tailbud was at the commencement of bending towards the dorsal side of the embryo.

4.2.5 Experimental manipulation of cilia on a *Ciona intestinalis* embryo

De-chorionation of *Ciona intestinalis* embryos at fertilisation did not prevent cilia formation at the late neurula and early tailbud stages of development. To assess whether cilia are required for correct laterality experimental manipulation was required to remove cilia. Experiments were conducted through microinjection with a morpholino against *IFT88,* an intraflagellar transport protein required for ciliogenesis, to perturb cilia formation. The number of experimental *Ciona intestinalis* embryos developing post *IFT88* morpholino microinjection was lower than required for further analysis. As a result another method of de-ciliation was required to generate large numbers of embryos for further analysis by SEM and *in situ* hybridisation. Any method must remove cilia whilst the chorion remains, so a link between cilia presence and laterality can be

detected without the complication of bilateral *Ci-Pitx* expression through de-chorionation at fertilisation. Previous experimentation in *Paracentrotus lividus* has demonstrated that the sea urchins respond to stress by de-ciliation (Casano et al. 1998) and especially from exposure to increased NaCl concentrations. Consequently, *Ciona intestinalis* embryos were exposed to high levels of NaCl and the presence of cilia reviewed. *Ciona intestinalis* embryos were grown in FSW until neurula stage and the commencement of ciliogenesis at which point experimental embryos were subjected to an increased amount of NaCl (4.45M) for 2 mins, and then returned to FSW to grow to late tailbud stage. Additional FSW was added to the control embryos to an equivalent volume. Embryos were de-chorionated and fixed for SEM 0 mins, 10 mins and 30 mins after the NaCl increase to evaluate the presence or absence of cilia. Embryos were also collected for *Ci-Pitx* in situ hybridisation at 60 mins, 90 mins and 120 mins, post NaCl increase.

The embryos fixed for SEM demonstrated cilia were present at the posterior of each cell in all conditions and time points (Fig, 4.5A-F'). The cilia were 1.5-2 μm in length in the control and experimental conditions at 0 mins, 10 mins and 30 mins. The cilia in the control condition at all time points (Fig. 4.5A, A', B, B', C, C', F, F') and the cilia at the experimental time point immediately post 4.45M NaCl exposure were always situated in a central to posterior position whereas the cilia in the experimental condition 10 mins (Fig. 4.5D, D') and 30 mins (Fig. 4.5F, F') after exposure were positioned at the very posterior of each cell.

Initial SEM images of embryos at 0 mins after exposure to NaCl were similar to the control embryos (Fig. 4.5A, B) but the embryos collected 10 and 30 mins after exposure to NaCl suggested that cilia were positioned further to the posterior of each cell (Fig. 4.5D, F). In total, individual cells (n=54) on nine control neurula and cells (n=42) on five NaCl neurula were analysed to assess the effect at 0 mins after exposure to 4.45M NaCl has on cilia position. In

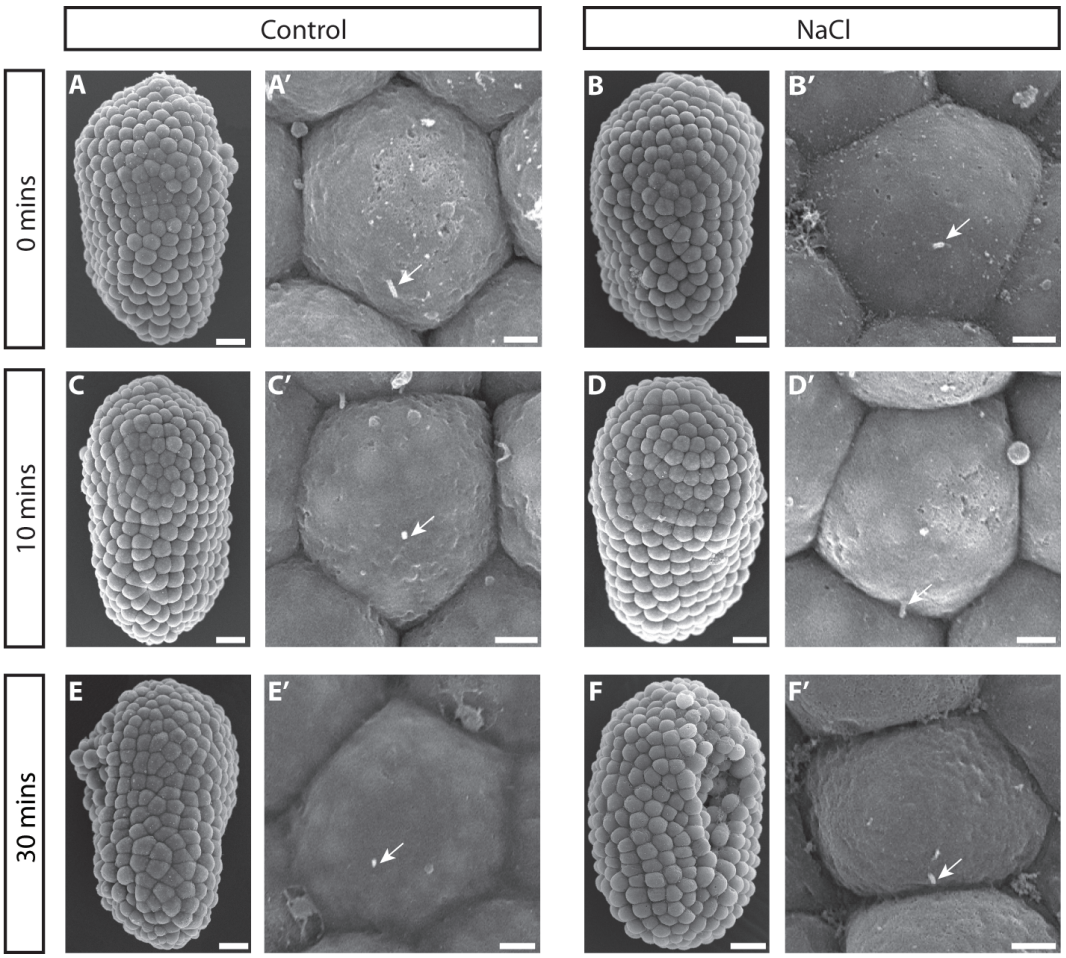


Figure 4.5: The position of cilia along the AP axis on *Ciona intestinalis* embryos 10 and 30 mins after exposure to NaCl.

A, **C**, **E**: SEM of control embryos at 0 mins, 10 mins and 30 mins. **A′**, **C′**, **E′**: High magnification images of cilia (white arrows). **B**, **B′**: SEM of experimental embryos at 0 mins immediately after a 2 min exposure to 4.45M NaCl. **D**, **D′**, **F**, **F′**: SEM of experimental embryos at 10 mins and 30 mins after a 2 min exposure to 4.45M NaCl. All embryos developed within the chorion which was removed prior to fixation for SEM.
Bar = 20µm (A, B, C, D, E, F); bar = 2µm (A′, B′, C′, D′, E′, F′)

both the control and experimental condition 100% of the cilia are positioned posterior to the centre-point (Fig. 4.6A). The distribution of cilia along the AP axis of the cell is similar in both conditions. However, in the control condition the highest proportion of cilia were positioned 81-90% along the cell AP axis against 91-100% along the AP axis in the experimental condition (Fig. 4.6A). The average distance along the AP axis in the control embryos (81.3%) and NaCl embryos (82.6%) was only a 1.3% difference between the conditions. The alignment of the cilium along the AP axis demonstrated the similar distribution in both the control and the NaCl condition

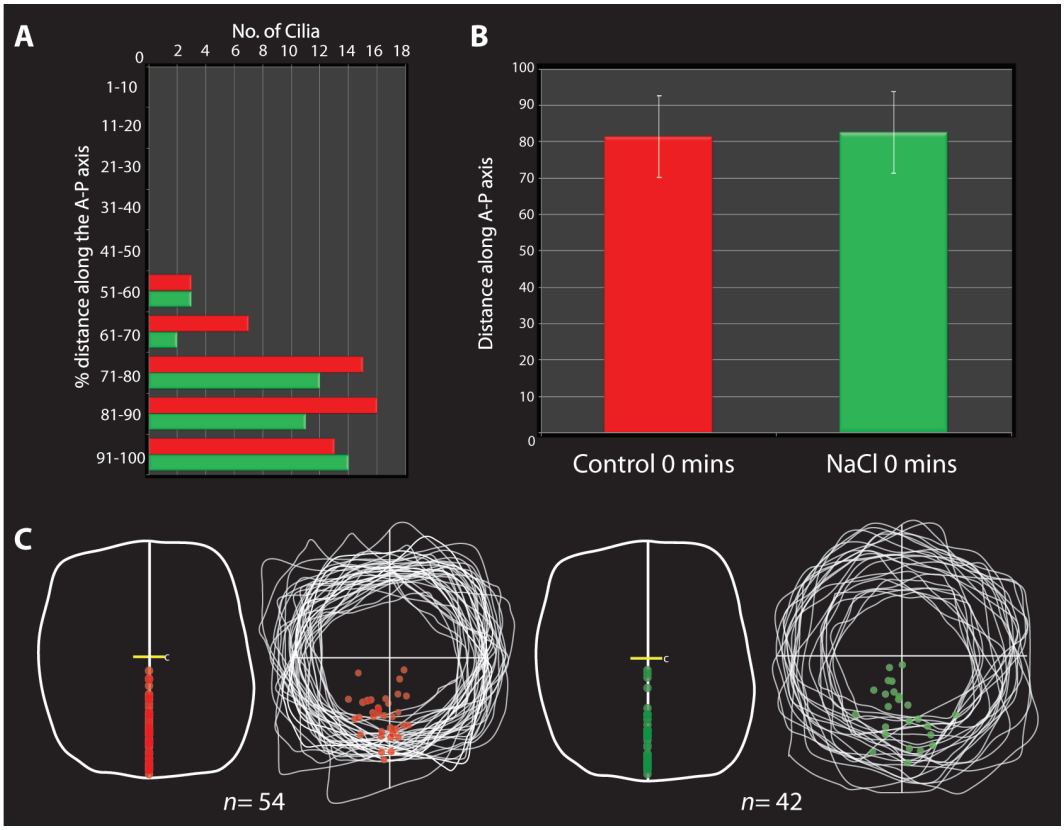


Figure 4.6: The effect of NaCl exposure on the cilia position along the AP axis on a developing *Ciona intestinalis* embryo 0 mins after exposure.

A: A graph to demonstrate the location of each cilium projection as a percentage along the AP axis of each individual cell in the control (red) and NaCl condition (green). Experimental embryos were subjected to an increased amount of NaCl for 2 mins at the early neurula stage and then immediately fixed. The position of cilia on individual cells (n=54) on 9 control neurula stage embryos were analysed alongside cells (n=42) on 5 NaCl condition embryos. **B**: A graph to show the average distance along the cell A-P axis that cilia are positioned for control embryos (81.3%) and NaCl embryos (82.6%). **C**: A cartoon cell to demonstrate the position of cilia along the AP axis posterior to the centre point (c, yellow line). In both 54 control cells and 42 NaCl exposed cells 100% of cilia were postioned posteriorly. A trace of each cell was overlain by the centrepoint shows the position of each cilium.

(Fig. 4.6C). The individual cells were traced and overlain by the centre-point and colour co-ordinated depending on the cell location on the embryo (as previously described at Fig. 4.1) (Fig. 4.6C). The distribution of the cilia is comparable between the two conditions.

In contrast, the distribution of cilia along the AP axis was very different 10 mins after exposure to 4.45M NaCl. Individual cells (*n*=73) on nine control embryos and cells (*n*=24) on five experimental embryos were measured and calculated at 10 mins after exposure. The control distribution was a standard bell curve with the highest number of cilia between 71-80% along

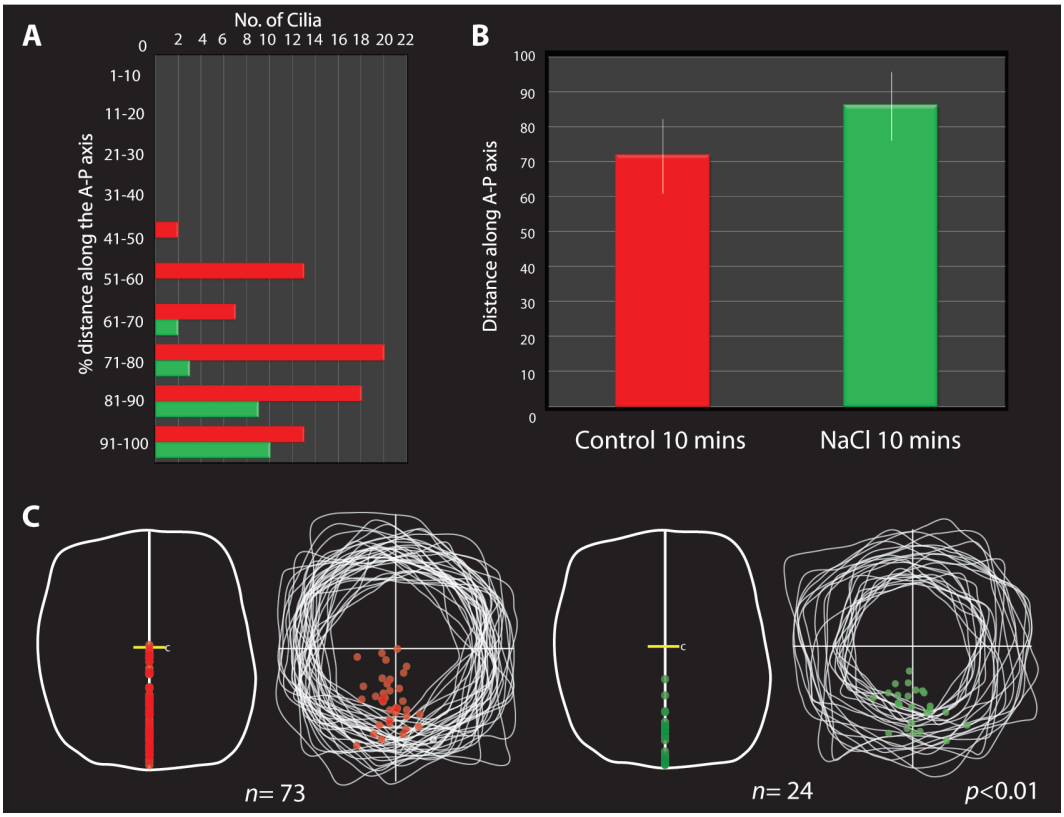


Figure 4.7: The effect of NaCl exposure on cilia position along the AP axis on a developing *Ciona intestinalis* embryo 10 mins after exposure.

A: A graph to demonstrate the location of each cilium projection as a percentage along the AP axis of each individual cell in the control (red) and NaCl condition (green). Experimental embryos were subjected to an increased amount of NaCl for 2 mins at the early neurula stage and then allowed to grow in normal FSW conditions for 10 mins. The position of cilia on individual cells (*n*=73) on 9 control neurula stage embryos were analysed alongside cells (*n*=24) on 5 NaCl condition embryos. **B**: A graph to show the average distance along the cell AP axis that cilia are positioned for control embryos (69%) and NaCl embryos (86.5%). **C**: A cartoon cell to demonstrate the position of cilia along the AP axis posterior to the centre point (c, yellow line). In 73 control cells, 97.2% of cilia are positioned in the posterior half of the cell and in 24 NaCl exposed cells 100% of cilia were postioned posteriorly. In NaCl exposed cells 100% of cilia were positioned in the posterior 25% of the cell. A trace of each cell was overlain by the centrepoint shows the position of each cilium.

the AP axis and the lowest <41% (Fig. 4.7A). In the experimental condition the region 91-100% along the AP axis had the highest number of cilia with no cilia present in the anterior 60% of the cell (Fig. 4.7A). The average percentage distance along the AP axis the cilia were situated in the control condition (69%) was lower than the experimental condition (86.5%) (Fig. 4.7B). In 73 control cells, 97.2% of cilia were positioned in the posterior half of the cell and in 24 NaCl exposed cells 100% of cilia were positioned posteriorly. In NaCl exposed cells 100% of cilia were positioned in the posterior 25% of the cell (Fig. 4.7A). The alignment of cilia along the AP axis of

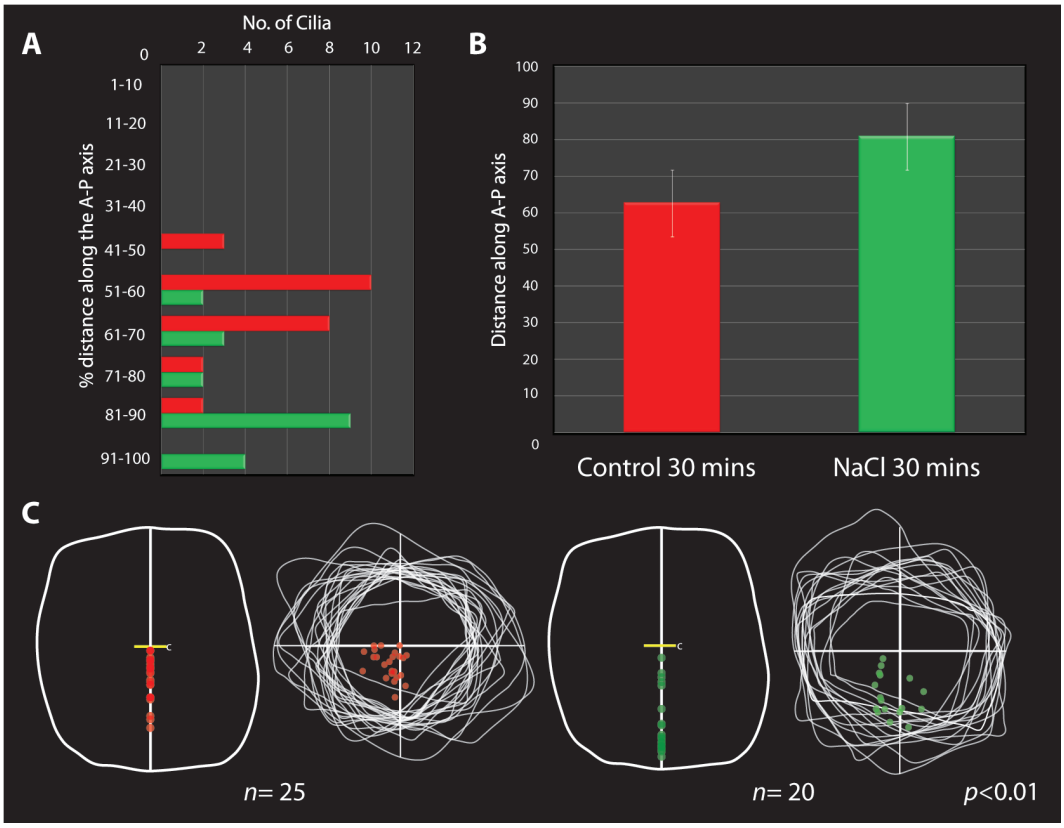


Figure 4.8: The effect of NaCl exposure on cilia position along the AP axis on a developing *Ciona intestinalis* embryo 30 mins after exposure.

A: A graph to demonstrate the location of each cilium projection as a percentage along the AP axis of each individual cell in the control (red) and NaCl condition (green). Experimental embryos were subjected to an increased amount of NaCl for 2 mins at the early neurula stage and then allowed to grow in normal FSW conditions for 30 mins. The position of cilia on individual cells (*n*=25) on 7 control neurula stage embryos were analysed alongside cells (*n*=20) on 6 NaCl condition embryos. **B**: A graph to show the average distance along the cell AP axis that cilia are positioned for control embryos (62.7%) and NaCl embryos (80.9%). **C**: A cartoon cell to demonstrate the position of cilia along the AP axis posterior to the centre point (c, yellow line). In 25 control cells, 100% of cilia are positioned in the posterior half of the cell and in 20 NaCl exposed cells 100% of cilia were postioned posteriorly. A trace of each cell was overlain by the centrepoint shows the position of each cilium.

a cartoon cell demonstrates the contrast between the more posterior experimental embryo cilia and the control embryo cilia (Fig. 4.7C).

At 30 mins after exposure to either FSW or NaCl, individual cells (*n*=25) on seven control embryos and cells (*n*=20) on six NaCl were measured. The control embryos cilia were distributed between 41 and 90% with the highest number of cilia situated between 51-60% along the AP axis. The experimental embryos cilia were predominantly 81-90% along the AP axis with 45% of the cilia positioned in this region (Fig. 4.8A). The average control embryo cilium is positioned, 62.7%

along the AP axis and the experimental embryo cilium, 80.9% (Fig. 4.8B). The experimental embryo cilia are situated 18.2% further towards the posterior of the cell than the control embryo cilia (Fig. 4.8C). Statistics using an ANOVA test (as discussed in part 4.2.3) have shown that the high levels of NaCl did not affect the cilia position at 0 mins after exposure ($F_{4,237,}$ $p>0.05$) but at 10 and 30 mins after the cilia are positioned at a more posterior position along the cell AP axis ($F_{4,237}$, $p<0.01$).

As well as the distance along the AP axis each cilium is positioned, the angle from the centre was recorded for all the different conditions and times. The angle measurement was taken using the same method discussed earlier (Fig. 4.2A). The distribution of the angle at different time points post exposure to 4.45M NaCl was plotted on bar charts. In both the control and the NaCl condition the cilia were located in between, except in one case, the 90° and 270° angle from the centre (Fig. 4.9B, C, D). The average angle from the centre at 0 mins, 10 mins and 30 mins differed by 32.48° in both conditions and was not significantly different between the different time points.

4.2.6 The effect of exposure to 4.45M NaCl on *Ci-Pitx* expression in *Ciona intestinalis* embryos

SEM analysis and measurements have demonstrated that cilia are positioned in a more posterior position along each cell's AP axis in embryos that were exposed to 4.45M NaCl for 2 mins during the neurula stage. Embryos were harvested for SEM immediately, 10 mins and 30 mins after NaCl exposure to assess the effect high NaCl concentrations have on cilia development in a developing *Ciona intestinalis* embryo. To determine if exposure to 4.45M NaCl has an effect on left-right

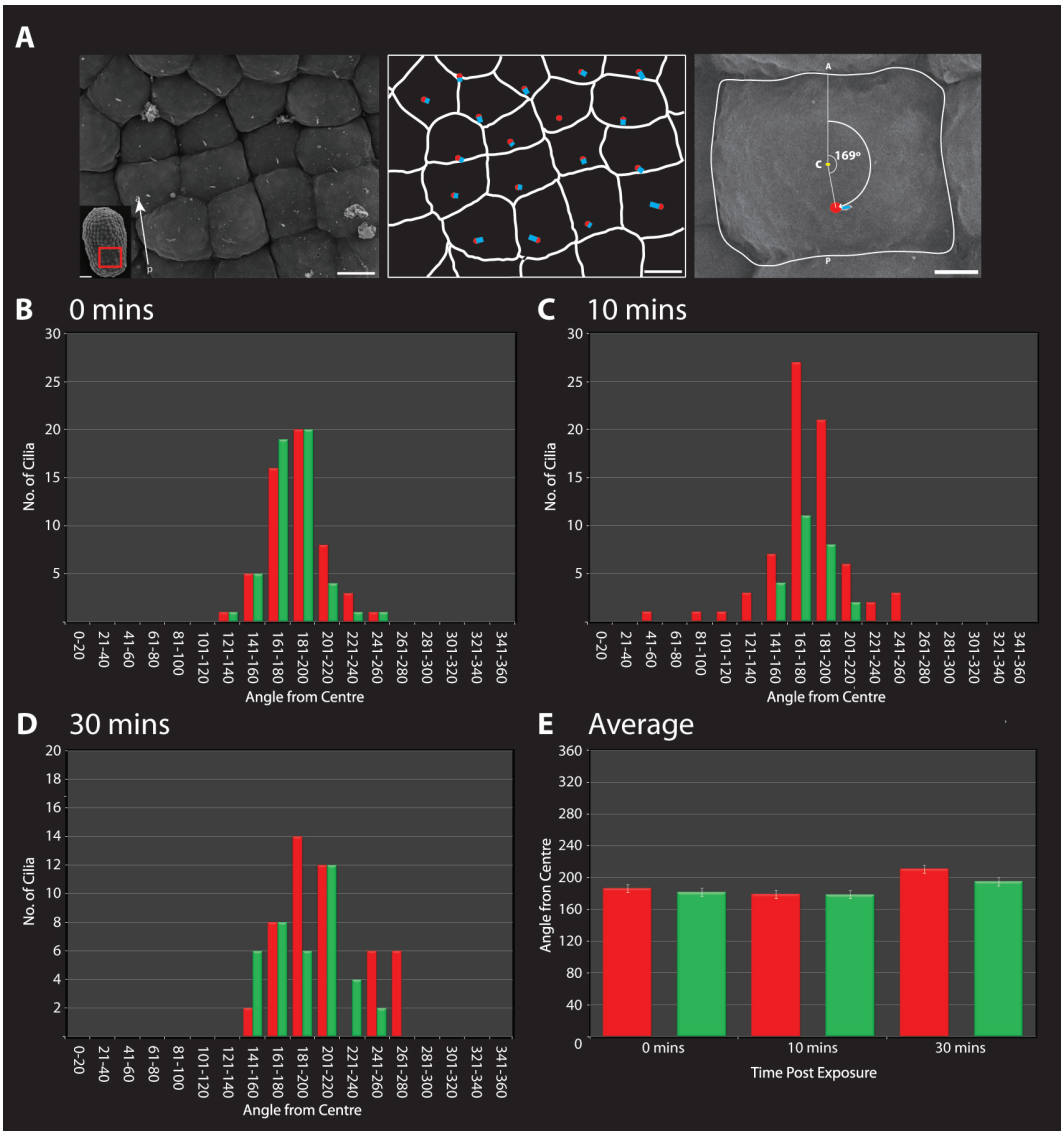


Figure 4.9: The effect of NaCl exposure on *Ciona intestinalis* neurula stage cilia angle from the centre of each cell.

A: A High magnification SEM image of a neurula embryo showing the presence of one cilium per cell on the outer ectoderm. Low magnification image of the embryo in the inset shows the anterior (a) and posterior (p). The red boxed area is shown at a higher magnification in A. A corresponding cartoon of A with an outline of each cell with the location of each cilium anchor (red) and direction of each cilium projection (blue) (Maisonneurve et al. 2009) (same images from Fig. 4.1). A diagram to show the method used to determine the angle from the centre of a cell each cilium was positioned. **B**: A graph to show the number of cilia projections in 20º segments from the AP axis and centrepoint immediately after exposure to 4.45M NaCl for control (red, *n*=54) and experimental (green, *n*=51) embryos. **C**: Experimental embryos were subjected to an increased amount of NaCl for 2 mins at the early neurula stage and then allowed to grow in normal FSW conditions for 10 mins. The position of cilia on individual cells (*n*=72) on 9 control neurula stage embryos were analysed alongside cells (*n*=25) on 5 NaCl condition embryos. **D**: The angle of cilia, after exposure to 4.45M NaCl and then allowed to grow in normal FSW conditions for 30 mins, for the control (*n*=24) and experimental (*n*=19). **E**: A graph to show the average angle from the centre of each cell to the position of the cilium at the three time points after exposure to NaCl.
Bar = 20 µm (inset A): bar = 5 µm (ectoderm); bar = 2 µm (individual cell).

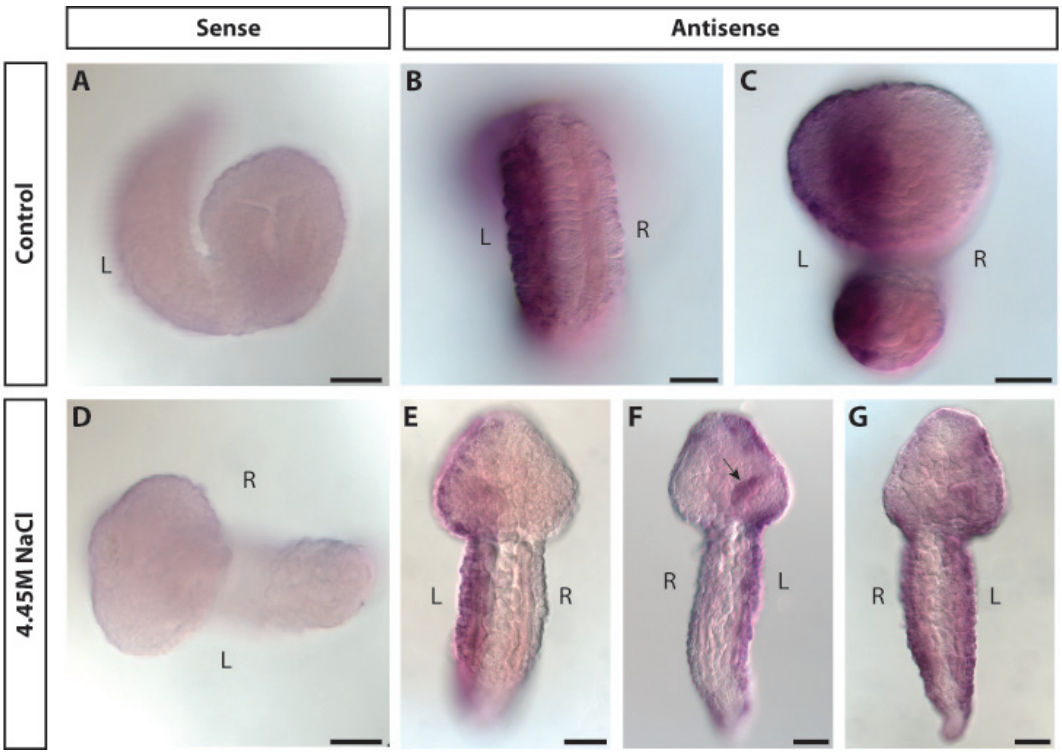


Figure 4.10: The localisation of *Ci-Pitx* expression in the left ectoderm and mesenchyme of 4.45M NaCl exposed *Ciona intestinalis* embryos.

A-C: Control Tailbud embryos hybridised with sense and antisense probes for *Ci-Pitx*. **A**: No staining in the embryo hybridised with the sense probe. **B**: Dorsal view of the tailbud region of an embryo with anterior to the top. *Ci-Pitx* expression is shown in left-side (L) ectoderm. **C**: Dorsal view of the head and tailbud region of a tailbud embryo with the anterior to the top. In both the head and tail region left-sided (L) *Ci-Pitx* expression is shown in the ectoderm. **D-G**: Tailbud embryos were exposed to 4.45M NaCl for 2 mins at the late neurula/early tailbud stage and allowed to grow in FSW to the mid tailbud stage. **D**: No staining in the embryos hybridised with the sense probe. **E**: A dorsal view of an experimental embryo with normal left-sided *Ci-Pitx* expression. **F**: The ventral view of an experimental embryo with *Ci-Pitx* expression in the left-side tail and head ectoderm and head mesenchyme (arrow). **G**: Dorsal view of an experimental embryo with bi-lateral *Ci-Pitx* expression. All embryos were grown within the chorion until immediately before fixation. R, right. Bar = 25 µm (A-G)

asymmetry with a potential link to cilia, embryos were allowed to grow to the late tailbud stage in FSW. Previous experiments have shown that a left-right determinant, *Ci-Pitx*, is expressed in the left mesenchyme and ectoderm of a tailbud *Ciona intestinalis* embryo (Boorman & Shimeld, 2002). *Ci-Pitx* expression is first detected in the Buccal Cavity (BC) but later is expressed in the left-side of the head and tail region. Removal of the chorion after fertilisation disrupts *Ci-Pitx* expression with ectopic and bilateral expression (Shimeld & Levin 2006) and brain asymmetry. *Ci-Pitx* is a molecular marker for *Ciona intestinalis* left-right asymmetry and was used here to

determine if NaCl treatment positioning leads to ectopic, bilateral or normal *Ci-Pitx* expression. *Ci-Pitx in situ* hybridisations were conducted on 4% PFA fixed tailbud embryos allowed to develop for 90 and 120 mins after exposure to 4.45M NaCl. A sense and antisense *Ci-Pitx* probe were made with the sense acting as the control. In neither the control nor the experimental embryos hybridised with the sense probe was there any staining (Fig. 4.10A, D). In 46.15% of control embryos (*n*=18/39), *Ci-Pitx* expression was restricted to the left mesenchyme and ectoderm (Fig. 4.10B, C) when observed from the dorsal side of the embryo. The other 53.85% had *Ci-Pitx* expression in the head and tail bilaterally (5.13%), buccal cavity only (15.38%) or no detectable *Ci-Pitx* expression at all (33.34%) (Fig. 4.11). The embryos that had no evidence of *Ci-Pitx* expression in any tissue were removed from further analysis because it is not possible to distinguish between a genuine change and a failure in the *in situ* hybridisation process. Once the no *Ci-Pitx* expression embryos were removed from the analysis *Ci-Pitx* expression was still pre-dominantly in the left-side of the embryo (69.23%) or the buccal cavity (23.08%) with only 7.69% of embryos with additional *Ci-Pitx* expression in the right tail (Fig. 4.11).

In experimental embryos, *Ci-Pitx* expression was predominantly found in the left-side head and tail of the embryo (38.27%) (*n*=31/81) but there were more embryos with ectopic *Ci-Pitx* expression (Fig. 4.10G). The other 61.73% had *Ci-Pitx* expression in the head and tail bilaterally (8.64%), buccal cavity only (11.11%) or no *Ci-Pitx* expression at all (29.63%) (Fig. 4.11). The 29.63% of experimental embryos with no *Ci-Pitx* expression were removed from the analysis as before. Once the no *Ci-Pitx* expression embryos were removed from the analysis *Ci-Pitx* expression was still pre-dominantly in the left-side of the embryo (54.39%) or the buccal cavity (15.79%) with 12.28% of embryos with additional *Ci-Pitx* expression in the right tail (Fig. 4.10G). *Ci-Pitx* expression was also limited to just the left head region with no tail expression

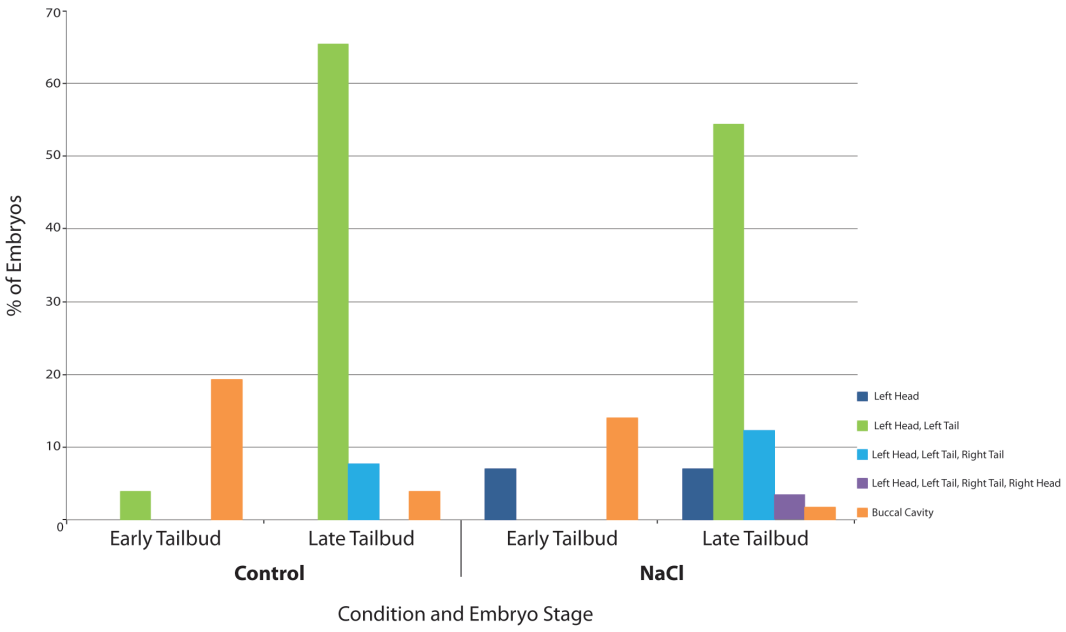


Figure 4.11: *Ci-Pitx* expression in *Ciona intestinalis* early and late tailbud embryos after exposure to 4.45M NaCl.

Ciona intestinalis embryos were exposed to 4.45M NaCl or, as a control, FSW at the onset of ciliogenesis for 2 mins then allowed to grow in FSW until late tailbud stage. *In situ* hybridisations for *Ci-pitx*, a molecular asymmetric marker, were conducted on both sets of embryos. Previous experiments have demonstrated *Ciona intestinalis* tailbud embryos express *Ci-pitx* in the left mesenchyme and ectoderm (Boorman and Shimeld, 2002). Control and experimental embryos were scored on the location of *Ci-pitx* expression at two developmental stages.

in the experimental condition which was not observed in the control embryos (14.04%) (Fig. 4.11). Through using an ANOVA test no significant difference was found between the two conditions. Thus altering the position of cilia on the *Ciona intestinalis* embryo does not prevent the asymmetric distribution of *Ci-Pitx*.

4.3 DISCUSSION

As discussed in Chapter 3, cilia are present on a late neurula/early tailbud stage *Ciona intestinalis* embryo immediately prior to asymmetric molecular, *Ci-Nodal* and *Ci-Pitx*, expression (Boorman & Shimeld 2002a; Morokuma et al. 2002; Yoshida & Saiga 2008; Mita & Fujiwara 2007) and persist for one hour from when they first emerge. The cilia do not have a central pair or dynein

arms required for motility and the nine doublet microtubule axoneme with nine fold symmetry breaks down ~140 nm from the transition zone as the cell exits the cell. Although the cilia do not appear to have a conserved motile role in the establishment of left-right asymmetry the timing of their presence still points towards a role in left-right asymmetry. Analysis of the ultrastructure indicates that the cilia have a sensory role in development and could potentially be the cellular site of H^+/K^+-ATPase ion flux first described in *Xenopus* (Levin et al. 2002). In this chapter, I examine the positioning constraints of cilia on the *Ciona intestinalis* embryo as well as the effect the manipulation of cilia presence and positioning has on the establishment of molecular left-right asymmetry to try to elucidate their role in the invertebrate model.

4.3.1 Polarisation of *Ciona intestinalis* cilia

On the late neurula and early tailbud *Ciona intestinalis* embryo the cilia appear to project from the posterior of each cell which suggests they are under strict positioning control (Fig. 3.8). To assess whether this observation was true, measurements of the cilium location along the AP axis and angle from the centre of each cell were collected. The distance of the cilium along the AP axis of the cell was converted to a percentage, to incorporate differences in cell size, and the angle of each cilium were both collated to determine if cilia are positioned at the posterior of each cell. In 432 cells measured the cilium projects posterior to the centre-point of the cell with no cilium projections from the anterior 40% of the cell (Fig. 4.1). Additionally, 83% of cilia were positioned in the 136-225º segments and no cilia were positioned between 0-45º and 316-360º from the centre of the cell (Fig. 4.2). It is clear that the positioning of cilia on a *Ciona intestinalis* embryo is under strict control and there are particular constraints to position cilia at the posterior.

4.3.2 Planar Cell Polarity in organisms

Polarisation of cells in the apical plane is a common feature in the Metazoan clade and is known to be instructed by the Planar Cell Polarity (PCP) pathway (see reviews Jones & Chen 2007; Simons & Mlodzik 2008). The PCP pathway controls the polarisation of cells across an epithelial sheet or the migration and intercalation of cells during convergent extension. In *Drosophila melanogaster*, the PCP pathway is required for the uniform pattern formed by distally oriented hairs that cover the dorsal and ventral surfaces of the wing. During pupal development each cell has a single wing hair composed of bundled actin filaments which is assembled at the distal vertex of the hexagon shaped cells (Wong & Adler 1993). Any mutation which results in a lack of PCP signalling results in disorganisation of hairs. The orientation of the tiny hairs on the *Drosophila melanogaster* fly wing was one of the first models used to elucidate the PCP pathway and the PCP genes, known as the core genes, required for polarisation (Strutt & Strutt 2005; Klein & Mlodzik 2005; Gubb & Garcia-Bellido 1982).

4.3.3 Planar Cell Polarity pathway in vertebrates

In vertebrates, the PCP pathway is required for the body hair orientation, polarisation of the sensory epithelium in the inner ear and the directed movement of mesenchymal cell populations during gastrulation (Dabdoub 2003; Guo et al. 2004; Keller 2002; Montcouquiol et al. 2003). In particular the role of PCP has been observed in Convergent Extension (CE) in vertebrates, a the process by which the tissue of an embryo is restructured to converge along one axis and

elongate along a perpendicular axis by cellular movement (Kuhl et al. 2001; Van Aelst & Symons 2002; Wallingford et al. 2002). Orthologues of the core *Drosophila melanogaster* PCP proteins, Dishevelled (DVL2, DVL3), Frizzled (FZ3, FZ6), Van Gogh like (VANGL2) and Prickle (PK2) were found in mammalian species expressed asymmetrically in tissues which display PCP (Wang et al. 2006a; Hamblet 2002; Wang & Nathans 2007; Wang et al. 2006b; Etheridge et al. 2008; Montcouquiol et al. 2003; Montcouquiol et al. 2006; Deans et al. 2007). *Dsh* is required for the apical docking and planar polarisation of basal bodies in the *Xenopus* ciliated epidermis (Park et al. 2008). Downstream *Drosophila melanogaster* PCP effector genes are also highly conserved in the vertebrates with Rho/Rac GTPases, Rho kinase2 and JNK all present in vertebrate genomes (Habas et al. 2001; Habas et al. 2003; Marlow et al. 2002; Yamanaka et al. 2002).

Frizzled (Fz) and Dishevelled (Dsh) (Axelrod 2001) are the central proteins in the PCP signalling pathway and are controlled through Stbm/Vang and Pk which together inhibit the Fz-Dsh PCP pathway (Jenny et al. 2003; Tree et al. 2002). It is not yet known what initiates Fz-PCP but research has shown that the interaction with Stbm/Vang/Pk and other proteins like Flamingo (Fmi) (Das et al. 2002; Shimada et al. 2001) regulate the pathway. The interaction between these proteins aligns them at the opposite side of cells setting up a gradient in-between. Any disorganisation of the localisation of these proteins causes disruption to PCP (Carreira-Barbosa 2003; Goto & Keller 2002). Downstream of Fz is the protein, Dsh, a cytoplasmic phosphoprotein which is part of the canonical Wnt pathway (Wallingford et al. 2000). Both Fz and Dsh are components of the canonical Wnt pathway but in the PCP pathway there is no evidence for a role for the other Wnt pathway proteins which feature in this particular pathway. The downstream effectors of the PCP pathway differ depending on the context, either cytoskeletal reorganisation or transcriptional response but involve Rho/Rac GTPases.

4.3.4 The control of cilia organisation in the vertebrate inner ear

Cilia are also organised and positioned under the strict control of the PCP pathway in the inner ear of vertebrates. A Kinocilium is a single microtubule based cilium which is surrounded by actin based hairs known as stereocilia in the vertebrate inner ear. The stereocilia and kinocilia are regularly patterned bundles of actin-rich hairs with a central kinocilium which transduces extracellular, mechanical signals into the cell by opening ion channels. All the core PCP proteins have been implemented in the tight control of sensory cilia in the inner ear. In PCP core protein mutant mice, the stereocilia remain patterned around the kinocilium but the kinocilium is randomly positioned (Wang et al. 2006; Wang et al. 2005; Montcouquiol et al. 2003; Curtin et al. 2003). These experiments prove that the positioning of cilia can be controlled by the PCP pathway.

4.3.5 PCP in left-right asymmetry

The posterior positioning of cilia is a feature associated with nodal cilia and the establishment of left-right asymmetry and is required for the rotational movement of the cilia to generate a leftward flow (Hashimoto et al. 2010; Hirokawa et al. 2006; Nonaka et al. 2005; Okada et al. 2005). The posterior positioning of cilia, in homologous structures to the mouse ventral node, in rabbit, zebrafish and *Xenopus*, has shown that this is a conserved precondition for cilia left-right asymmetry establishing leftward flow (Essner et al. 2005; Schweickert et al. 2007; Feistel & Blum 2006). Recent research has shown that core genes in the vertebrate Planar Cell Polarity (PCP)

pathway are required for the positioning of cilia at the posterior of the mouse node and *Xenopus* GRP (Antic et al. 2010).

The role of PCP in the precise positioning and polarisation of bristles on the *Drosophila melanogaster* wing and the stereocilia hair cells in the vertebrate ear led many to believe that it also had a role in nodal cilia polarisation. Research has shown that the PCP pathway is vital for the normal functioning of cilia at the mouse ventral node and *Xenopus* GRP and therefore, the establishment of left-right asymmetry. PCP core proteins Vangl1 and Pk2 are asymmetrically localised in the mouse ventral node and in *Xenopus vangl2* mutants, the posterior positioning of cilia in the GRP is disrupted which ultimately affects nodal flow and downstream left-right asymmetry (Antic et al. 2010). *BicC* recruits *dsh* from the Wnt canonical pathway for the PCP pathway so is an essential protein for normal cilia positioning and left-right asymmetry (Maisonneuve et al. 2009). The research has shown that the PCP pathway, first observed in *Drosophila melanogaster*, is a conserved mechanism in both mouse and *Xenopus* and is important for the correct patterning of the vertebrate body plan. Vandenberg & Levin (2010) have suggested that PCP acts before, and not exclusively through, nodal cilia and spreads LR orientation throughout the blastoderm. The requirement of Vangl2 in the establishment of asymmetry in the chick embryo, which has previously been shown not to have nodal cilia and a leftward flow (Zhang & Levin 2009), has complicated the role for PCP in left-right asymmetry as purely an organiser of cilia positioning.

4.3.6 PCP genes in *Ciona intestinalis*

A genome survey has shown that PCP genes are present in the *Ciona intestinalis* embryo

genome. It was found that almost all of the PCP core genes are present in the genome, with less redundancy than vertebrates (Sasakura et al. 2003). Orthologues of *Fz*, *Dsh*, *Stbm*/*Vang*/*Pk*, *Daam-1*, *JNK* and *Rho*/*Rac*/*cdc42* are present in the *Ciona intestinalis* genome which suggests that PCP is also a signalling pathway utilised in the embryo and/or adult organism (Sasakura et al. 2003; Hotta et al. 2003; Hotta et al. 2007). The PCP pathway has been implicated in ascidian convergent extension because embryos transgenic for *dsh* did not have tail elongation and cells of the notochord did not intercalate properly (Keys et al. 2002). Additionally, embryos with a *Pk* null mutation were able to begin convergence but could not maintain the connections and *dsh* expression was not polarised (Jiang & Smith 2007; Jiang et al. 2005).

The precise localisation of cilia on the posterior of *Ciona intestinalis* ectoderm cells, in a similar fashion to nodal cilia, suggests that PCP may play a role. The highly conserved PCP core genes are present in the *Ciona intestinalis* genome and have a role in convergent extension of the notochord so have the capacity to have a role here. However, the main components of the PCP pathway were not found in the tailbud stage embryo, with some genes absent and others not expressed in the relevant tissue (Imai et al. 2004; Ikuta et al. 2010). It remains unclear if the immunolocalisation experiments for these genes were conducted in embryos that were de-chorionated at fertilisation or immediately prior to fixation which could affect the results. As shown in previous research, the removal of the chorion at fertilisation alters the expected asymmetric expression of *Ci-Pitx* and this research has shown (in next paragraph) that de-chorionation dramatically affects the development and appearance of the embryo. The removal of the chorion could compromise the expression of the genes normally required for cilia positioning.

Future work should focus on this pathway to analyse its role in positioning of early stage *Ciona intestinalis* cilia. The expression of PCP pathway genes in the tailbud stage embryo needs

to be validated by experimentation on embryos which are only de-chorionated immediately before fixation. Experimentation using the ROCK inhibitor, Y-27632, a member of the PCP pathway was conducted on neurula stage *Ciona intestinalis* embryos to attempt to disrupt the cilia positioning (data not shown). However, the affect on the actin cytoskeleton, and other parts of the PCP pathway was pronounced and the embryos were not able to development beyond the tailbud stage. The requirement for cilia to localise to the posterior of each cell suggests that it is important for their role on the embryo. Analysis of the *Ciona intestinalis* cilia structure strongly indicates a non-motile role on the embryo so the positioning is not required for cilia rotation, as in the mouse ventral node. It is unknown why these cilia are constrained to the posterior of the cell but it is likely to be important in some way for their potential role.

4.3.7 The position of cilia at different locations on the late neurula/early tailbud *Ciona intestinalis* embryo

Embryos were analysed to determine if the location of the cilia on each cell was affected by the cell's location on the embryo. The motile cilia which generate a leftward flow and left-right asymmetry in mouse are constrained within a concave pit structure, whereas cilia on the *Ciona intestinalis* embryo are found on every cell of the embryo. This could be a result of a lack of organiser region homologous to the mouse ventral node on the *Ciona intestinalis* embryo (Dehal et al. 2002). To analyse if a particular population of cells on the embryo differed in their positioning of the cilia, which could have an independent role in left-right asymmetry establishment in *Ciona intestinalis*, the position of the cilia in different regions were recorded.

Statistical analysis showed that the cilia on the left face of the embryo in position 2 (mid-

way along the embryo AP axis) were positioned in a significantly different position along the individual cell AP axis. It could be that although *Ciona intestinalis* do not have an organiser region on the developing embryo a differently positioned population of cilia could have a different role which acts as a distinct region like the mouse ventral node. The possibility that this small population of cilia are motile and generate a flow which is detected by the other cilia of the embryo can be largely discounted. This is due to the fact that amongst 75 photographed cilia (and numerous more cilia that were not photographed) located on the *Ciona intestinalis* embryo, not one cilium had a 9+2 structure or the dynein arms required for motility. It is therefore not understood why this population of cilia are positioned in a different point on the cell AP axis or how this affects their role. The elucidation of the role these cilia play on the *Ciona intestinalis* embryo at the late neurula or early tailbud embryo might shed light on why they are positioned differently.

4.3.8 The effect of de-chorionation on cilia presence

As discussed in Chapter 3, the chorion protects *Ciona intestinalis* embryos during the early stages of embryogenesis and removal of the chorion causes bi-lateral expression of *Ci-Pitx* (Shimeld & Levin, 2006). Here it has been shown that the chorion does not interact with cilia (Chapter 3) but the timing of cilia emergence at the point before molecular asymmetries has suggested that de-chorionation at fertilisation could disrupt cilia and therefore, left-right asymmetry. The absence of cilia and the effect of problems with asymmetry could provide a link between these cilia and the establishment of left-right asymmetry. *Ciona intestinalis* embryos were allowed to develop within the chorion or de-chorionated at fertilisation, fixed for SEM at the late neurula/

early tailbud stage and examined for presence of cilia. The removal of the chorion at fertilisation did not inhibit ciliogenesis as cilia were present on the de-chorionated embryos at the time point expected from chorionated embryos. It is, therefore, unlikely that the disruption to left-right asymmetry observed in embryos de-chorionated at fertilisation is due to a lack of cilia. Analysis of the surface structure and texture of the *Ciona intestinalis* embryos by SEM may give an indication of how the removal of the chorion results in bilateral *Ci-Pitx* expression.

Despite the fact that cilia were observed on embryos de-chorionated at fertilisation, SEM analysis of de-chorionated embryos has demonstrated that the removal of the chorion has other effects on the *Ciona intestinalis* tailbud embryo. The cells of the embryo had a flatter apical surface and less distinct cell boundaries which suggest a problem with the embryo cytoskeleton. Additionally, the tail of the embryo at the mid-tailbud stage has begun to bend towards the dorsal side of the embryo rather than the expected bend to the ventral side. Embryos which are de-chorionated at fertilisation exhibit abnormalities later in development, with all embryo development arresting before the hatchling stage.

Although, this research does not demonstrate why embryos de-chorionated at fertilisation have defects in laterality it does indicate that general embryo abnormalities combined together could result in bilateral *Ci-Pitx* expression. The removal of the chorion changes the immediate physical environment of the embryo including the mechanical forces, enzymatic activity and ionic environment. These results, in combination with previous de-chorionation experiments (Shimeld & Levin 2006), show the importance of maintaining *Ciona intestinalis* within the chorion during development when analysing gene expression. Most methods of gene manipulation in *Ciona intestinalis* (excluding microinjection although rates of injection through the chorion are very low), require the chorion to be removed at fertilisation which as shown here

disrupts normal development and therefore, ultimately compromises the experimental results. All these data suggest that, although the removal of the chorion could remove a vital space for a morphogen or mechanical motion which generates a physical interaction with the cilia. Left-right asymmetry defects in de-chorionated embryos are not due to the loss of cilia.

4.3.9 The effect of experimental manipulation on cilia

To truly confirm or deny that the cilia on the late neurula/early tailbud *Ciona intestinalis* embryo have a role in left-right asymmetry a morpholino against *IFT88*, an intraflagellar protein, was made. The IFTs are essential for ciliogenesis through their rapid movement of multi-subunit protein particles along flagellar microtubules and are required for the assembly and maintenance of eukaryotic flagella (see review Rosenbaum & Witman 2002). *IFT88 Chlamydomonas reinhardtii* mutants have normal development except for the absence of a flagellum, and mouse mutants have PKD (Pazour et al. 2000). Morpholinos against this gene were intended to be injected into the *Ciona intestinalis* oocyte at fertilisation to prevent ciliogenesis and molecular asymmetries examined to assess if left-right asymmetry was disrupted. However, the microinjection process is commonly used on de-chorionated embryos as injection through the chorion blocks the needle and speed is essential to inject a large number of embryos before cleavage. After numerous attempts to produce replicable results the method was abandoned due to the requirement for the chorion to remain attached so molecular asymmetry could be assessed.

The requirement for the chorion to remain attached limited the methods available to remove cilia and there is not a known drug which reliably removes cilia without disruption to the cytoskeleton and general development. However, previous experimentation in *Paracentrotus*

lividus has demonstrated that the sea urchins respond to stress by de-ciliation and especially from exposure to increased NaCl concentrations (Casano et al. 1998). It is not known though, why exactly the increase in Ca^{2+} results in the loss of cilia. Therefore, *Ciona intestinalis* embryos at the late neurula/early tailbud stage of development were exposed to a high concentration (4.45M) of NaCl (an additive saline concentration of 470mM, double the normal concentration of sea water) and the effect on cilia presence and positioning examined. Although cilia were present on embryos at 0, 10 and 30 mins after exposure, their positioning appeared different. Subsequent *in situ* hybridisation experiments of the gene *Ci-Pitx* were conducted on the embryos to determine if the more posterior position of cilia disrupted the left-sided expression.

The lack of disruption to normal left-sided *Ci-Pitx* expression suggests that the position of each cilium is not important for its role if they are involved in left-right asymmetry. Unfortunately, due to the requirement for the removal of the chorion before fixation in both the control and experimental condition which takes approximately 10 mins in total to achieve, another time point in between 0 and 10 mins could not be harvested. The more posterior position of cilia on each cell 30 mins after exposure to high levels of NaCl suggests that the cilia are not reabsorbed and then built again after the NaCl is diluted to normal levels.

4.3.10 Conclusion

Measurements of the cilia position along the AP axis and the angle from the centre-point of each cell showed that cilia are positioned in the posterior half of each cell, a characteristic of nodal cilia. The precise positioning of cilia to the posterior of the cell might be a constraint enforced on the cilia to enable them to function for their role on the embryo. Analysis of previous research

has suggested a role for the PCP pathway in establishing a gradient within each cell to restrict the cilia to the posterior. The PCP pathway has been implicated in other organisms and polarised tissues as well as positioning cilia on the *Xenopus* epidermis and vertebrate inner ear. *Ciona intestinalis* have the core PCP genes as well as a potential role for the pathway in convergent extension which suggests that the pathway could also be controlling the position of cilia on the cells of the ectoderm. The ultrastructure of these cilia suggests they have a mechanosensory role during this point in development but it still remains unknown why the cilia are positioned posteriorly. The requirement for posterior positioning in the mouse ventral node is related to their role as generators of a directional flow but although the positioning is present in *Ciona intestinalis*, it is not for motility.

Cilia are positioned on the *Ciona intestinalis* embryo immediately prior to the asymmetric expression of *Ci-Nodal* and *Ci-Pitx* which led to the proposal that the cilia are linked with the establishment of left-right asymmetry. The structure of the cilia show that they do not rotate and generate a flow on the surface of the embryo but they could be the site of ion channels and other proteins involved in left-right asymmetry. Experiments tried to determine if the removal of cilia results in defects in the asymmetric expression of *Ci-Pitx*. *Ciona intestinalis* embryos do not respond to high levels of salt by de-ciliation, a characteristic of the sea urchin, *Paracentrotus lividus*. Instead the cilia are positioned further along the AP axis of the cell which does not result in bilateral or reversed *Ci-Pitx* expression. These results show that this difference in cilia position is not important for the cilia if they have a role in left-right asymmetry. Further experiments to remove cilia are required to see if there is a direct link between cilia and the establishment of left-right asymmetry. However, other techniques such as electroporation and RNAi all rely on de-chorionation of embryos at fertilisation which we know affects left-right asymmetry. The

most usable method would be drug inhibition which has been used effectively on embryos still within their chorion, but as yet there is not a drug available which removes cilia and does not have an effect on centrioles required for normal cell division.

CHAPTER 5

Phylogenetic Analysis of the Genes Involved in the Establishment of Left-right Asymmetry in Mouse and Human across the Eukaryotes

5.1 INTRODUCTION

Previous chapters have focused on the morphology and surface structures of neurula stage *Ciona intestinalis* embryos, however, substantial amounts of research in the model organisms has analysed the role of proteins in the establishment of left-right asymmetry. Concurrently to morphological experiments, over the years, research in the field of left-right asymmetry has identified genes that are vital for the correct positioning of organs within model organisms. Mutations which cause human diseases and mouse mutants have led to new advances in the search for the mechanisms that set up left-right asymmetry. To parallel morphology, this chapter will investigate the conservation of genes linked with left-right asymmetry establishment, as implied by mutant phenotype, across the eukaryotes. In particular the presence of these proteins in the ascidian *Ciona intestinalis* genome will be analysed to compare with the morphological analyses in previous chapters.

The eurkaryotes are a large domain of organisms whose cells contain complex structures enclosed within membranes and in particular their membrane bound nucleus within which

genetic material is contained. In this analysis, the eukaryotes are segregated into seven kingdoms; Animalia, Fungi, Amoebozoa, Plantae, Chromalveolata, Rhizaria and Excavata. Many organisms within these kingdoms utilise cilia or flagella during their life cycle, as a requirement for organism motility or as sensors. Cilia are present at some stage during development on each examined holozoan, although only non-motile cilia are found in *Caenorhabditis elegans*. The Metazoa are multicellular organisms which incorporate organisms with radial, bilateral and no symmetry, with the bilateria encompassing a large proportion of the studied organisms. In particular, the vertebrates and some invertebrates have been analysed to assess the mechanisms that establish the left-right axis during development (as discussed in more depth in Chapter 1). The analysis of proteins linked with left-right asymmetry establishment in the vertebrates across the eukaryotes will provide an interesting survey of gene presence or absence to coincide with the morphological analyses.

In order to generate a comprehensive survey of genes linked to the human and mouse phenotype, *situs inversus,* a method of finding genes that when mutated result in the incorrect positioning of organs was utilised. *Situs inversus* is a congenital condition in which the major visceral organs are reversed or mirrored from their normal positions. The normal arrangement is known as *situs solitus* and the reversed condition presents in 1 in 8000 to 1 in 20000 (Nursal et al. 2004). The reversal of the organs does not impair the individual phenotypically unlike *situs ambiguous* which is a more complicated disorder with only individual organs displaced. This left-right asymmetry disorder provides a standardised phenotype to search for genes that are required for the correct patterning of left-right asymmetry which can in turn be searched for in the 45 genomes selected due to their complete or near-complete genome sequence and evolutionary spread across the eukaryotes. Additionally organisms were chosen on whether

species produce a cilium or flagellum during their lifecycle, and within the Holozoa, species were selected to represent a wide distribution of known left-right asymmetry mechanisms.

Here I show that from the search of orthologues in the 45 genomes it was demonstrated that the structural and motor proteins were present in every organism that produces a cilium during development. This showed that the proteins that normally build and move cilia were mutated in the diseases that have laterality defects and are ancestral proteins that have previously been shown to be vital for ciliogenesis and motility. This demonstrated that although the node cilia have a rarer 9+0 cilia structure, they are still built and motility generated in the same manner as other eukaryote species. The transcription factor orthologues were generally restricted to the Holozoa where their expansion is related to the advent of multicellularity. The other proteins involved in left-right asymmetry were mainly found in the Holozoa, except PKD2. The *Ciona intestinalis* orthologue of DNAH11 is not expressed in the early stages of development which supplements the data from the previous chapters that dynein arms are not present on the cilia of tailbud stage *Ciona intestinalis*.

5.2 RESULTS

5.2.1 Identification of proteins involved in the initial break in symmetry in humans and mice

The mechanisms involved in breaking symmetry have been analysed in several vertebrate systems and although not extensively understood, key genes have been discovered. Particular genes have been linked to the initial break in symmetry in the mouse, *Xenopus* and Zebrafish system. To understand the evolution of these genes across eukaryotes and their potential conserved link

with left-right asymmetry the phylogenetic presence and absence of these proteins was analysed.

An exhaustive list of genes annotated to have an involvement in left-right asymmetry was collated through the OMIM (Online Mendelian Inheritance in Man) and MGI (Mouse Genome Informatics) database. Online Mendelian Inheritance in Man (OMIM), a database of human genes and genetic disorders was used to search for genes involved in disorders which present *situs inversus*, a phenotype observed when the initial break in symmetry is disrupted. *Situs inversus* is a phenotype of 12 human disorders, where the incidence is greater than one case, and is linked with 30 genes (Table 5.1). In some disorders nine gene locations are known to be linked with the phenotype *situs inversus* but the exact gene responsible for the disorder is not yet known. In particular, there are 12 Bardet-Biedl Syndrome (BBS) gene map loci known but only six genes are known to be responsible for the disorder.

The MGI database phenotypes/alleles project enables access to spontaneous, induced, and genetically-engineered mutations and their strain-specific phenotypes. To maintain continuity the phenotype *situs inversus* was used to search the database for mouse mutants which displayed problems with their left-right asymmetry. During the development of 27 mouse mutants there is some disruption to left-right asymmetry with problems in left-right axis patterning and abnormal embryonic turning (Table 5.2). The results were refined to only include the genes which have a known direct link with left-right asymmetry in vertebrate organisms or have a high incidence of *situs inversus*, >48% (Table 5.3).

5.2.2 Phylogenetic distribution of left-right linked proteins

As a result of the survey to find genes associated with left-right asymmetry 14 genes were taken

Table 5.1: Human Diseases with the phenotype, *situs inversus*. The phenotype *situs inversus* was used to search the OMIM database for mutated genes in the disorders which display this phenotype.

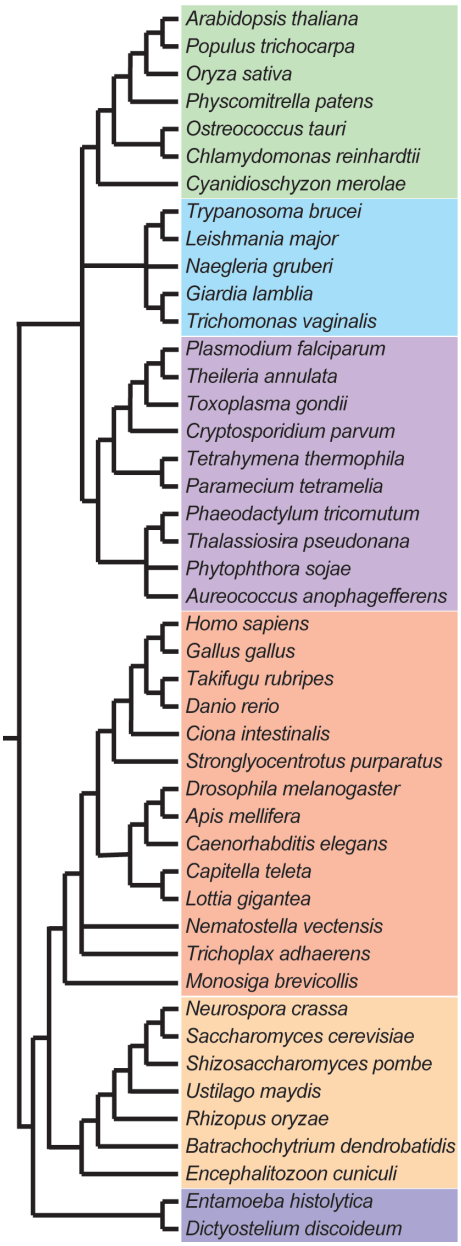
Disease		Alternative Names	Gene Map Locus	Gene	Protein	LR Asymmetry
Situs Inversum Viscerum	SIV		7p21	DNAH11	Dynein Heavy Chain	Situs inversus
Heterotaxy	HTX1	Visceral, 1, X-linked	Xq26.2	ZIC3	Zinc Finger Transcription Factor	Randomisation of LR
Kartagener's Syndrome			9p21-p13	DNAI1	Dynein Light Chain	Situs inversus
			7p21	DNAI1	Dynein Light Chain	
			5p15-p14	DNAH5	Dynein Heavy Chain	
			7p21	DNAH11	Dynein Heavy Chain	
Primary Cilia Dyskinesia	PCD	Primary Immotile Cilia Syndrome	9p21-p13	DNAI1 (CILD1)	Dynein Light Chain	Situs inversus
			5p15-p14	DNAH5 (CILD3)	Dynein Heavy Chain	
			15q13.1-q15.1	(CILD4)	Unknown	
			17p14	TXNDC3 (CILD6)	Thioredoxin Domain-Containing Protein	
			17q25	DNAI2 (CILD9)	Dynein Light Chain	
			14q21.3	KTU (CILD10)	Kintoun	
			16q24.1	LRRC50	Leucine Rich Repeat Containg Protein 50	
Laterality Defect/Autosomal Dominant			6p21	Unknown	Unknown	Situs inversus Situs ambiguous Situs solitus
Renpenning Syndrome	RENS1	MRXS3, MRXS8, MRX55	Xp11.23	PQBP1	Polyglutamine-Binding Protein 1	N/A
Johanson-Blizzard Syndrome	JBS	Nasal Alar Hypoplasia, Hypothyroidism	15q15-q21.1	UBR1	Ubiquitin-Protein Ligase E3 Component N-Recognin 1	Neonate Situs inversus
Thiamine-responsive megaloblastic anemia syndrome	TRMA	Megalobalstic anemia	1q23.3	SLC19A2	Thiamine Transporter Protein	Situs inversus
Bardet-Biedl Syndrome	BBS	BBS1-12	11q13	(BBS1)	Unknown	Randomisation of LR
			16q21	(BBS2)	Unknown	
			3p12-q13	ARL6 (BBS3)	ADP-ribosylation factor (ARF)-like-6 gene	
			15q22.3-q23	(BBS4)	Unknown	
			2q31	(BBS5)	Unknown	
			20p12	(BBS6)	Unknown	
			4q27	(BBS7)	Unknown	
			14q32.1	TTC8 (BBS8)	Tetratricopeptide Repeat Protein	Randomisation of LR
			7p14	PTHB1 (BBS9)	Parathyroid Hormone-Responsive Gene B1	
			12q	C12ORF58 (BBS10)	Chromosome 12 ORF 58	
			9q33.1	TRIM32 (BBS11)	Tripartite Motif-Containing Protein-32 Gene	
			4q27	C4ORF24 (BBS12)	Chromosome 4 ORF 24	
Heterotaxy	HTX, HTX2	Visceral, 2, X-linked	2q21.1	CFC1 (HTX2)	CRYPTIC Protein	Abdominal Situs inversus
Meckel Syndrome Type 1	MKS1		17q23	MKS1	Unknown	Situs inversus totalis
Nephronophthisis	NPHP		9	NPHP2	Unknown	Situs inversus
			3	NPHP3	Unknown	

Table 5.2: Mouse mutants which display the phenotype *situs inversus*. The phenotype *situs inversus* was used to search the MGI database for mutated genes in mouse mutants which display this phenotype. Duplicate gene names occur from different mutation screens and methods (targeted, gene trap, chemically induced or spontaneous) or mutations in different exons of the same gene.

Mouse Mutant	Chr	Synonyms	Survival	Observed Phenotypes in Mouse			Other Comments
				Embryogenesis	Growth and Size	Similar Human Diseases	
Bbs1	19	Bbs1^{-}	~ 50% die by E10.5		No Situs Inversus	Bardet-Biedl Syndrome 1	Olfactory cilia mis-orientated
Bbs4	9	Bbs4^{-}	~ 50% die by E10.6		No Situs Inversus	Bardet-Biedl Syndrome 4	Olfactory cilia mis-orientated
Cfc1	1	Cryptic	Homozygotes die by 2wks after birth	Abnormal LR axis patterning Abnormal Embryonic Turning	~50% Situs inversus of Organs	Asplenia with Cardiovascular Anomalies	Randomised cardiac looping
Cited2	10	Cited2-		Abnormal Embryonic Turning	9% Abdominal Visceral Situs inversus		
Dand5	8	cerl-2^{-}	35% die within 48 hrs of birth	Abnormal LR axis patterning	Situs inversus		
Dnahc11	12	iv			~50% Situs Inversus		
Dnahc11	12	lrd		Paralysed monocilia	Situs inversus		Decreased Litter Size and absent Ca^{2+} channel
Dnahc11	12	lrd-		Abnormal LR axis patterning Paralysed monocilia	Situs inversus	Situs Inversus Viscerum	
Dnahc5	15	Mdnah5-	Most die by 2-3 wks after birth		Complete, partial or no Situs inversus	Ciliary Dykinesia, Primary 3 Kartagener Syndrome	Cilia are immotile and lack dynein
Foxj1	11	HFH-4-	Homozygotes die by E16.5	Abnormal LR axis patterning	48.1% Situs inversus	Kartagener Syndrome	Sperm lack flagella
Foxj1	11	HFH-4-	Most die at birth		~50% Situs inversus	Kartagener Syndrome	Absence of 9+2 in airway
Gdf1	8	Gdf1^{-}	66% survive to E14.5 All die within 48 hrs of birth	Abnormal LR axis patterning	~50% Situs inversus of Organs		
Gpg2	UNK	gpg2			Situs inversus		Heterotaxia, no heart looping
Gpg4	15	gpg4			Situs inversus		Heterotaxia
Gpg6	8	gpg6			Situs inversus		Heretotaxia, isomerism and abnormal cilia morphology
Invs (FVB)	4	inv	All die by 7 days after birth	Abnormal Embryonic Turning	Situs inversus	Situs Inversus Viscerum	
Kif3a	11	KIF3A^{-}	All die by E10	Abnormal LR axis patterning Abnormal Embryonic Turning Abnormal Node	Situs inversus		Lack of cilia in node
Lefty1	1	lefty-1-	60% die between E10.5 and E13.5		1 case of Situs inversus		Major cardiovascular problems
Lrm1	1				Situs inversus		pulmonary isomerism
Lrm2	11				Situs inversus		pulmonary isomerism
Mgat1	11		Homozygotes die by E10.5	Abnormal LR axis patterning Abnormal Embryonic Turning	Homozygotes Situs inversus		
Mgrn1	16	md^{2J}	60% die by 3 wks after birth	Abnormal LR axis patterning	< 1% Situs inversus		
Pitx2	3	deltac		Abnormal LR axis patterning	11% Right-sided Stomachs		
Pkd2	5	Pkd2$^{-/-}$	All die by E12.5	Abnormal LR axis patterning Abnormal Embryonic Turning	Abdominal Situs inversus	Polycystic Kidney Disease 2, PKD2	
Poll	19	Pol lambda^{-} /-	50% -/- die by 3 weeks after birth		19% Situs inversus totalis	Primary Ciliary Dyskinesia, PCD	Sperm have snaggy tails and respiratory cilia fail to adopt 9+2 arrangment and lack inner dynein arms
Rfx3	19	Rfx3^{tm1Rsw}	50% -/- die by E11 - E12	Abnormal LR axis patterning Abnormal Embryonic Turning	6 % Situs inversus		19% Inversion of cardiac looping
Tgif1	17	Tgif^{-}	Growth retardation		13% Situs inversus		

Table 5.3: Genes of Interest. Genes with a 48% or higher incidence of *situs inversus*.

Gene	Protein	Disease or Condition	LR Asymmetry
BICC1	Bi-caudal C 1	Polycystic Kidney Disease	
DNAI1	Dynein Light Chain 1	Kartagener's Syndrome	Situs inversus
		Primary Cilia Dyskinesia	
DNAI2	Dynein Light Chain 2	Primary Cilia Dyskinesia	
DAND5	DAN Domain Family, Member 5 (BMP Antagonists)		
DNAH11	Dynein Heavy Chain	Situs Inversum Viscerum	
		Kartagener's Symdrome	
DNAH5	Dynein Heavy Chain	Kartagener's Symdrome	
		Primary Cilia Dyskinesia	
FOXJ1	Forkhead Box J1 Transcription Factor		
GDF1	Growth Determination Factor (BMP family)		
Invs (FVB)	Ankyrin Repeats and 2 IQ calmodulin-binding domains	Situs Inversus Viscerum	
		Nephronophthisis type 2	
KIF3A	Kinesin-like Protein 3A	Polycystic Kidney Disease	
PKD2	Polycystin Protein Family	Polycystic Kidney Disease	Abdominal Situs inversus
RFX3	Regulatory Factor 3		Situs Inversus
ZIC3	Zinc Finger Transcription Factor	Heterotaxy	Randomised



Eukaryote Clade	Common Name	M or S	Organismal Asymmetry
Plantae	Rock Cress	M	Mixed
	Black Cottonwood	M	No Symmetry
	Asian Rice	M	
	Moss	M	Mixed
	Green Algae	S	
	Green Algae	S	
	Red Algae	S	
Excavata	Sleeping Sickness Parasite	S	
	Leishmaniasis Parasite	S	
	AmoeboFlagellate	S	
	Giardisis Parasite	S	
	Trichomoniasis Parasite	S	
Chromalveolata	Malaria Parasite	S	
	Theileriosis Parasite	S	
	Toxoplasmosis Parasite	S	
	Cryptosporidiosis Parasite	S	
	Ciliated Protozoa	S	
	Ciliated Protozoa	S	
	Diatom	S	
	Diatom	S	
	Soil Borne Plant Pathogen	S	
	Algae	S	
Holozoa	Human	M	
	Red Jungle Fowl	M	
	Pufferfish	M	
	Zebrafish	M	
	Sea Squirt	M	
	Californian Sea Urchin	M	Bilateral
	Fruit Fly	M	
	African Honey Bee	M	
	Round Worm	M	
	Polychaete Worm	M	
	Owl Limpet	M	
	Starlet Sea Anemone	M	Radial
	Trichoplax	M	No Symmetry
	Choanoflagellate	S	
Fungi	Red Bread Mould	M	
	Budding Yeast	S	
	Fisson Yeast	S	
	Corn Smut	S	
		S	
	Chytridiomycosis Fungus	S	
	Intracellular Parasite	S	
Amoebozoa	Amoebiasis parasite	S	
	Slime Mould	M/S	

Figure 5.1: Phylogenetic relationship of the eukaryotes.

The six main groups of the eukaryotes: Plantae (green), Excavata (turquoise), Chromalveolata (purple), Holozoa (red), Fungi (orange) and Amoebozoa (Blue). All the species included have a complete or near-complete genome. The species also include multicellular (M) and unicellular (S) organisms which encompass the two main groups of symmetry: bilateral and radial as well as those species with no whole organism symmetry (left blank).

forward to analyse their phylogenetic distribution across the six major groups; Plantae, Excavata, Chromalveolata, Holozoa, Fungi and Amoebozoa. 45 genomes were selected due to their complete or near-complete genome sequence and evolutionary spread across the eukaryotes (Fig. 5.1) (Appendix Table 1.1). Research has demonstrated that cilia have an important role in left-right asymmetry in vertebrates so organisms were selected to represent species that either produce a cilium or flagellum during their lifecycle (*n*=29) or do not (*n*=16). Within the Holozoa, species were selected to represent diversity and similarity between known left-right asymmetry mechanisms. The 14 genes involved in disease/disorders, mouse mutants which display *situs inversus* or manipulated model species experiments were used to interrogate the 45 predicted proteomes for orthologous sequences.

The approach used was based on the clustering of proteins by BLASTp score (first used and described by Wickstead & Gull, 2007) which was previously validated by analysing γ-tubulin (Hodges et al. 2010). Hodges et al. 2010 showed that the approach could identify homologous sequences in multiple organisms as well as paralogous families. Initially potential orthologues of the human protein sequence for each gene were identified by a reciprocal best BLASTp search with an e-value threshold of 10^{-5}. Orthologues found by this method in the other 45 proteomes (e-value threshold of $<10^{-2}$) were also used to perform BLASTp to find additional instances missed originally. Results from this search were then formed into clusters using a distance matrix derived from BLASTp scores (Wickstead & Gull 2007). The orthologous cluster was defined by eye, aligned, trimmed and then used in Maximum Likelihood (ML) and Bayesian phylogenetic inference (Guindon & Gascuel 2003; Ronquist 2003) (as described in Materials and Methods) (Phylogenies are found in the Appendix 1.1-1.11). The *Branchiostoma floridae* genome was searched separately for orthologues using BLAST and sequences incorporated into the analysis

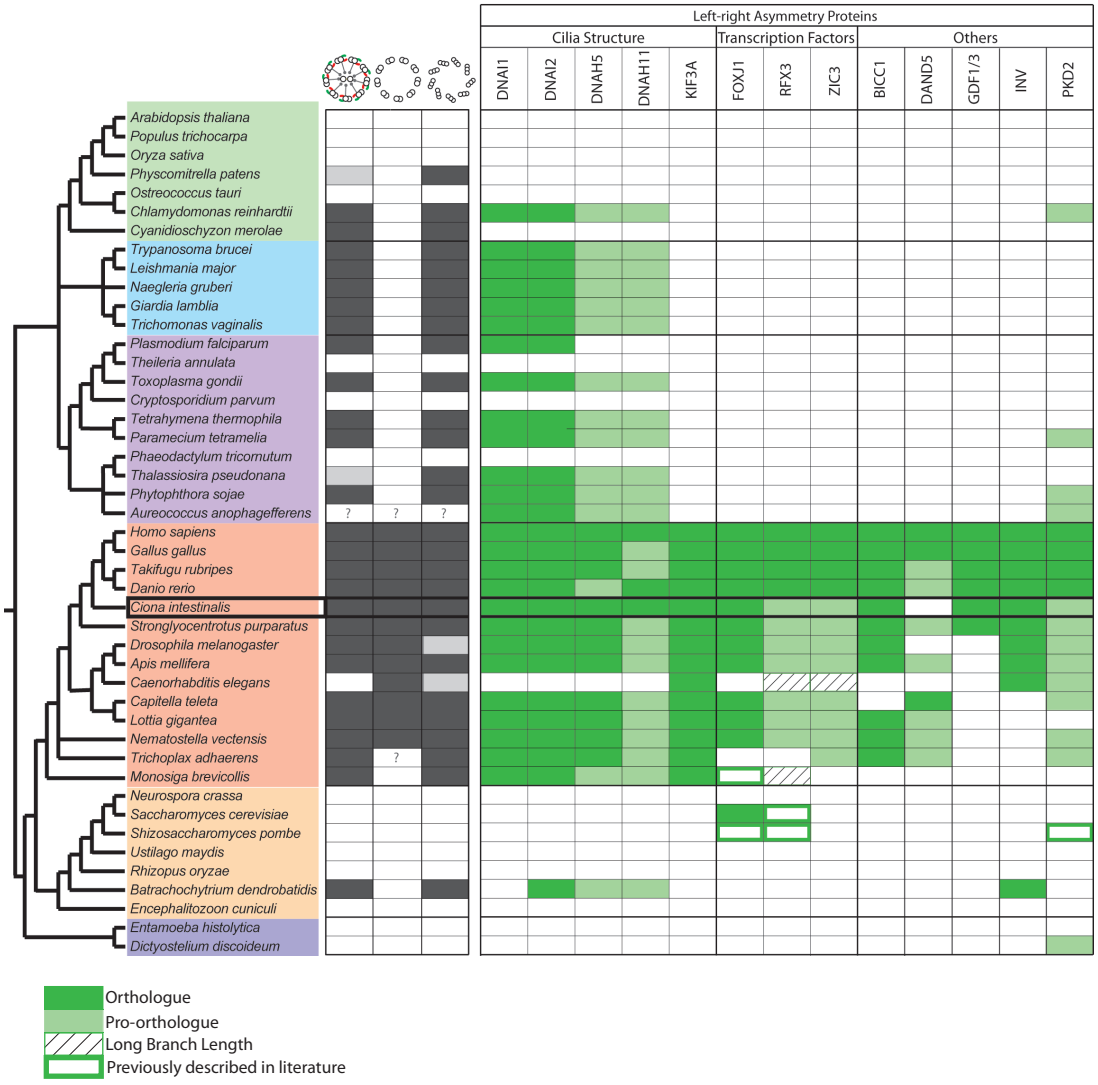


Figure 5.2: Distribution of proteins involved in left-right asymmetry in vertebrates among the eukaryotes.

Protein homologues were indentified in 45 eukaryotic genomes, including 29 species with motile cilia, 12 species with immotile cilia and 29 species with triplet basal body structure (dark grey box). Species with cilia or basal body structures different from the standard structure are marked with a light grey box. *P. patens* has no dynein arms, *T. pseudonana* has dynein arms but no central pair or radial spokes, *D. melanogaster* has an additional basal body structure of doublet microtubules and *C. elegans* has a singlet microtubule basal body. The presence of orthologue(s) is indicated by a green box. Pro-orthologues are indicated by a light green box. Sequences present in the BLASTp clustering method but removed from the analysis due to long branch lengths are indicated by a striped green box. Divergent homologues known in the literature but not identified by this approach are highlighted by a green border. 'Structural' proteins are associated with ciliogenesis and cilia motility. 'Transcription Factors' are proteins which bind to specific sequences and control the transcription of genes involved in left-right asymmetry. 'Other' are proteins which have a role in left-right asymmetry but are not categorised. The six main groups of the eukaryotes: Plantae (green), Excavata (turquoise), Chromalveolata (purple), Holozoa (red), Fungi (orange) and Amoebozoa (Blue). All the species included have a complete or near-complete genome.

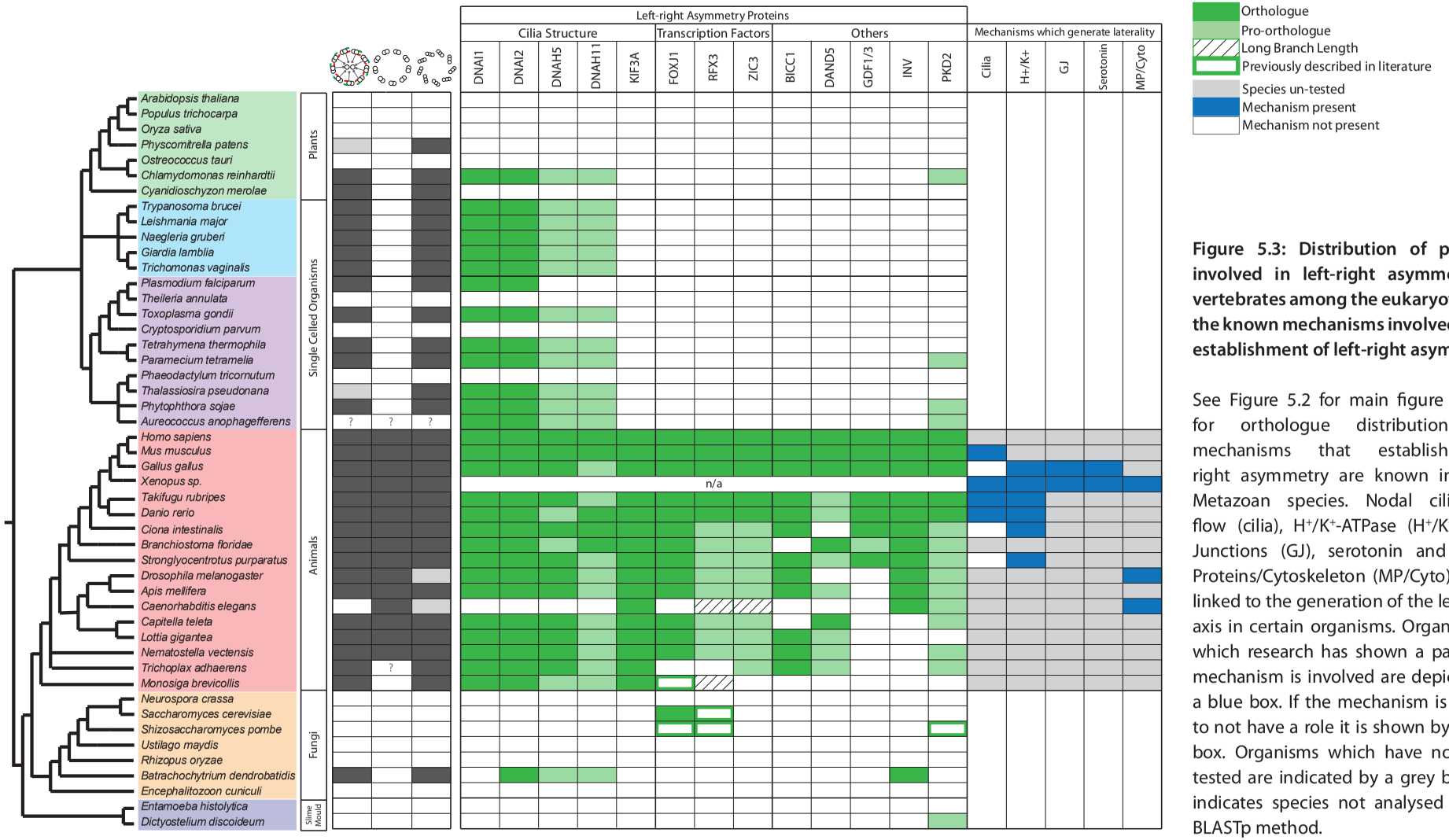


Figure 5.3: Distribution of proteins involved in left-right asymmetry in vertebrates among the eukaryotes and the known mechanisms involved in the establishment of left-right asymmetry.

See Figure 5.2 for main figure legend for orthologue distribution. The mechanisms that establish left-right asymmetry are known in some Metazoan species. Nodal cilia and flow (cilia), H^+/K^+-ATPase (H^+/K^+), Gap Junctions (GJ), serotonin and Motor Proteins/Cytoskeleton (MP/Cyto) are all linked to the generation of the left-right axis in certain organisms. Organisms in which research has shown a particular mechanism is involved are depicted by a blue box. If the mechanism is known to not have a role it is shown by a clear box. Organisms which have not been tested are indicated by a grey box. n/a indicates species not analysed by the BLASTp method.

prior to ML and Bayesian phylogenetic inference.

The proteins were ordered through their cellular role and the results of the BLASTp score method and phylogenetic analysis incorporated to show the presence of protein orthologues in the 45 species analysed (Fig. 5.2). Additionally, information on the presence and absence of motile and immotile cilia as well as basal body structure were included. Most motile cilia have a 9+2 ultrastructure with a central pair, radial spokes and dynein arms which have highly conserved functions across the eukaryotes. In contrast, immotile cilia have a 9+0 structure, but the mechanisms involved in ciliogenesis are conserved between the two kinds of cilia. The cilia of the node have a much rarer ultrastructure, 9+0 with dynein arms, and although they are able to rotate it is a different movement from other 9+2 cilia (discussed in Chapter 1). The proteins involved in the ciliogenesis and movement from cilia are highly conserved across the eukaryotes and are termed structural proteins in this analysis and include the dyneins and kinesins. The transcription factors, in comparison to the ancient structural proteins, are found predominantly in the Metazoa. Several other proteins, which are harder to categorise in this situation, were found in the initial search and are termed 'others' in this analysis. Each group of proteins will next be analysed in turn and their link to the known mechanisms involved in the establishment of left-right asymmetry in the Metazoa included (Fig. 5.3).

5.2.2.1 Phylogenetic distribution of the structural proteins essential for ciliogenesis

The dynein and kinesin gene families are essential for the correct formation of cilia through their roles as retrograde and anterograde motor proteins respectively. Mutations in these genes result in a lack of cilia or impaired cilia function which has been shown to be essential for normal left-right asymmetry in vertebrates. The dynein family encompasses a group of force-generating

ML

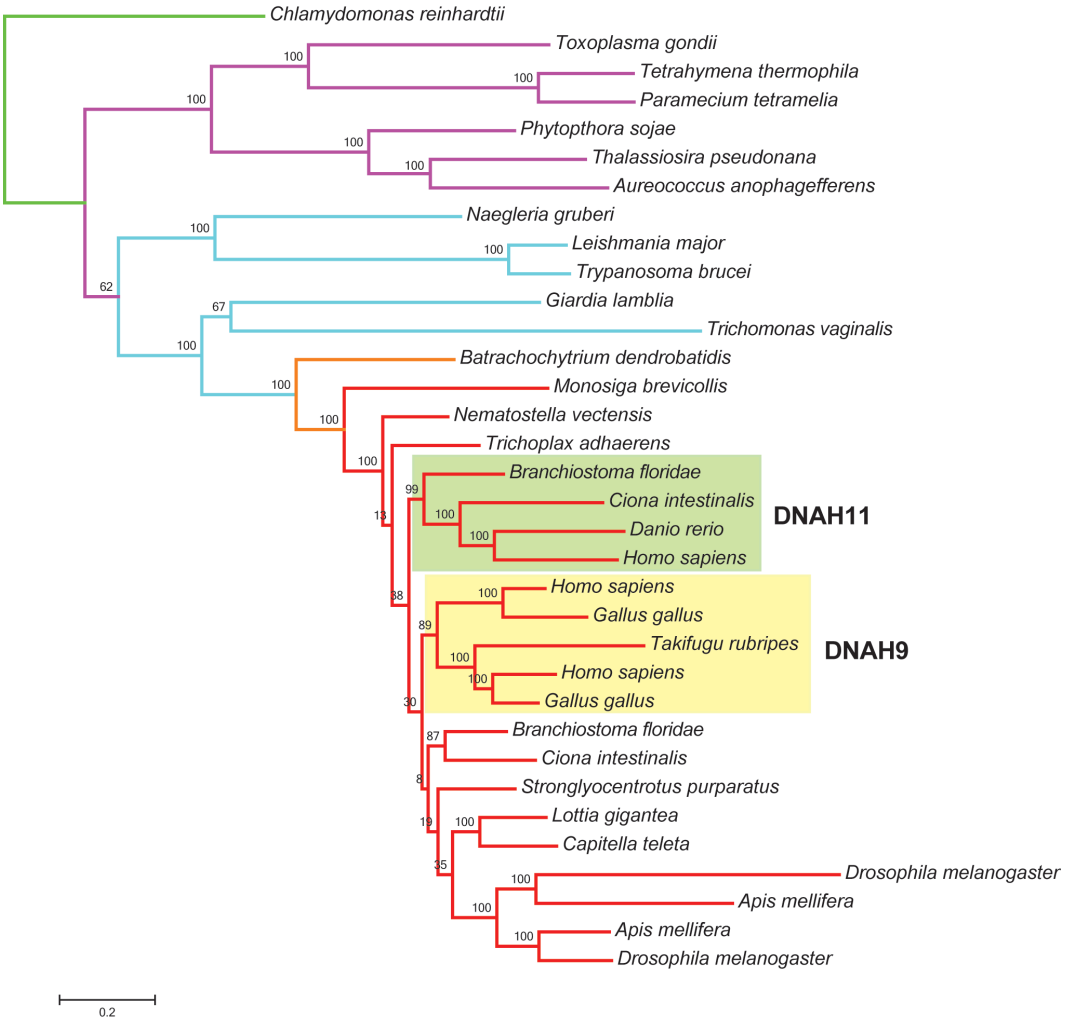


Figure 5.4: DNAH11 Phylogeny.

Maximum Likelihood and Bayesian trees were produced for DNAH11, including DNAH9. Amino acid sequence alignments were produced using MAFFT and trimmed to remove poorly aligned positions. Maximum likelihood phylogentic trees were constructed using PhyMLv3.0 (100 replicates, LG matrix, 4 gamma categories, random starting tree). Bayesian trees were inferred using MrBayesv3.1.2 (random starting tree, 4 chains of temperature 0.2, WAG substitution matrices, 4 discrete categories of gamma distribution substitution rate, 250 000 generations). Topology support for nodes is indicated (bootstrap). Generally, groups with >90% bootstrap support were considered to be well supported and those with >70% bootstrap support to have some support. The tree contains organisms from 5 of the 6 major clades: Plantae (Green), Chromalveolata (Purple), Excavata (Turquoise), Holozoa (Red) and Fungi (Orange).

adenosine triphosphatases (ATPases) that move along eukaryotic microtubules. The dyneins are divided into two groups; cytoplasmic and axonemal with the latter required for cilia/flagella motility. The axonemal dynein complex comprises 14 heavy chain, two intermediate chain,

Bayesian

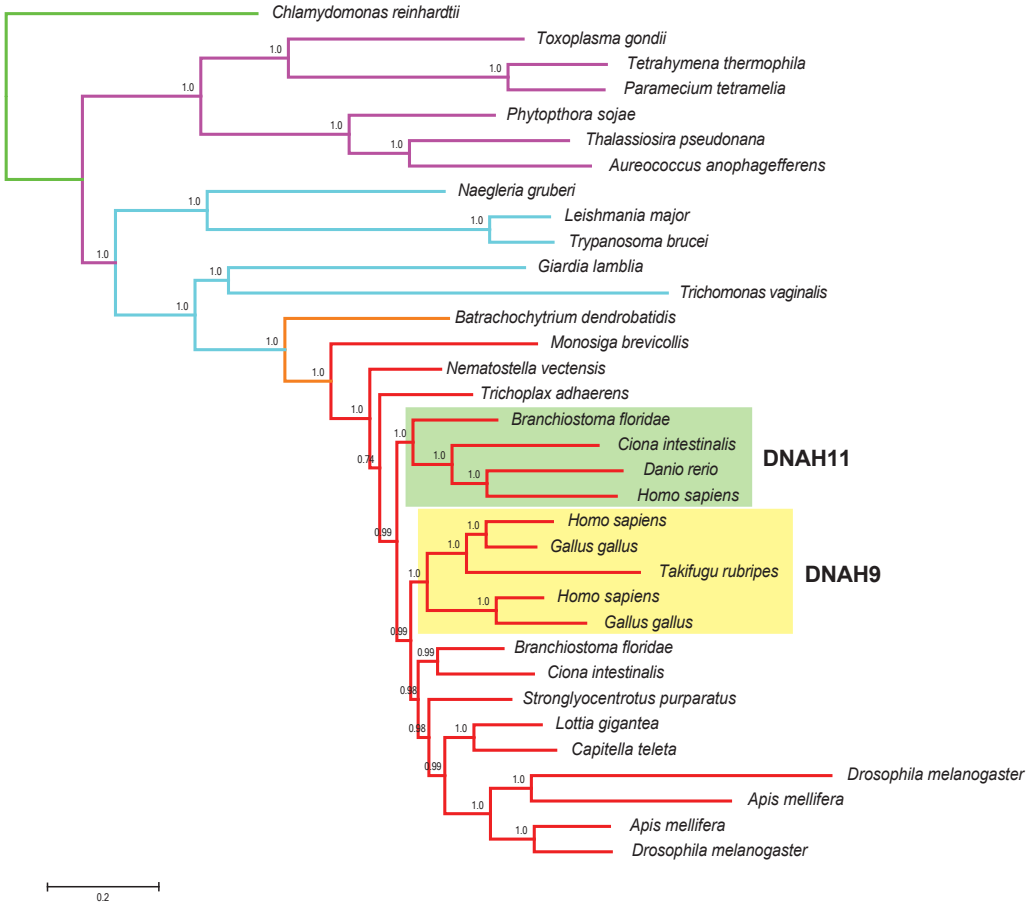


Figure Legend on previous page.

one light intermediate chain and two light chain proteins. They are also split into six families: outer-arm dynein (OAD)α, OADβ, OADγ, inner-arm dynein (IAD)-1α, IAD-1β and the single headed dyneins. Importantly, two of the heavy chain proteins (DNAH11 and DNAH5) and two intermediate chain proteins (DNAI1 and DNAI2) have been shown to have a role in defining laterality in vertebrate organisms.

DNAH11, also known as Lrd, is an outer dynein arm (ODA) protein which is essential for cilia motility at the mouse ventral node (Okada et al. 1999). The *lrd* gene was first implicated in left-right asymmetry through inherited diseases, such as *situs inversus viscerum* and Kartagener's

syndrome, and mouse mutants, such as the *iv* mouse mutant (Hummel & Chapman 1959; Lowe et al. 1996; Singh et al. 1991; Supp et al. 1997; Schreiner et al. 1993) which has a 50% incidence of inverted visceral organ positioning (Layton 1976). GFP-tagged lrd fused protein in mouse embryos demonstrated that lrd has an exclusively ciliary location and function and is localised to the cilia at the centre of the mouse ventral node (McGrath et al. 2003). In the analysis using the BLASTp score method a DNAH11 orthologue or pro-orthologue was found in all the species that generate a cilium/flagellum at some point in their life cycle (Fig. 5.4). An orthologue was present in *Danio rerio*, *Ciona intestinalis* and *Branchiostoma floridae* but not outside the chordates. A highly similar heavy chain protein, DNAH9 clustered with the DNAH11 family which is expected as they both belong to the OAD-β group. The BLASTp method clustered members of the non-metazoan OAD-γ, non-metazoan OAD-β and metazoan OAD-β (as described by Wickstead & Gull 2007) but the non-metazoan OAD-γ group of dyneins was removed from the analysis in the ML and Bayesian phylogenies because only one ancestral dynein group was required as an outgroup to the Metazoa. Further analysis concentrated solely on the metazoan orthologues. Orthologues were absent in the higher plants and red algae, an observation made previously (Wickstead & Gull 2007; Lawrence et al. 2001). An orthologue was not present in the *Plasmodium falciparum* proteome but this parasite builds flagella by an IFT-independent mechanism and has been shown to have highly divergent or absent dynein proteins (Wickstead & Gull 2007).

Orthologues of DNAH5, another axonemal heavy chain protein and part of the OADα group, were also detected through the BLASTp method (Fig. 5.2). Mutations in DNAH5 cause primary ciliary dyskinesia (PCD) and randomisation of left-right asymmetry (Olbrich et al. 2002). *In situ* hybridisations in mouse have localised *dnah5* to the mouse ventral node 7.0 to 8.0 d.p.c and

TEM utilised to show ODAs in nodal cilia are absent (Olbrich et al. 2002). ODAs are essential for cilia motility and defects in the heavy chain paralyse the cilia and perturb nodal flow at the mouse ventral node (Hornef et al. 2006). Orthologues of DNAH5 were found in all Metazoa except *Caenorhabditis elegans*, which never builds motile cilia (Fig. 5.2). Like DNAH11 and DNAH9, DNAH5 is clustered with another closely related dynein heavy chain protein, DNAH8 (Appendix Fig. 1.1). A common ancestral orthologue was found in all the species analysed which form a flagella or cilia at some point during their life cycle, except *Plasmodium falciparum* (as discussed for DNAH11).

DNAI1 and DNAI2 are both intermediate chain dyneins and mutations in either gene result in abnormal ciliary ultrastructure and function associated with primary ciliary dyskinesia and Kartagener Syndrome (Guichard et al. 2001; Loges et al. 2008). *DNAI1*, is the human orthologue of the *Chlamydomonas reinhardtii IC78* gene and mutations in this gene account for 2-13% of PCD patients with defined ODA defects (Guichard et al. 2001). DNAI2 is required for ODA assembly throughout the ciliary axoneme which suggests a role in nodal cilia motility and, like DNAH11, defects perturb flow and cause randomised asymmetry (Loges et al. 2008). Both of the proteins were found in the same species as DNAH11 and DNAH5 which is consistent with the presence of cilia at some point in their life cycle (Fig. 5.2). *Physcomitrella patens* does not have outer dynein arms so the absence of the axonemal dyneins analysed was expected. A *Plasmodium falciparum* orthologue was present for both DNAI1 and DNAI2 but the long branch lengths suggest a highly divergent sequence (Appendix Fig. 1.2 and Fig. 1.3). A DNAI1 orthologue was not found in *Batrachochytrium dendrobatidis* unlike the other dyneins analysed (Appendix Fig. 1.2).

Another structural protein KIF3A, a member of the heterotrimeric, microtubular, anterograde

motor kinesin-2 family, was mutated in the first experiments which suggested a role for cilia in the development of left-right asymmetry (Nonaka et al. 1998). The absence of KIF3A results in a lack of cilia at the mouse ventral node so the absence of leftward nodal flow results in randomised left-right asymmetry (Takeda et al. 1999; Okada et al. 1999; Nonaka et al. 1998). KIF3A and KIF3B, together with an associated protein KAP3, form a heterotrimer named the KIF3 complex. A KIF3A orthologue was present in all metazoan species analysed including *Caenorhabditis elegans*, which only assembles immotile cilia (Fig. 5.2). The clustering method employed in this analysis did not find other kinesin-2 family members KIF3B, KIF3C, KIF-17 or the *Chlamydomonas reinhardtii* homologue, FLA-10 but was restricted to the KIF3A subset (Appendix Fig. 1.4).

5.2.2.2 Phylogenetic distribution of known Transcription Factors (TFs) involved in left-right asymmetry

Transcription factors bind to specific DNA sequences, thereby controlling the transcription of genetic information from DNA to mRNA. Four transcription factors were identified in the OMIM and MGI gene survey and analysed through the BLASTp score method. FOXJ1, a member of the forkhead family of transcription factors, has been shown to regulate the transcription of genes that control the production of motile cilia (Brody et al. 2000) as well as function in mouse left-right determination (Zhang et al. 2004). The use of the BLASTp method showed FOXJ1 orthologues were restricted to the Holozoa except one in yeast (Fig. 5.2). FOXJ1 orthologues were not found in both *Caenorhabditis elegans* and *Trichoplax adhaerens*. An orthologue of FOXJ1 was found in *Saccharomyces cerevisiae* and orthologues have been previously described in *Monosiga brevicollis* and *Shizosaccharomyces pombe* but were not identified in this screen.

Interestingly, no FOXJ genes have previously been observed in the ecdysozoans (Mazet et al. 2003) but this method has shown a FOXJ1 orthologue in both *Drosophila melanogaster* and *Apis mellifera* (Appendix Fig. 1.5).

RFX3, a member of the regulatory factor X (RFX) family of transcription factors has been shown to be involved in the assembly of primary cilia and laterality (El Zein et al. 2009; Bonnafe et al. 2004). There are five known members of the RFX family of transcription factors in mammals and my analysis found three of the family (Appendix Fig. 1.6). RFX1-3 proteins have higher similarity to each other outside the RFX DNA binding domain motif than with RFX4 and RFX5 (Emery et al. 1996) which suggests why they were missed by the BLASTp method. *RFX3* is expressed in the mouse ventral node and is essential for cilia assembly through the regulation of *D2lic*, a gene implicated in intraflagellar transport (Bonnafe et al. 2004). Sak1 in *Schizosaccharomyces pombe* (Wu & McLeod 1995), a gene in *Saccharomyces cerevisiae* and a gene in *Caenorhabditis elegans* (Emery et al. 1996) have all been previously described as RFX and although a potential *Caenorhabditis elegans* orthologue was found in this analysis neither yeast gene was found. A potential RFX1-3 orthologue was found in *Caenorhabditis elegans* and *Monosiga brevicollis* but both were removed from the analysis due to long branch lengths which suggest a high level of sequence diversity (Fig. 5.2). One orthologue was found in each of the rest of the Metazoa, except *Trichoplax adhaerens*, with the *Ciona intestinalis* and *Branchiostoma floridae* genes positioned outside the vertebrate genes in both ML and Bayesian phylogenies (Appendix Fig. 1.6).

X-linked heterotaxy (HTX1) is a rare developmental disorder which presents problems with laterality and results from mutations in the *zic3* gene (Purandare et al. 2002; Gebbia et al. 1997). ZIC3, a member of a family of zinc finger transcription factors, is involved in laterality in

humans (Gebbia et al. 1997), mouse (Ware et al. 2006) and *Xenopus* (Kitaguchi et al. 2000). ZIC3 is expressed symmetrically at the mouse ventral node and within the primitive streak during gastrulation and is required to maintain *nodal* expression (Purandare et al. 2002). Five ZIC proteins were found in *Homo sapiens*, *Gallus gallus*, *Takifugu rubripes* and *Danio rerio* which was consistent with previous analyses (Merzdorf 2007) with one ZIC gene in *Drosophila melanogaster* known as the *odd-paired* (*opa*) gene (Aruga et al. 1996) (Fig. 5.2). In *Drosophila melanogaster* *opa* is essential for the parasegmental subdivision of the early embryo (Benedyk et al. 1994). The first intron-exon boundary is conserved in all five genes but the second intron-exon boundary is conserved between ZIC1, ZIC2 and ZIC3, but not ZIC4 or ZIC5 (Appendix Fig. 1.7) (Grinberg & Millen 2005). A ZIC orthologue was found in the vertebrate species analysed and a ZIC family pro-orthologues were found in the rest of the metazoan species, except *Caenorhabditis elegans*. A ZIC pro-orthologue has been characterised in the protostome *Caenorhabditis elegans* as an open reading frame from the genome, named C47C12.3 (Benedyk et al. 1994; Knight & Shimeld 2001) but was removed due to long branch length after ML phylogenies. A ZIC pro-orthologue was found in *Ciona intestinalis*, which has previously been described and named *Ci-macho* (Satou et al. 2002) (Fig. 5.2).

5.2.2.3 Phylogenetic distribution of proteins involved in the movement of cilia and other factors in the development of laterality

As well as structural proteins and transcription factors involved in left-right asymmetry in the vertebrates other proteins were also found as causes of the phenotype *situs inversus*. Proteins involved in the positioning of nodal cilia, transduction of left-ward flow through calcium channels and inhibition and regulation of nodal are also required for normal laterality. The *inv*

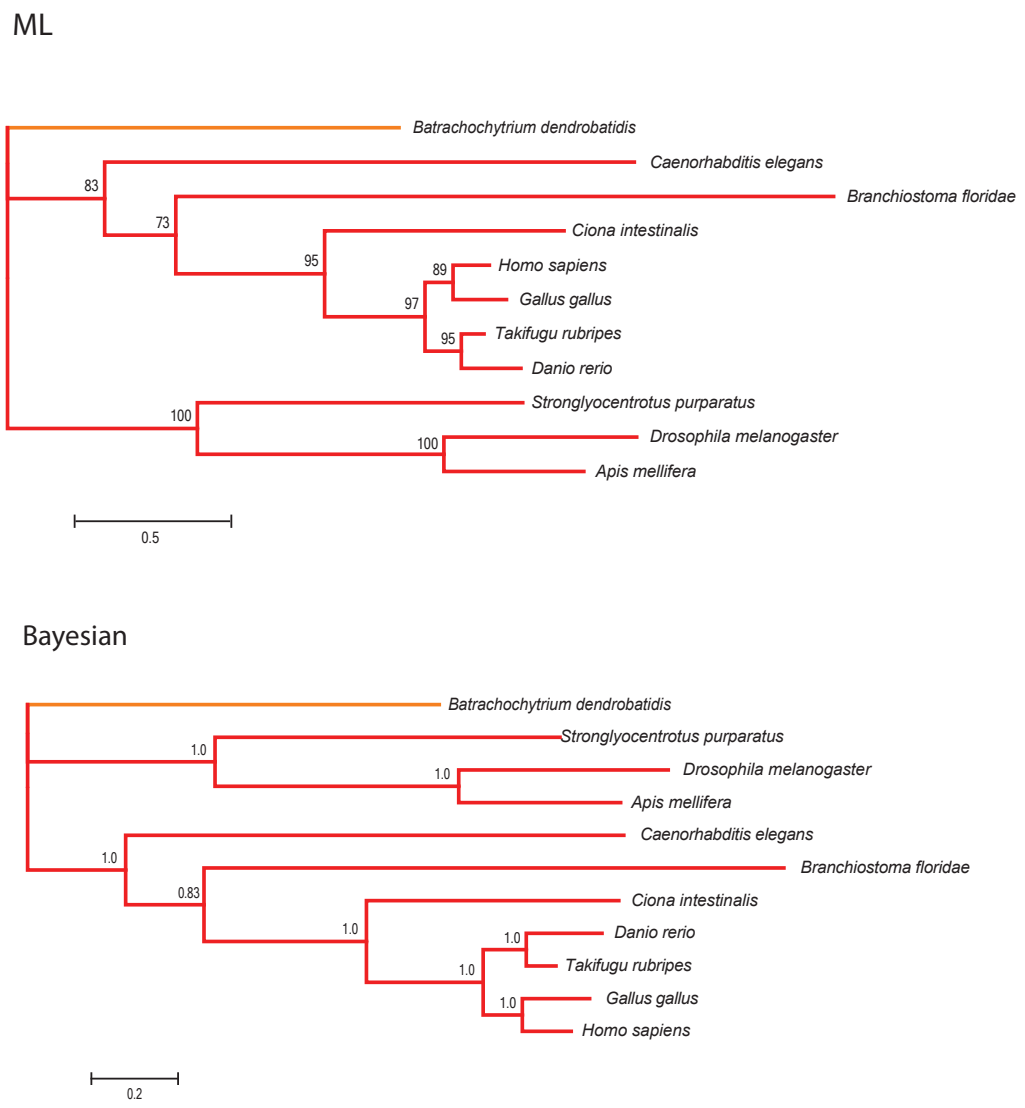


Figure 5.5: INV Phylogeny.

Maximum Likelihood and Bayesian trees were produced for INV. Amino acid sequence alignments were produced using MAFFT and trimmed to remove poorly aligned positions. Maximum likelihood phylogentic trees were constructed using PhyMLv3.0 (100 replicates, LG matrix, 4 gamma categories, random starting tree). Bayesian trees were inferred using MrBayesv3.1.2 (random starting tree, 4 chains of temperature 0.2, WAG substitution matrices, 4 discrete categories of gamma distribution substitution rate, 250 000 generations). Topology support for nodes is indicated (bootstrap). Generally, groups with >90% bootstrap support were considered to be well supported and those with >70% bootstrap support to have some support. The tree contains organisms from 2 of the 6 major clades: Holozoa (Red) and Fungi (Orange).

mouse was generated through a recessive insertional mutation within the *inversin* gene, which removes a coding sequence of 1000 amino acids (Yokoyama et al. 1993; Morgan et al. 1998). The *inversin* gene encodes an intracellular protein with ankyrin repeats in the C-terminal domain.

The mutation results in 100% of homozygous transgenic mice displaying *situs inversus* instead of the randomised laterality observed in mouse mutants of other genes (Yokoyama et al. 1993). Inversin is localised in the primary cilia on nodal cells (Watanabe et al. 2003) and although the cilia maintain nodal flow, the disorganisation of nodal cilia posterior positioning and the aberrant rotation of cilia have been shown to affect the speed of nodal flow in *inv* mouse mutants (Okada et al. 2005). The BLASTp analysis was the first to assess the inversin protein phylogeny and has shown that Inversin orthologues are found across the holozoan species incorporated in this analysis (Fig. 5.2 and Fig. 5.5).

The Transforming Growth Factor-β (TGF-β) superfamily comprises a large group of structurally related polypeptides that are capable of regulating cell growth and differentiation. One of the TGF-β superfamily, Growth Differentiation Factor 1 (GDF1), a mammalian orthologue of the amphibian Vg1, has been implicated in left-right determination through its role in the early gene activation pathway which leads to the establishment of left-right asymmetry (Rankin et al. 2000; Andersson et al. 2007). GDF1 (and the closely related GDF3) have deuterostome orthologues in *Ciona intestinalis* and *Stronglyocentrotus purparatus* (Fig. 5.2 and Appendix Fig. 1.8).

Polycystic Kidney Disease is an autosomal dominant genetic disorder characterised by the formation of cysts, which are predominantly found in the ducts of the kidney and liver (Torres & Harris 2006). Two of the genes responsible for the disease, *PKD1* and *PKD2* encode Polycystin-1 and Polycystin-2 which are membrane glycoproteins (Woolf et al. 1995; Mochizuki et al. 1996; Hayashi et al. 1997). Polycystin-2 is predicted to have cytoplasmic N-termini and C-termini and six transmembrane domains which create a nonselective cation channel that is highly permeable to calcium (Gonzelez-Perrett et al. 2001; Vassilev et al. 2001; Koulen et al. 2002; Hayashi et al. 1997). Homozygous *Pkd2* mouse mutants display left-right asymmetry due to the failure to

activate detectable levels of nodal expression in the lateral plate mesoderm (Pennekamp et al. 2002). The BLASTp analysis found PKD2 orthologues in all the Holozoa except *Lottia gigantea* and *Monosiga brevicollis* (Fig. 5.2). PKD2-like 2 and PKD2-like-1 *Homo sapiens* and *Gallus gallus* proteins were found as well as a fish (*Takifugu rubripes* and *Danio rerio*) PKD2-like1protein (Appendix Fig. 1.9). The invertebrate genes of the Metazoa included in this analysis are all positioned outside the vertebrates. No orthologues were found in the Excavata or Fungi but three were observed in the Chromalveolata (*Aureococcus anophagefferens*, *Paramecium tetramelia* and *Phytophthora sojae*) clade of eukaryotes. One Amoebozoa, *Dictyostelium discoideum* and one Plantae, *Chlamydomonas reinhardtii* orthologue (C_420012), previously found in a proteomic analysis was found (Pazour et al. 2005; Li et al. 2004).

Bicaudal C (*BicC1*) was originally identified in *Drosophila melanogaster* as a gene in which heterozygous females produced embryos with 'double-abdomen' phenotypes (Mohler & Wieschaus 1986). BicC1 encodes an evolutionary conserved RNA-binding molecule that consists of five N-terminal KH RNA-binding domains and a C-terminal protein-protein interaction SAM (sterile alpha motif) domain. BicC1 has been implicated in left-right asymmetry because inhibition of BicC1, through homologous recombination in embryonic stem (ES) cells, disrupts normal planar positioning of cilia and therefore, fluid flow which results in randomised left-right asymmetry (Maisonneuve et al. 2009). The BLASTp analysis found an orthologue in all the holozoan species except *Caenorhabditis elegans* and *Monosiga brevicollis* (Fig. 5.2 and Appendix Fig. 1.10).

DAND5 is a member of a novel family which included *Cerberus* and *Gremlin* and are all related through the conserved DAN domain (Hsu et al. 1998). They are all secreted proteins which block Bone Morphogenetic Protein (BMP) signalling by binding to BMPs and preventing them from

binding to receptors. DAND5 blocks the expression of the TGFβ superfamily member *nodal* on the right of the mouse ventral node (Hashimoto et al. 2004; Marques et al. 2004). Cerberus and Dante orthologues grouped together as did the Gremlin orthologues. A Cerberus orthologue was found in all the vertebrate species as well as a cephalochordate species, *Branchiostoma floridae* but no orthologue was found in *Ciona intestinalis*. Gremlin orthologues were also found in the vertebrates and two invertebrate species *Capitella teleta* and *Lottia gigantea* (Fig. 5.2 and Appendix Fig. 1.11). Previous research has found a potential *Ciona intestinalis* Gremlin orthologue but it was unsure if the protein was ancestral to just the Gremlin clade or the whole DAN family (Hino et al. 2003).

5.2.3 The presence of left-right asymmetry proteins in *Ciona intestinalis*

5.2.3.1 *Ciona intestinalis* proteins

In Chapters 3 and 4, the conservation of monocilia on the ectoderm of *Ciona intestinalis* embryos was analysed as well as their potential role in nodal flow and left-right asymmetry establishment. To inform the previous morphological analysis the proteins linked with left-right asymmetry which were analysed across the eukaryotes were also analysed in the *Ciona intestinalis* embryo and their Expression Sequence Tag data assessed. This research was able to analyse whether the proteins essential for the correct positioning of organs in the vertebrates were present in the *Ciona intestinalis* embryo.

Ciona intestinalis has an orthologue of each structural protein involved in left-right asymmetry in its genome. The dyneins are highly conserved axonemal motor proteins required for cilia motility which has led to their requirement in the axoneme of nodal cilia in the establishment of

vertebrate left-right asymmetry. A single orthologue was found for both the Dynein Intermediate chain proteins, DNAI1 and DNAI2 and both orthologues resolved to immediately outside the vertebrate clade. The anterograde protein, KIF3A, required for ciliogenesis through its role as a motor protein was also found in the *Ciona intestinalis* predicted proteome. A single orthologue was present and in both methods of phylogenetic inference was situated outside the vertebrate clade and inside the cephalochordate, *Branchiostoma floridae*. DNAH5, an axonemal heavy chain protein and part of the OADα group is essential for the establishment of motile nodal cilia and left-right asymmetry. The BLASTp method found four potential *Ciona intestinalis* orthologues which all resolved inside the metazoan DNAH5/8 clade inside the non-holozoan ancestral orthologues. One of the potential orthologues grouped outside the vertebrate DNAH8 clade and two others grouped with an invertebrate DNAH5/8 clade. One DNAH5 orthologue was observed grouped outside the vertebrate DNAH5 clade which suggests that this sequence is a true DNAH5 *Ciona intestinalis* orthologue. The dynein motor protein DNAH11 orthologues grouped with DNAH9 orthologues which encode another dynein motor protein. The *Ciona intestinalis* DNAH11 orthologue grouped with the vertebrate DNAH11 sequences but no DNAH9 orthologue was found although a *Ciona intestinalis* protein did group with other invertebrate proteins in a DNAH11/9 clade. One KIF3A *Ciona intestinalis* orthologue was found which grouped outside the vertebrates and inside *Branchiostoma floridae*.

A pro-orthologue of the transcription factors RFX3 and ZIC3 was found in the *Ciona intestinalis* predicted proteome lying outside the RFX1/2/3 and ZIC1/2/3/4/5 vertebrate clades respectively in phylogenetic analyses. The *Ciona intestinalis* pro-orthologues were grouped with other invertebrate pro-orthologues. A clear orthologue was not found for FOXJ1 with a potential orthologue grouping outside the invertebrates with low support values in both phylogenetic

	Left-right Asymmetry Proteins												
	Structural					Transcription Factors			Others				
Stage of Development	DNAI1	DNAI2	DNAH5	DNAH11	KIF3A	FOXJ1	RFX3	ZIC3	BICC1	GDF1	INV	PKD2	Total
Egg	0	1	0	0	1	2	8	3	0	4	1	4	32587
Cleaving Embryo	0	0	0	1	1	2	3	0	0	0	0	3	34025
Gastrula and Neurula	1	1	0	2	0	1	1	0	0	2	0	5	26154
Tailbud	0	1	0	0	1	0	3	4	2	0	1	1	34185
Larvae	0	0	0	0	0	0	1	8	0	0	3	0	33245
Whole Embryo	0	1	0	0	0	0	1	1	0	0	1	2	18194
Juvenile	0	1	2	2	1	0	1	1	0	0	0	3	30098
Young Adult	0	4	0	1	1	3	5	0	0	0	2	3	32584
Mature Adult	10	14	5	0	1	7	6	0	3	6	0	6	33721
Whole Animal	0	0	0	0	0	0	0	0	0	0	0	0	82
Neural Complex	0	0	0	1	0	1	0	4	1	0	0	2	11105
Heart	1	1	1	0	0	0	0	0	1	3	0	2	13892
Endostyle	0	0	0	0	0	0	0	0	0	0	1	0	2690
Digestive Gland	3	6	0	1	0	1	2	0	0	1	0	4	17951
Gonad	0	0	1	0	0	0	3	0	0	1	0	0	17265
Testis	0	1	0	0	1	0	0	0	1	0	0	0	5726
Haemocytes	0	0	1	0	0	0	0	0	0	0	1	0	33633
Unpublished Library	0	0	0	0	0	0	0	0	0	0	0	0	998
Egg to Neurula	9	3	2	0	5	1	9	14	30	17	0	24	157985

Figure 5.6: EST numbers of 13 genes in the adult and embryo *Ciona intestinalis* gene collection (Satou et al. 2003). Total indicates the total ESTs from this library.

inferences. For both the INV and BicC1 protein, a *Ciona intestinalis* orthologue was found that grouped outside the vertebrates and inside the invertebrates and for the PKD2 protein a pro-orthologue of the PKD2/PKD2-like1/2 protein was extracted. An orthologue of the GDF1 protein was found and grouped outside the vertebrates and inside the echinoderm, *Stronglyocentrotus purparatus*. No *Ciona intestinalis* orthologue was found for the DAND5 protein.

5.2.3.2 The expression of proteins involved in left-right asymmetry in *Ciona intestinalis*

An orthologue or pro-orthologue of 13 of the 14 proteins, known to have an important involvement in establishing laterality, was found in the *Ciona intestinalis* proteome using the BLASTp method previously described. Large-scale Expression Sequence Tag (EST) analyses of transcripts expressed in *Ciona intestinalis* have been conducted and provide detailed information on the expression of particular genes in numerous tissues and embryonic stages (Satou et al. 2003). Figure 5.6 collates the EST information for each of the proteins analysed previously

(excluding DAND5 which the BLASTp method found no orthologue in *Ciona intestinalis*). As described in previous chapters, *Ci-Pitx* expression, the first molecular evidence of asymmetry, is first detected in the mid-tailbud stage of development. To assess the potential role of the BLASTp analysed proteins in establishing the left-sided *Ci-Pitx* expression the ESTs at the gastrula and neurula stage as well as earlier stages are of particular importance. Six of the proteins (*n*=13) are expressed at the gastrula and neurula stage of development (DNAI1, DNAI2, DNAH11, FOXJ1, RFX3, GDF1 and PKD2) and the same seven proteins as well as three more are expressed at the cleaving embryo stage or earlier (KIF3A, TBX6 and ZIC3). PKD2 has the highest number of ESTs at the gastrula and neurula stage with five whilst DNAH11 and GDF1have two and DNAI1, DNAI2, FOXJ1 and RFX3 have one (Fig. 5.6).

5.2.3.3 The Expression Patterns of *DNAH11* in the developing *Ciona intestinalis* embryo

DNAH11, also known as *lrd*, is one of the few genes expressed exclusively in the cilia of the mouse ventral node (McGrath et al. 2003) which makes it an interesting gene to study when analysing left-right proteins and their role in the developing *Ciona intestinalis* embryo. Phylogenetics has demonstrated that DNAH11 appears to be a chordate specific protein with *Ciona intestinalis* and *Branchiostoma floridae* orthologues discovered which do not cluster with the highly similar DNAH9 protein (Fig. 5.4). Further analysis has shown that during embryogenesis two ESTs are present in the gastrula and neurula stage libraries and one from the stage at which the embryo is undergoing cleavage (Fig. 5.6). Several early stages of *Ciona intestinalis* embryogenesis were fixed and *DNAH11 in situ* hybridisations for two *DNAH11* probes performed. Embryos were hybridised with a dioxygenin labelled RNA probe and stained to assess localisation of *DNAH11*

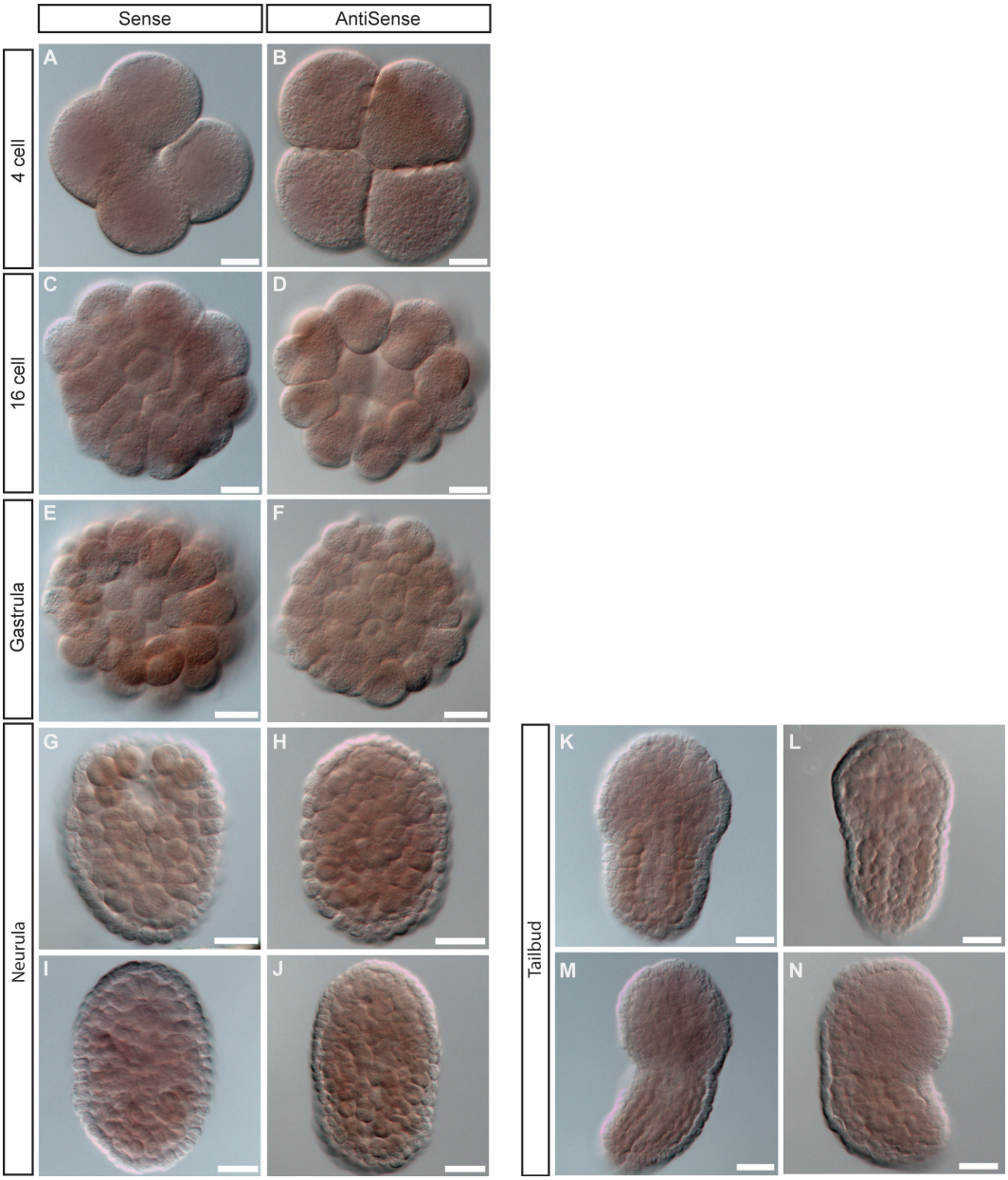


Figure 5.7: *DNAH11* is not expressed in the early stages of *Ciona intestinalis* embryogenesis.

A, **C**, **E**, **G**, **I**, **K**, **M**: Control *in situ* hybridisations for *DNAH11* using a sense probe. Embryos are staged at 4 cell, 16 cell, 76 cell, gastrula, late neurula and tailbud and there is no expression in any embryos. **B**, **D**, **F**, **H**, **J**, **L**, **N**: Experimental *in situ* hybridisations for *DNAH11* using an antisense probe. Embryos were the same age and show no staining. Bar = 50µm (All)

gene expression. In both the probes the sense and antisense hybridised embryos had no evidence of any staining until background stain levels predominated (Fig. 5.7).

5.3 DISCUSSION

Defects in the normal mechanisms which establish the left-right axis result in numerous human disorders which normally present with other common features, such as immotile or absent cilia. Additionally, numerous mouse mutants have abnormal positioning of organs and heart looping. To assess whether proteins associated with these diseases and syndromes are conserved among the eukaryotes a survey was conducted to compile a list of the proteins involved in left-right asymmetry development and their phylogenetic distribution analysed. *Situs inversus*, a term to describe the complete reversal of the positioning of internal organs in organisms, provided a standardised phenotype to search OMIM and MGI to find genes involved in the establishment of left-right asymmetry.

The initial survey identified numerous genes that result in *situs inversus* in both human and mouse but only those that have an incidence in greater than 48% of cases were retained for further analysis. These genes are linked with five diseases or syndromes which commonly present with left-right asymmetry defects. PKD2, BicC1 and KIF3A are all mutated proteins that cause Polycystic Kidney Disease (PKD), an autosomal inherited disorder which occurs in ~1 in 1000 people within the Caucasian community and is characterised by the formation of fluid-filled cysts in the kidneys. The onset of these cysts results in renal parenchyma and eventually end-stage renal failure (ESRF) with the formation of cysts in other organs such as the liver and pancreas (Gabow 1993). The PKD2 gene is located on the chromosome 4q21-23 and is mutated in 15% of PKD sufferers. The *jcpk* mouse mutant phenotype closely resembles human PKD which is due to a mutation in the *BicC1* gene (Bouvrette et al. 2008). Additionally, the removal of

cilia in a *kif3a* knockout mouse presented renal cysts and a PKD phenotype which demonstrated the importance of cilia in this disease (Lin et al. 2003).

Primary Ciliary Dyskinesia, (PCD) was previously known as Immotile Cilia Syndrome, along with Kartagener's Syndrome and results from mutations including DNAH11, DNAH5, DNAI1 and DNAI2 (Noone et al. 1999). The disease is pleiotropic including immotile sperm and respiratory cilia and mirror-image organ distribution. It has been described in more detail in Chapter 1 and in the results section in Chapter 5. Mutations in the gene *zic3* cause Heterotaxy 1 which results in congenital heart defects, a defect which is found in 1% of all live births (Gebbia et al. 1997).

The genes involved in these disorders and mouse mutants were taken forward to study their prevalence across ciliated and non-ciliated organisms in six major clades. 45 species genomes from the Plantae, Excavata, Chromalveolata, Holozoa, Fungi and Amoebozoa clades were searched for the 13 genes. Species were chosen to represent the six major clades, incorporate organisms that require a cilium/flagellum at some point in their life-cycle and, in the Holozoa, have different mechanisms involved in the breaking of symmetry and the establishment of left-right asymmetry. The interrogation of the predicted proteomes utilised the Reciprocal Best BLASTp search and clustering method (method described in more detail in Chapter 2). The orthologous clusters were defined by eye, aligned, trimmed and then used in ML and Bayesian phylogenetic inference. This analysis is the first widespread evolutionary survey of genes involved in the establishment of left-right asymmetry in mouse and human.

5.3.1 The presence and absence of proteins involved in left-right asymmetry and nodal flow in the human and mouse models

5.3.1.1 Structural Proteins

The 9+2 motile cilium is widely found across the eukaryotes, from the green algae (*Chlamydomonas reinhardtii*) to humans and has a highly conserved structure and function. These motile cilia are able to beat through the central pair and dynein arms which are attached to the A-tubule (described in more detail in Chapter 1). The primary cilia, 9+0 without dynein arms or radial spokes, are restricted to the Eumetazoa (excluding placozoans). A third type of cilia, known as nodal cilia, have been shown to have a 9+0 structure with dynein arms (Hirokawa et al. 2006). Videomicroscopy experiments have shown that although these cilia do not have a central pair they are able to beat (Nonaka et al. 1998). The beat differs from the conventional 9+2 cilia whip-like movement as the cilia rotate on a posterior tilt to generate an overall directional flow. However, it is not clear whether the same proteins involved in motility and ciliogenesis in 9+2 motile cilia are essential in building and function of nodal cilia.

As expected the dynein axonemal heavy chain and intermediate chain proteins (DNAH11, DNAH5, DNAI1 and DNAI2) orthologues, or pro-orthologues, were found in all species that have motile cilia at some point in their life cycle. No dyneins were present in the higher plants or the non-flagellate red algae (*Cyanidioschyzon merolae*), which does not have dynein motor proteins at all, which is in line with previous research. An ancestral orthologue of all four dynein proteins analysed was found in all five Excavata genomes surveyed. Within the Chromalvaeolata, the species selected which do have cilia or flagella at some point in their life cycle had a pro-orthologue of the dyneins involved in left-right asymmetry except *Plasmodium falciparum*.

Comparative analyses like this one cannot distinguish between proteins that have been lost entirely and those that have diverged in sequence to the point where they are undetectable by this approach. For instance, the *Plasmodium falciparum* builds a flagellated microgamete using an IFT independent mechanism (Briggs et al. 2004) and has divergent dynein sequences so although an orthologue was not found for DNAH11 or DNAH5 it could be a result of a highly divergent sequence and not a complete absence (Wickstead & Gull 2007). A pro-orthologue was found in *Thalassiosira pseudonana*, an organism which has motile cilia with no central pair or radial spokes but still contains the full complement of dyneins analysed here. An orthologue or a pro-orthologue of all the dynein proteins analysed was found in each holozoan species surveyed except for *Caenorhabditis elegans* which does not build a motile cilia. A DNAH11 and DNAH5 pro-orthologue and DNAI2 orthologue was found in the only one fungi species, *Batrachochytrium dendrobatidis* which has a flagellated zoospore.

Proteins of the kinesin superfamily are ubiquitous to all eukaryotes although this analysis only concentrated on KIF3A, a protein required for node ciliogenesis. All kinesin proteins share a conserved globular motor domain, usually found at the N-terminus and a more divergent tail region which interacts with kinesin light chain proteins, cargoes or other macromolecules. KIF3A belongs to the kinesin-2 family of kinesin proteins which share a common ancestor and a conserved cellular role. They are found in species that build a cilium or flagellum at some point in their life cycle. Although other members of the kinesin-2 family were not pulled out in this search, a KIF3A orthologue was found in every species of the Holozoa analysed but in no species outside this group.

The results from the protein survey of structural proteins show that although the nodal cilia are potentially a new cilial structure, with a 9+0 structure with dynein arms, the structure and

assembly require the ancestral genes involved in the conventional 9+2 motile cilia ciliogenesis and movement. The absence of any of the four dynein proteins analysed here results in a lack of normal nodal flow and left-right asymmetry defects in numerous model species which suggests the cilia are built and motile by ancestral genes conserved from as distantly related organisms as *Chlamydomonas reinhardtii*. A new group of genes are not essential for the potentially unique cilia structure of nodal cilia.

5.3.1.2 Transcription Factors

The proteins which all encode Transcription Factors, FOXJ1, RFX3 and ZIC3, were pre-dominantly found in the Metazoa, an already observed consequence of the advent of multicellularity (Larroux et al. 2008). Transcription Factors act as regulatory nodes in developmental specification and patterning events and with their expansion in early metazoan evolution may have enabled the advent of metazoan axial patterning and multicellularity (Larroux et al. 2006). Within the Metazoa there is a large variation of body plans with the cnidarians exhibiting radial symmetry, the deuterostomes and protostomes displaying bilateral asymmetry and sponges no symmetry. It has been previously discussed that sponges may have a narrower suite of transcription factors which could link with their diminished complexity compared to the bilaterian lineages, including the more complex symmetric body plans (Larroux et al. 2006; Simionato et al. 2007). The choanoflagellate, *Monosiga brevicollis* represents the outgroup to the Metazoa and demonstrates that a large number of signalling pathway components and transcription factors are unique to organisms after the divergence between choanoflagellates and the Metazoa.

In particular, this analysis focused on transcription factors known to have an important role in the development of left-right asymmetry to analyse their spread across the eukaryotes.

FOXJ1, a member of the Forkhead family of transcription factors, controls the production of motile cilia (Brody et al. 2000) as well as function in mouse left-right asymmetry determination (Zhang et al. 2004). FOXJ1 is expressed in the ventral cells of the node and, although the nodal cilia are still present, its absence results in the randomised expression of *nodal* and *pitx2*, as well as the complete absence of *lefty* expression (Zhang et al. 2004). RFX3, a member of the regulatory X family, is expressed in the node and is important in the assembly of cilia through an IFT implicated gene, *D2lic*. ZIC3, was first implicated in left-right asymmetry through the developmental disorder, HTX1, whose sufferers show laterality problems. It is expressed in the node and maintains nodal expression in the node and the LPM.

An orthologue or pro-orthologue of these transcription factors was found in all of the Metazoa, except *Caenorhabditis elegans*. A highly divergent sequence was detected through the BLASTp method in this species for RFX3 and ZIC3 but both sequences were removed due to their very different sequences but have both been described in previous studies. An orthologue of each protein was found in the vertebrates but only pro-orthologues were found for RFX3 and ZIC3 in the rest of the Metazoa. Three RFX proteins (RFX1-3) and five ZIC proteins (ZIC1-5) were only found in the vertebrates. However, an orthologue was found in each selected Metazoa species (except *Caenorhabditis elegans*) for FOXJ1, although the *Ciona intestinalis* sequence grouped outside the invertebrates and not in the expected phylogenetic position outside the vertebrates. A *Ciona intestinalis* orthologue has not been described for the FOXJ1 protein which suggests that this is a very divergent protein which must be considered carefully as a true orthologue. RFX3 and FOXJ1 pro-orthologues in the two yeast species have been described in previous analyses but the highly divergent sequences were removed in this analysis due to very long branch lengths in the phylogenetic analyses.

5.3.1.3 Other proteins

Other proteins that cannot be as easily grouped together as the structural proteins and transcription factors were also identified in the initial gene survey to have a role in the establishment of left-right asymmetry. *BicC1* and *inversin* are two genes involved in the positioning of nodal cilia in mice and their distribution across the eukaryotes has not been previously analysed. This research has identified new species which have an orthologue of each protein within the predicted proteomes. BicC1, bicaudal C1, is expressed in the mouse ventral node and the *Xenopus* Hensen's node where it is responsible for the organised posterior positioning of nodal cilia (Wessely et al. 2001; Tran et al. 2007). Inhibition of BicC1 results in the disorganised positioning of cilia and the disruption to the directional flow which is essential for the downstream establishment of left-right asymmetry. Previously, a homologue of the *Drosophila melanogaster BicC1* gene has been described in the mouse, *Xenopus* and zebrafish (Bouvrette et al. 2010) but in this analysis, orthologues are also found in all the metazoans analysed except *Caenorhabditis elegans* and *Capitella teleta*

Inversin is localised to the node cilia and is believed to work in parallel with BicC1 to polarise nodal cilia by directly inhibiting Dvl1 in the canonical Wnt signalling pathway (Maisonneuve et al. 2009). Inversin is present in the *Caenorhabditis elegans* predicted proteome, which BicC1 is not, but is restricted to the Deuterostomes and ecdysozoans with no orthologues found in the lophotrochozoans organisms analysed. However, the growth differentiation factor family protein, GDF1, which is involved in the early gene activation pathway which leads to the establishment of left-right asymmetry, was only found in the deuterostomes.

PKD2, is the one of the two genes responsible for the autosomal dominant genetic disorder,

Polycystic Kidney Disease (PKD). *PKD2* encodes Polycystin-2 which is a six transmembrane spanning protein which is a nonselective cation channel that is highly permeable to calcium (Gonzalez-Perrett et al. 2001; Vassilev et al. 2001; Koulen et al. 2002; Hayashi et al. 1997). In organisms homozygous to *PKD2* exhibit randomised left-right asymmetry as a result of an ability to activate detectable levels of *nodal* expression in the LPM (Pennekamp et al. 2002). An orthologue was found in the vertebrate organisms, a PKD2-like-1 protein in the same organisms and a PKD2-like-2 protein in only the human and chick models.

A PKD2 pro-orthologue was found in the rest of the Metazoa except *Lottia gigantea* as well as in organisms in the Plantae, Chromalveolata, Fungi and Amoebozoa groups. PKD2 in *Chlamydomonas reinhardtii* is cleaved in the cell body and then moves to the flagellar membrane where it is enriched (Huang et al. 2007). Most of the protein remains static in the flagella but some moves at a similar rate to IFT and is essential in the efficient mating of gametes of opposing mating types. The touching of flagella results in the initiation of a Ca^{2+} signalling pathway which is required for the fusion of gametes. The result suggests an ancestral role for the protein as a calcium channel in a wide diversity of organisms both with and without cilia, and has more than just a role in left-right asymmetry in these single-celled organisms and plants. The calcium channel could have been co-opted to the node cilia in vertebrates to act as a channel important in left-right asymmetry. These other proteins generating *situs inversus* are primarily found in the Metazoa, with no orthologues in the metazoan outgroup, the choanoflagellates. Only the calcium channel encoding protein, PKD2 was found in organisms outside the Metazoa.

5.3.2 Protein presence and left-right asymmetry mechanisms

As described in the introduction, several different mechanisms are involved in the establishment of left-right asymmetry in vertebrates. Nodal flow is a characteristic of the mammalian, amphibian and fish models but is completely absent in the avian model. In addition, several other mechanisms are also known to be involved in the generation of laterality in the avian, amphibian and fish models. H^+/K^+-ATPase, Gap junctions and Serotonin are all implicated in the chick and *Xenopus* embryo and are dependent on each other. H^+/K^+-ATPase is also implicated in the development of left-right asymmetry in zebrafish. The different mechanisms known to have a role in particular organisms compared to the presence and absence of proteins involved in mammalian left-right asymmetry showed that all 13 proteins were present in all the chordates that have numerous and different left-right mechanisms. Although, the chick embryo does not have nodal cilia that produce a directional flow the predicted proteome still maintains a full complement of proteins involved in left-right asymmetry.

Nodal and *pitx2* expression on the left-side of the node is a conserved feature in the vertebrates and the left-sided expression in the embryo as a whole is a feature of most invertebrates with the exception of the ecdysozoan species analysed. Most proteins were absent from the *Caenorhabditis elegans* predicted proteome which is the only Holozoa organism analysed that does not have motile cilia at any point in its life cycle. The lack of dynein proteins was expected due to absence of motile cilia but an orthologue was only found for three proteins (KIF3A, INV and PKD2) although others may not have been detected due to the fast evolving genome and highly divergent sequences. A particular set of proteins did not seem to be associated with the nodal flow mechanism, or any other mechanism. This may be due to the pleiotropic roles that

the proteins have in development. This set of proteins was not exhaustive but instead focussed on mammalian proteins. It would be interesting to extend the search to proteins in other organisms which have mechanisms.

ZIC3 was restricted to the Metazoa, with no orthologues found in organisms in the other five clades; a finding validated in previous research. Five Zinc Finger transcription factors found in the vertebrates all contain highly conserved five tandem C2H2 type ZF domains which are thought to be derived from a common ancestral gene (Aruga 2004). ZIC1-3 are most closely related in the mouse, while ZIC4 and ZIC5 are more divergent (Furushima et al. 2000). Of the five ZIC genes found in mouse, four orthologues are found in *Xenopus* (ZIC1, ZIC2, ZIC3 and ZIC5), three in chick and zebrafish (ZIC1-3), two in ascidians (ZICL/ZICN and macho-1) (Gostling & Shimeld 2003; Satou et al. 2002; Nishida & Sawada 2001; Wada & Saiga 2002) and one in both *Drosophila melanogaster* (opa) (Benedyk et al. 1994) and *Caenorhabditis elegans* (C47C12.3) (Alper & Kenyon 2002). The vertebrate species analysed had three RFX genes (RFX1-3) whereas the invertebrate species only had one pro-orthologue. The expansion of the *ZIC* and *RFX* genes in the vertebrates could have enabled the vertebrates to evolve a specialised mechanism at the organiser to establish left-right asymmetry.

5.3.3 Proteins involved in the establishment of left-right asymmetry in *Ciona intestinalis*

An orthologue or pro-orthologue was found in the *Ciona intestinalis* predicted proteome for all the proteins associated with left-right asymmetry, except DAND5. The structural proteins, DNAH11, DNAH5, DNAI1, DNAI2 and KIF3A were all found in the *Ciona intestinalis* proteome

which is a common factor in all organisms which have cilia at some point in their life cycle. Interestingly, a DNAH11 orthologue was found in the *Ciona intestinalis*, but not in *Gallus gallus* or *Takifugu rubripes*, proteome. An absence of a DAND5 orthologue is not conclusive and could be an artefact of the method used to search for orthologues. An EST survey of the 12 proteins analysed through ML and Bayesian phylogenetic inference show that at the stages prior to the asymmetric expression of *Ci-Nodal*, *Ci-Pitx* and *Ci-Lefty* there is evidence that every protein, except DNAH5, is expressed. The lack of DNAH5 could be a result of very low expression levels which are not detected by the screen or could be an absence of expression at all.

The presence of a DNAH11 orthologue in human, *Danio rerio*, *Ciona intestinalis* and *Branchiostoma floridae* but not in any other organism analysed was an interesting finding because it appears to be a deuterostome specific protein. Two ESTs of the gene were found in the *Ciona intestinalis* gene collection (Satou et al. 2003) and the localisation of DNAH11 in the early stages of *Ciona intestinalis* development was tested through *in situ* hybridisation. No staining was observed on any embryo from the oocyte stage to the late tailbud stage when *Ci-Nodal* and *Ci-Pitx* are expressed asymmetrically. In conjunction with previous work in this thesis, the cilia of the late neurula *Ciona intestinalis* are non-motile with no evidence of dynein arms through TEM analysis which could explain the lack of *DNAH11* expression.

5.4 CONCLUSION

The survey of proteins which when mutated cause disorders that result in *situs inversus* provided a concise list of proteins involved in the establishment of left-right asymmetry in humans and mouse. The proteins were linked to five human diseases and disorders, including PCD,

Kartagener's syndrome and PKD, from which multiple findings in the investigation into the development of the left-right axis have been found. The symptoms and structure of cilia in these diseases were invaluable in the discovery that cilia are important in the establishment of left-right asymmetry and the normal body plan.

The normal motile cilium structure has nine outer doublet microtubules with a central pair and accessories such as dynein arms and radial spokes. Node cilia are motile but have an unconventional structure with nine outer doublet microtubules but no central pair. Dynein arms on the A-tubule enable the cilia to rotate and function. Outer and inner dynein arm proteins were identified in the initial protein screen which when mutated or removed cause laterality defects. These proteins are found across the eukaryotes and are highly conserved in all species which generate a cilium/flagellum at some point in their life cycle which suggests that the same proteins are used to build nodal cilia as the conventional motile cilium.

Transcription factors were predominantly found in the Holozoa with the advent of multicellularity and the other proteins involved in the development of left-right asymmetry were also mainly found restricted to the Holozoa, except PKD2. Repeatedly I only found single gene-copy or single representatives for particular proteins in the *Ciona intestinalis* predicted proteome. An orthologue was found in the *Ciona intestinalis* translated genome for each protein except DAND5 and the only protein not found in the EST survey, at the neurula or tailbud stage, was DNAH5 which shows that all the genes are expressed at the right time and place to function in a role in left-right asymmetry in *Ciona intestinalis* development. DNAH11 expression was analysed for localisation in the early stages of embryogenesis but in line with the structural TEM in earlier chapters does not appear to function in the embryo at this stage.

CHAPTER 6

Conclusions

The positioning of the urochordates, including the ascidian species *Ciona intestinalis*, immediately outside the vertebrates means that they provide an interesting model for analysing the conservation of particular developmental mechanisms in a basal chordate (Delsuc et al. 2006). As a result this thesis has focused on the conservation of known vertebrate mechanisms in the establishment of left-right asymmetry and their potential role in the developing *Ciona intestinalis* embryo.

Left-right asymmetry mechanisms have been elucidated in several vertebrates (as discussed in Chapter 1) although there remain many unanswered questions. The mouse model has enabled several new findings to emerge in the discovery of the mechanisms which generate the left-right axis (Nonaka et al. 1998; Takeda et al. 1999). SEM demonstrated that cilia were present on the mouse ventral node and were able to rotate in a vortical motion which generated a leftward flow across the node (Sulik et al. 1994; Nonaka et al. 1998). The cilia were able to generate this rotation due to their posterior positioning on the cells of the node as well as the 40°±10° tilt of the cilia (Hashimoto et al. 2010; Nonaka et al. 2005). Downstream of nodal flow is the left-sided localisation of *nodal* (Collignon et al. 1996), *lefty* (Meno et al. 1996) and *pitx2* (Ryan et al. 1998) and subsequent asymmetric positioning of internal organs. The exact method in which the flow is converted into asymmetric localisation of *nodal* is not yet understood although two hypotheses have been proposed.

Nodal flow is a conserved mechanism in the vertebrates, with the same mechanism found in both the fish and amphibian models (Schweickert et al. 2007; Okada et al. 2005). Other mechanisms influential in the establishment of left-right asymmetry have also been detected in these models, as well as the avian model, which lacks monocilia on the node and, therefore, nodal flow (Levin & Mercola 1999). These mechanisms include H^+/K^+-ATPase (Levin et al. 2002), Gap junctions (Levin & Mercola 1999) and Serotonin (Fukumoto et al. 2005) which all occur during the early stages of development and prior to the presence of cilia and nodal flow. Asymmetric distribution of *nodal*, *pitx2* and *lefty* is highly conserved throughout the invertebrates but as yet only H^+/K^+-ATPase has been analysed as a mechanism for the establishment of left-right asymmetry in these species (Morokuma et al. 2002; Mita & Fujiwara 2007; Yu et al. 2002; Boorman & Shimeld 2002a; Duboc et al. 2005; Hibino et al. 2006; Grande & Patel 2009). This thesis has aimed to analyse how far the conservation of nodal flow extends beyond the vertebrates and into the invertebrates.

The adult *Ciona intestinalis* is a sessile filter feeder but the larva is a free swimming tadpole with many characteristics of the chordates. The urochordates are the closest living relative to vertebrates and, therefore, an interesting model to analyse nodal flow conservation (Delsuc et al. 2006; Tsagkogeorga et al. 2009). SEM has previously been used to analyse the surface structure and textures of the closely related ascidian *Halocynthia roretzi* species (Satoh & Deno 1984), but this is the first study to analyse the surface structures of the early *Ciona intestinalis* embryo. Careful consideration of fixation, to preserve microtubule structures like cilia, has enabled the detection of cilia, through SEM, on the surface ectoderm of a late neurula/early tailbud stage embryo. The cilia project from every cell of the embryo at a length of 1.5-2 μm and persist until the mid tailbud stage of development. The presence of cilia on the embryo immediately prior to the left-sided expression of *Ci-Pitx* led me to hypothesise that these cilia may have a role

homologous to the mouse node cilia.

Ciona intestinalis embryos do not have an organiser region (Lemaire 2011) which is homologous to the mouse ventral node, which could explain the presence of cilia on every cell of the ectoderm, but if the cilia do generate a leftward flow they must be motile. Live imaging of the cilia on the embryo suggested that they were not motile but analysis of their structure would enable me to determine if the cilia were able to move. TEM demonstrates that the cilia of the *Ciona intestinalis* embryo do not have the same structure as motile cilia, or that of the motile mouse node cilia. Instead immediately after the cilium has exited the cell the nine doublet microtubules are arranged in a ring structure but taper along the length of the cilium. At the distal tip there is no organised distribution of doublets and some doublets have disintegrated into singlets. This structure was also observed on cilia of the mouse endoderm and has been previously described in mammalian cell lines and *Leishmania mexicana* (Gluenz et al. 2010). Accessories associated with cilia, such as the central pair, radial spokes and dynein arms, which are synonymous with motile cilia, were never observed on the *Ciona intestinalis* cilia. The disorganised structure of these cilia makes it unlikely that they are motile but that instead they may have a sensory role on the developing embryo. This role could still be linked with the establishment of left-right asymmetry but not in the same capacity as the cilia of the mouse ventral node.

Both motile and immotile cilia are found on many different organisms where they have numerous roles, including sensory. Sensory motile cilia are essential for mating in *Chlamydomonas reinhardtii* (Huang et al. 2007) and immotile cilia have been shown to be a site of Hh and Wnt signalling (Haycraft et al. 2005; Corbit et al. 2005; Corbit et al. 2008). However, the expression of genes involved in these two pathways, as well as polycystins, is not found in the *Ciona intestinalis* embryo at the late neurula/early tailbud stage. As a result, I postulate that

if the cilia on the *Ciona intestinalis* embryo are involved in left-right asymmetry, they could be a location for H^+/K^+-ATPase channels which are known to establish left-right asymmetry in this species.

A characteristic of mouse node cilia, the posterior positioning of the cilia on each cell, is also conserved in cilia of the late neurula/early tailbud stage *Ciona intestinalis* embryo. Measurements have shown that the cilia of the *Ciona intestinalis* embryo are positioned in the posterior half of each cell along the AP axis. The PCP pathway has been implicated in the positioning of mouse ventral node cilia (Dabdoub 2003; Antic et al. 2010), as well as the cilia of the inner ear, and is the most likely mechanism which restricts the cilia to the posterior of each cell. The core pathway genes are present in the *Ciona intestinalis* genome and are known to be essential for convergent extension in the late tailbud embryo (Keys et al. 2002; Sasakura et al. 2003; Hotta et al. 2003; Hotta et al. 2007). Current gene expression analysis suggests that the genes are nor expressed in the late neurula/early tailbud embryo but these experiments were conducted in embryos de-chorionated at fertilisation. The removal of the chorion dramatically disrupts development (Shimeld & Levin 2006) and, therefore, these results cannot be considered as definitive and the genes could still be expressed. Future gene expression studies on embryos grown within the chorion and genetic manipulation of the genes is required to determine if the PCP pathway could be essential in the positioning of these cilia.

The cilia are positioned at the posterior of each cell of the embryo, although one small population of cells on the left face of the embryo in the region between the head and the tail have cilia positioned at a slightly different point along the cell AP axis. These cilia could have a different role which acts as a distinct region like the mouse ventral node. It can largely be discounted that the cilia are positioned at the posterior of each cell in order for the cilia to rotate

because the disorganised ultrastructure of these cilia but it could still be important for their role. The disruption of cilia positioning through exposure to high concentrations of NaCl does not affect the asymmetric expression *Ci-Pitx*. Although the cilia exposed to NaCl are positioned in a significantly different position it is still within the posterior half of the cell which may not affect their potential role in left-right asymmetry.

Previous experiments have demonstrated the importance of the chorion during the early development of the *Ciona intestinalis* embryo, especially in the development of left-right asymmetry (Shimeld & Levin 2006). To understand more the role that the chorion plays in *Ciona intestinalis* asymmetry development, the ultrastructure of the chorion and associated structures was analysed at the late neurula/early tailbud stage. The cilia are not in direct contact with chorion so it is unlikely that the removal of the chorion breaks a physical attachment. The disruption to left-right asymmetry could be a result of general abnormal embryo development due to changes in the immediate physical environment which alter mechanical forces, enzymatic activity and ionic environment. These experiments do not elucidate why the removal of the chorion affects left-right asymmetry but do suggest that the general disruption to development could cause this disorganisation.

In conjunction with morphological experiments, the genes involved in the establishment of left-right asymmetry have been surveyed across the eukaryotes with particular attention to those present in *Ciona intestinalis*. I investigated conservation of genes linked to left-right asymmetry as implied by mutant phenotypes that display *situs inversus*. This survey collated a list of genes which are all linked to left-right asymmetry and can be categorised by their cellular roles. The ancient dynein and kinesin proteins, which are essential for ciliogenesis and motility, are found in all organisms which build a cilium at some stage in their life cycle. The link with the structural

proteins and defects in left-right asymmetry indicate that although the cilia of the mouse ventral node have a different cilia structure, they are still built and maintained using ancestral genes. The newer transcription factors which have been linked to the advent of multicellularity were mainly restricted to the metazoa. Other proteins that cannot be categorised in this instance were present in most Metazoan species with only PKD2 found repeatedly outside this clade.

The morphological experiments (described in Chapter 3 and 4) demonstrate that cilia are present on the developing *Ciona intestinalis* embryo prior to asymmetric distribution of *nodal* which indicates a potential role in the development of left-right asymmetry. Although it can be concluded that the cilia are not motile, the presence of proteins involved in left-right asymmetry in humans and mice was analysed in *Ciona intestinalis*. All the proteins except DAND5 were found in the *Ciona intestinalis* genome and the only protein not found in the EST survey, at the neurula or tailbud stage was DNAH5. This shows that the genes are expressed at the right time and place to have a role in the establishment of left-right asymmetry in *Ciona intestinalis*. The genes involved in nodal flow and left-right asymmetry are present in the *Ciona intestinalis* embryo at the exact time point that left-right asymmetry is established which could mean that they have a conserved role in the invertebrate species. However, the pleiotropic nature of these genes could mean that they are actually working in another capacity.

Future experiments are required to focus on the role of these cilia on the ectoderm of the *Ciona intestinalis* embryo. The short time span in which these cilia emerge is indicative of a precise role at this point of development although it is not known what this role could be. Treatment of embryos with high concentrations of NaCl and the ROCK inhibitor Y-27632 has failed to remove the cilia or has affected the overall embryo development so a direct link between cilia loss and disruption to *Ci-Pitx* asymmetric expression cannot be measured. The removal of

the chorion for most manipulative techniques is detrimental to the asymmetric expression of *Ci-Pitx* so limits their use to answer this question. It might be that the experiment must wait until there are reliable methods of microinjection through the chorion of *Ciona intestinalis* or the generation of a drug inhibitor of genes required for ciliogenesis which do not affect other cellular processes.

REFERENCES

Van Aelst, L. & Symons, M., 2002. Role of Rho family GTPases in epithelial morphogenesis. *Genes & Development*, 16(9), pp.1032-54.

Afzelius, B.A., 1976. A Human Syndrome Caused by Immotile Cilia. *Science*, 193(4250), pp.317-319.

Allen, R., 1965. Isolated cilia in inner retinal neurons and in retinal pigment epithelium. *Journal of Ultrastructure Research*, 12(5-6), pp.730-747.

Alper, S. & Kenyon, C., 2002. The zinc finger protein REF-2 functions with the Hox genes to inhibit cell fusion in the ventral epidermis of *C. elegans*. *Development*, 129(14), pp.3335-3348.

Altschul, S.F. et al., 1990. Basic Local Alignment Search Tool. Methods, 215(3), pp.403-410.

Andersson, O., Bertolino, P. & Ibáñez, C.F., 2007. Distinct and cooperative roles of mammalian *Vg1* homologs *GDF1* and *GDF3* during early embryonic development. *Developmental Biology*, 311(2), pp.500-11.

Antic, D. et al., 2010. Planar cell polarity enables posterior localization of nodal cilia and left-right axis determination during mouse and *Xenopus* embryogenesis. *PloS one*, 5(2), p.e8999.

Aruga, J., 2004. The role of *Zic* genes in neural development. *Molecular and Cellular Neurosciences*, 26(2), pp.205-21.

Aruga, J. et al., 1996. The mouse *zic* gene family. Homologues of the *Drosophila* pair-rule gene odd-paired. *The Journal of Biological Chemistry*, 271(2), pp.1043-7.

Axelrod, J.D., 2001. Unipolar membrane association of *Dishevelled* mediates *Frizzled* planar cell polarity signaling. *Genes & Development*, 15, pp.1182-1187.

Beddington, R.S., 1994. Induction of a second neural axis by the mouse node. *Development*, 120(3), pp.613-620.

Bellomo, D. et al., 1996. Cell proliferation in mammalian gastrulation: the ventral node and notochord are relatively quiescent. *Developmental Dynamics*, 205(4), pp.471-85.

Belmont, J.W. et al., 2004. Molecular genetics of heterotaxy syndromes. *Current Opinion in Cardiology*, 19(3), pp.216-20.

Benedyk, M.J., Mullen, J.R. & DiNardo, S., 1994. *odd-paired*: a zinc finger pair-rule protein required for the timely activation of *engrailed* and *wingless* in *Drosophila* embryos. *Genes & Development*, 8(1), pp.105-117.

Berbari, N.F. et al., 2009. The primary cilium as a complex signaling center. *Current Biology*, 19(13), pp.R526-35.

Blum, M. et al., 1992. Gastrulation in the mouse: The role of the homeobox gene goosecoid. *Cell*, 69(7), pp.1097-1106.

Bonnafe, E. et al., 2004. The Transcription Factor RFX3 Directs Nodal Cilium Development and Left-Right Asymmetry Specification. *Molecular and Cellular Biology*, 24(10), pp.4417-4427.

Boorman, C.J. & Shimeld, S.M., 2002a. *Pitx* homeobox genes in *Ciona* and *amphioxus* show left-right asymmetry is a conserved chordate character and define the ascidian adenohypophysis. *Evolution & Development*, 4(5), pp.354-65.

Boorman, C.J. & Shimeld, S.M., 2002b. The evolution of left-right asymmetry in chordates. *BioEssays*, 24(11), pp.1004-11.

Borovina, A. et al., 2010. Vangl2 directs the posterior tilting and asymmetric localization of motile primary cilia. *Nature Cell Biology*, 12(4), pp.407-12.

Boucher, R.C., 2004. New concepts of the pathogenesis of cystic fibrosis lung disease. *European Respiratory Journal*, 23(1), pp.146-158.

Bouvrette, D.J., Price, S.J. & Bryda, E.C., 2008. K homology domains of the mouse polycystic kidney disease-related protein, Bicaudal-C (Bicc1), mediate RNA binding in vitro. *Nephron. Experimental Nephrology*, 108(1), pp.e27-34.

Bouvrette, D.J. et al., 2010. Knockdown of *bicaudal C* in zebrafish (*Danio rerio*) causes cystic kidneys: a non mammalian model of polycystic kidney disease. *Comparative Medicine*, 60(2), pp.96-106.

Brennan, J., Norris, D.P. & Robertson, E.J., 2002. *Nodal* activity in the node governs left-right asymmetry. *Genes & Development*, 16(18), pp.2339-44.

Briggs, L.J. et al., 2004. More than one way to build a flagellum: comparative genomics of parasitic protozoa. *Current Biology*, 14(15), pp.R611-2.

Brody, S.L. et al., 2000. Ciliogenesis and left-right axis defects in forkhead factor HFH-4-null mice. *American Journal of Respiratory Cell and Molecular Biology,* 23(1), pp.45-51.

Brown, N.A. & Wolpert, L., 1990. The development of handedness in left/right asymmetry. *Development*, 109(1), pp.1-9.

Brueckner, M., 2001. Cilia propel the embryo in the right direction. *American Journal of Medical Genetics*, 101(4), pp.339-44.

Buceta, J. et al., 2005. Nodal cilia dynamics and the specification of the left/right axis in early vertebrate embryo development. *Biophysical Journal*, 89(4), pp.2199-209.

Burighel, P. & Cloney, R.A., 1997. Urochordata: Ascidiacea. In F. W. Harrison & E. E. Ruppert, eds. *Microscopic Anatomy of Invertebrates: Hemichordata, Chaetognatha and the Invertebrate Chordates*. New York: Wiley-Liss, p. 280.

Campione, M. et al., 1999. The homeobox gene *Pitx2*: mediator of asymmetric left-right signaling in vertebrate heart and gut looping. *Development*, 126(6), pp.1225-1234.

Carreira-Barbosa, F., 2003. *Prickle 1* regulates cell movements during gastrulation and neuronal migration in zebrafish. *Development*, 130(17), pp.4037-4046.

Casano, C. et al., 1998. Deciliation: A stressful event for *Paracentrotus lividus* embryos. *Biochemical and Biophysical Research Communications,* 248(3), pp.628-34.

Cheng, A.M. et al., 2000. The *lefty*-related factor *Xatv* acts as a feedback inhibitor of *nodal* signaling in mesoderm induction and L-R axis development in *Xenopus*. *Development*, 127(5), pp.1049-1061.

Collignon, J., Varlet, I. & Robertson, E.J., 1996. Relationship between asymmetric *nodal* expression and the direction of embryonic turning. *Nature*, 381, pp.155-58.

Corbit, K.C. et al., 2005. Vertebrate *Smoothened* functions at the primary cilium. *Nature*, 437(7061), pp.1018-21.

Corbit, K.C. et al., 2008. *Kif3a* constrains beta-catenin-dependent Wnt signalling through dual ciliary and non-ciliary mechanisms. *Nature Cell Biology*, 10(1), pp.70-6.

Cotelli, F. et al., 1981. Differentiation of the Vitelline Coat in the Ascidian *Ciona intestinalis* : *An Ultrastructural Study. Roux's Archives of Developmental Biology*, 190, pp.252-258.

Coutelis, J.B. et al., 2008. Left-right asymmetry in *Drosophila*. *Seminars in Cell* & *Developmental Biology*, 19(3), pp.252-62.

Crowther, R.J. & Whittaker, J.R., 1994. Serial repetition of cilia pairs along the tail surface of an ascidian larva. *The Journal of Experimental Zoology*, 268(1), pp.9-16.

Cui, C., Little, C.D. & Rongish, B.J., 2009. Rotation of organiser tissue contributes to left-right asymmetry. *The Anatomical Record*, 292(4), pp.557-561.

Curtin, J.A. et al., 2003. Mutation of *Celsr1* Disrupts Planar Polarity of Inner Ear Hair Cells and Causes Severe Neural Tube Defects in the Mouse. *Current Biology*, 13(13), pp.1129-1133.

Dabdoub, A., 2003. Wnt signaling mediates reorientation of outer hair cell stereociliary bundles in the mammalian cochlea. *Development*, 130(11), pp.2375-2384.

Dahl, H.A., 1963. Fine structure of cilia in rat cerebral cortex. *Zeitschrift fur Zellforschung und Mikroskopische Anatomie*, 60(3), pp.369-386.

Das, G., Reynolds-Kenneally, J. & Mlodzik, M., 2002. The Atypical Cadherin Flamingo Links Frizzled and Notch Signaling in Planar Polarity Establishment in the *Drosophila* Eye. *Developmen*tal *Cell*, 2(5), pp.655-666.

Deans, M.R. et al., 2007. Asymmetric distribution of *prickle-like 2* reveals an early underlying polarization of vestibular sensory epithelia in the inner ear. *The Journal of Neuroscience*, 27(12), pp.3139-47.

Degasperi, V. et al., 2009. Muscle differentiation in a colonial ascidian: organisation, gene expression and evolutionary considerations. *BMC Developmental Biology*, 9, p.48.

Dehal, P. et al., 2002. The draft genome of *Ciona intestinalis*: insights into chordate and vertebrate origins. *Science*, 298(5601), pp.2157-67.

Delsuc, F. et al., 2006. Tunicates and not cephalochordates are the closest living relatives of vertebrates. *Nature*, 439(7079), pp.965-8.

Dilly, P.N., 1969. Studies on the receptors in *Ciona intestinalis*. *Zeitschrift fur Zellforschung und Mikroskopische Anatomie*, 96(1), pp.63-65.

Downing, K.H. & Sui, H., 2007. Structural insights into microtubule doublet interactions in axonemes. *Current Opinion in Structural Biology*, 17(2), pp.253-9.

Duboc, V. et al., 2005. Left-Right Asymmetry in the Sea Urchin Embryo Is Regulated by *Nodal* Signaling on the Right Side. *Developmen*tal *Cell*, 9, pp.147-158.

El Zein, L. et al., 2009. RFX3 governs growth and beating efficiency of motile cilia in mouse and controls the expression of genes involved in human ciliopathies. *Journal of Cell Science*, 122(Pt 17), pp.3180-9.

Emery, P. et al., 1996. RFX proteins, a novel family of DNA binding proteins conserved in the eukaryotic kingdom. *Nucleic Acids Research*, 24(5), pp.803-7.

Emlet, R.B., 1995. Larval spicules, cilia, and symmetry as remnants of indirect development in the direct developing sea urchin *Heliocidaris erythrogramma*. *Developmental Biology*, 167(2), pp.405-15.

Essner, J.J. et al., 2005. Kupffer's vesicle is a ciliated organ of asymmetry in the zebrafish embryo that initiates left-right development of the brain, heart and gut. *Development*, 132(6), pp.1247-60.

Essner, J.J. et al., 2002. Conserved function for embryonic nodal cilia. *Nature*, 418(6893), pp.37-8.

Etheridge, S.L. et al., 2008. Murine *dishevelled 3* functions in redundant pathways with *dishevelled 1* and *2* in normal cardiac outflow tract, cochlea, and neural tube development. *PLoS Genetics*, 4(11), p.e1000259.

Feistel, K. & Blum, M., 2006. Three types of cilia including a novel 9+4 axoneme on the notochordal plate of the rabbit embryo. *Developmental Dynamics*, 235(12), pp.3348-58.

Field, S. et al., 2011. Pkd1l1 establishes left-right asymmetry and physically interacts with Pkd2. *Development*, 138(6), pp.1131-42.

Fliegauf, M. & Omran, H., 2006. Novel tools to unravel molecular mechanisms in cilia-related disorders. *Trends in Genetics,* 22(5), pp.241-5.

Fukumoto, T., Kema, I.P. & Levin, M., 2005. Serotonin signaling is a very early step in patterning of the left-right axis in chick and frog embryos. *Current Biology*, 15(9), pp.794-803.

Furushima, K. et al., 2000. A new murine zinc finger gene, *Opr. Mechanisms of Development*, 98(1-2), pp.161-164.

Gabow, P.A., 1993. Autosomal dominant polycystic kidney disease. *The New England Journal of Medicine,* 329(5), pp.332-342.

Gadelha, C. et al., 2006. Basal body and flagellum mutants reveal a rotational constraint of the central pair microtubules in the axonemes of trypanosomes. *Journal of Cell Science*, 119(Pt 12), pp.2405-13.

Gebbia, M. et al., 1997. X-linked situs abnormalities result from mutations in ZIC3. *Nature Genetics,* 17(3), pp.305-8.

Gluenz, E. et al., 2010. Beyond 9+0: noncanonical axoneme structures characterize sensory cilia from protists to humans. *The FASEB Journal*, 24(9), pp.3117-21.

Goldstein, L.S., 1993. With apologies to scheherazade: tails of 1001 kinesin motors. *Annual Review of Genetics*, 27, pp.319-51.

González-Perrett, S. et al., 2001. Polycystin-2, the protein mutated in autosomal dominant polycystic kidney disease (ADPKD), is a Ca^{2+}-permeable nonselective cation channel. *Proceedings of the National Academy of Sciences of the United States of America*, 98(3), pp.1182-7.

Goodenough, U.W., 1985. Substructure of inner dynein arms, radial spokes, and the central pair/projection complex of cilia and flagella. *The Journal of Cell Biology,* 100(6), pp.2008-2018.

Gostling, N.J. & Shimeld, S.M., 2003. Protochordate *Zic* genes define primitive somite compartments and highlight molecular changes underlying neural crest evolution. *Evolution & Development*, 5(2), pp.136-44.

Goto, T. & Keller, R., 2002. The planar cell polarity gene *strabismus* regulates convergence and extension and neural fold closure in *Xenopus*. *Developmental Biology*, 247(1), pp.165-81.

Grande, C. & Patel, N.H., 2009. *Nodal* signalling is involved in left-right asymmetry in snails. *Nature*, 457(7232), pp.1007-11.

Grinberg, I. & Millen, K.J., 2005. The *ZIC* gene family in development and disease. *Clinical Genetics*, 67(4), pp.290-6.

Gros, J. et al., 2009. Cell movements at Hensen's node establish left/right asymmetric gene expression in the chick. *Science*, 324(5929), pp.941-4.

Gubb, D. & Garcia-Bellido, A., 1982. A genetic analysis of the determination of cuticular polarity during development in *Drosophila melanogaster*. *Journal of Embryology and Experimental Morphology,* 68(1), pp.37-57.

Guichard, C. et al., 2001. Axonemal dynein intermediate-chain gene (*DNAI1*) mutations result in *Situs inversus* and primary ciliary dyskinesia (Kartagener syndrome). *American Journal of Human Genetics*, 68(4), pp.1030-5.

Guindon, S. & Gascuel, O., 2003. A Simple, Fast, and Accurate Algorithm to Estimate Large Phylogenies by Maximum Likelihood. *Systematic Biology*, 52(5), pp.696-704.

Guo, N., Hawkins, C. & Nathans, J., 2004. *Frizzled6* controls hair patterning in mice. *Proceedings of the National Academy of Sciences of the United States of America*, 101(25), pp.9277-81.

Habas, R., Dawid, I. B. & He, X., 2003. Coactivation of Rac and Rho by Wnt/Frizzled signaling is required for vertebrate gastrulation. *Genes & Development*, 17(2), pp.295-309.

Habas, R., Kato, Y. & He, X., 2001. *Wnt/Frizzled* Activation of Rho Regulates Vertebrate Gastrulation and Requires a Novel Formin Homology Protein *Daam1*. *Cell*, 107(7), pp.843-854.

Hamblet, N.S., 2002. *Dishevelled 2* is essential for cardiac outflow tract development, somite segmentation and neural tube closure. *Development*, 129(24), pp.5827-5838.

Han, Y.-G. et al., 2008. *Hedgehog* signaling and primary cilia are required for the formation of adult neural stem cells. *Nature Neuroscience*, 11(3), pp.277-84.

Hanaoka, K. et al., 2000. Co-assembly of polycystin-1 and -2 produces unique cation-permeable currents. *Nature*, 408(6815), pp.990-4.

Hara, Y. et al., 2003. Asymmetric formation and possible function of the primary pore canal in plutei of *Temnopleurus hardwicki*. *Development, Growth & Differentiation*, 45(4), pp.295-308.

Harada, Y. et al., 2008. Mechanism of self-sterility in a hermaphroditic chordate. *Science*, 320(5875), pp.548-50.

Hashimoto, H. et al., 2004. The Cerberus/Dan-family protein Charon is a negative regulator of Nodal signaling during left-right patterning in zebrafish. *Development*, 131(8), pp.1741-53.

Hashimoto, M. et al., 2010. Planar polarization of node cells determines the rotational axis of node cilia. *Nature Cell Biology*, 12(2), pp.170-6.

Hayashi, M. et al., 2005. Left-right asymmetry in the alimentary canal of the *Drosophila* embryo. *Development, Growth & Differentiation*, 47(7), pp.457-60.

Hayashi, T. et al., 1997. Characterization of the exon structure of the polycystic kidney disease 2 gene (PKD2). *Genomics*, 44(1), pp.131-6.

Haycraft, C.J. et al., 2005. Gli2 and Gli3 localize to cilia and require the intraflagellar transport protein polaris for processing and function. G. Barsh, ed. *PLoS Genetics*, 1(4), p.e53.

Hibino, T. et al., 2006. Ion flow regulates left-right asymmetry in sea urchin development. *Development Genes and Evolution*, 216(5), pp.265-76.

Hino, K. et al., 2003. A genomewide survey of developmentally relevant genes in *Ciona intestinalis*. VI. Genes for *Wnt*, *TGFbeta*, *Hedgehog* and *JAK/STAT* signaling pathways. *Development Genes and Evolution*, 213(5-6), pp.264-72.

Hirokawa, N., Tanaka, Y. & Okada, Y., 2009. Left-right determination: involvement of molecular motor *KIF3*, cilia, and nodal flow. *Cold Spring Harbor Perspectives in Biology,* 1(1), p.a000802.

Hirokawa, N. et al., 2006. Nodal flow and the generation of left-right asymmetry. *Cell*, 125(1), pp.33-45.

Hodges, M.E. et al., 2010. Reconstructing the evolutionary history of the centriole from protein components. *Journal of Cell Science*, 123(Pt 9), pp.1407-13.

Hornef, N. et al., 2006. DNAH5 mutations are a common cause of primary ciliary dyskinesia with outer dynein arm defects. *American Journal of Respiratory and Critical Care Medicine*, 174(2), pp.120-6.

Hotta, K. et al., 2003. A genome-wide survey of the genes for planar polarity signaling or convergent extension-related genes in *Ciona intestinalis* and phylogenetic comparisons of evolutionary conserved signaling components. *Gene*, 317, pp.165-185.

Hotta, K. et al., 2007. *Brachyury*-downstream notochord genes and convergent extension in *Ciona intestinalis* embryos. *Development, Growth & Differentiation*, 49, pp.373-382.

Hozumi, S. et al., 2006. An unconventional myosin in *Drosophila* reverses the default handedness in visceral organs. *Nature*, 440(7085), pp.798-802.

Hsu, D.R. et al., 1998. The *Xenopus* Dorsalising Factor Gremlin Identifies a Novel Family of Secreted Proteins that Antagonize BMP Activities. *Cell*, 1, pp.673-683.

Huang, K. et al., 2007. Function and dynamics of PKD2 in *Chlamydomonas reinhardtii* flagella. *The Journal of Cell Biology,* 179(3), pp.501-14.

Huangfu, D. & Anderson, K.V., 2006. Signaling from *Smo* to *Ci/Gli:* conservation and divergence of Hedgehog pathways from *Drosophila* to vertebrates. *Development*, 133(1), pp.3-14.

Hudson, C. & Yasuo, H., 2005. Patterning across the ascidian neural plate by lateral *Nodal* signalling sources. *Development*, 132(6), pp.1199-210.

Hummel, K.P. & Chapman, D.B., 1959. Visceral inversion and associated anomalies in the mouse. *Journal of Heredity.* 50, pp.9-13.

Ikuta, T., Satoh, N. & Saiga, H., 2010. Limited functions of Hox genes in the larval development of the ascidian *Ciona intestinalis*. *Development*, 137(9), pp.1505-13.

Imai, K.S. et al., 2004. Gene expression profiles of transcription factors and signaling molecules in the ascidian embryo: towards a comprehensive understanding of gene networks. *Development*, 131(16), pp.4047-58.

Jenny, A. et al., 2003. *Prickle* and *Strabismus* form a functional complex to generate a correct axis during planar cell polarity signaling. *The EMBO Journal*, 22(17), pp.4409-20.

Jiang, D. & Smith, W.C., 2007. Ascidian notochord morphogenesis. *Developmental Dynamics*, 236(7), pp.1748-57.

Jiang, D., Munro, E.M. & Smith, W.C., 2005. Ascidian *prickle* Regulates Both Mediolateral and Anterior-Posterior Cell Polarity of Notochord Cells. *Current Biology*, 15(1), pp.79-85.

Jiang, J.X. & Goodenough, D.A., 1996. Heteromeric connexons in lens gap junction channels. *Proceedings of the National Academy of Sciences USA*, 93, pp.1287-1291.

Jones, C. & Chen, P., 2007. Planar cell polarity signaling in vertebrates. *BioEssays*, 29(2), pp.120-32.

Jurand, A., 1974. Some aspects of the development of the notochord in mouse embryos. *Journal of Embryology and Experimental Morphology*, 32(1), pp.1-33.

Kartagener, M. & Stucki, P., 1962. Bronchiectasis with *Situs inversus. Archives of Pediatrics,* 79, pp.193-207.

Katoh, K. et al., 2002. MAFFT: a novel method for rapid multiple sequence alignment based on fast Fourier transform. *Nucleic Acids Research*, 30(14), pp.3059-66.

Katz, M.J., 1983. Comparative Anatomy of the Tunicate Tadpole, *Ciona intestinalis*. *Biological Bulletin*, 164(1), pp.1-27.

Kaufman, M.H., 1992. The atlas of mouse development Matthew H. Kaufman, ed., *San Diego: Academic Press.*

Kawakami, M. & Nakanishi, N., 2001. The role of an endogenous PKA inhibitor, PKIalpha, in organizing left-right axis formation. *Development*, 128(13), pp.2509-15.

Kawakami, Y. et al., 2005. Retinoic acid signalling links left-right asymmetric patterning and bilaterally symmetric somitogenesis in the zebrafish embryo. *Nature*, 435(7039), pp.165-71.

Kawasumi, A. et al., 2011. Left-right asymmetry in the level of active Nodal protein produced in the node is translated into left-right asymmetry in the lateral plate of mouse embryos. *Developmental Biology*.

Keller, R., 2002. Shaping the vertebrate body plan by polarized embryonic cell movements. *Science*, 298(5600), pp.1950-4.

Kelly, K.A., Wei, Y. & Mikawa, T., 2002. Cell death along the embryo midline regulates left-right sidedness. *Developmental Dynamics*, 224(2), pp.238-44.

Kessel, R. & Kemp, N., 1962. An electron microscope study on the oocyte, test cells and follicular envelope of the tunicate, *Molgula manhattensis*. *Journal of Ultrastructure Research*, 6(1), pp.57-76.

Keys, D.N. et al., 2002. Control of intercalation is cell-autonomous in the notochord of *Ciona intestinalis*. *Developmental Biology*, 246(2), pp.329-40.

Kinder, S.J. et al., 2001. The organizer of the mouse gastrula is composed of a dynamic population of progenitor cells for the axial mesoderm. *Development*, 128(18), pp.3623-34.

Kiprilov, E.N. et al., 2008. Human embryonic stem cells in culture possess primary cilia with hedgehog signaling machinery. *The Journal of Cell Biology*, 180(5), pp.897-904.

Kitaguchi, T. et al., 2000. *Zic3* is involved in the left-right specification of the *Xenopus* embryo. *Development*, 127(22), pp.4787-95.

Klein, T.J. & Mlodzik, M., 2005. Planar cell polarization: an emerging model points in the right direction. *Annual Review of Cell and Developmental Biology*, 21, pp.155-76.

Klingenberg, C.P., McIntyre, G.S. & Zaklan, S.D., 1998. Left-right asymmetry of fly wings and the evolution of body axes. *The Royal Society Proceedings: Biological Sciences,* 265(1402), pp.1255-9.

Knight, R.D. & Shimeld, S.M., 2001. Identification of conserved C2H2 zinc-finger gene families in the Bilateria. *Genome Biology*, 2(5), p.RESEARCH0016.

Konno, A. et al., 2010. Distribution and structural diversity of cilia in tadpole larvae of the ascidian *Ciona intestinalis*. *Developmental Biology*, 337(1), pp.42-62.

Kosaki, K. & Casey, B., 1998. Genetics of human left-right axis malformations. *Seminars in Cell & Developmental Biology*, 9(1), pp.89-99.

Koulen, P. et al., 2002. Polycystin-2 is an intracellular calcium release channel. *Nature Cell Biology*, 4(3), pp.191-7.

Kozminski, K.G. et al., 1993. A motility in the eukaryotic flagellum unrelated to flagellar beating. *Proceedings of the National Academy of Sciences of the United States of America*, 90(12), pp.5519-23.

Kramer-Zucker, A.G. et al., 2005. Cilia-driven fluid flow in the zebrafish pronephros, brain and Kupffer's vesicle is required for normal organogenesis. *Development*, 132(8), pp.1907-21.

Kuroda, R. et al., 2009. Chiral blastomere arrangement dictates zygotic left-right asymmetry pathway in snails. *Nature*, 462(7274), pp.790-4.

Kühl, M. et al., 2001. Antagonistic regulation of convergent extension movements in *Xenopus* by Wnt/β-catenin and Wnt/Ca^{2+} signaling. Mechanisms of *Development*, 106(1-2), pp.61-76.

Lambert, C.C. & Lambert, G., 1978. Tunicate Eggs Utilize Ammonium Ions for Flotation. *Science*, 200(4337), pp.64-65.

Larroux, C. et al., 2006. Developmental expression of transcription factor genes in a demosponge: insights into the origin of metazoan multicellularity. *Evolution & Development*, 8(2), pp.150-73.

Larroux, C. et al., 2008. Genesis and expansion of metazoan transcription factor gene classes. *Molecular Biology and Evolution*, 25(5), pp.980-96.

Lawrence, C.J. et al., 2001. Dyneins have run their course in plant lineage. *Traffic*, 2(5), pp.362-3.

Layton, W.M., 1976. Random determination of a developmental process: reversal of normal visceral asymmetry in the mouse. *The Journal of Heredity,* 67(6), pp.336-8.

Lee, J.D. & Anderson, K.V., 2008. Morphogenesis of the node and notochord: the cellular basis for the establishment and maintenance of left-right asymmetry in the mouse. *Developmen*tal *Dynamics,* 237(12), pp.3464-76.

Lemaire, P., 2011. Evolutionary crossroads in developmental biology: the tunicates. *Development*, 138(11), pp.2143-2152.

Lemaire, P., 2009. Unfolding a chordate developmental program, one cell at a time: invariant cell lineages, short-range inductions and evolutionary plasticity in ascidians. *Developmental Biology*, 332(1), pp.48-60.

Levin, M. & Mercola, M., 1999. Gap junction-mediated transfer of left-right patterning signals in the early chick blastoderm is upstream of *Shh* asymmetry in the node. *Development*, 126(21), pp.4703-14.

Levin, M. & Palmer, R., 2007. Left-right patterning from the inside out: widespread evidence for intracellular control. *BioEssays*, 29(3), pp.271-87.

Levin, M. et al., 1995. Determining Left-Right Asymmetry in Chick Embryogenesis. *Cell*, 82, pp.803-814.

Levin, M. et al., 2002. Asymmetries in H^+/K^+-ATPase and cell membrane potentials comprise a very early step in left-right patterning. *Cell*, 111(1), pp.77-89.

Li, J. et al., 2004. Comparative genomics identifies a flagellar and basal body proteome that includes the *BBS5* human disease gene. *Cell*, 117(4), pp.541-52.

Ligoxygakis, P., Strigini, M. & Averof, M., 2001. Specification of left-right asymmetry in the embryonic gut of *Drosophila*. *Development*, 128(7), pp.1171-4.

Lin, F. et al., 2003. Kidney-specific inactivation of the KIF3A subunit of kinesin-II inhibits renal ciliogenesis and produces polycystic kidney disease. *Proceedings of the National Academy of Sciences of the United States of America*, 100(9), pp.5286-91.

Liu, A., Wang, B. & Niswander, L.A., 2005. Mouse intraflagellar transport proteins regulate both the activator and repressor functions of Gli transcription factors. *Development*, 132(13), pp.3103-11.

Logan, C.Y. & Nusse, R., 2004. The Wnt signaling pathway in development and disease. *Annual Review of Cell and Developmental Biology*, 20, pp.781-810.

Loges, N.T. et al., 2008. *DNAI2* mutations cause primary ciliary dyskinesia with defects in the outer dynein arm. *American Journal of Human Genetics*, 83(5), pp.547-58.

Lopes, S.S. et al., 2010. Notch signalling regulates left-right asymmetry through ciliary length control. *Development*, 137(21), pp.3625-32.

Lowe, L.A. et al., 1996. Conserved left-right asymmetry of *nodal* expression and alterations in murine *Situs inversus*. *Nature*, 381, pp.158-161.

Lustig, K.D. et al., 1996. A *Xenopus nodal*-related gene that acts in synergy with noggin to induce complete secondary axis and notochord formation. *Development*, 122(10), pp.3275-3282.

Maisonneuve, C. et al., 2009. *Bicaudal C*, a novel regulator of *Dvl* signaling abutting RNA-processing bodies, controls cilia orientation and leftward flow. *Development*, 136(17), pp.3019-30.

Mancuso, V., 1965. An electron microscope study of the test cells and follicle cells of *Ciona intestinalis* during oogenesis. *Acta Embryologiae et Morphologiae Experimentalis*, 8(3), pp.239-66.

Mancuso, V., 1973. Changes in fine structure associated with the test formation in the ectoderm cells of *Ciona intestinalis* embryo. *Acta Embryologiae Experimentalis*, 3, pp.247-57.

Manni, L. et al., 2005. Stomodeal and neurohypophysial placodes in *Ciona intestinalis*: insights into the origin of the pituitary gland. *Journal of Experimental Zoology. Part B, Molecular and Developmental Evolution,* 304(4), pp.324-39.

Marlow, F. et al., 2002. Zebrafish Rho Kinase 2 Acts Downstream of Wnt11 to Mediate *Cell* Polarity and Effective Convergence and Extension Movements. *Current Biology*, 12(11), pp.876-884.

Marques, S. et al., 2004. The activity of the *Nodal* antagonist *Cerl-2* in the mouse node is required for correct L/R body axis. *Genes & Development*, 18(19), pp.2342-7.

May, S.R. et al., 2005. Loss of the retrograde motor for IFT disrupts localization of *Smo* to cilia and prevents the expression of both activator and repressor functions of *Gli. Developmental Biology*, 287(2), pp.378-89.

Mazet, F. et al., 2003. Phylogenetic relationships of the *Fox* (Forkhead) gene family in the Bilateria. *Gene*, 316, pp.79-89.

McGrath, J. et al., 2003. Two populations of node monocilia initiate left-right asymmetry in the mouse. *Cell*, 114(1), pp.61-73.

Medawar, P., 1951. Asymmetry of Larval Amphioxus. *Nature*, 167, pp.852-3.

Meno, C. et al., 1999. Mouse Lefty2 and Zebrafish Antivin Are Feedback Inhibitors of *Nodal* Signaling during Vertebrate Gastrulation. *Molecular Cell*, 4(3), pp.287-298.

Meno, C. et al., 1996. Left-right asymmetric expression of the TGFB-family member *lefty* in mouse embryos. *Nature*, 381, pp.151-155.

Merchant, S.S. et al., 2007. The *Chlamydomonas* genome reveals the evolution of key animal and plant functions. *Science*, 318(5848), pp.245-50.

Merzdorf, C.S., 2007. Emerging roles for *zic* genes in early development. *Developmental Dynamics*, 236(4), pp.922-40.

Mita, K. & Fujiwara, S., 2007. *Nodal* regulates neural tube formation in the *Ciona intestinalis* embryo. *Development Genes and Evolution*, 217(8), pp.593-601.

Mita-Miyazawa, I., Ikegami, S. & Satoh, N., 1985. Histospecific acetylcholinesterase development in the presumptive muscle cells isolated from 16-cell-stage ascidian embryos with respect to the number of DNA replications. *Journal of Embryology and Experimental Morphology*, 87, pp.1-12.

Mitchell, D.R. & Nakatsugawa, M., 2004. Bend propagation drives central pair rotation in *Chlamydomonas reinhardtii* flagella. *The Journal of Cell Biology*, 166(5), pp.709-15.

Mochizuki, T. et al., 1998. Cloning of *inv,* a gene that controls left-right asymmetry and kidney development. *Nature*, 395, pp.177-181.

Mochizuki, T. et al., 1996. *PKD2*, a gene for polycystic kidney disease that encodes an integral membrane protein. *Science*, 272(5266), pp.1339-42.

Mohler, J. & Wieschaus, E.F., 1986. Dominant maternal-effect mutations of *Drosophila melanogaster* causing the production of double-abdomen embryos. *Genetics*, 112(4), pp.803-22.

Montcouquiol, M. et al., 2003. Identification of *Vangl2* and *Scrb1* as planar polarity genes in mammals. *Nature*, 423(6936), pp.173-7.

Montcouquiol, M. et al., 2006. Asymmetric localization of *Vangl2* and *Fz3* indicate novel mechanisms for planar cell polarity in mammals. *The Journal of Neuroscience*, 26(19), pp.5265-75.

Morgan, D. et al., 1998. *Inversin*, a novel gene in the vertebrate left-right axis pathway, is partially deleted in the *inv* mouse. *Nature Genetic*s, 20(2), pp.149-56.

Morokuma, J. et al., 2002. *HrNodal,* the ascidian *nodal*-related gene, is expressed in the left side of the epidermis, and lies upstream of *HrPitx*. *Development Genes and Evolution,* 212(9), pp.439-46.

Narayan, D. et al., 1994. Unusual inheritance of primary ciliary dyskinesia (Kartagener's syndrome). *Journal of Medical Genetics,* 31(6), pp.493-496.

Nielsen, S.K. et al., 2008. Characterization of primary cilia and Hedgehog signaling during development of the human pancreas and in human pancreatic duct cancer cell lines. *Developmental Dynamics*, 237(8), pp.2039-52.

Nishida, H., 1987. Cell lineage analysis in ascidian embryos by intracellular injection of a tracer enzyme. III. Up to the tissue restricted stage. *Developmental Biology*, 121(2), pp.526-41.

Nishida, H., 1983. Cell lineage analysis in ascidian embryos by intracellular injection of a tracer enzyme: I. Up to the eight-cell stage. *Developmental Biology*, 99(2), pp.382-394.

Nishida, H. & Satoh, N., 1985. Cell lineage analysis in ascidian embryos by intracellular injection of a tracer enzyme: II. The 16- and 32-cell stages. *Developmental Biology*, 110(2), pp.440-454.

Nishida, H. & Sawada, K., 2001. *macho-1* encodes a localized mRNA in ascidian eggs that specifies muscle fate during embryogenesis. *Nature*, 409(6821), pp.724-9.

Nonaka, S. et al., 2002. Determination of left – right patterning of the mouse embryo by artificial nodal flow. *Nature*, 418, pp.96-99.

Nonaka, S. et al., 1998. Randomization of left-right asymmetry due to loss of nodal cilia generating leftward flow of extraembryonic fluid in mice lacking KIF3B motor protein. *Cell*, 95(6), pp.829-37.

Nonaka, S. et al., 2005. De novo formation of left-right asymmetry by posterior tilt of nodal cilia. *PLoS Biology*, 3(8), p.e268.

Noone, P.G. et al., 1999. Discordant organ laterality in monozygotic twins with primary ciliary dyskinesia. *American Journal of Medical Genetics*, 82(2), pp.155-60.

Noone, P.G. et al., 2007. Mutations in *DNAI1* (*IC78*) Cause Primary Ciliary Dyskinesia Mutations. *Chest*, 121, pp.97-98.

Numata, N. et al., 2008. Molecular mechanism of force generation by dynein, a molecular motor belonging to the AAA+ family. *Biochemical Society Transactions,* 36(Pt 1), pp.131-5.

Nursal, T.Z. et al., 2004. Laparoscopic cholecystectomy in a patient with *Situs inversus totalis. Journal of Laparoendoscopic & Advanced Surgical Techniques. Part A,* 11(4), pp.239-41.

Ocbina, P.J.R. & Anderson, K.V., 2008. Intraflagellar transport, cilia, and mammalian Hedgehog signaling: analysis in mouse embryonic fibroblasts. *Developmental Dynamics*, 237(8), pp.2030-8.

Okada, Y. et al., 1999. Abnormal nodal flow precedes *Situs inversus* in *iv* and *inv* mice. *Molecular Cell*, 4(4), pp.459-68.

Okada, Y. et al., 2005. Mechanism of nodal flow: a conserv ed symmetry breaking event in left-right axis determination. *Cell*, 121(4), pp.633-44.

Olbrich, H. et al., 2002. Mutations in *DNAH5* cause primary ciliary dyskinesia and randomization of left-right asymmetry. *Nature Genetics,* 30(2), pp.143-4.

Omoto, C. K. & Kung, C., 1979. The pair of central tubules rotates during ciliary beat in *Paramecium*. *Nature*, 279(5713), pp.532-534.

Park, T.J. et al., 2008. *Dishevelled* controls apical docking and planar polarization of basal bodies in ciliated epithelial cells. *Nature Genetics,* 40(7), pp.871-9.

Pazour, G. & Whitman, G., 2003. The vertebrate primary cilium is a sensory organelle. *Current Opinion in Cell Biology,* 15(1), pp.105-110.

Pazour, G.J. et al., 2005. Proteomic analysis of a eukaryotic cilium. *The Journal of Cell Biology,* 170(1), pp.103-13.

Pazour, G.J. et al., 2000. *Chlamydomonas IFT88 a*nd its mouse homologue, polycystic kidney disease gene *tg737*, are required for assembly of cilia and flagella. *The Journal of Cell Biology,* 151(3), pp.709-18.

Pennekamp, P. et al., 2002. The ion channel polycystin-2 is required for left-right axis determination in mice. *Current Biology*, 12(11), pp.938-43.

Praetorius, H.A. & Spring, K.R., 2001. Bending the MDCK Cell Primary Cilium Increases Intracellular Calcium. *Journal of Membrane Biology,* 184(1), pp.71-79.

Purandare, S.M. et al., 2002. A complex syndrome of left-right axis , central nervous system and axial skeleton defects in *Zic3* mutant mice. *Development*, 129, pp.2293-2302.

Quarmby, L.M. & Parker, J.D.K., 2005. Cilia and the cell cycle? *The Journal of Cell Biology,* 169(5), pp.707-10.

Rankin, C.T. et al., 2000. Regulation of left-right patterning in mice by growth/differentiation factor-1. *Nature Genetics,* 24(3), pp.262-5.

Raya, A. et al., 2004. Notch activity acts as a sensor for extracellular calcium during vertebrate left-right determination. *Nature*, 427(6970), pp.121-8.

Rebagliati, M.R. et al., 1998. Zebrafish nodal-related genes are implicated in axial patterning and establishing left-right asymmetry. *Developmental Biology*, 199(2), pp.261-72.

Rodríguez-Esteban, C. et al., 2001. *Wnt* signaling and *PKA* control *Nodal* expression and left-right determination in the chick embryo. *Development*, 128(16), pp.3189-95.

Rohatgi, R., Milenkovic, L. & Scott, M.P., 2007. Patched1 regulates hedgehog signaling at the primary cilium. *Science*, 317(5836), pp.372-6.

Ronquist, F., 2003. MrBayes 3: Bayesian phylogenetic inference under mixed models. *Bioinformatics,* 19(12), pp.1572-1574.

Rosati, F. & de Santis, R., 1978. Studies on fertilization in the ascidans. *Experimental Cell Research,* 112(1), pp.111-119.

Rosenbaum, J.L. & Witman, G.B., 2002. Intraflagellar transport. *Nature Reviews. Molecular Cell Biology,* 3(11), pp.813-25.

Ross, A.J. et al., 2005. Disruption of Bardet-Biedl syndrome ciliary proteins perturbs planar cell polarity in vertebrates. *Nature Genetics*, 37(10), pp.1135-40.

Ryan, A.K. et al., 1998. *Pitx2* determines left-right asymmetry of internal organs in vertebrates. *Nature*, 394(6693), pp.545-51.

De Santis, R., Jamunno, G. & Rosati, F., 1980. A study of the chorion and the follicle cells in relation to the sperm-egg interaction in the ascidian, *Ciona intestinalis*. *Developmental Biology*, 74(2), pp.490-9.

Sasakura, Y. et al., 2003. A genomewide survey of developmentally relevant genes in *Ciona intestinalis*. VII. Molecules involved in the regulation of cell polarity and actin dynamics. *Development Genes and Evolution*, 213(5-6), pp.273-83.

Satir, P. & Christensen, S.T., 2007. Overview of structure and function of mammalian cilia. *Annual Review of Physiology,* 69, pp.377-400.

Sato, Y. & Morisawa, M., 1999. Loss of test cells leads to the formation of new tunic surface cells and abnormal metamorphosis in larvae of *Ciona intestinalis* (Chordata, Ascidiacea). *Development Genes and Evolution*, 209(10), pp.592-600.

Satoh, N., 1978. *Cell*ular morphology and architecture during early morphogenesis of the ascidian egg: an SEM study. *The Biological Bulletin*, 155(3), pp.608-14.

Satoh, N. & Deno, T., 1984. Periodic appearance and disappearance of microvilli associated with cleavage cycles in the egg of the ascidian, *Halocynthia roretzi. Developmental Biology*, 102(2), pp.488-92.

Satoh, N., Numakunai, T. & Hori, R., 1982. Behavior and cellular morphology of the test cells during embryogenesis of the ascidian *Halocynthia roretzi. Journal of Morphology,* 171(2), pp.219-223.

Satou, Y. et al., 2003. Large scale EST analyses in *Ciona intestinalis*: its application as Northern blot analyses. *Development Genes and Evolution,* 213(5-6), pp.314-8.

Satou, Y. et al., 2002. *macho-1*-Related genes in *Ciona* embryos. *Development Genes and Evolution,* 212(2), pp.87-92.

Schlueter, J. & Brand, T., 2007. Left-right axis development: examples of similar and divergent strategies to generate asymmetric morphogenesis in chick and mouse embryos. *Current Opinion in Genetics & Development,* 117(1-4), pp.256-67.

Schreiner, C.M. et al., 1993. Correlation of Forelimb Malformation Asymmetries with Visceral Organ Situs in Transgenic Mouse Insertional Mutation, legless. *Developmental Biology*, 158(2), pp.560-562.

Schweickert, A. et al., 2007. Cilia-driven leftward flow determines laterality in *Xenopus*. *Current Biology,* 17(1), pp.60-6.

Shih, J. & Fraser, S E, 1996. Characterizing the zebrafish organizer: microsurgical analysis at the early-shield stage. *Development*, 122(4), pp.1313-22.

Shimada, Y. et al., 2001. Asymmetric co-localization of Flamingo, a seven-pass transmembrane cadherin, and Dishevelled in planar cell polarization. *Current Biology*, 11(11), pp.859-863.

Shimeld, S.M. & Levin, M., 2006. Evidence for the regulation of left-right asymmetry in *Ciona intestinalis* by ion flux. *Developmental Dynamics*, 235(6), pp.1543-53.

Shiratori, H. & Hamada, H., 2006. The left-right axis in the mouse: from origin to morphology. *Development*, 133(11), pp.2095-104.

Shook, D.R., Majer, C. & Keller, R., 2004. Pattern and morphogenesis of presumptive superficial mesoderm in two closely related species, *Xenopus laevis* and *Xenopus tropicalis*. *Developmental Biology*, 270(1), pp.163-85.

Simionato, E. et al., 2007. Origin and diversification of the basic helix-loop-helix gene family in metazoans: insights from comparative genomics. *BMC Evolutionary Biology,* 7(1), p.33.

Simons, M. & Mlodzik, M., 2008. Planar Cell Polarity Signaling: From fly development to Human Disease. *Annual Review of Genetics*, 42, p.517.

Singh, G. et al., 1991. *Legless* Insertional Mutation: Morphological, Molecular, and Genetic Characterization. *Genes & Development*, 5(12a), pp.2245-2255.

Small, K.S. et al., 2007. A haplome alignment and reference sequence of the highly polymorphic *Ciona savignyi* genome. *Genome Biology*, 8(3), p.R41.

Smith, E.F. & Yang, P., 2004. The radial spokes and central apparatus: mechano-chemical transducers that regulate flagellar motility. *Cell Motility and the Cytoskeleton*, 57(1), pp.8-17.

Spemann, H. & Mangold, H., 1924. über Induktion von Embryonalanlagen durch Implantation artfremder Organisatoren. *Archiv für Mikroskopische Anatomie und Entwicklungsmechanik*, 100(3-4), pp.599-638.

Spéder, P., Adám, G. & Noselli, S., 2006. Type ID unconventional myosin controls left-right asymmetry in *Drosophila*. *Nature*, 440(7085), pp.803-7.

Stokes, M.D. & Holland, N.D., 1995. Ciliary Hovering in Larval Lancelets (= *Amphioxus*). *Biological Bulletin*, 188(3), p.231.

Storm van's Gravesande, K. & Omran, H., 2005. Primary ciliary dyskinesia: clinical presentation, diagnosis and genetics. *Annuals of Medicine,* 37(6), pp.439-49.

Strutt, H. & Strutt, D., 2005. Long-range coordination of planar polarity in *Drosophila*. *BioEssays*, 27(12), pp.1218-27.

Sulik, K. et al., 1994. Morphogenesis of the murine node and notochordal plate. *Developmental Dynamics*, 201(3), pp.260-78.

Supp, D.M. et al., 1997. Mutation of an axonemal dynein affects left-right asymmetry in *inversus viscerum* mice. *Nature*, 389(6654), pp.963-966.

Takamura, K. et al., 1996. Immunohistology with Antibodies Specific to Test Cells in the Ascidian *Ciona intestinalis* Suggests Their Role in Larval Tunic Formation. *Zoological Science*, 13(2), pp.241-251.

Takatori, N., Satou, Y. & Satoh, N., 2002. Expression of *hedgehog* genes in *Ciona intestinalis* embryos. *Mechanisms of Development*, 116(1-2), pp.235-8.

Takeda, S. et al., 1999. Left-right asymmetry and Kinesin superfamily protein KIF3A: New Insights in Determination of Laterality and Mesoderm Induction by *kif3A-/-* mice analysis. The *Journal of Cell Biology*, 145(4), pp.825-836.

Tamm, S.L. & Tamm, S., 1981. Ciliary reversal without rotation of axonemal structures in ctenophore comb plates. *The Journal of Cell* Biology, 89(3), pp.495-509.

Tanaka, Y., Okada, Y. & Hirokawa, N., 2005. FGF-induced vesicular release of Sonic hedgehog and retinoic acid in leftward nodal flow is critical for left-right determination. *Nature*, 435(7039), pp.172-7.

Teilmann, S.C. et al., 2005. Localization of transient receptor potential ion channels in primary and motile cilia of the female murine reproductive organs. *Molecular Reproduction and Development*, 71(4), pp.444-52.

Teilmann, S.C. et al., 2006. Expression and localization of the progesterone receptor in mouse and human reproductive organs. *The Journal of Endocrinology,* 191(3), pp.525-35.

Torban, E. et al., 2004. Independent mutations in mouse *Vangl2* that cause neural tube defects in looptail mice impair interaction with members of the Dishevelled family. *The Journal of Biological Chemistry*, 279(50), pp.52703-13.

Torrence, S.A. & Cloney, R.A., 1982. Nervous system of ascidian larvae: Caudal primary sensory neurons. *Zoomorphology,* 99(2), pp.103-115.

Torres, V.E. & Harris, P.C., 2006. Mechanisms of Disease: autosomal dominant and recessive polycystic kidney diseases. *Nature clinical practice. Nephrology*, 2(1), pp.40-55; quiz 55.

Tran, U. et al., 2007. *Xenopus* Bicaudal-C is required for the differentiation of the amphibian pronephros. *Developmental Biology*, 307(1), pp.152-64.

Tree, D.R.P. et al., 2002. Prickle Mediates Feedback Amplification to Generate Asymmetric Planar Cell Polarity Signaling. *Cell*, 109(3), pp.371-381.

Tsagkogeorga, G. et al., 2009. An updated 18S rRNA phylogeny of tunicates based on mixture and secondary structure models. *BMC Evolutionary Biology,* 9, p.187.

Vandenberg, L.N. & Levin, M., 2010. Far from solved: a perspective on what we know about early mechanisms of left-right asymmetry. *Developmental Dynamics*, 239(12), pp.3131-46.

Vassilev, P.M. et al., 2001. Polycystin-2 is a novel cation channel implicated in defective intracellular $Ca^{(2+)}$ homeostasis in polycystic kidney disease. *Biochemical and Biophysical Research Communications*, 282(1), pp.341-50.

Veland, I.R. et al., 2009. Primary cilia and signaling pathways in mammalian development, health and disease. *Nephron. Physiology*, 111(3), pp.p39-53.

Wada, S. & Saiga, H., 2002. *HrzicN*, a new *Zic* family gene of ascidians, plays essential roles in the neural tube and notochord development. *Development*, 129(24), pp.5597-5608.

Waddington, C.H., 1932. Experiments on the Development of Chick and Duck Embryos, Cultivated *in vitro*. *Philosophical Transactions of the Royal Society B: Biological Sciences,* 221(474-482), pp.179-230.

Wallingford, J B et al., 2000. Dishevelled controls cell polarity during *Xenopus* gastrulation. *Nature*, 405(6782), pp.81-5.

Wallingford, J. B., Fraser, S. E. & Harland, R. M., 2002. Convergent Extension: The Molecular Control of Polarized *Cell* Movement during Embryonic *Development*. *Developmen*tal *Cell*, 2(6), pp.695-706.

Wang, J., Hamblet, N.S., et al., 2006. Dishevelled genes mediate a conserved mammalian PCP pathway to regulate convergent extension during neurulation. *Development*, 133(9), pp.1767-78.

Wang, J. et al., 2005. Regulation of polarized extension and planar cell polarity in the cochlea by the vertebrate PCP pathway. *Nature Genetics*, 37(9), pp.980-5.

Wang, Y. & Nathans, J., 2007. Tissue/planar cell polarity in vertebrates: new insights and new questions. *Development*, 134(4), pp.647-58.

Wang, Y., Guo, N. & Nathans, J., 2006. The role of Frizzled3 and Frizzled6 in neural tube closure and in the planar polarity of inner-ear sensory hair cells. *The Journal of Neuroscience*, 26(8), pp.2147-56.

Ware, S.M., Harutyunyan, K.G. & Belmont, J.W., 2006. Heart defects in X-linked heterotaxy: evidence for a genetic interaction of *Zic3* with the *nodal* signaling pathway. *Developmental Dynamics*, 235(6), pp.1631-7.

Wargo, M.J. & Smith, E.F., 2003. Asymmetry of the central apparatus defines the location of active microtubule sliding in *Chlamydomonas* flagella. *Proceedings of the National Academy of Sciences of the United States of America*, 100(1), pp.137-42.

Warner, F.D., 1970. New Observations on flagella fine structure: The Relationship Between Matrix Structure and the Microtubule Component of the Axoneme. *The Journal of Cell Biology,* 47(1), pp.159-182.

Warner, F.D. & Satir, P., 1974. The structural basis of ciliary bend formation: Radial Spoke Positional Changes Accompanying Microtubule Sliding. *The Journal of Cell Biology*, 63(1), pp.35-63.

Watanabe, D. et al., 2003. The left-right determinant Inversin is a component of node monocilia and other 9+0 cilia. *Development*, 130(9), pp.1725-1734.

Wessely, O. et al., 2001. Identification and expression of the mammalian homologue of *Bicaudal-C*. Mechanisms of *Development*, 101(1-2), pp.267-270.

Wheatley, D.N., 2005. Landmarks in the first hundred years of primary (9+0) cilium research. *Cell Biology Internationa*l, 29(5), pp.333-9.

Whelan, S. & Goldman, N., 2001. A general empirical model of protein evolution derived from multiple protein families using a maximum-likelihood approach. *Molecular Biology and Evolution*, 18(5), pp.691-9.

Wickstead, B. & Gull, K., 2007. Dyneins across eukaryotes: a comparative genomic analysis. *Traffic*, 8(12), pp.1708-21.

Witman, G.B., 1978. *Chlamydomonas* flagellar mutants lacking radial spokes and central tubules. Structure, composition, and function of specific axonemal components. *The Journal of Cell Biology,* 76(3), pp.729-747.

Wong, L.L. & Adler, P.N., 1993. Tissue polarity genes of *Drosophila* regulate the subcellular location for prehair initiation in pupal wing cells. *The Journal of Cell Biology,* 123(1), pp.209-221.

Woods, A. et al., 1989. Definition of individual components within the cytoskeleton of Trypanosoma brucei by a library of monoclonal antibodies. *Journal of Cell Science,* 93 (Pt 3), pp.491-500.

Woolf, E.A. et al., 1995. Polycystic kidney disease: the complete structure of the *PKD1* gene and its protein. The International Polycystic Kidney Disease Consortium. *Cell*, 81(2), pp.289-98.

Wu, S.-Y. & McLeod, M., 1995. The *sak1* Gene of *Schizosaccharomyces pombe* Encodes an RFX Family DNA-Binding Protein That Positively Regulates Cyclic AMP-Dependent Protein Kinase-Mediated Exit from the Mitotic Cell Cycle. *Microbiology*, 15(3), pp.1479-1488.

Yagi, T. & Kamiya, R., 2000. Vigorous beating of *Chlamydomonas* axonemes lacking central pair/radial spoke structures in the presence of salts and organic compounds. *Cell Motility and the Cytoskeleton*, 46(3), pp.190-9.

Yamanaka, H. et al., 2002. JNK functions in the non-canonical Wnt pathway to regulate convergent extension movements in vertebrates. *EMBO Reports,* 3(1), pp.69-75.

Yamanaka, Y. et al., 2007. Live imaging and genetic analysis of mouse notochord formation reveals regional morphogenetic mechanisms. *Developmen*tal *Cell*, 13(6), pp.884-96.

Yamazaki, H. et al., 1996. Cloning and characterization of KAP3: A novel kinesin superfamily-associated protein of KIF3A/3B. *Proceedings of the National Academy of Science*s, 93(16), pp.8443-8448.

Yamazaki, H. et al., 1995. KIF3A/B: a heterodimeric kinesin superfamily protein that works as a microtubule plus end-directed motor for membrane organelle transport. *The Journal of Cell Biology,* 130(6), pp.1387-1399.

Yasui, K. et al., 2000. Left-right asymmetric expression of *BbPtx*, a Ptx-related gene, in a lancelet species and the developmental left-sidedness in deuterostomes. *Development*, 127(1), pp.187-95.

Yin, Y. et al., 2009. The *Talpid3* gene (KIAA0586) encodes a centrosomal protein that is essential for primary cilia formation. *Development*, 136(4), pp.655-64.

Yokoyama, T. et al., 1993. Reversal of left-right asymmetry: a *Situs inversus* mutation. *Science*, 260(5108), pp.679-82.

Yoshida, K. & Saiga, H., 2008. Left-right asymmetric expression of *Pitx* is regulated by the asymmetric *Nodal* signaling through an intronic enhancer in *Ciona intestinalis*. *Development Genes and Evolution,* 218(7), pp.353-60.

Yoshida, T. et al., 1989. Analysis of mammalian dynein using antibodies against A polypeptides of sea urchin sperm flagellar dynein. *Experimental Cell Research*, 184(2), pp.440-8.

Yu, J.-K., Holland, L.Z. & Holland, N.D., 2002. An amphioxus *nodal* gene (*AmphiNodal*) with early symmetrical expression in the organizer and mesoderm and later asymmetrical expression associated with left-right axis formation. *Evolution & Development*, 4(6), pp.418-25.

Yu, J.-K. et al., 2007. Axial patterning in cephalochordates and the evolution of the organizer. *Nature*, 445(7128), pp.613-7.

Zhang, M. et al., 2004. Foxj1 regulates asymmetric gene expression during left-right axis patterning in mice. *Biochemical and Biophysical Research Communications*, 324(4), pp.1413-20.

Zhang, Y. & Levin, M., 2009. Left-right asymmetry in the chick embryo requires core planar cell polarity protein Vangl2. *Genesis*, 47(11), pp.719-728.

APPENDICES

Species	Source	Version	Web Reference
Apis mellifera	beebase	v2 (pre-release)	racerx00.tamu.edu
Arabidopsis thaliana	TAIR	TAIR7	www.arabidopsis.org/
Aureococcus anophagefferens	JGI	v1.0	www.jgi.doe.gov/
Batrachochytrium dendrobatidis	Broad Institute	v1.0	www.broad.mit.edu/annotation/fgi/
Caenorhabdatis elegans	WormBase	WS170	www.wormbase.org/
Capitella teleta	JGI	v1.0	www.jgi.doe.gov/
Chlamydomonas reinhardtii	JGI	v3.1	www.jgi.doe.gov/
Ciona intestinalis	JGI	v2.0	www.jgi.doe.gov/
Cryptosporidium parvum	CryptoDB	v.3.4	www.cryptodb.org/
Cyanidioschyzon merolae	C.merolae genome project	v1	merolae.biol.s.u-tokyo.ac.jp/
Danio rerio	VEGA	May 2007	vega.sanger.ac.uk/
Dictyostelium discoideum	dictyBase	05-20-2007	dictybase.org/
Drosophila melanogaster	ENSEMBL	BDGP4.3, 44.43b	www.ebi.ac.uk/ensembl/
Encephalitozoan cuniculi	NCBI	1	www.ncbi.nlm.nih.gov/
Entamoeba histolytica	geneDB	17102005	www.genedb.org/
Gallus gallus	ENSEMBL	WASHUC2, 44.2b	www.ebi.ac.uk/ensembl/
Giardia lamblia	GiardiaDB	v1.0	www.giardiadb.org/
Homo sapiens	VEGA	Jun-07	vega.sanger.ac.uk/
Leishmania major	geneDB	v5.2	www.genedb.org/

Lottia gigantea	JGI	v1.0	www.jgi.doe.gov/
Monosiga brevicollis	JGI	v1.0	www.jgi.doe.gov/
Naegleria gruberi	JGI	v1.0	www.jgi.doe.gov/
Nematostella vectensis	JGI	v1.0	www.jgi.doe.gov/
Neurospora crassa	Broad Institute	v7.0	www.broad.mit.edu/annotation/fgi/
Oryza sativa	TIGR	v5.0	www.tigr.org/tdb/e2k1/osa1/
Ostreococcus tauri	JGI	v2.0	www.jgi.doe.gov/
Paramecium tetraurelia	ParameciumDB	v1.04	paramecium.cgm.cnrs-gif.fr/
Phaeodactylum tricormutum	JGI	v2.0	www.jgi.doe.gov/
Physcomitrella patens	JGI	v1.1	www.jgi.doe.gov/
Phytophthora sojae	JGI	v1.1	www.jgi.doe.gov/
Plasmodium falciparum	PlasmoDB	v5.2	www.plasmodb.org/
Populus trichocarpa	JGI	v1.1	www.jgi.doe.gov/
Rhizopus oryzae	Broad Institute	v3.0	www.broad.mit.edu/annotation/fgi/
Saccharomyces cerevisiae	Saccharomyces genome database	20070713	www.yeastgenome.org/
Schizosaccharomyces pombe	Sanger	v19	www.sanger.ac.uk/Project/S_Pombe/
Stronglyocentrotus purparatus	Baylor College of Medicine	Spur_2.1, v4	www.hgsc.bcm.tmc.edu/
Takifugu rubripes	ENSEMBL	Assembly4, 44.4e	www.ebi.ac.uk/ensembl/
Tetrahymena thermophila	TIGR	10/24/2006	www.tigr.org/tdb/e2k1/tta1/
Thalassiosira pseudonana	JGI	v3.0	www.jgi.doe.gov/
Theilera annulata	GeneDB	v4	www.genedb.org/
Toxoplasma gondii	ToxoDB	v4.1	www.toxodb.org/
Trichomonas vaginalis	TIGR	20050331	www.tigr.org/tdb/e2k1/tvg/
Trichoplax adhaerens	JGI	v1.0	www.jgi.doe.gov/
Trypanosoma brucei	geneDB	v4	www.genedb.org/
Ustilago maydis	Broad Institute	v1.0	www.broad.mit.edu/annotation/fgi/

Bayesian



Appendix Figure1.1: DNAH5 Phylogeny.

Maximum Likelihood and Bayesian trees were produced for DNAH5, including DNAH8. Amino acid sequence alignments were produced using MAFFT and trimmed to remove poorly aligned positions. Maximum likelihood phylogentic trees were constructed using PhyMLv3.0 (100 replicates, LG matrix, 4 gamma categories, random starting tree). Bayesian trees were inferred using MrBayesv3.1.2 (random starting tree, 4 chains of temperature 0.2, WAG substitution matrices, 4 discrete categories of gamma distribution substitution rate, 250 000 generations). Topology support for nodes is indicated (bootstrap). Generally, groups with >90% bootstrap support were considered to be well supported and those with >70% bootstrap support to have some support. The tree contains organisms from 5 of the 6 major clades: Plantae (Green), Chromalveolata (Purple), Excavata (Turquoise), Holozoa (Red) and Fungi (Orange).

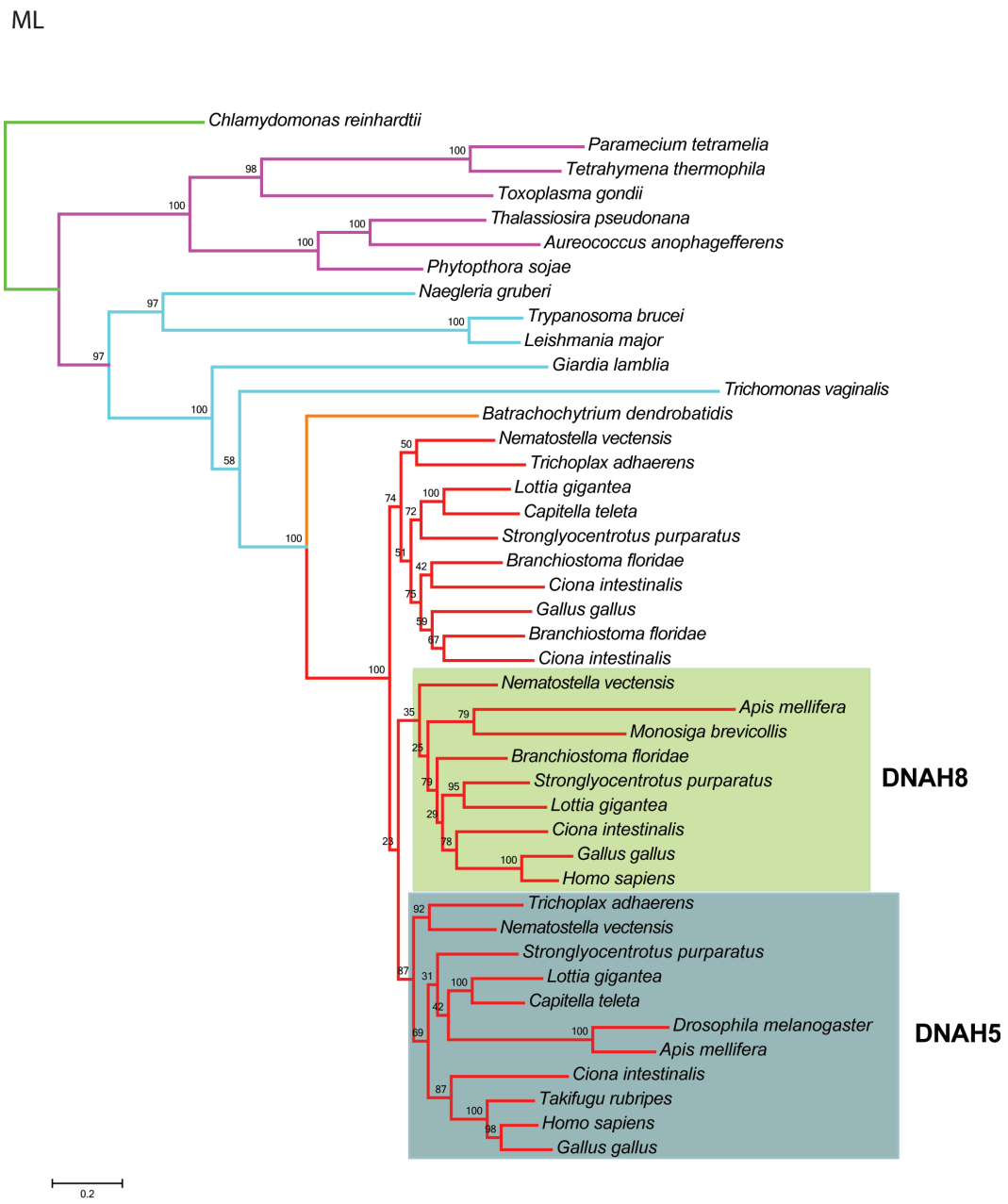
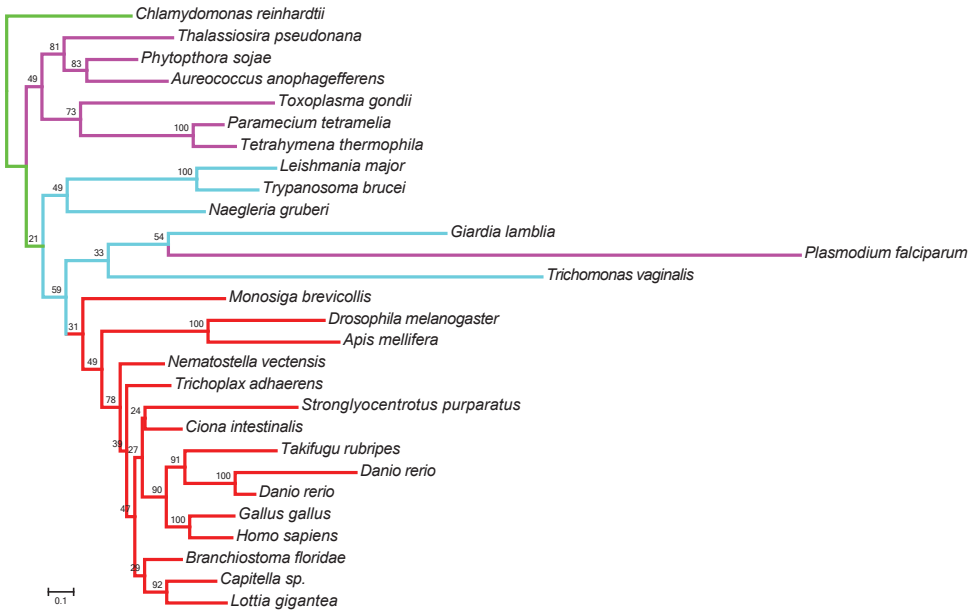
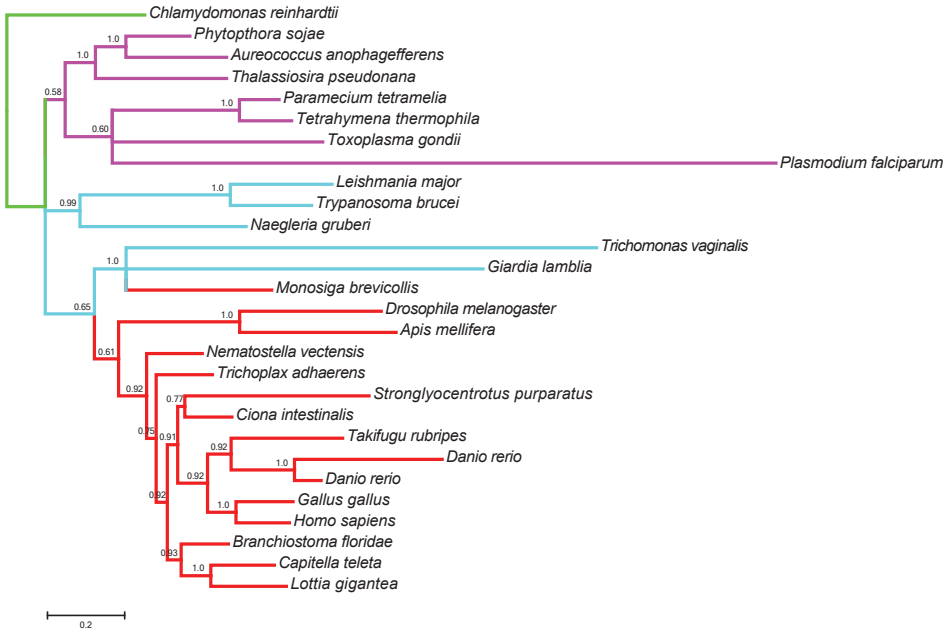


Figure legend on previous page

ML

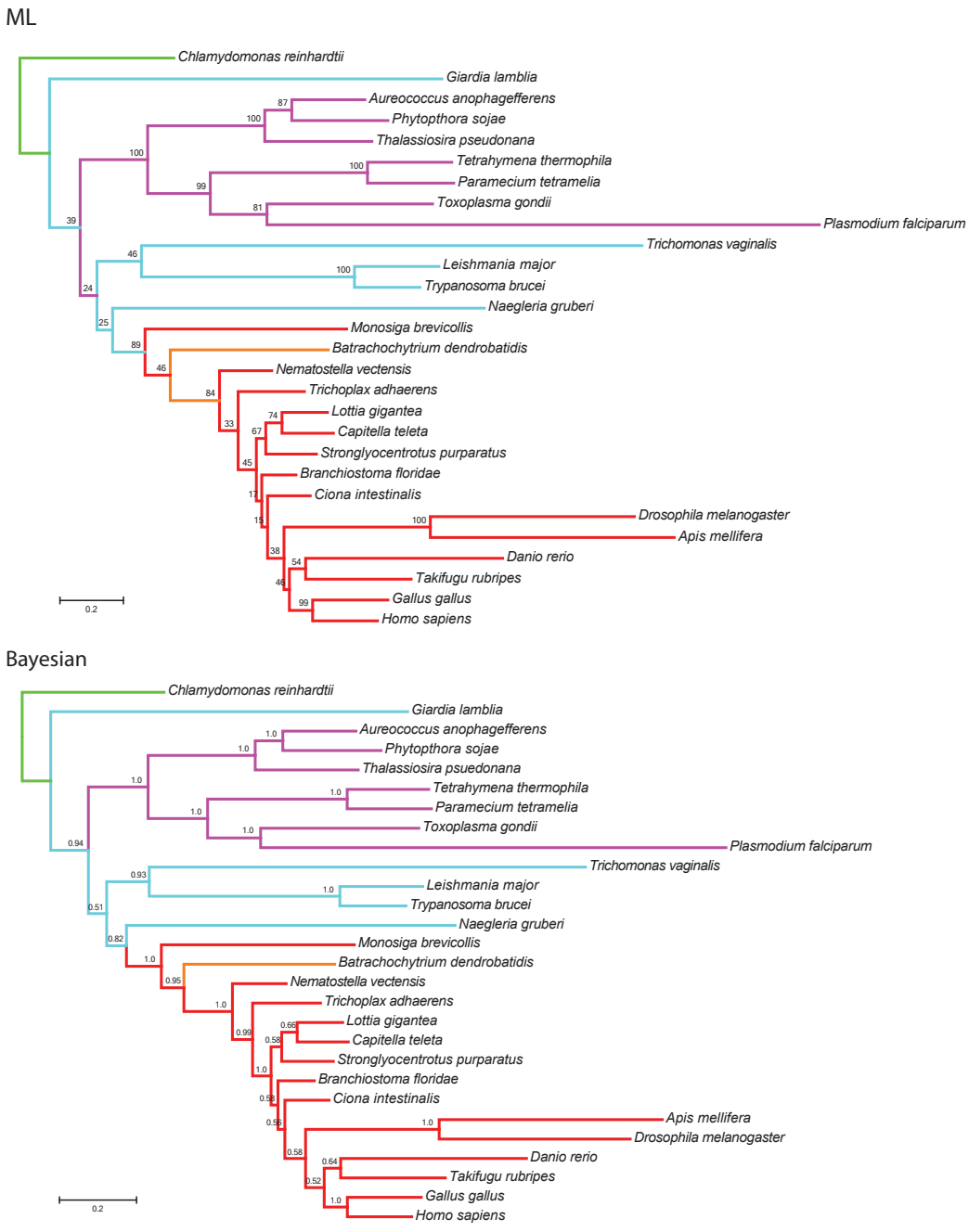


Bayesian



Appendix Figure 1.2: DNAI1 Phylogeny.

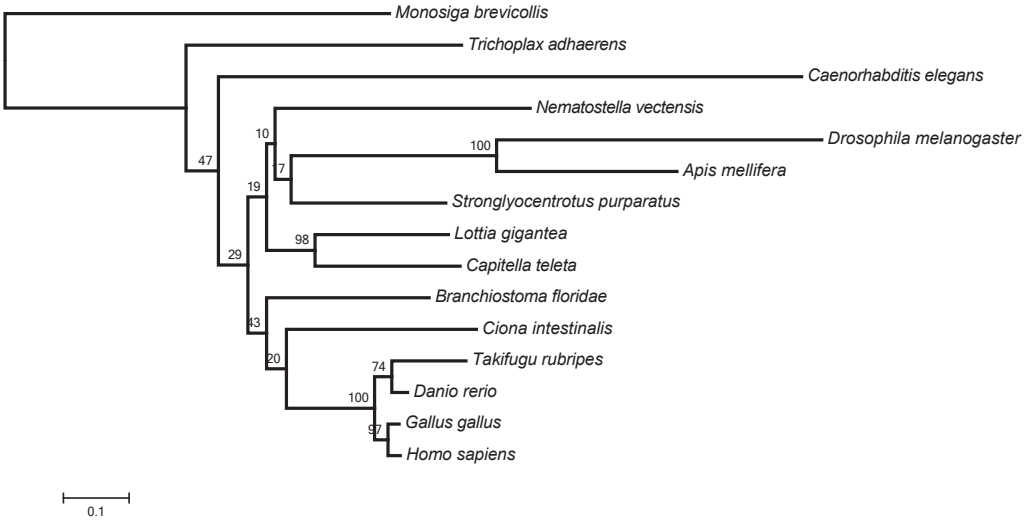
Maximum Likelihood and Bayesian trees were produced for DNAI1. Amino acid sequence alignments were produced using MAFFT and trimmed to remove poorly aligned positions. Maximum likelihood phylogentic trees were constructed using PhyMLv3.0 (100 replicates, LG matrix, 4 gamma categories, random starting tree). Bayesian trees were inferred using MrBayesv3.1.2 (random starting tree, 4 chains of temperature 0.2, WAG substitution matrices, 4 discrete categories of gamma distribution substitution rate, 250 000 generations). Topology support for nodes is indicated (bootstrap). Generally, groups with >90% bootstrap support were considered to be well supported and those with >70% bootstrap support to have some support. The tree contains organisms from 4 of the 6 major clades: Plantae (Green), Chromalveolata (Purple), Excavata (Turquoise) and Holozoa (Red).



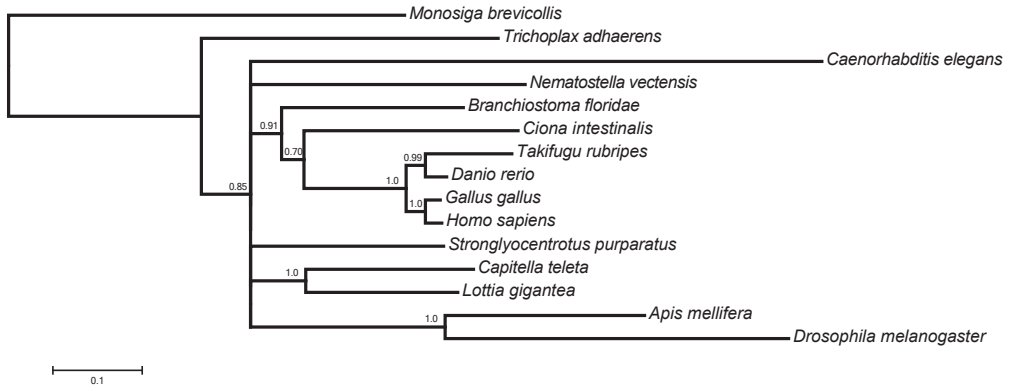
Appendix Figure 1.3: DNAI2 Phylogeny.

Maximum Likelihood and Bayesian trees were produced for DNAI2. Amino acid sequence alignments were produced using MAFFT and trimmed to remove poorly aligned positions. Maximum likelihood phylogentic trees were constructed using PhyMLv3.0 (100 replicates, LG matrix, 4 gamma categories, random starting tree). Bayesian trees were inferred using MrBayesv3.1.2 (random starting tree, 4 chains of temperature 0.2, WAG substitution matrices, 4 discrete categories of gamma distribution substitution rate, 250 000 generations). Topology support for nodes is indicated (bootstrap). Generally, groups with >90% bootstrap support were considered to be well supported and those with >70% bootstrap support to have some support. The tree contains organisms from 5 of the 6 major clades: Plantae (Green), Chromalveolata (Purple), Excavata (Turquoise), Holozoa (Red) and Fungi (Orange).

ML

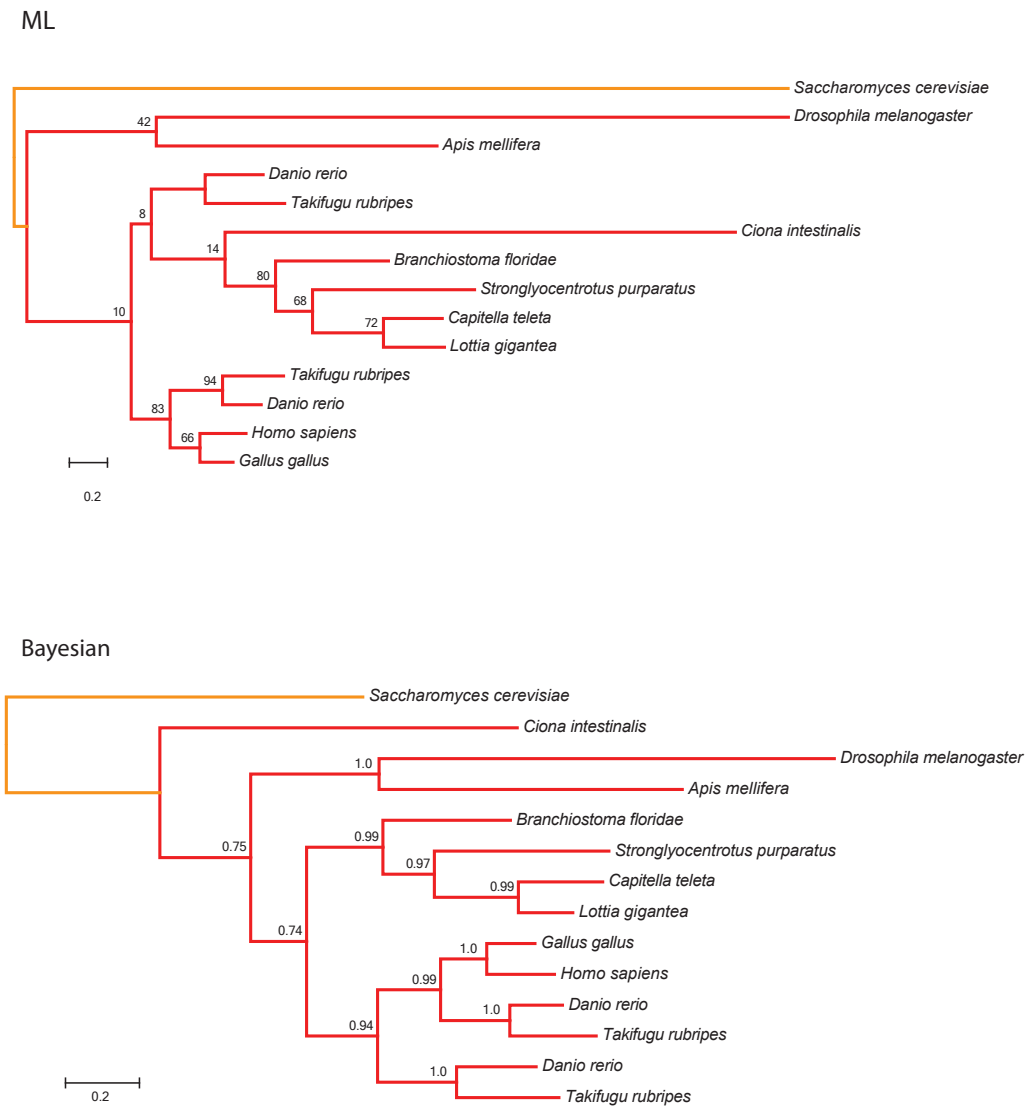


Bayesian



Appendix Figure 1.4: KIF3A Phylogeny.

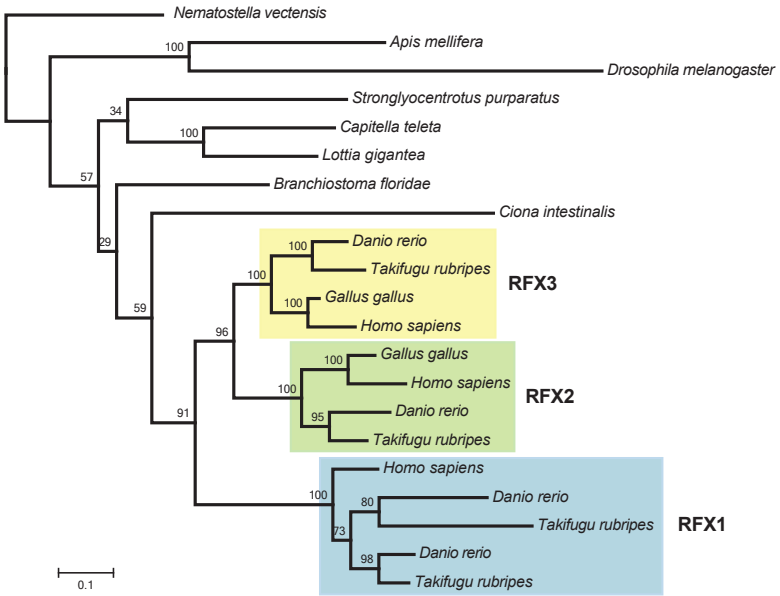
Maximum Likelihood and Bayesian trees were produced for KIF3A. Amino acid sequence alignments were produced using MAFFT and trimmed to remove poorly aligned positions. Maximum likelihood phylogentic trees were constructed using PhyMLv3.0 (100 replicates, LG matrix, 4 gamma categories, random starting tree). Bayesian trees were inferred using MrBayesv3.1.2 (random starting tree, 4 chains of temperature 0.2, WAG substitution matrices, 4 discrete categories of gamma distribution substitution rate, 250 000 generations). Topology support for nodes is indicated (bootstrap). Generally, groups with >90% bootstrap support were considered to be well supported and those with >70% bootstrap support to have some support.



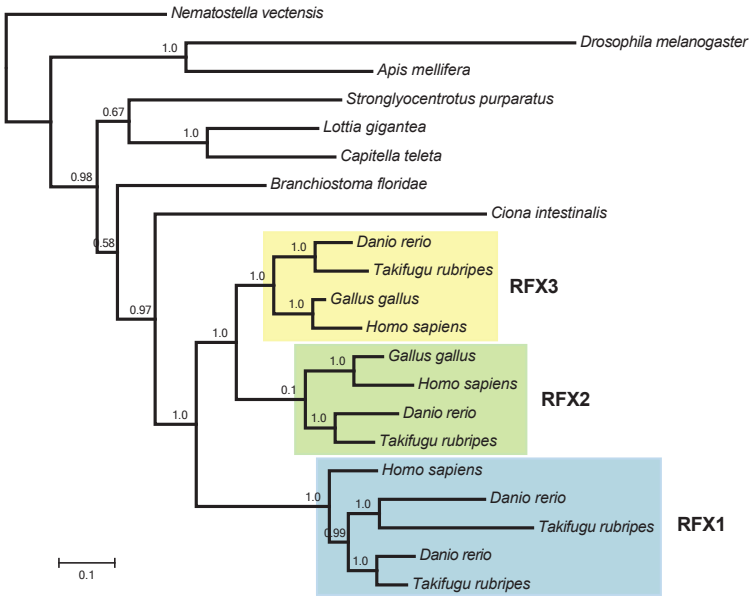
Appendix Figure 1.5: FOXJ1 Phylogeny.

Maximum Likelihood and Bayesian trees were produced for FOXJ1. Amino acid sequence alignments were produced using MAFFT and trimmed to remove poorly aligned positions. Maximum likelihood phylogentic trees were constructed using PhyMLv3.0 (100 replicates, LG matrix, 4 gamma categories, random starting tree). Bayesian trees were inferred using MrBayesv3.1.2 (random starting tree, 4 chains of temperature 0.2, WAG substitution matrices, 4 discrete categories of gamma distribution substitution rate, 250 000 generations). Topology support for nodes is indicated (bootstrap). Generally, groups with >90% bootstrap support were considered to be well supported and those with >70% bootstrap support to have some support.

ML



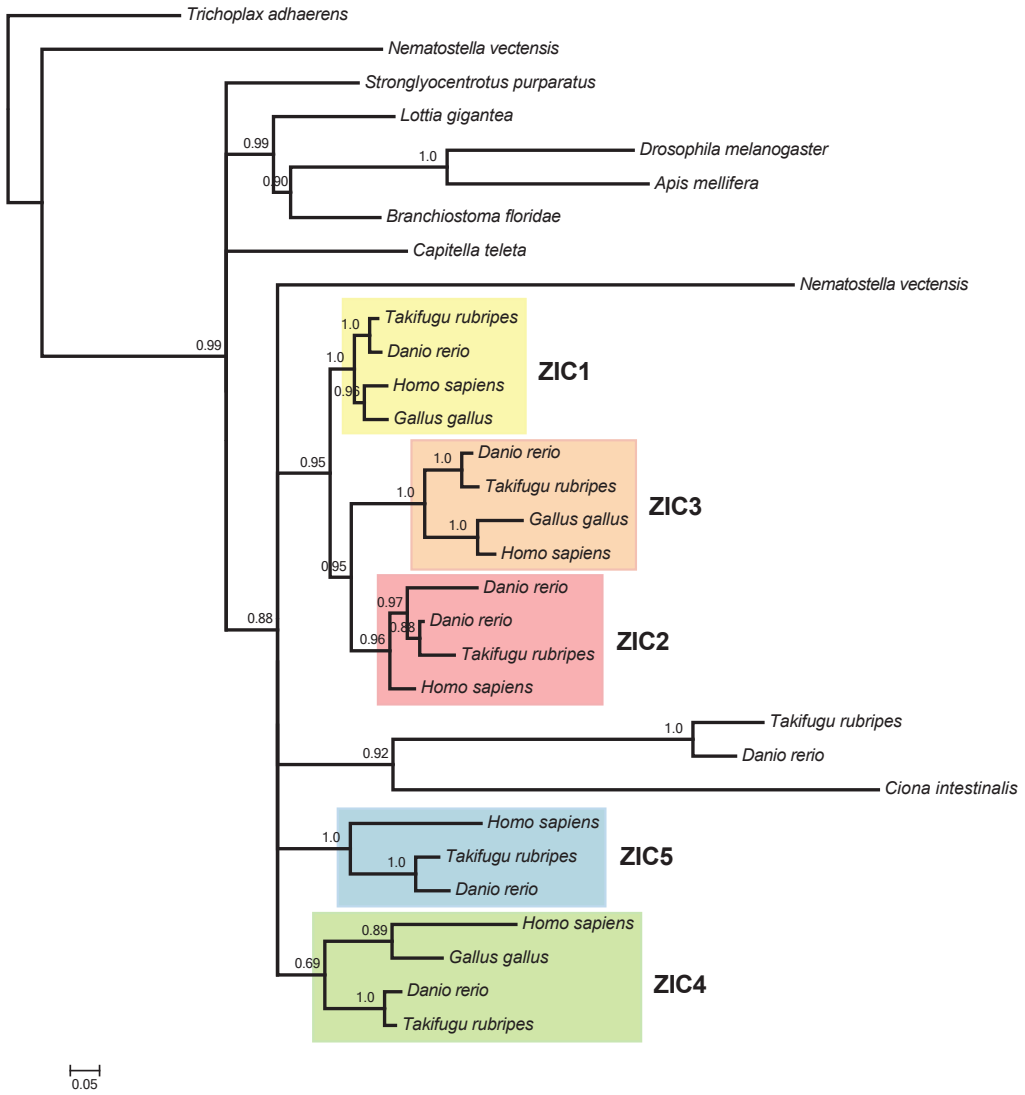
Bayesian



Appendix Figure 1.6: RFX3 Phylogeny.

Maximum Likelihood and Bayesian trees were produced for RFX3, including RFX1 and RFX2. Amino acid sequence alignments were produced using MAFFT and trimmed to remove poorly aligned positions. Maximum likelihood phylogentic trees were constructed using PhyMLv3.0 (100 replicates, LG matrix, 4 gamma categories, random starting tree). Bayesian trees were inferred using MrBayesv3.1.2 (random starting tree, 4 chains of temperature 0.2, WAG substitution matrices, 4 discrete categories of gamma distribution substitution rate, 250 000 generations). Topology support for nodes is indicated (bootstrap). Generally, groups with >90% bootstrap support were considered to be well supported and those with >70% bootstrap support to have some support.

Bayesian



Appendix Figure 1.7: ZIC3 Phylogeny.

Maximum Likelihood and Bayesian trees were produced for ZIC3. Amino acid sequence alignments were produced using MAFFT and trimmed to remove poorly aligned positions. Maximum likelihood phylogentic trees were constructed using PhyMLv3.0 (100 replicates, LG matrix, 4 gamma categories, random starting tree). Bayesian trees were inferred using MrBayesv3.1.2 (random starting tree, 4 chains of temperature 0.2, WAG substitution matrices, 4 discrete categories of gamma distribution substitution rate, 250 000 generations). Topology support for nodes is indicated (bootstrap). Generally, groups with >90% bootstrap support were considered to be well supported and those with >70% bootstrap support to have some support.

ML

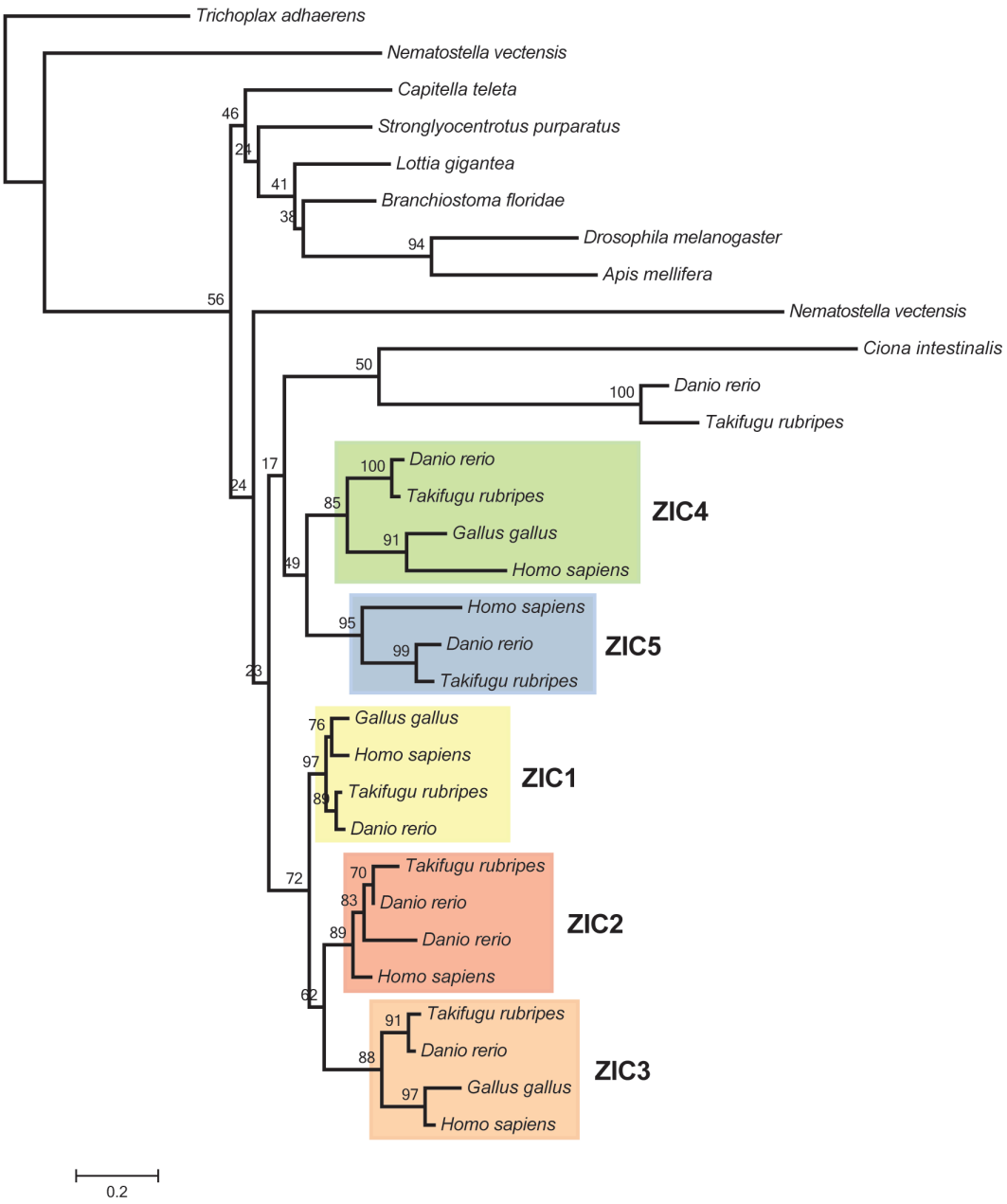
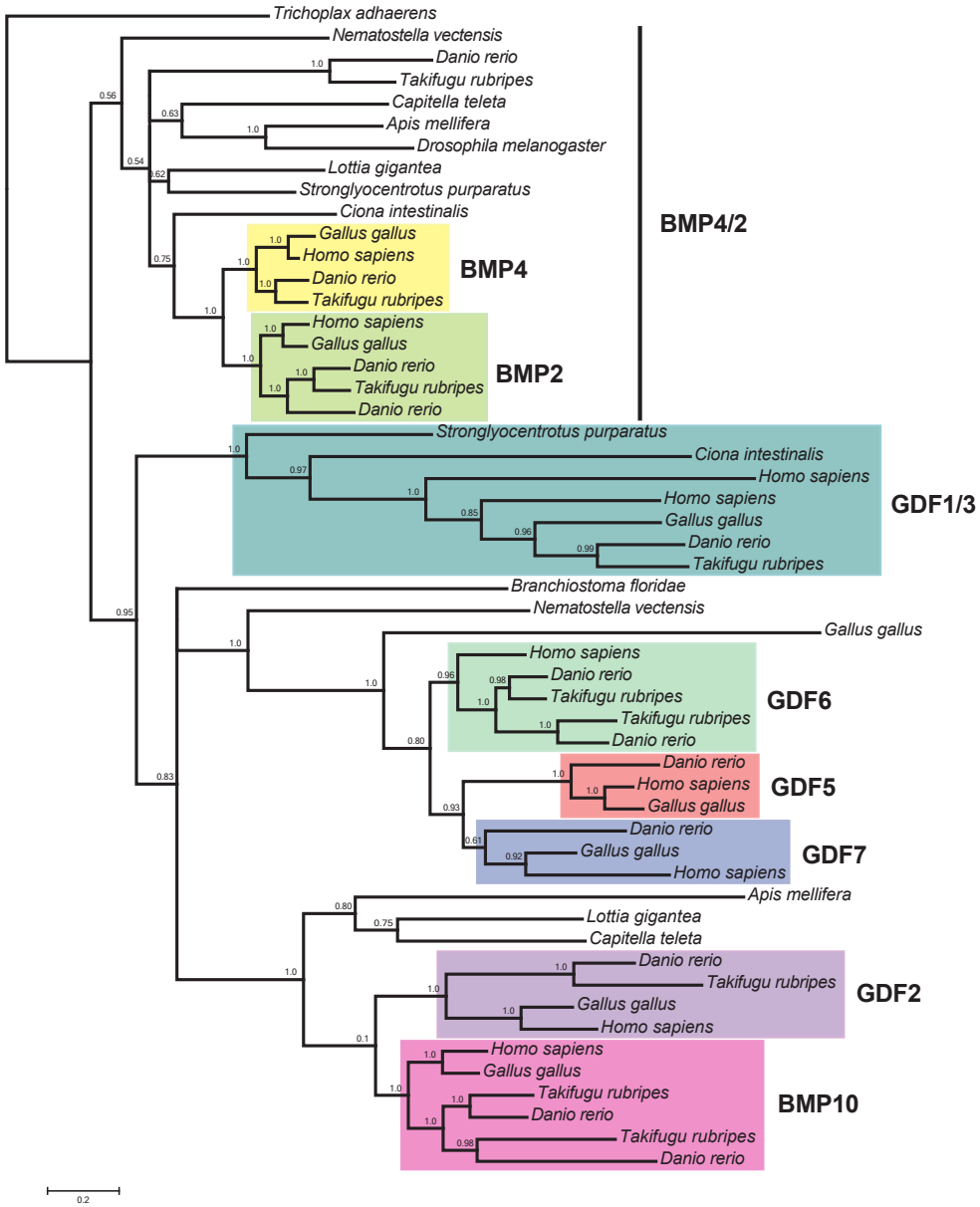


Figure legend on previous page.

Bayesian



Appendix Figure 1.8: GDF1 Phylogeny.

Maximum Likelihood and Bayesian trees were produced for GDF1. Amino acid sequence alignments were produced using MAFFT and trimmed to remove poorly aligned positions. Maximum likelihood phylogentic trees were constructed using PhyMLv3.0 (100 replicates, LG matrix, 4 gamma categories, random starting tree). Bayesian trees were inferred using MrBayesv3.1.2 (random starting tree, 4 chains of temperature 0.2, WAG substitution matrices, 4 discrete categories of gamma distribution substitution rate, 250 000 generations). Topology support for nodes is indicated (bootstrap). Generally, groups with >90% bootstrap support were considered to be well supported and those with >70% bootstrap support to have some support.

ML

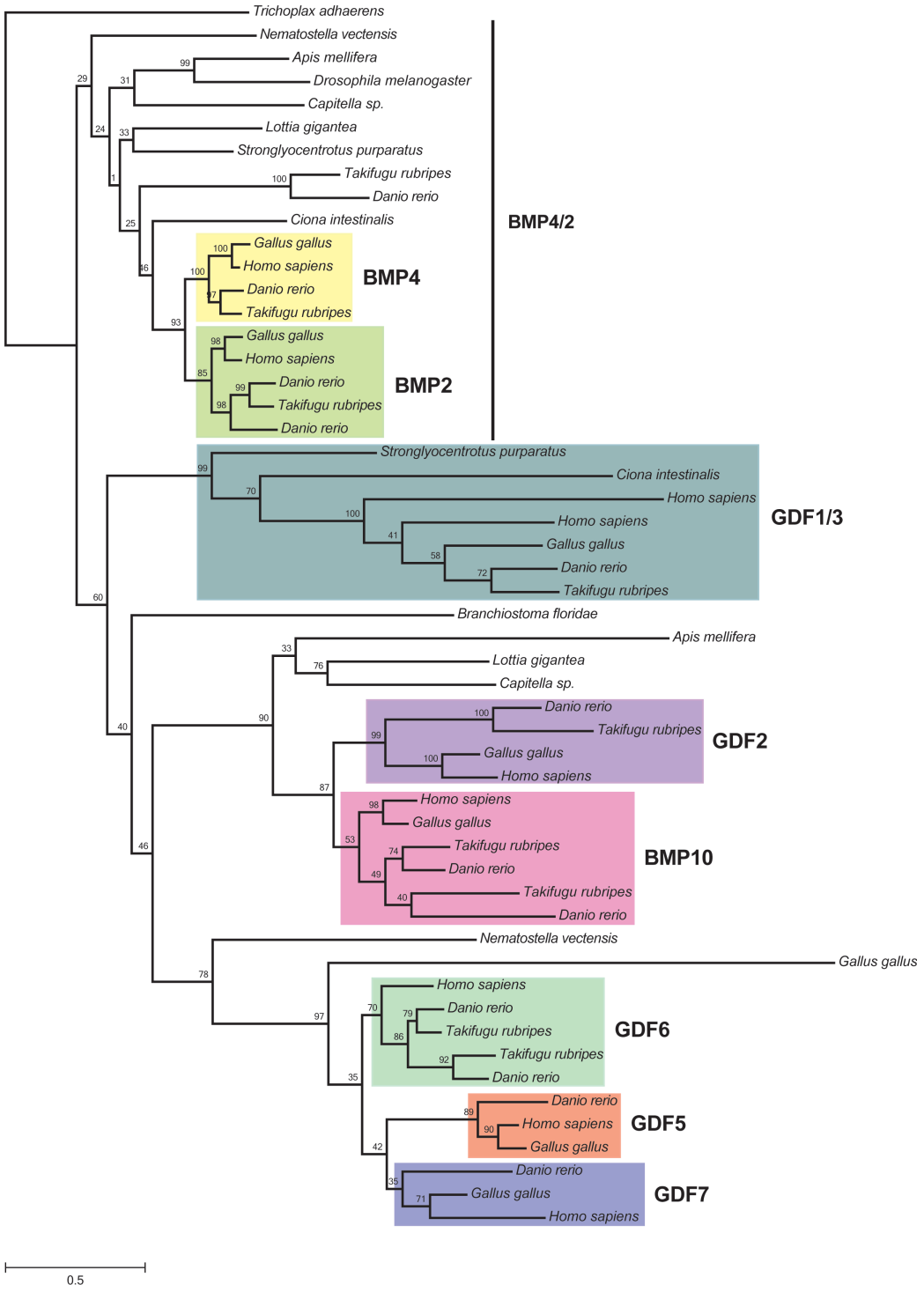
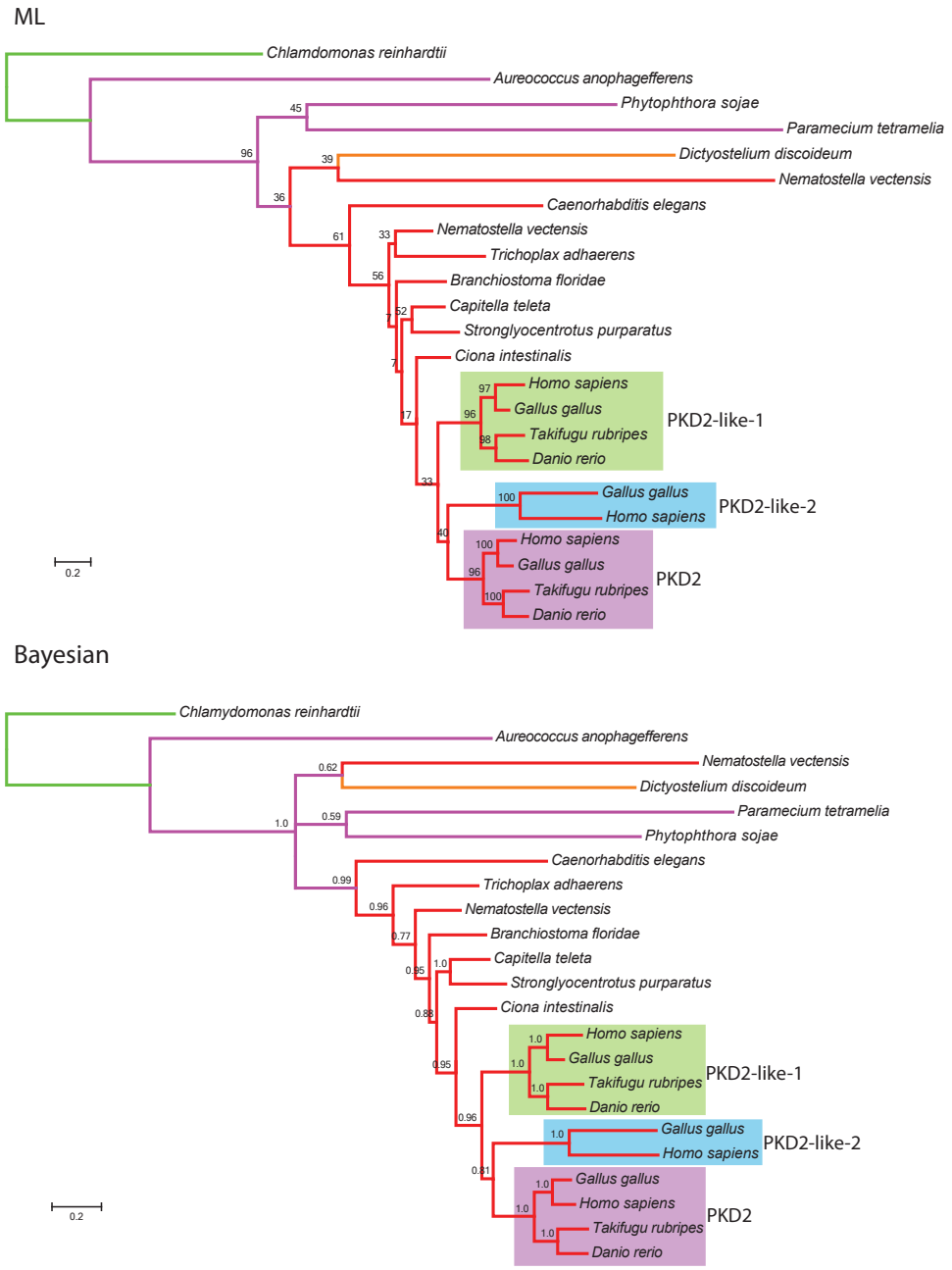


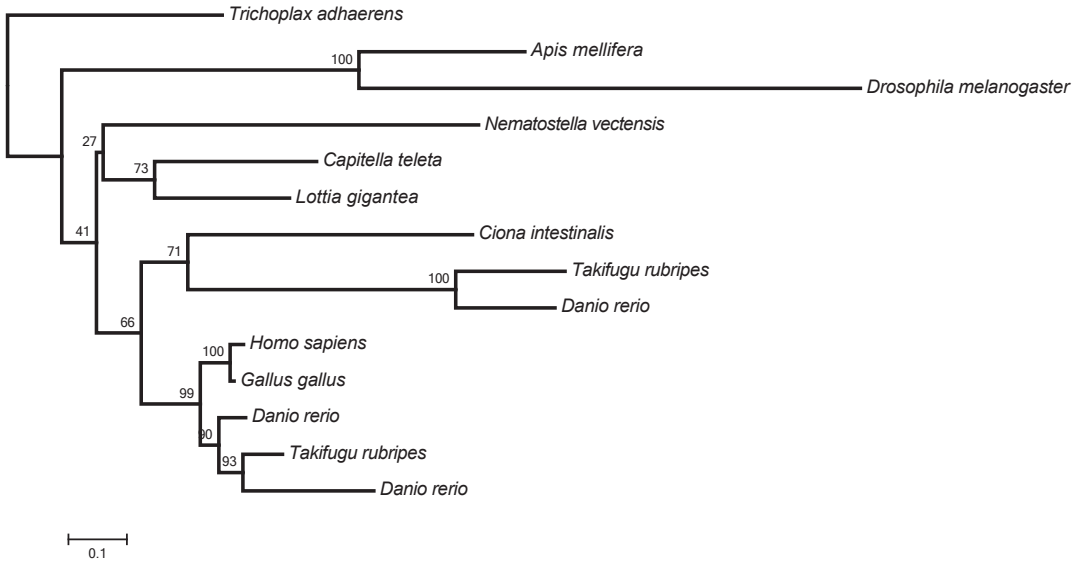
Figure legend on previous page.



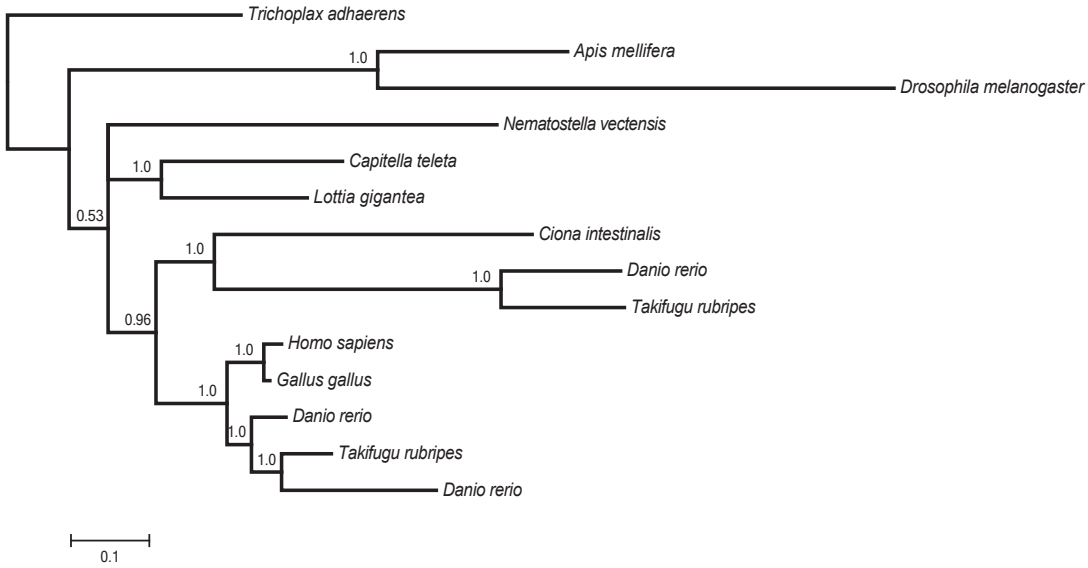
Appendix Figure 1.9: PKD2 Phylogeny.

Maximum Likelihood and Bayesian trees were produced for PKD2. Amino acid sequence alignments were produced using MAFFT and trimmed to remove poorly aligned positions. Maximum likelihood phylogentic trees were constructed using PhyMLv3.0 (100 replicates, LG matrix, 4 gamma categories, random starting tree). Bayesian trees were inferred using MrBayesv3.1.2 (random starting tree, 4 chains of temperature 0.2, WAG substitution matrices, 4 discrete categories of gamma distribution substitution rate, 250 000 generations). Topology support for nodes is indicated (bootstrap). Generally, groups with >90% bootstrap support were considered to be well supported and those with >70% bootstrap support to have some support. The tree contains organisms from 4 of the 6 major clades: Plantae (Green), Chromalveolata (Purple), Holozoa (Red) and Fungi (Orange).

ML



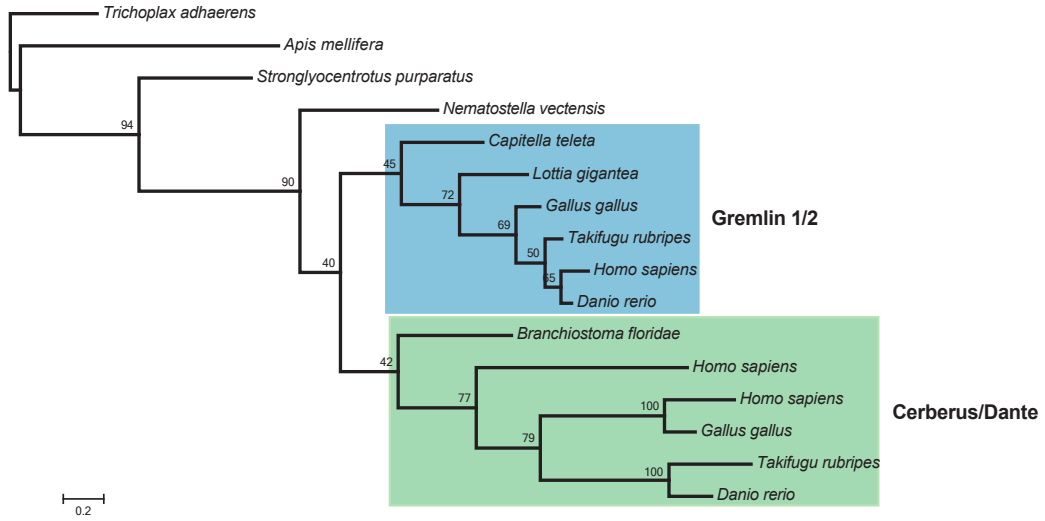
Bayesian



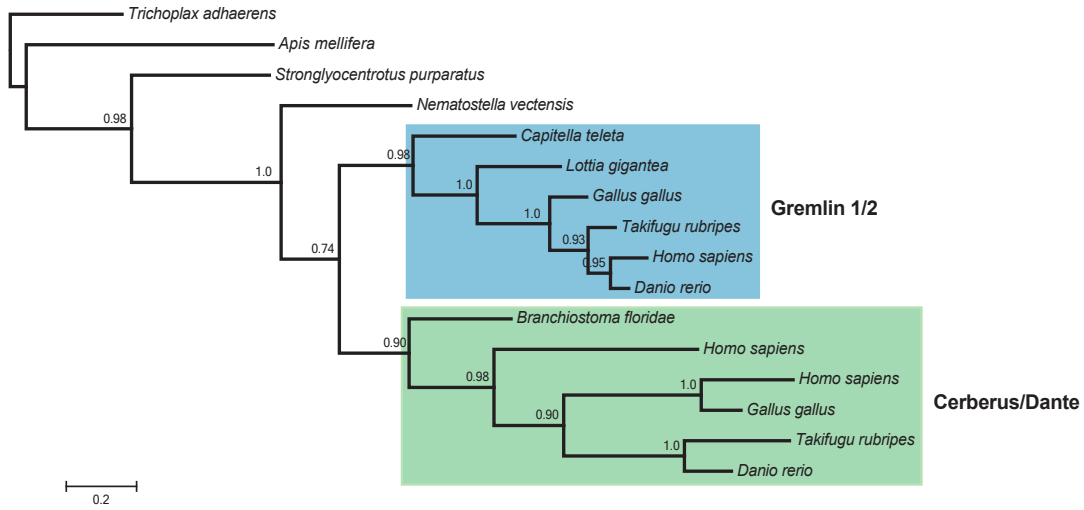
Appendix Figure 1.10: BICC1 Phylogeny.

Maximum Likelihood and Bayesian trees were produced for BICC1. Amino acid sequence alignments were produced using MAFFT and trimmed to remove poorly aligned positions. Maximum likelihood phylogentic trees were constructed using PhyMLv3.0 (100 replicates, LG matrix, 4 gamma categories, random starting tree). Bayesian trees were inferred using MrBayesv3.1.2 (random starting tree, 4 chains of temperature 0.2, WAG substitution matrices, 4 discrete categories of gamma distribution substitution rate, 250 000 generations). Topology support for nodes is indicated (bootstrap). Generally, groups with >90% bootstrap support were considered to be well supported and those with >70% bootstrap support to have some support.

ML



Bayesian



Appendix Figure 1.11: DAND5 Phylogeny.

Maximum Likelihood and Bayesian trees were produced for DAND5. Amino acid sequence alignments were produced using MAFFT and trimmed to remove poorly aligned positions. Maximum likelihood phylogentic trees were constructed using PhyMLv3.0 (100 replicates, LG matrix, 4 gamma categories, random starting tree). Bayesian trees were inferred using MrBayesv3.1.2 (random starting tree, 4 chains of temperature 0.2, WAG substitution matrices, 4 discrete categories of gamma distribution substitution rate, 250 000 generations). Topology support for nodes is indicated (bootstrap). Generally, groups with >90% bootstrap support were considered to be well supported and those with >70% bootstrap support to have some support.